ATB
Leibniz-Institut für Agrartechnik
Potsdam-Bornim e.V.

IGZ

Universität Potsdam

3rd Global Workshop on Proximal Soil Sensing

26 – 29 May 2013
Potsdam, Germany

International Union of Soil Sciences

Organized under the auspices of the International Union of Soil Sciences
Working Group on Proximal Soil Sensing

Bornimer Agrartechnische Berichte

Heft 82

Potsdam-Bornim 2013

3rd Global Workshop on Proximal Soil Sensing 2013

26 – 29 May 2013
Potsdam, Germany

International Union of Soil Sciences

International Union of Soil Sciences
Working Group on Proximal Soil Sensing

Bornimer Agrartechnische Berichte
Heft 82

Potsdam-Bornim 2013

Editors:
Dr. Robin Gebbers
Leibniz-Institut für Agrartechnik Potsdam-Bornim e.V.
Dr. Erika Lück
Universität Potsdam
Dr. Jörg Rühlmann
Leibniz-Institut für Gemüse- und Zierpflanzenbau

Layout and typesetting:
Dipl.-Ing. (FH) Katrin Witzke

Publisher:
Published by the Leibniz-Institute for Agricultural Engineering Potsdam-Bornim (Leibniz-Institut für Agrartechnik Potsdam-Bornim e.V., ATB) with support by the German Federal Ministry of Food, Agriculture and Consumer Protection (Bundesministerium für Ernährung, Landwirtschaft und Verbraucherschutz, BMELV) and the Ministry of Science, Research and Culture of the State of Brandenburg (Ministerium für Wissenschaft, Forschung und Kultur, MWFK).

Leibniz-Institut für Agrartechnik Potsdam-Bornim e.V.
Max-Eyth-Allee 100
14469 Potsdam-Bornim
☎: +49 (0)331-5699-0
Fax: +49 (0)331-849
E-mail: atb@atb-potsdam.de
Internet: http://www.atb-potsdam.de

Herausgegeben vom Leibniz-Institut für Agrartechnik Potsdam-Bornim e.V. (ATB) mit Förderung durch den Bund (Bundesministerium für Ernährung, Landwirtschaft und Verbraucherschutz BMELV), das Land Brandenburg (Ministerium für Wissenschaft, Forschung und Kultur MWFK).

ISSN 0947-7314

Content

Preface

Spatial information about soils at a fine spatial and temporal scale is scarce. Despite the importance of soil for food production, bio-geochemical recycling, carbon storage, and as a cultural heritage, remarkably little is known about its spatial variation and how to address it. Conventional methods of soil analysis, though accurate, are often too expensive and time consuming to be used for soil assessment at distances of less than 50 m. For example, geostatistics tells us that we need sampling intervals of less than 30 m in landscapes formed by the last ice age. Archaeological surveys of ancient human settlements or investigations of polluted sites require information at even finer resolution. To efficiently address soil spatial variability, we need sensor systems that provide cost- and time-effective quantitative information. In response to this demand the discipline of proximal soil sensing has emerged. Proximal soil sensing is dedicated to the development and application of field-based sensors from close by (say within 2 m), or within the soil body (Viscarra Rossel, McBratney & Minasny, 2010).

The Global Workshop on Proximal Soil Sensing 2013 (GWPSS2013) in Potsdam, Germany was arranged by the Leibniz-Institute of Agricultural Engineering (ATB), the Leibniz-Institute of Vegetable and Ornamental Crops (IGZ), and the University of Potsdam. The GWPSS2013 is the third in a row. The first workshop was organized by Dr. Raphael Viscarra Rossel 2008 in Sydney, Australia. The second was held in Montreal, Canada in 2011 by Prof. Dr. Viacheslav Adamchuck. All of them were arranged under the auspices of the International Union of Soil Sciences (IUSS).

The GWPSS2013 will bring together researchers from various disciplines, including soil science, agricultural engineering, geophysics, chemistry, agronomy, archaeology, spatial statistics, as well as commercial entities involved in the development and use of proximal sensors. The workshop's focus is on mobile multi-sensor systems, sensor data fusion and applications of proximal soil sensing. More than 80 attendees have registered to the workshop. We collected nearly 60 contributions in this book. A large number of contributions are related to soil spectroscopy in the visible and near infrared (Vis-NIR) which has gained increasing interest over the last years. Nevertheless, classical and advanced geo-electrical methods are still considered as very valuable tools for proximal soil sensing. According to the contributions, they received nearly as much attention as Vis-NIR spectroscopy. A lot of progress has been made in the combination of soil sensors. In particular, the combination of geo-electrical methods with passive gamma ray radometry and/or radar has been investigated. It is evident that there is no single sensor that can handle all situations and meet all requirements. Thus sensor data fusion and advanced mathematical methods for data analysis are an integral part of proximal soil sensing. In particular, it is a great challenge to derive process based models with sensor data and to develop empirical models that can be transferred from one place to another. Several contributions to the GWPSS2013 deal with this problem. A couple of technolo-

gies new to proximal soil sensing will be presented as well. These include: terahertz transmission, cosmic ray neutron sensing, photo-acoustic spectroscopy and advanced electrochemical methods. Applications ranged from agriculture (soil fertility, soil moisture, soil biology, pH, soil texture) to archaeology and to environmental protection.

The organisers would like to thank their institutions for their support and all of their colleagues for their hard work in preparing the workshop. We wish to acknowledge the advice of Raphael Viscarra Rossel and Viachselav Adamchuck and we are very grateful for the excellent review of the submissions by the scientific committee. Last but not least, we like to thank the participants and the commercial supporters - without them the workshop would not have happened.

Germany Robin Gebbers

Erika Lück

Jörg Rühlmann

Viscarra Rossel, R. A.; McBratney, A. B.; Minasny, B., 2010. Proximal soil sensing. Preface. Springer, Dordrecht, The Netherlands

Scientific Committee

Viacheslav Adamchuk: McGill University, Canada

Annamaria Castrignanò: Agricultural Research Council CRA-SCA, Italy

Richard Ferguson: University of Nebraska-Lincoln, USA

Robin Gebbers: Leibniz-Institute for Agricultural Engineering, Germany

Carolyn Hedley: Landcare Research, Newzealand

Erika Lück: University of Potsdam, Germany

Abdul Mouazen: Cranfield University, United Kingdom

Jörg Rühlmann: Institute of Vegetable and Ornamental Crops, Germany

Sakae Shibusawa: Tokyo University of Ag. and Technology, Japan

Bosse Stenberg: Swedish University, Sweeden

Kenneth Sudduth: USDA-ARS, USA

Marc Van Meirvenne: University Gent, Belgium

Raphael Viscarra Rossel: CSIRO Land and Water, Australia

Chris Waring: ANSTO Australian Nuclear Science and Technology Organisation, Australia

Pierre Roudier: Landcare research Ltd., Newzealand

Simone Priori: Research Center of Agrobiology and Pedology, Italy

Timothy Saey: University Gent, Belgium

Kristin Piikki: Swedish University, Sweeden

Zhou Shi: Zhejiang University, China

Eckart Kramer: University of Sustainable Development, Germany

Bornimer Agrartechnische Berichte • Heft 82
ISSN 0947-7314
Leibniz-Institut für Agrartechnik Potsdam-Bornim e.V. (ATB)

Development of a proximal multi sensor system for measuring soil condition

R. Visacarra Rossel*

CSIRO Land and Water, Bruce E. Butler Laboratory, PO Box 1666, Canberra, ACT 2601, Australia

**E-mail: Raphael.Viscarra-Rossel@csiro.au*

Abstract

In this presentation I will discuss the importance of soil measurement and review proximal soil sensing (PSS): the technologies that are currently available and their use for measuring soil properties. I will discuss the sampling dilemma and using the range of frequencies in the electromagnetic spectrum as a framework, describing technologies that can be used for PSS, including electrochemical and mechanical sensors, telemetry, geographic positioning and elevation, multisensor platforms, and core measuring and down borehole sensors.

Because soil properties can be measured with different proximal soil sensors examples will be given of the alternative techniques that are available for measuring soil properties. The developmental stage of technologies for PSS will be reported and the current approximate cost of commercial sensors. The presentation will focus on the development of PSS over the past 30 years, on its current state and the future.

I will report results of research to develop a multi-sensor system to measure soil organic carbon, bulk density and thus organic carbon stores. Results will show that the multi-sensor system can be used to derive accurate estimates of soil carbon content and carbon stores, which might then be used for baselining and with appropriate designs also monitoring.

Potentials of terahertz transmission measurements as a new methodology for proximal soil sensing

V. Dworak[1*], S. Augustin[2], J. Selbeck[1], R. Gebbers[1]

[1]Leibniz Institute for Agricultural Engineering, Max-Eyth-Allee 100, 14469 Potsdam, Departement Engineering for Crop Production, Germany

[2]German Aerospace Center (DLR), Institute for Planetary Research, Experimental Planetary Physics (XP), Rutherfordstr. 2, 12489 Berlin, Germany

[*]E-mail: vdworak@atb-potsdam.de

Abstract

Soil is a scarce resource which requires due attention. Developing soil sensors with the possibility of continuous online measurement is a major challenge in soil science. Terahertz (THz) electromagnetic radiation may provide the opportunity for the measurement of organic material density, water content and other soil parameters at different soil depths. Penetration depth and information content is important for a functional soil sensor. First results (Dworak, 2011) with frequencies of 340 GHz to 360 GHz and 1.627 THz to 2.523 THz show an existing frequency dependency. The results demonstrate the potential of this THz approach for both soil analysis and imaging of buried objects.

1 Introduction

Proximal soil sensing competes with traditional sampling plus laboratory analysis and with remote sensing. The efficiency of proximal soil sensing relies on measurement methods that can a) be integrated into mobile system, b) are insensitive to or can be protected from ambient conditions, c) can rapidly process samples, and d) have a sound relationship with soil properties of interest. Additionally, the methodology should use low-cost sensors, should not use/produce toxic substances and should be non-invasive if possible. Many measurement technologies in proximal soil sensing such as Vis-NIR spectroscopy or radar are based on the interaction of electromagnetic radiation with soil (Mouazen, 2005; Collins, 2008; Baghdadi, 2007). Electromagnetic radiation in the terahertz (THz) range (100 µm to 1 mm) is new to soil sensing because the technology has been developed more recently, over the last two decades. It shows some similarities to radar, which operates at the MHz to low GHz range and has already been used for soil sensing. Due to the constant decline of prices for THz equipment it becomes more and more affordable. THz is non-invasive and environmentally sound. So it is of interest to explore the potentials of THz in proximal soil sensing. The objectives of the initial work presented her was a) to identify organic objects within a mineral soil matrix; b) to obtain absorption coefficients from soil and see whether these can be used to distinguish soil properties. To accomplish this, an appropriate setup of a THz system was to be designed.

2 Material and methods

2.1 Soil samples

Four different soil samples (Table 1) were used in order to estimate the absorption of THz radiation at different frequencies. They were selected with respect to variation in important soil parameters, namely organic matter (OM) and particle size distribution (soil texture) and with respect to the physical bulk density. Differences between the soil samples were important to induce contrasts for the THz approach. Three samples were natural soils collected in Potsdam, Germany (soils 1 to 3 in Table 1). One was an artificial soil, composed to obtain a sample with medium organic matter content (soil 4 in Table 1). The samples were ground, sieved to 2 mm and air dried. The air dried samples contained a certain amount of water as shown in Table 1, which may be relevant for THz attenuation. All samples were exposed to the same humidity conditions during the measurement campaign. They were analyzed for organic matter and water content (Table 1).

Table 1. Analysis of the air dried soil samples. The difference to 100% is the leftover which is so called “mineral ashes”.

Sample name	DM105 %	OM %	C %	N %	S %
Soil 1	99.97	0.238	0.010	0.001	0.006
Soil 2	99.75	1.554	0.451	0.017	0.030
Soil 3	93.50	30.50	15.50	0.142	3.61
Soil 4	93.57	6.55	0.748	0.009	0.026

DM 105 is the dry matter of the sample after oven-drying for 24 h at 105 °C; OM is the amount of organic matter; C, N, and S are the concentrations of carbon, nitrogen, and sulfur, respectively.

Particle size distribution was analyzed by sieving with different meshes. Figure 1 shows the distribution of particle sizes over eight classes.

Figure 1 shows differences in particle fractions of 25 µm to 63 µm and 355 µm to 500 µm between the four soil samples. The fractions of the smaller particle sizes were correlated with organic matter content in the soil samples (see OM in Table 1), except for Soil 4.

Bulk density of soils may be another influencing factor on THz attenuation. Therefore, bulk density was measured with a wedge sample holder and a measuring cup. Results of 10 repetitions for each sample are summarized in Table 2.

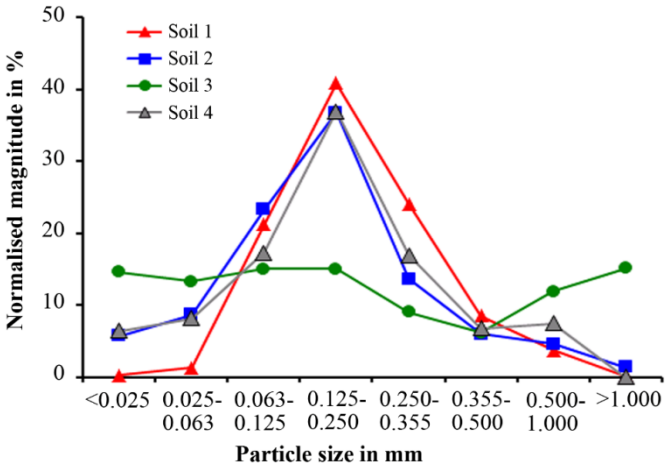

Figure 1. Particle size distribution of the four soil samples.

Table 2. Bulk densities of the four soil samples.

Container	Density in g/cm³							
	Soil 1		Soil 2		Soil 3		Soil 4	
Wedge	1.7879	±0.0430	1.2860	±0.0315	1.0123	±0.0371	1.0511	±0.0241
Measuring cup	1.7937	±0.0274	1.3987	±0.0242	1.0031	±0.0151	1.0551	±0.0160

2.2 Transmission measurements at 1.6 and 2.5 THz

For the evaluation of transmission greater than 1 THz, an optically pumped molecular gas laser was used. This laser operates at discrete frequencies between 0.7 THz and 5.2 THz, and it has an output power of up to 10 mW. The transmission measurements were done at frequencies of 1.627 THz and 2.523 THz. The measurements showed no sufficient transmission of THz radiation at this frequency range.

2.3 THz setup for determining the absorption coefficient

THz frequencies from 340 GHz to 360 GHz were generated with an yttrium iron garnet (YIG)-oscillator operating at 11–12 GHz as fundamental source. Multiplier diodes were used to upconvert the signal of the YIG oscillator (VDI-TX-S119, Virginia Diodes, Inc., Charlottesville, VA, USA). The power was emitted from a horn antenna with a Gaussian beam shape of 9° divergence at approximately 1 mW output power. The beam was optically modulated with a chopper wheel with frequencies ranging from 23 Hz to 27 Hz and then amplified by a lock-in amplifier. A lens made of TPX® was used to focus the emitted power on the sample [Figure 2(a,b)]. A second lens was used to collect the power transmitted through the soil sample and to focus it onto a Golay cell detector (Tydex, St. Peterburg, Russia). The transmitted power was amplified with a lock-in amplifier (SR850, Stanford Research Systems, Inc., Sunnyvale, CA, USA), which in turn

was referenced to the optical chopper. Data acquisition was done automatically with a computer.

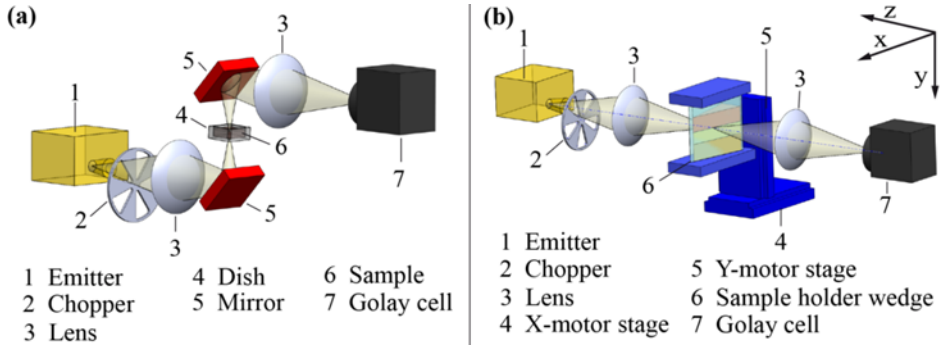

Figure 2. (a) Setup for the transmission measurement using the sample dish (approach 1). (b) Transmission measurement using the wedge sample holder (approach 2).

Two setups were tested for exposing the samples to the THz radiation. In the first setup, the soil was placed in a Teflon sample dish. After putting the soil into the dish, the sample was carefully compacted, and its thickness was measured [Figure 2(a)]. The second setup employed a wedge sample holder of 6 cm height (y-direction), 6 cm length (x-direction) and of varying width from 0 cm to 2 cm (z-direction). The walls of the wedge sample holder were made of 2 mm high density polyethylene (HDPE) plates. This second setup was designed to reduce the complexity in determining the soil absorption coefficient. Based on the constant thickness of the walls and their plain surfaces absorption and refection coefficients of the wedge sample holder were independent from the position of the THz beam as shown in Figure 3. This was also true for the interface to the soil sample, because the diameter of the divergent beam was much larger than the soil particles.

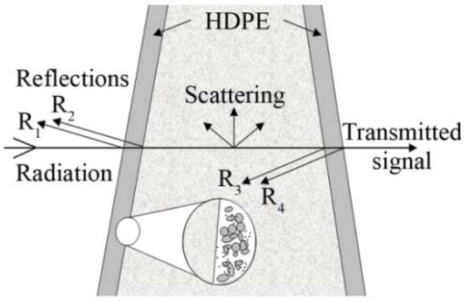

Figure 3. Wedge sample holder. The reflection coefficient of the surface to wall material interface is approximately constant by design.

The transmitted power received by the Golay cell detector, Pt, is given by:

$$P_t(d) = P_e T_{atm} T_1 T_2 e^{-\alpha d} \quad (1)$$

$$\frac{P_t(d)}{P_e} = T_{atm} T_1 T_2 e^{-\alpha d} \tag{2}$$

where P_e is the power emitted from the source, T_{atm} is the atmospheric transmission, T_1, T_2 are the transmission of the HDPE windows of the sample holder, d is the thickness of the soil at the measuring position and α is the absorption coefficient of the soil. The transmitted electromagnetic wave must pass all materials in series and therefore the transmission coefficients must be multiplied as given in Equation (1).

From this the absorption coefficient is derived as:

$$\ln\left(\frac{P_t(d)}{P_e}\right) = \alpha d - \ln(T_{atm} T_1 T_2) \tag{3}$$

The atmospheric transmission and the transmission of the HDPE windows are constant and appear as an offset to the Equation (3). Equation (3) explains why linear regression can be used to determine the absorption coefficient and why the unknown reflection-coefficients do not affect the soil dependent absorption coefficient. The soil samples were compacted by knocking the wedge on a table. The soil density in the wedge varied from high to low from the bottom to the top of the wedge, caused by the soil's own weight. The same protocol was applied to all soil samples. The wedge was scanned with a xy-positioning stage ([Figure 2(b)]. The increment in x- and y-direction was set to 1 mm while the focus of the beam was adjusted to the wedge mid-position in the z-direction. Lock-in integration time at each grid point of the xy-array was 1 s. By this we obtained an image of 60 columns and 60 rows summing up to 360 pixels.

2.4 Determination of absorption coefficients

The absorption coefficients were derived from the wedge-scanning approach (second setup) by linear regression. Only data from the mid-region of the image were used. Data from the boarders were omitted due to distortion effects at the edges. Every column of data, collected along the y-direction, corresponded to a known, constant thickness of the sample. The sample thickness was 2 cm at the x-position (6 cm) for the wedge used, and so the absorption coefficient (in decibels per millimeter) needed to be multiplied by a factor of three. For regression analysis, data were averaged along the columns and then related to the respective sample thicknesses [Equation (4)]. Only those columns were used that have more than 20 values exceeding the least significant bit of the analog to digital converter. Linear regression models were fitted to the data by means of ordinary least squares. The slope of the regression line is a direct estimate of the absorption coefficient as expressed in decibels per millimeter. This can be explained as follows:

(a) No offset zeroing was needed for the absorption of the HDPE wedge wall material;

(b) No emitter amplitude adjustment was required (as long as the output power was stable during at least one scan);

(c) The absorption coefficient was given by the slope of the linear regression, thereby making it independent of the sample thickness. Therefore, the x-position did not need to be adjusted for the measurement series.

The following equations were used:

$$mean(x) = \frac{\sum_{i=1}^{n} I(x; y_i)}{n} \tag{4}$$

$$S(x) = 10 \cdot \log\left[mean\left(x\right)\right] \tag{5}$$

$$S(x) = offset + \alpha x / 3 \tag{6}$$

$$d = x / 3 \tag{7}$$

where I(*x;y)* is the signal intensity at the xy-position in the image from the lock-in amplifier output, and *S(x)* are the mean values along each column (y_i) on a decibel scale. At each day of measurement, temperature and humidity were recorded.

3 Results and discussion

The analysis with frequencies of 1.627 THz and 2.523 THz show no transmission of detectable intensities. This setup had no options for separating scattering effects from damping effects, but both parameters could be high, because of the manifold composition of soil samples.

3.1 Evaluation of different experimental setups

The small soil sample area in the 25 mm × 25 mm dish caused poor repeatability among the reproductions of sample preparations (data not shown). The main reasons for the poor repeatability included variations in the soil sample, an insufficient thickness preparation procedure with respect to the stamp and variations in the emitter power on different days. However, some differences for the transmitted signal intensity among the soil samples were detectable. The second approach, which made use of the wedge sample holder, was more efficient because all sample thicknesses were measured in one scan and the influence of the soil density was averaged over the y-direction. Therefore, the dish setup was only used with a 75 mm × 75 mm dish to image buried test objects in the soil.

Theoretically, the wedge sample holder should have provided the advantage that no position adjustments or calibrations were needed to determine the absorption coefficients. However, the usability of this setup was evaluated. Therefore, the empty wedge

sample holder was measured at three frequencies in order to estimate its influence on the transmitted signal intensity. It turned out that an undistorted region in the center of the sample holder was visible at all three frequencies making it suitable for further application.

3.2 Absorption coefficients

As listed in Table 3, nearly equal frequencies were used to measure the local transmitted signal intensity. The resulting images, shown in Figure 4, indicate why averaging along the y-direction was required. One can observe strong local signal variations. Thus, a single point measurement could be misleading and would not be adequate for characterizing these difficult soil samples.

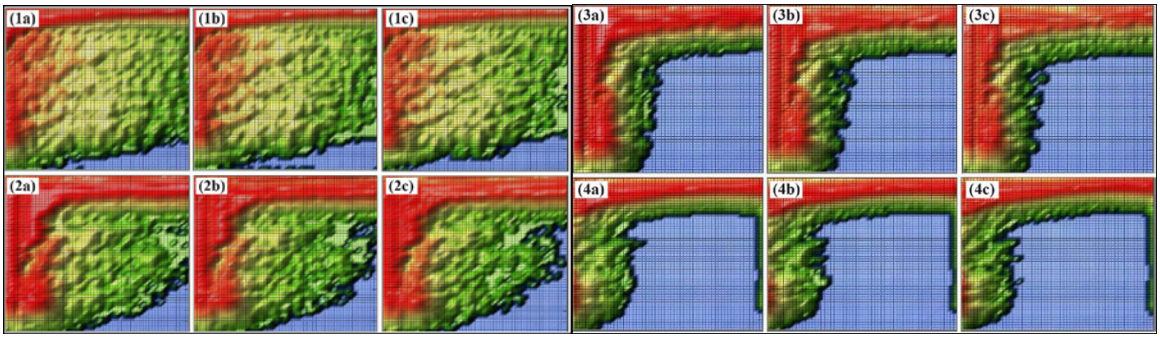

Figure 4. (1a, 1b and 1c) Transmission images of Soil 1 at 340 GHz, 351 GHz and 360 GHz. (2a, 2b and 2c) Transmission images of Soil 2 at 340 GHz, 351 GHz and 360 GHz. (3a, 3b and 3c) Transmission images of Soil 3 at 340 GHz, 351 GHz and 360 GHz. (4a, 4b and 4c) Transmission images of Soil 4 at 340 GHz, 351 GHz and 360 GHz. All images are in arbitrary units in rainbow colors from red (high intensity) to blue (low intensity). Each square in the images is equal to one square millimeter and the image size is 60 mm by 60 mm.

The blue regions in the acquired images (Figure 4) represent a measured intensity of zero, meaning that the signal intensity was below the detection limit of the setup in this configuration. Because zero cannot be a permissible value on the decibel scale, all zeros were ignored in the consecutive analysis. The mean value and standard deviation for each column are plotted in Figure 5. Every plot was adjusted with an additional offset to separate the graphs and to improve visibility. Lengths of plots vary in Figure 5 for the different soil samples, because only those signal amplitudes were included that are based on more than 20 nonzero measurements in a column.

Figure 5 shows representative plots of the signal absorption for the four soil samples measured with three different frequencies. The results varied with the size and position of the used inner xy-array of the data points. Therefore, the estimated absorption coefficients are inaccurate as shown by the repeated measurements at 340 GHz in Table 3.

Thus they should not be used for precise predictions. However, the differences between the absorption coefficients were obvious.

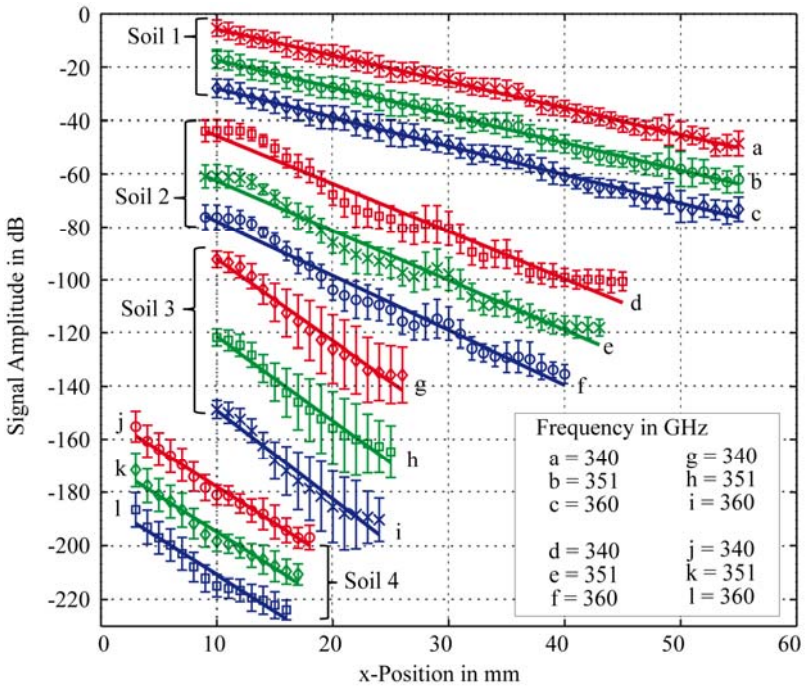

Figure 5. Plots of transmission signal amplitude versus x-position of the wedge sample holder for the four soil samples at three different frequencies (the x position is related to the soil thickness by d = x/3). All plots are adjusted with an additional offset for better visibility.

Table 3. Absorption coefficient estimation with linear regression.

Freq GHz	Soil 1		Soil 2		Soil 3		Soil 4	
	D dB mm^{-1}	R^2	D dB mm^{-1}	R^2	D dB mm^{-1}	R^2	D dB mm^{-1}	R^2
340	−0.98 ± 0.02	0.996	−1.80 ± 0.124	0.961	−3.08 ± 0.271	0.975	−2.76 ± 0.21	0.983
351	−1.03 ± 0.022	0.995	−1.88 ± 0.115	0.971	−3.18 ± 0.278	0.977	−2.72 ± 0.291	0.969
360	−1.07 ± 0.023	0.995	−2.05 ± 0.132	0.971	−3.36 ± 0.377	0.966	−2.74 ± 0.4	0.949
340	−1.02 ± 0.031	0.991	−1.42 ± 0.088	0.981	−3.82 ± 0.284	0.996		

These results demonstrated the feasibility of discriminating soils by THz radiation. With a more sensitive and stable setup as well as a more reproducible sample preparation, quantitative measurements may be possible. A well defined calibration protocol is required. With respect to the error of estimate of the absorption coefficient (Table 3), higher absorption can be assumed with higher measuring frequencies for the first three soil samples (Table 3). This rule is not applicable to the THz analysis of the fourth soil sample. We may conclude that spectral information in the THz region contains additional information about different absorption mechanisms. To verify this in further

experiments more stable measurements over a wider frequency range are required. The influence of water, carbon, nitrate and other soil ingredients needs to be analyzed in more detail. The amount of water and carbon increased in the same manner for the first three soil samples (Table 1). Therefore, the mechanism that dominates the absorption effect cannot be defined with this preparation. Moreover, the influence of the particle size distribution may be responsible for the different spectral behavior of the fourth soil sample. The first three soil samples had the same sequence for the value of the absorption coefficient and the amount of large and small particles, and the sequences were inversed for the middle particle size. Soil 4 had the same amount of medium size particle as Soil 2, but proportions of small and large particles were different (Figure 1). The water content of Soil 3 and Soil 4 was nearly identical. Thus water content cannot have caused differences in the spectral behavior.

Bulk density (Table 2) of the four soil samples had little effect on the signal absorption. This can be concluded from the fact that Soil 1 had the highest density but the lowest absorption. Therefore, the absorption is dominated by the conductivity and dielectric properties of the soil constitutes and not by the bulk density.

A time independent measurement in the wedge will allow for better quantitative measurements in future experiments. This new approach is demonstrated in Figure 6(a) with the first three soil samples. The beam divergence caused a triangle overlay in the signal between the soil samples. Therefore, a larger wedge sample holder or a smaller beam divergence is required.

3.3 Imaging

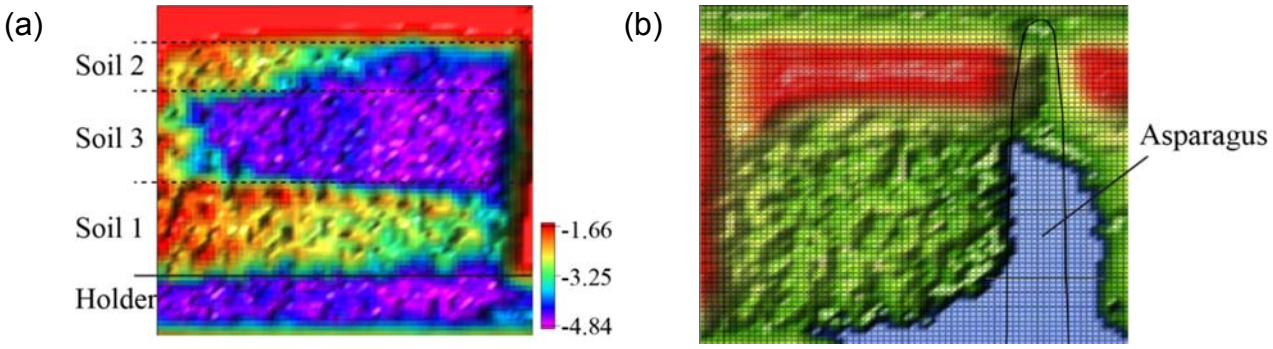

Figure 6. (a) The transmission image of the first three soil samples with a logarithmic scale in arbitrary units. From top to bottom: Soil 2, Soil 3 and Soil 1. The image size is 60 mm by 60 mm. (b) The transmission image of the wedge sample holder filled with Soil 1 and asparagus. The image is in arbitrary units in rainbow colors from red, high intensity, to blue, low intensity. The image size is 60 mm by 60 mm.

The ability to focus the THz beam has the advantage of a high spatial resolution of localized absorption causes, thus, enabling imaging. Visualizing with high spatial resolution in terms of images is an important application for a sensor setup. The potential of

this visualization method is shown in Figure 6(a) by an image of three different soil samples in the wedge sample holder. The high water content of vegetables caused signal absorption for the transmitted THz wave. Figure 6(b) shows the absorption image of the asparagus prepared in the wedge sample holder.

4 Conclusions

In this study, the feasibility of the THz imaging of soils was demonstrated. The local parameter variations of different soil samples were detectable. In addition, it was possible to differentiate soil samples by their absorption coefficients (see Table 3 and Figure 5). Soils with higher organic matter have higher absorption coefficients. Using wavelengths of less than 1 mm, a positive correlation was observed between absorption and the particle size fraction of 0.5 mm to 1 mm. However, the alignment of an optical THz system is difficult. For example, stationary waves and scattered emissions have to be avoided. The setup presented here is far from being optimum. Nevertheless, the practical outcome of this study is the establishment of an approach to perform soil analyses by THz radiation. With a more sensitive detector and better calibration, it may be possible to make a quantitative assessment of soil parameters. Furthermore, analysis of spectral information should help to separate the information overlay of different soil parameters.

Measurements need to be more accurate to establish the absorption coefficient in a quantitative manner. To solve accuracy issues, two options should be investigated in the future: First, a THz setup with more powerful signal sources, larger lenses and more sensitive detectors, such as a heterodyne amplifier should be employed. Second, measurements with a known and unknown soil samples should be carried out in tandem to improve prediction. This requires a larger wedge sample holder and smaller beam divergence.

References

DWORAK, V., AUGUSTIN, S., GEBBERS, R. 2011. Application of Terahertz Radiation to Soil Measurements: Initial Results. Sensors 11, 9973-9988.

MOUAZEN, A.M., DE BAERDEMAEKER, J., RAMON, H. 2005. Towards development of on-line soil moisture content sensor using a fibre-type NIR spectrophotometer. Soil Till. Res. 80, 171-183.

COLLINS, M.E. 2008. History of Ground-Penetrating Radar Applications in Agriculure. In Handbook of Agricultural Geophysics; Allred, B.J., Daniels, J.J., Ehsani, M.R., Eds.; CRC Press, Taylor and Francis Group: New York, NY, USA; pp 45-55.

BAGHDADI, N., AUBERT, M., CERDAN, O., FRANCHISTEGUY, L., VIEL, C., MARTIN, E., ZRIBI, M., DESPRATS, J.F. 2007. Operational mapping of soil moisture using synthetic aperture radar data: Application to the Touch Basin (France). Sensors 7, 2458-2483.

Spatial modelling of soil attributes using a combination of in-situ proximal sensing methods

P. Roudier*, C. Hedley, C. Ross

Landcare Research – Manaaki Whenua, Private Bag 11052, Manawatu Mail Centre, Palmerston North 4442, New Zealand.
**E-mail: roudierp@landcareresearch.co.nz*

Abstract

In this study visible near infra-red spectroscopy (VNIR) was trialled as a non-destructive and cost-efficient field method to estimate and map soil carbon stocks in an arable field. Volumetric total soil organic carbon (SOC) estimates (to 0.3 m) at one hundred positions have been combined with electromagnetic (EM) survey data to develop a volumetric SOC mapping method. Volumetric SOC was estimated at each sampling site by (1) laboratory analysis and (2) chemometric processing of the VNIR soil spectra collected from the core in the field, using partial least square regression (PLSR). SOC estimates were then combined with the EM and terrain attribute layers to calibrate a ten-fold cross-validated random forest regression model.

Keywords: digital soil mapping, carbon stocks, in-situ spectroscopy.

1 Introduction

The emergence of proximal and remote sensing technologies provides opportunities to develop refined methods for spatial modelling of soil attributes. This aims to improve on conventional methods which are time consuming and expensive. In this study, we estimate and map volumetric soil organic carbon (SOC) stocks at paddock scale using a combination of proximal sensing technologies: VNIR (visible – near infrared) spectroscopy and EM (electromagnetic) mapping. Spectroscopy provides a fast and cost-effective way to measure volumetric SOC from soil cores (Morgan et al., 2009). VNIR estimates are combined with EM and terrain attributes to map SOC stocks.

This study compares two digital soil mapping strategies: the first method uses conventional laboratory analysis for all collected samples, while the second one uses VNIR spectroscopy to reduce the number of required laboratory analyses; hence improving the cost-efficiency of the method. Point estimates are combined with EM and terrain covariates using spatial modelling to map soil attributes.

2 Material and methods

2.1 Study site

The field research site is a 71.1 ha irrigated maize *(Zea mays)* field in the Manawatu Sand Country, New Zealand. The topography is a sand plain, surrounded by low sand dunes, with a short range micro-relief of small crescent-shaped dunes. Soils are variably influenced by a high and fluctuating water table (Hedley et al, 2012).

2.2 Soil covariates

An EM mapping system was used to quantify soil variability. Elevation data collected by the EM survey has been used to create a 5-m resolution digital elevation model (DEM), from which a suite of terrain covariates has been derived (Figure 1). 100 positions were selected for soil sampling by stratifying the EM38 dataset. Soil cores were collected to 30-cm depth, and scanned in the field at 1-cm intervals using an ASD FieldSpec3 spectrometer. The cores were then collected for lab analysis.

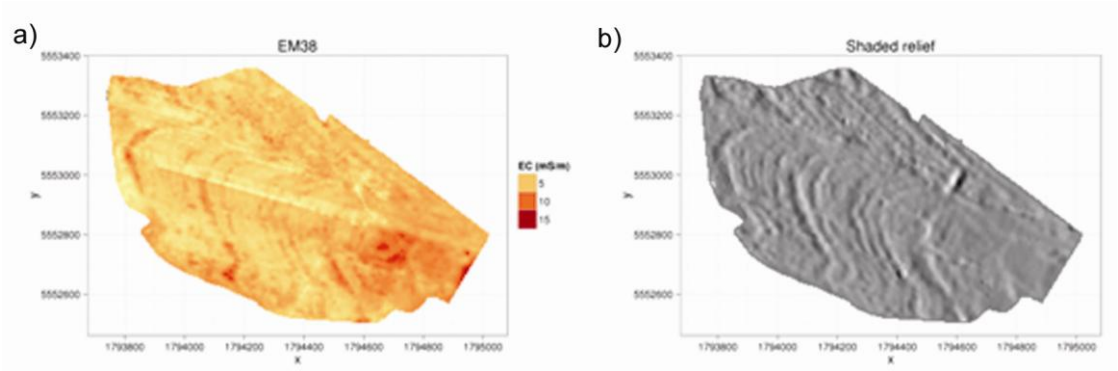

Figure 1. (a) EM38 map interpolated from the EM survey of the study site. (b) Shaded relief map of the DEM derived from the RTK-DGPS data collected during the EM survey.

2.3 Spectroscopy

Partial least square regression (PLSR) modelling was used to predict volumetric SOC from the VNIR field spectra. The influence of the size of the calibration set on the performance of SOC assessment has been studied for 10 different calibration set sizes (10% to 100%). Each calibration set has been determined using the Kennard-Stone algorithm (Kennard and Stone, 1969).

2.4 Spatial modeling

Mapping of SOC has been carried out for each depth interval using random forest regression. SOC has been modelled between 0 and 0.3 m from EM and DEM-derived covariates, because SOC is related to texture and microtopography. The lab-based approach has 3 depth intervals (10-cm slices). The VNIR method allows SOC to be estimated every centimetre, resulting in 30 depth intervals. In order to be able to improve

the robustness of the model and derive uncertainty information, a cross-validation procedure has been implemented (Ließ et al., 2012).

3 Results

3.1 SOC prediction

PLSR models return a cross-validated $RMSEP_{PLS}$ < 6 T/ha when using 90% samples in the calibration set. Models using between 40 and 80% of the dataset in the calibration set return a cross-validated $RMSEP_{PLS}$ < 7 T/ha. A calibration set using 30% or less of the samples for calibration, returns a cross-validated $RMSEP_{PLS}$ < 8 T/ha (Figure 2).

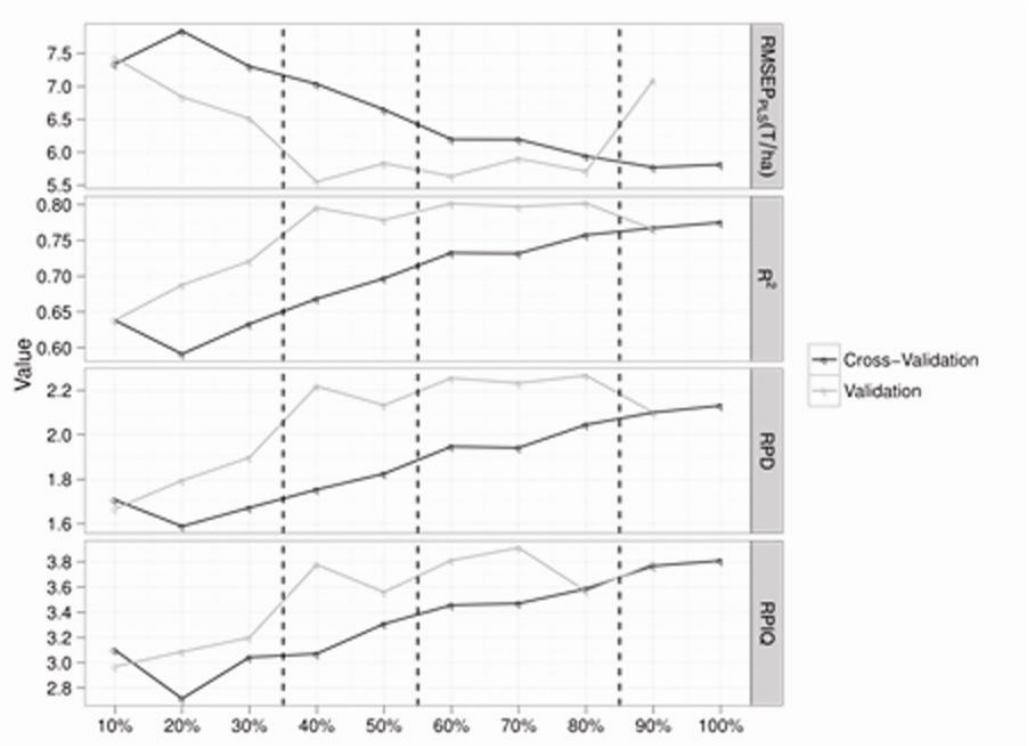

Figure 2. Evolution of the performance indicators for the PLS regression with the relative size of the calibration set. The black line shows results for the ten-fold cross-validation calibration, while grey line shows results on the validation set.

3.2 Spatial modeling

Spatial modelling results (Figure 3) suggest the performance of the digital soil mapping procedure is affected by the number of samples used by the PLSR calibration, and consequently by the overall performance of the PLSR. However, this effect seems limited. The best results are obtained by the lab-based approach ($RMSEP_{RF}$ of 11.88 T/ha), while the $RMSEP_{RF}$ of the VNIR-based approach ranges from 14.01 to 18.66 T/ha depending on the size of the PLSR calibration set (100% and 20% respectively in this example). This was expected as field VNIR estimation of SOC adds a supplementary source of uncertainty. However, a systematic over-estimation can be observed on the

VNIR predictions. This offset is due to the Kennard-Stone sampling method, which over-represents the 0-10 cm horizon in the successive calibration sets, because this is the horizon showing the most variability.

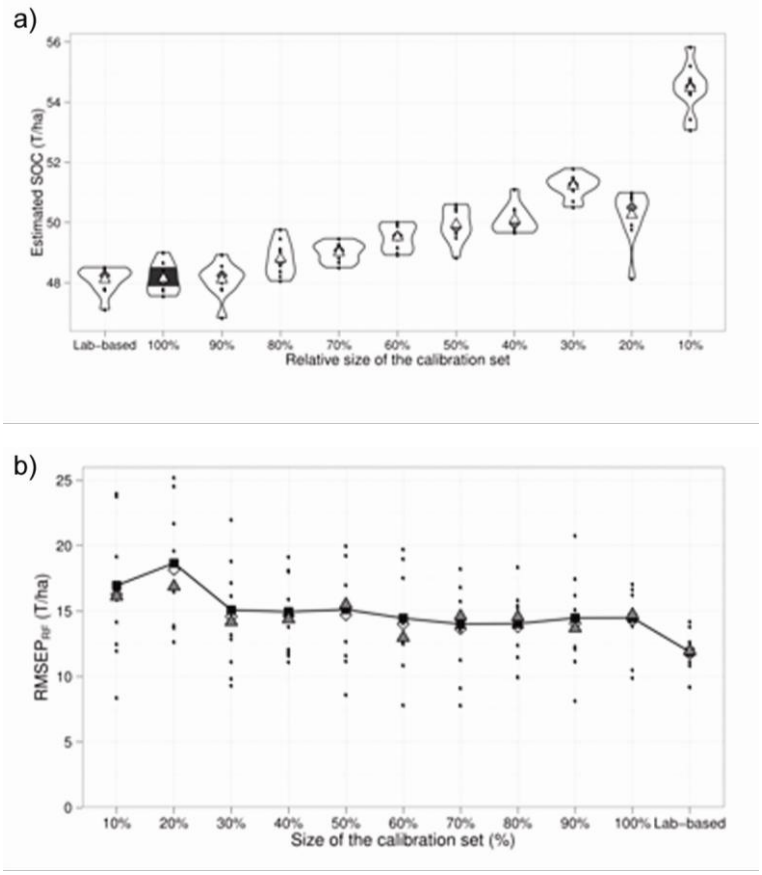

Figure 3. Evolution of the performance of the SOC mapping with the relative size of the calibration set. The circles represent the $RMSEP_{RF}$ (resp. SOC) values for each of the ten simulations. The grey triangles and white diamonds represent the median and mean of the $RMSEP_{RF}$ (resp. SOC) values for each of the ten simulations.(a) Estimated SOC for the study site. (b) Uncertainty associated with the predictions.

4 Discussion

In-field spectroscopy reduces the need for lab analysis, therefore improving the cost and time efficiency of digital soil mapping. The ability to take many spectra in the field for SOC prediction, in combination with on-the-go proximal sensing technologies such as EM, provides a method to investigate spatial variability at high resolution (5 m in this study). Additionally, the core scanning procedure provides a direct measurement of soil carbon at 1-cm intervals, improving depth resolution, and detecting subtle but important changes that may occur at each centimetre of soil profile.

In order to keep the number of lab analyses to a minimum, we are developing a national spectral library dedicated to soil attribute prediction from air-dried soil samples. Spiking

this national spectral library with a limited number of local samples could help keep the costs and uncertainties to a minimum (Sankey et al, 2008).

5 Conclusions

The PLS results from the cross-validation process supports the possibility to predict directly volumetric SOC from VNIR spectra collected on fresh cores: cross-validated RMSEP values < 8 T/ha were achieved. These VNIR estimates have then been combined with EM and DEM derivatives. The spatial regression modelling step introduced larger uncertainties than those of VNIR-based predictions of volumetric SOC at the sampling positions.

References

HEDLEY, C. B., ROUDIER, P., YULE, I. J., EKANAYAKE, J., BRADBURY, S. 2013. Soil water status and water table depth modelling using electromagnetic surveys for precision irrigation scheduling. Geoderma, **199** 22-29.

LIEß, M., GLASER, B., HUWE, B. 2012. Uncertainty in the spatial prediction of soil texture: Comparison of regression tree and Random Forest models. Geoderma, **170** 70-79.

KENNARD, R.W., STONE, L.A. 1969. Computer aided design of experiments. Technometrics, **11** 137–148.

MORGAN, C. L., WAISER, T. H., BROWN, D. J., HALLMARK, C. T. 2009. Simulated in situ characterization of soil organic and inorganic carbon with visible near-infrared diffuse reflectance spectroscopy. Geoderma, **151**(3) 249-256.

SANKEY, J.B., BROWN, D.J., BERNARD, M.L., LAWRENCE, R.L. 2008. Comparing local vs. global visible and near-infrared (VisNIR) diffuse reflectance spectroscopy (DRS) calibrations for the prediction of soil clay, organic C and inorganic C. Geoderma, **148**(2) 149-158.

Use of a new electrostatic resistivity-meter - first results

M. Dabas[1*], A. Tabbagh[2], S. Flageul[2]

[1]*Géocarta SA, 2 galerie Vivienne, 75002 Paris, France*
[2]*UMR 7619 Sisyphe, UPMC/CNRS, case 105, 4 place Jussieu, 75252 Paris Cedex05, France*
[*]*E-mail: dabas@gecarta.net*

Abstract

We present in this paper a new type of resistivity-meter for measuring the apparent Electrical Resistivity (ERa) of soils in Agriculture. The use of such instruments and especially in a continuous mode overcomes some difficulties encountered in the classical galvanic methods like the one related to contact resistance. A careful design of both electrodes (capacitive plates) and electronics open new possibilities: this resistivity-meter is able both to measure the frequency-dependence of ERa and also makes the separation of in-phase and out of phase components of ERa. Three examples are displayed in civil engineering, -agriculture and archaeological mapping.

Keywords: electrical resistivity, galvanic coupling, capacitive coupling, spectral resistivity, compaction, water content.

1 Introduction

Measurement of Apparent Electrical Resistivity (ERa) is known to be one of the most valuable parameter for the estimation of the soil spatial variability in Agriculture and is considered to be the entrance gate for Precision Agriculture together with parameters related to the plant growth. In geophysics, measurement of ERa by resistivity-meters with galvanic coupling with ground surface (often quoted Direct Current Methods, -DC-) or measurement of apparent Electrical Conductivity (ECa) by Electromagnetic Induction instruments (EMI) with no contact with ground surface is widespread. Both instrumentations have its own advantages and drawbacks: for example, the use of EMI enables an easy and continuous recording while moving over the profiles (even if the sensor should be as low as possible to ensure the highest signal/noise ratio). Use of DC instruments enable several depths of investigations and an easy calibration of measurements (Dabas and Tabbagh, 2003; Gebbers et al., 2009). Drawbacks of EMI are known: calibration difficult to perform, sensitivity to metal and generally speaking to any EM Interference, investigation depth not as precise as with DC instruments and finally a very low response over resistive areas. For DC instruments, the workload of deploying these instruments in the field is high, and the tolerance to contact resistance can be a problem, specially with towed systems like VERIS or even with ARP© system with its carefully designed resistivity-meter (Dabas, 2009).

Taking into account these drawbacks (workload - high contact resistance), we have decided to develop since a long time new instruments for measuring the ER by using electrostatic poles in the air above the ground that can be considered as capacitively coupled electrodes (Grard and Tabbagh, 1991; Panissod et al., 1998). The first applications of these instruments were for archaeological investigations over tarmac areas and inside buildings (Dabs et al., 2000).

2 Instrument design and laboratory test

The new developed system is named SECR-1 for Spectral Electrostatic Complex Resistivity-meter (Flageul et al., 2013). It is a multi-frequency system (2mHz – 100kHz) representing a very low input capacitance and a high phase sensitivity (1 milliradian).

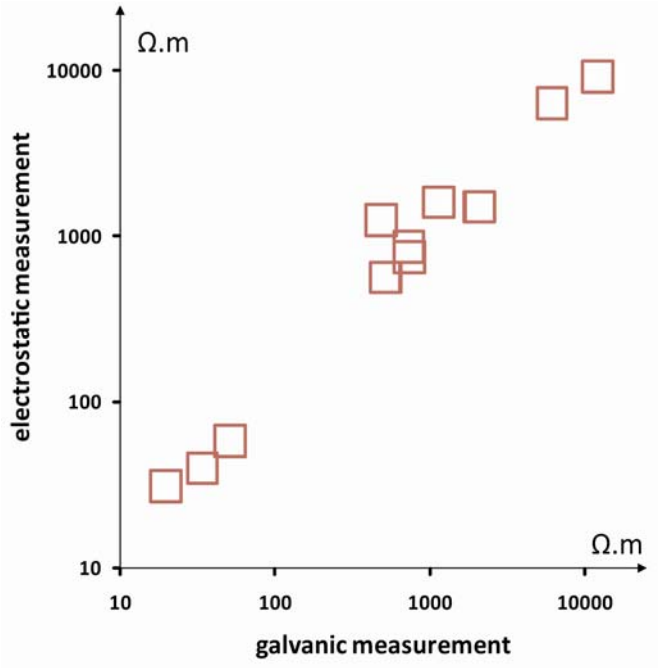

Figure 1. Correlation of electrical resistivities measured by electrostatic measurements (SECR-1) and with a standard DC resistivity-meter.

The main difficulty in the application of this method lies in the choice of the most suitable frequency; this results in the need for a compromise between three constraints:

1. The frequency *f* must be sufficiently high to ensure that the impedance of each pole is sufficiently low.
2. If the electrical conductivity σ is to be measured, the condition $\sigma >> \varepsilon\omega$ ($\omega = 2\pi f$ being the angular frequency and ε the dielectric permittivity) must be respected. It is however possible to determine both σ and ε, by measuring both the in-phase and the quadrature (out of phase) components of the voltage (Tabbagh *et al.* 1993).

3. In order to avoid induction effects that would drastically reduce the depth to which materials could be measured (Benderitter *et al.,* 1994; Tabbagh and Panissod, 2000) the induction number $IN=\sigma\mu\omega L^2$ must verify $IN<<1$, μ being the magnetic permeability and L the characteristic length of the instrument.

The poles are located in the air, outside the medium under study, and generate the electric field. They constitute an open capacitor. The voltage is measured between a different set of poles.

Good agreement was observed between measurements using our multipole, and those made using galvanic contact resistivity measurements in which the electrode array accurately reproduced the pole geometry.

3 Field experiments

SECR-1 was tested for different applications prior to precision agriculture: civil engineering and archaeological mapping. In the first application, a small electrostatic hexapole (maximum distance 25cm between poles, see figure 2) is located over the different stones of historical monuments in order to characterize their water content.

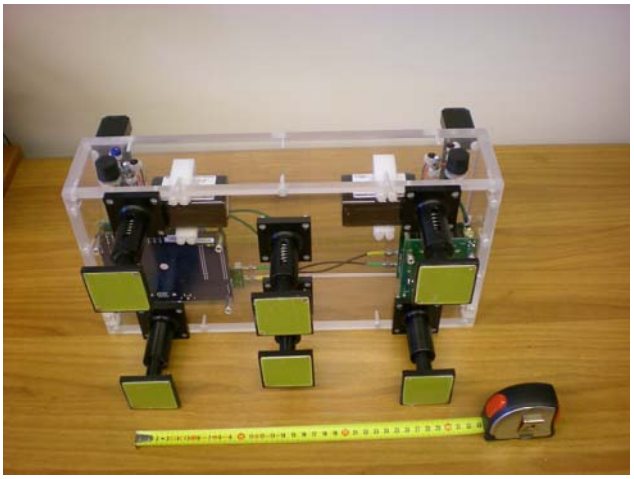

Figure2. Photograph of the SECR-1 developed for small scale studies

In a second application, the system was used for the characterization of soil compaction (delta clods) in a luvisoil. The ERa were measured at 4 different period of the year with 2 quadrupoles. The results shown in figure 3 indicate that (1) the large quadripole is able to detect the most strongly compacted zones and (2) this detection is facilitated when the soil is in its driest state (the macro-pores are filled with air, blue curve - July). From all of the collected data, the compact clods appear to be more conductive than the surrounding loosened soil, where the water content is also reduced in accordance with the greater size of pores. Due to its lesser capability for deep soundings, the short quadripole did not allow the clods to be clearly delineated.

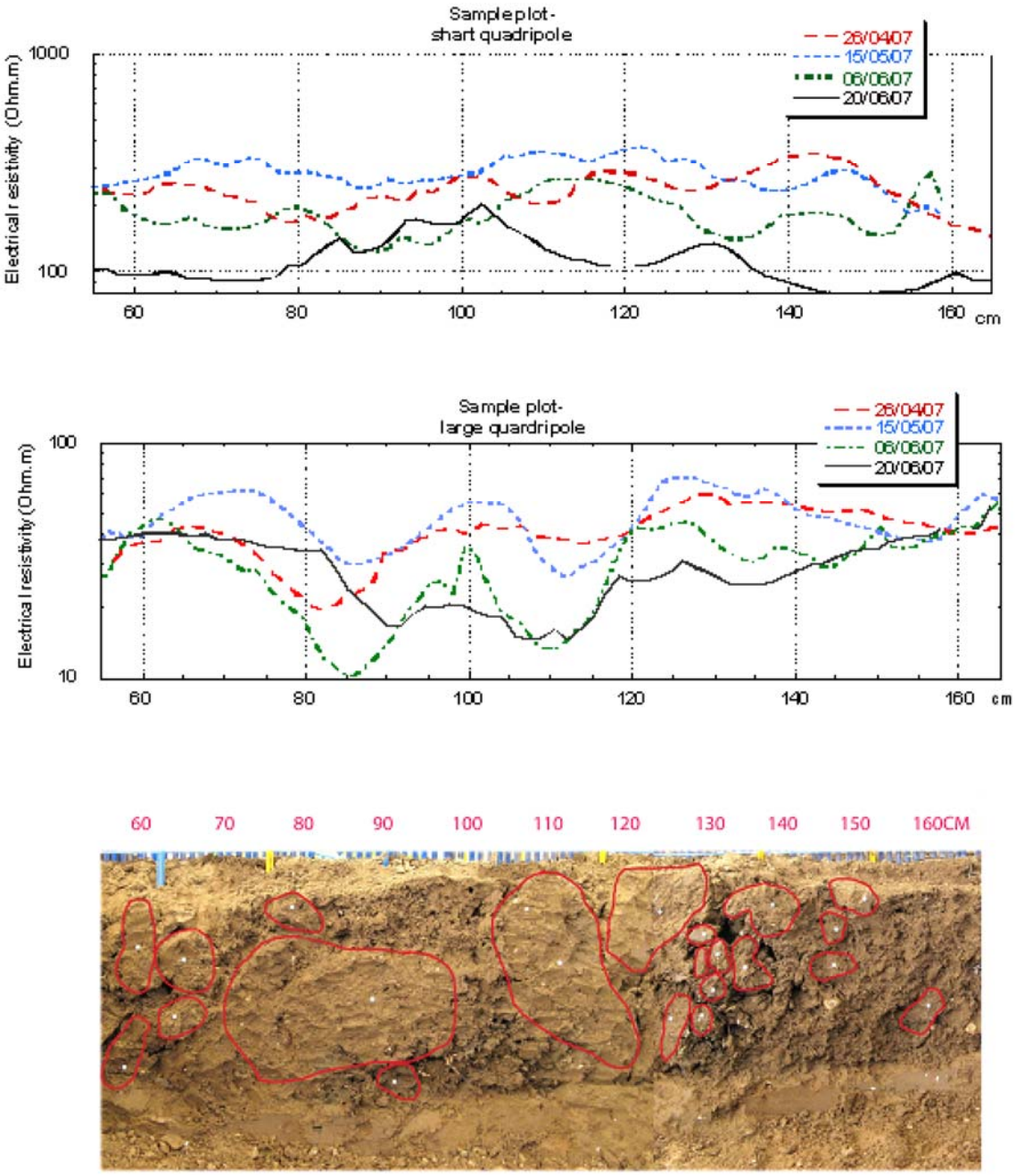

Figure 3. Apparent Electrical resistivities measured by SECR-1 (up: small quadripole ,down: large quadripole) at 4 different periods over a luvisoil. Photo of the trench made after measurements showing the clods (highlighted in red).

The last experiment was for detection of buried archaeological remains. This test is the closest to what is done in Precision Agriculture. The spatial variability which was depicted by the two electrostatic dipoles was found to be in very good agreement to the one obtained in a second step with a DC resistivity-meter (see Flageul et al., 2013).

Figure 4. SECR-1 with two dipoles for soil mapping at large scale

4 Conclusions

We have shown that it was possible to make measurements of ERa without galvanic electrodes over the soil using the new resistivity-meter specifically designed for these measurements. This opens new opportunities to measure ERa in difficult conditions when the electrical contact resistance is high (>100Kohm). This system has to be hardened to be used in industrial applications and research has to be undertaken to understand the usefulness of complex spectral measurements in agriculture.

References

BENDERITTER, Y., JOLIVET, A., MOUNIR, A., TABBAGH, A. 1994. Application of the electrostatic quadripole to sounding in the hectometric range of depth. Journal of Applied Geophysics*, 31,* 1-6.

DABAS, M., CAMERLYNCK, C. , PERE FREIXAS I CAMPS 2000. Simultaneous use of electrosatic quadrupole and GPR in urban context: investigation of the basement of the cathedral of Girona (Catalunya, Spain). Geophysics, 65-2, 526-532.

DABAS, M., TABBAGH A. 2003. A comparison of EMI and DC methods used in soil mapping-theoretical considerations for precision agriculture, p. 121-129, in: Precision Agriculture, ed. J. Stafford and A. Werner, Wageningen Academic Publishers, Muencheberg, 783p.

DABAS, M. 2009. Theory and practice of the new fast electrical imaging system ARP©, in: Seeing the Unseen, Geophysics and Landscape Archaeology, Campana and Piro eds., CRC Press, Taylor and Francis Group, 2009, p. 105-126.

FLAGEUL, S., DABAS M., THIESSON, J., REJIBA, F., TABBAGH, A. 2013. First in situ tests of a new electrostatic resistivity meter, Near Surface Geophysics, in press.

GRARD, R., TABBAGH, A. 1991. A mobile four-electrode array and its application to the electrical survey of planetary grounds at shallow depths. J.G.R 96, B-3, 4117-4123.

GEBBERS, R., LÜCK E., DABAS, M., DOMSCH, H. 2009. Comparison of instruments for geoelectrical soil mapping at the field scale, Near Surface Geophysics, 7, 179-190.

PANISSOD, C., DABAS, M., HESSE, A., JOLIVET, A., TABAGH A., TABBAGH J. 1998. Recent developments in shallow-depth electrical and electrostatic prospecting using mobile arrays, Geophysics, 63, 5, p. 1542-1550.

SOUFFACHÉ, B., COSENZA, P., FLAGEUL, S., PENCOLÉ, J.-P., SELADJI, S., TABBAGH, A. 2010. Electrostatic multipole for electrical resistivity measurements at decimetric scale. Journal of Applied Geophysics, 71-1, 6-12.

TABBAGH, A., HESSE, A. GRARD, R. 1993. Determination of electrical properties of the ground shallow depth with an electrostatic quadrupole: field trials on archaeological sites. Geophysical Prospecting*, 41-4,* 579-597.

TABBAGH, A., PANISSOD, C. 2000. 1D complete calculation for electrostatic soundings interpretation. Geophysical Prospecting*,* 48-3, 511-520.

Hydrostratigraphic analysis using electromagnetic induction data and a quasi-three-dimensional electrical conductivity imaging

J. Triantafilis[1*], F. A. Monteiro Santos[2]

[1]*Biosciences Building Store, University of New South Wales (UNSW), Faculty of Science Store, Lowy Cancer Research Centre C25, via gate 11 Botany Street, RANDWICK NSW 2052*
[2]*Centro de Geofísica da Universidade de Lisboa, 1749-016 Lisboa, Portugal*
[*]*E-mail: j.triantafilis@unsw.edu.au*

Abstract

Efforts are being made to improve water use efficiency in the irrigated areas of the Murray-Darling River Basin in order to deal with predicted rainfall decline in south eastern Australia and also reduce the incidence of secondary soil and water salinisation. The latter commonly occurs as a result of poor location of water storage reservoirs and conveyance infrastructure upon relic drainage channels and the subsequent interaction of deep draining waters from them with natural stores of salts (e.g. connate salts stored in geological sediments). This is the case in the irrigated area surrounding Bourke in the Darling River valley. In order to better understand and hence manage the Riverine plain upon which irrigation is undertaken, information is required about the spatial distribution of soil types and the stratigraphic features (e.g. alluvial sands interbedded in clay strata) which are capable of redistributing deep draining water. In previous research electromagnetic (EM) induction instruments, such as the root-zone measuring EM38, have been used to map the areal distribution of soil types and hydrological properties. This is similarly the case for the EM34, which has been used to map the spatial distribution of vadose-zone features and groundwater associated with hydrogeological units. However, describing the nexus of the soil and vadose zone has not been adequately investigated. One of the reasons is the lack of suitable software to jointly invert the apparent electrical conductivity (sigma-a) data collected by these types of EM instruments. The aim of this research is to demonstrate how a joint inversion of EM38 and EM34 sigma-a data collected in an irrigated area around Bourke, and at a reconnaissance level, can be used to infer the areal distribution of soil types, physiographic and hydrogeological units by inputting EM38 and EM34 sigma-a data into a 1D laterally constrained algorithm for quasi three-dimensional conductivity imaging. We find that the 3-dimensional slices and 2-dimensional cross-sections of true electrical conductivity (sigma) model represent the known soil types, physiography and stratigraphy of the interbedded sands and clays which in places overly isolated outcrops of a Cretaceous marine mudstone, whereby the latter is thought to drive primary and point source secondary soil and water salinisation.

Proximal soil sensing for upscaling of soil biodiversity information in agricultural soils

M. Joschko[1*], R. Gebbers[2], M. Schirrmann[2], D. Barkusky[3], E. Kramer[4], J. Timmer[5,6]

[1]Leibniz-Zentrum für Agrarlandschaftsforschung (ZALF) e.V., Institut für Landschaftsbiogeochemie, Eberswalder Str. 84, 15374 Müncheberg, Germany
[2]Leibniz-Institut für Agrartechnik Potsdam-Bornim e.V., Abteilung Technik im Pflanzenbau, Max-Eyth-Allee 100, 14469 Potsdam, Germany
[3]Leibniz-Zentrum für Agrarlandschaftsforschung (ZALF) e.V, Forschungsstation, Eberswalder Str. 84, 15374 Müncheberg, Germany
[4]Hochschule für nachhaltige Entwicklung Eberswalde (FH), Friedrich-Ebert-Straße 28, 16225 Eberswalde, Germany
[5]Freiburger Zentrum für Datenanalyse und Modellbildung, Universität Freiburg, Eckerstr. 1, 79104 Freiburg, Germany
[6]Freiburg Institute for Advanced Studies (FRIAS), University of Freiburg, Albertstr. 19, 79104 Freiburg, Germany
[*]E-mail: mjoschko@zalf.de

Abstract

Information about spatial distribution of soil biota is needed for the design of adequate soil management strategies. Proximal soil sensing could become a suitable tool for upscaling soil biotic activity if close relationships between soil biota and soil sensor data could be ascertained. In a long-term field study on tilled soil, relationships between ECa (measured at plots and on-the-go) and earthworm abundances assessed during a decade were analysed. They indicate a close relationship between ECa and earthworm abundances especially under reduced tillage. The results confirm the suitability of proximal soil sensing for upscaling soil biodiversity information in agricultural soils.

Keywords: apparent electric conductivity, earthworm abundance, conventional tillage, reduced tillage, landscape.

1 Introduction

For the adequate management of agricultural soils, information about large scale patterns of soil biodiversity is essential. Proximal soil sensing could become a suitable tool for upscaling soil biotic activity if close relationships between soil biota and soil sensor data could be ascertained. For example, apparent electrical conductivity (ECa) might become important in assessing the spatial distribution of earthworm abundances at field scale because ECa can be coded to many soil parameters such as soil texture that have a direct influence on the earthworm habitat. This was recently shown by Valckx et al., 2009 and Joschko et al., 2010. Here, we report results from a study where we tested

the potential of ECa assessed by point measurements as well as Veris scanning for predicting earthworm abundances in reduced and conventional tilled sandy soils.

2 Materials and methods

Relationships between ECa and earthworm abundances were analyzed at 42 plots under reduced and conventional tillage management at a 74 ha field on sandy-loam soil in NE Germany. ECa was measured with a manually operated “4-Point-light” earth-resistivity meter using a Wenner electrode configuration and an electrode spacing of 0.5 m with four repititions in each plot (LGM Lippmann, Germany), in May 2005. Furthermore, the entire field was scanned for ECa with the geo-electrical sensor of the Veris Mobile Sensor platform (MSP, Veris Technologies, USA) using a tramline spacing of 18 m, in August 2012. For this study, the shallow ECa values were used (0.12 m) and were interpolated by block Kriging onto the 42 plots. Earthworm abundances were determined at the southern edge of each plot annually or biannually between May 1997 and September 2006, at a total of 14 occasions. Earthworms were sorted and counted by hand immediately after sampling one 0.5 m × 0.5 m × 0.2 m (width, length, depth) soil block. In the data analysis, Spearman correlation coefficients were calculated between ECa and mean earthworm abundances between 1997 and 2006 at each plot. We also took into account possible spatial variations in the relationship between ECa and earthworm abundance by applying spatial state-space analysis.

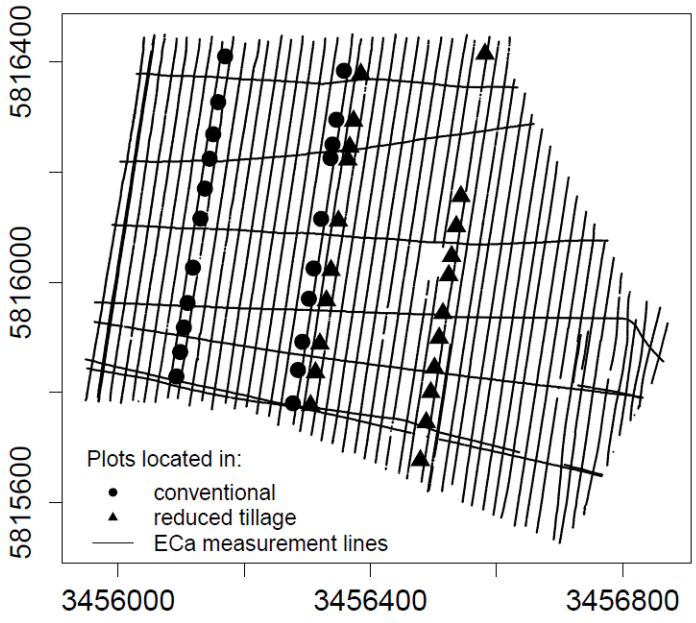

Figure 1. Lietzen observational study (since 1996) with 21 plots under conventional tillage (left) and 21 plots under reduced tillage (right).

Figure 2. The Veris Multi-Sensor platform used in this study.

3 Results

Significant global correlations between ECa and earthworm abundances were found especially under reduced tillage (precision cultivator, 15-80 cm tillage depth) using the "4-Point light" meter as well as the Mobile Sensor Platform (Fig. 3 and 4).

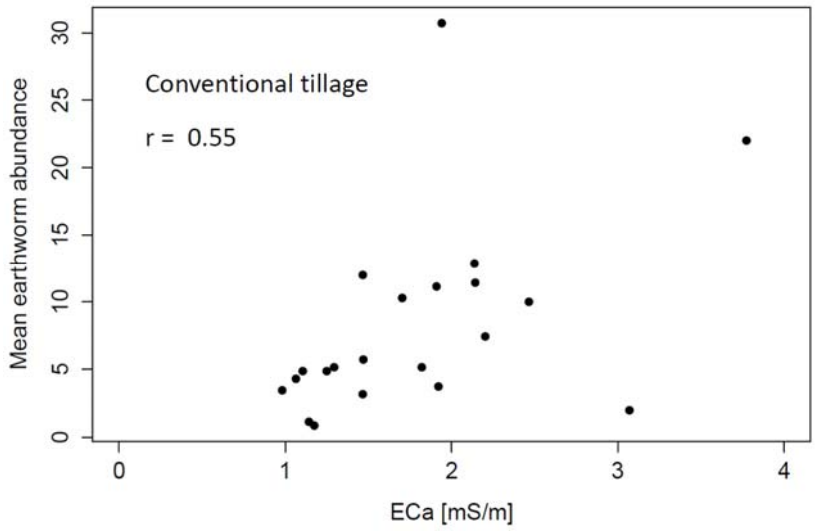

Figure 3. Relationship between ECa measured with the Veris Mobile Sensor, Platform and mean earthworm abundance [number*m^{-2}] between 1997 and 2006 at 21 locations under conventional tillage.

There was also a close correlation between "4-Point light" meter data and mobile sensor data, so that the on-the-go measurement error can be regarded as small. This confirms the stability of spatial EC pattern over time found in other studies which contributes to its usefulness in upscaling.

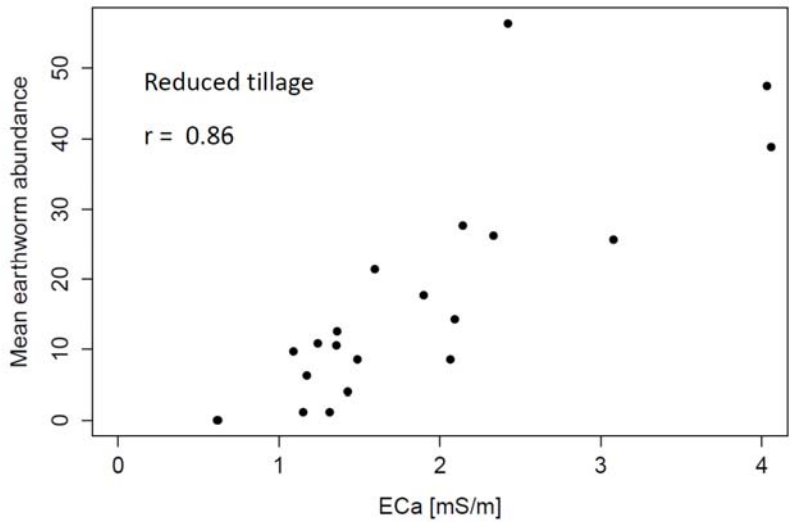

Figure 4. Relationship between ECa measured with the Veris Mobile Sensor, Platform and mean earthworm abundance [number*m^{-2}] between 1997 and 2006 at 21 locations under reduced tillage.

The application of local spatial statistics further improved the detection of quantitative relationships between ECa and earthworm abundances. Finally, it was found that in conventionally tilled soil larger uncertainties in the estimation of the earthworm abundances were present due to the weaker correlation between ECa and earthworms.

4 Conclusions

The results confirmed the applicability of ECa for soil biodiversity studies. The apparent electrical conductivity (ECa) is especially promising since it integrates information about soil texture and soil water content which are closely linked to the ecological requirements of soil biota. Proximal soil sensing might play a major role for upscaling to field scale spatial models of earthworm abundances using ECa as primary sensor information. However, other state variables that influence the earthworm habitat such as soil organic matter or soil pH should be assessed as well at best by using a sensor combination. Further research is needed to fully evaluate the potential of proximal soil sensing for predicting earthworm abundances and soil biota within fields.

Acknowledgements

The project was funded by the *Landwirtschaftliche Rentenbank* (Frankfurt/Main). Technical help by *Ursula Fuhr* and *Doris Beutler* (ZALF, Institute of Landscape Biogeochemistry) and the staff of the ZALF, Experimental Field Station Müncheberg) is gratefully acknowledged. We also thank *Gebhard Graf Hardenberg* and *Felix Gerlach* (Komturei Lietzen) for giving access to their fields and supporting the experiments.

References

JOSCHKO, M., GEBBERS, R., BARKUSKY, D., TIMMER, J. 2010. The apparent electrical conductivity as a surrogate variable for predicting earthworm abundances in tilled soils. J. Plant Nutr. Soil Sci. **73**, 584–590

VALCKX, J., COCKX, L., WAUTERS, J., VAN MEIRVENNE, M., GOVERS, G., HERMY, M., MUYS, B. 2009. Within-field spatial distribution of earthworm populations related to species interactions and soil apparent electrical conductivity. Applied Soil Ecology 41, 315-328

Interpreting the soil-landscape around the school of gladiators of Carnuntum by integrating multi-receiver EMI measurements

T. Saey[1*], M. Van Meirvenne[1], P. De Smedt[1], I. Trinks[2], G. Verhoeven[2], W. Neubauer[2]

[1]*Universiteit Gent, Department of Soil Management, Coupure links 653, Gent, Belgium*
[2]*Ludwig Boltzmann Institute for Archaeological Prospection and Virtual Archaeology (LBI ArchPro), Hohe Warte 38, Vienna, Austria*
[*]*E-mail: timothy.saey@ugent.be*

1 Introduction

Low frequency electromagnetic induction (EMI) methods are well introduced in proximal soil sensing and precision agriculture because measurements of the apparent electrical conductivity (ECa) allow the detailed characterization of the variability of soil properties such as texture, organic matter and moisture. Besides ECa, EMI methods measure simultaneously the apparent magnetic susceptibility (MSa). To enlarge their applicability, some EMI instruments have multiple receiver coils creating a potential for depth investigations of the electrically conductive and magnetic features. When such information is available over a larger area, the detailed reconstruction of the soil-landscape becomes possible. Such information is highly complementary to the understanding of buried archaeological structures revealed with other methods.

2 Objectives

Recently, the Ludwig Boltzmann Institute for Archaeological Prospection and Virtual Archaeology (LBI-ArchPro) announced the discovery of the buried remains of a gladiator school (a “ludus gladiatorius”) next to the excavated amphitheatre of the Roman city of Carnuntum, Austria. This was achieved by combining high-resolution magnetometry and multi-antennae GPR measurements. However, these methods did not provide information about the composition of the soil and its variability. The aim of this research is to evaluate the usefulness of a EMI survey with a multi-receiver instrument, registering simultaneously ECa and MSa, to characterize the soil variability around the gladiator school. We will especially focus on the ability to interpret the soil-landscape of this highly valuable archaeological site.

3 Materials and methods

Our study site represents a 5.6 ha arable field, embedding the gladiator school and bordering the excavated amphitheatre. It is located on slightly undulating, fluviatile and gravel-rich terraces of the nearby river Danube. Near the end of the Weichselian glacial period, this area was covered by aeolian loess deposits from a variable but generally

limited thickness. The study area has a slightly undulating topography with a range in elevation of 12.9 m.

The study area was investigated with an EMI sensor which consists of one transmitter coil and four receiver coils, the DUALEM-21S instrument (DUALEM, Milton, Canada). This multi-receiver EMI instrument allows measuring both the ECa and MSa of four different soil volumes.

4 Results

The mean ECa increases from the shallowest to the deepest measuring coil configurations indicating that the subsoil is on average much more conductive than the topsoil. The MSa measurements depict the archaeological structures related to the school of gladiators.

Integrating the simultaneous ECa or MSa measurements can be done by modelling the conductivity (EC) or magnetic susceptibility (MS) of a particular depth interval or slice. On the study site, EC-depth slicing resulted in an enhanced visibility of patterns. In the north-western part of the study site, a fine-scale polygonal network appears. Based on previous experience with EMI sensors we interpreted this network as frost-wedge pseudomorphs. In the central and northeastern parts of the study area, traces of surface drainage patterns are clearly visible. Most of these gullies flow into the lower part of the area where the frost-wedge pseudomorphs are present. Complementary to the EC-depth slices, MS-depth slicing enhances the visibility of the archaeological traces related to the school of gladiators and its associated structures. When both complementary EC and MS data are combined it becomes clear that the school was constructed on an area with low EC values and outside the area affected by erosion. The builders of the school obviously selected a location near to the amphitheatre which was situated at a higher position in the landscape with a stable (gravel rich) subsoil avoiding sloping and wet clay rich parts of the area.

5 Conclusions

The potential of multi-receiver EMI for soil-landscape research around archaeological sites situates in the ability to integrate the multiple signals of both the complementary electrical conductivity and magnetic susceptibility. Combining the multiple ECa measurements allowed to interpret the soil landscape. Moreover, the complementary MSa measurements enabled locating the buried archaeological remains.

The influence of conductivity on the microstrip soil moisture sensor

G. Kitić*, V. Crnojević Bengin

University of Novi Sad, Faculty of Technical Sciences, Trg Dositeja Obradovića 6, 21000 Novi Sad, Serbia
**E-mail: gkitic@gmail.com*

Abstract

In this work, the possibility to perform soil-independent measurement of soil moisture is investigated. By using test samples moisturized with water of different salinities, we analyse the influence of the soil conductivity on the output of the microstrip soil moisture sensor operated in the frequency range from 0.5 GHz to 2.5 GHz. The obtained results confirm that if the operating frequency is sufficiently high (i.e. 2.5 GHz or higher), the influence of soil conductivity on the calibration curves based on the mixing-model can be neglected. These results open way for the design of miniature soil-independent soil moisture sensors for applications in wireless sensor networks.

Keywords: soil moisture, microstrip sensor, conductivity influence.

1 Introduction

The measurement of soil moisture is needed in variety of applications in agriculture, various soil studies, ecosystem management, geo-engineering, and more. In general, methods for the measurement of soil moisture content can be divided into direct and indirect methods (Nussberger, 2005). Direct methods are based on drying the soil sample and measuring its weight before and after the drying process. They are very accurate but quite time consuming (24 h), destructive and do not allow repeatability of measurement on the same location. Indirect methods estimate the water content via a certain parameter that is directly influenced by moisture (Kramer et al, 1992; Topp et al, 1980; Dalton et al, 1984; Whalley et al, 1992). These methods differ in cost, accuracy, response time and durability.

The design of miniature low-cost soil-moisture sensors for applications in wireless sensor networks (WSN) presents a specific challenge today. Apart from operating on a single frequency, such sensors need to work independently of the soil type, i.e. of the soil conductivity. In this paper, we first analyse a miniature high-sensitivity microstrip fractal sensor which uses the phase shift method and in essence measures the soil permittivity which is a strong function of the soil volumetric water content (VWC). To allow low-cost production, the sensor is based on standard transmission line microstrip architecture and fabricated in a conventional printed circuit board technology.

To correlate the measured permittivity with VWC, we propose a method to construct the calibration curve by fitting the three-phase mixing model (TPMM) to the measurement results, (Roth et al, 1990). Then, we investigate the influence of the conductivity on the calibration curve and discuss the optimal operating frequency of the sensor. In that manner, we open way to the design of soil-moisture sensors which operate independently of the soil type.

2 Materials and methods

The phase shift method for determination of soil moisture content relies on the fact that the water content strongly affects the permittivity of soil, (George, 1999). VWC can be determined from the effective permittivity ε by measuring the phase shift of the electromagnetic wave that propagates along the sensor with the phase velocity v, (Kitić et al, 2010):

$$\vartheta = \left(\sqrt{\mu\varepsilon} \sqrt{\frac{1+\sqrt{1+\left(\frac{\sigma}{\omega\varepsilon}\right)^2}}{2}} \right)^{-1} \tag{1}$$

where ω is the operating angular frequency, μ is effective permeability and σ is conductivity of the soil. The phase shift $\Delta\varphi$ can be calculated as

$$\Delta\varphi = \omega \frac{L_{TL}}{v} \tag{2}$$

where L_{TL} is the length of the transmission line (i.e. the sensor).

To achieve very compact size and improved sensitivity, the sensor is designed using two parallel segments, each comprised of two Hilbert fractal lines of the third order and connected in series, Figure 1a. The sensor is realized on a 1.27 mm thick Taconic CER-10 substrate with ε_r = 9.8 and $tan\delta$ = 0.0025. The width of Hilbert lines is 0.4 mm, while the spacing between the lines is 0.2 mm. Ports and feed lines are placed on the same side of the substrate to allow easy accessibility when the sensor is inserted in the soil. The overall dimensions of the sensor are 32x19.4 mm. By removing the part of the ground plane directly under the line (Figure 1b), sensitivity of the sensor is additionally improved, (Radonić et al, 2010).

Quartz sand was used to validate the method since it provides the repeatability of measurements, it is suitable for sensor mounting and it has properties similar to soil. Dried sand was poured in plastic containers and phase shift measurements were performed for different moisture levels of the sand sample, at operating frequencies in the range of 0.5-2.5 GHz, Figure 1c.

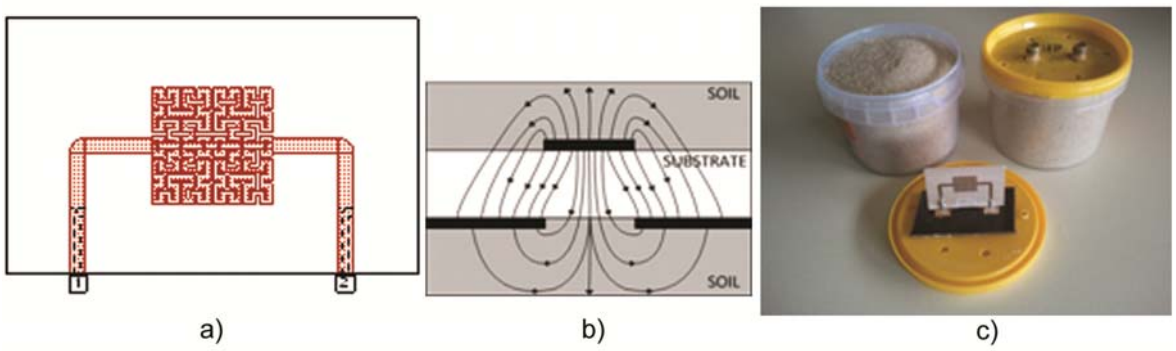

Figure 1. a) Top view of the sensor b) E-field lines of the sensor inserted in the soil c) sensor mounted on the container

The calibration curves were constructed by fitting the TPMM to the measurement results for various sand moistures, and for each analysed frequency. The model assumes that the actual phase shift $\Delta\varphi$ is the result of mixing of various sand components, each inflicting its phase: sand matrix $\Delta\varphi_s$, air $\Delta\varphi_a$ and water $\Delta\varphi_w$. VWC can be determined by using

$$\theta_v = \frac{\Delta\varphi^{\alpha} - (1-\phi)\,\Delta\varphi_s^{\alpha} - \phi\Delta\varphi_a^{\alpha}}{\Delta\varphi_w^{\alpha} - \Delta\varphi_a^{\alpha}} \tag{3}$$

where θ_v is VWC, α is a geometrical parameter and ϕ is porosity.

To investigate the influence of the conductivity on the calibration curves, the measurement procedure was repeated for the sand moisturized with water with two different salinities (conductivities): 29‰ and 70‰. The measurement procedure starts with a completely dry quartz sand sample. The phase of S_{21} parameter of the sensor was measured in the frequency range of 0.5-2.5 GHz. Then, the sample was moistened by 4-5 g of distilled water and left in sealed plastic bag for 24 hours so that water is evenly distributed in the sample. The procedure of successive phase shift measurement and moisturizing was repeated until saturation of the sample was achieved.

We show that if the operating frequency is sufficiently high to result in $(\sigma/\omega\varepsilon)^2 << 1$, then the conductivity can be neglected and the expression for phase velocity (1) can be simplified to $v = (\sqrt{\mu\varepsilon})^{-1}$. We analytically estimate the operating frequencies to be above 2.43 GHz and 3.23 GHz, respectively.

3 Results and discussion

Figure 2 shows the calibration curve of the sensor at the operating frequency of 2.5 GHz. The curve was designed by fitting 12 calibration points and it exhibits the maximum absolute error with the respect to calibration points of 0.018 m^3/m^3, i.e. 5.22 % of the full scale output (FSO). To validate the proposed method, another sample with four

different values of VWC was measured. The maximum absolute error in this case was 0.019 m^3/m^3, i.e. almost identical to that of the calibration curve.

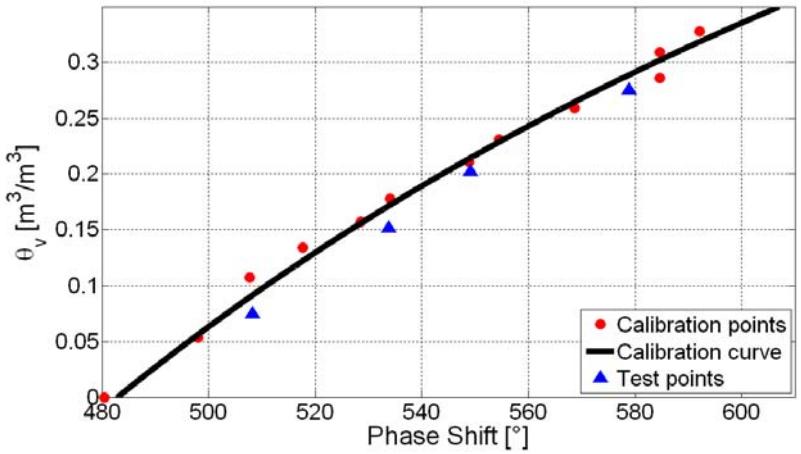

Figure 2. Calibration curve at 2.5 GHz.

In Figure 3, fitted calibration curves for the measurement performed at the edges of operational bands are presented, namely at 0.5 and 2.5 GHz. As can be seen, a significant difference between the calibration curves obtained from differently treated samples exists if the operating frequency is relatively low (i.e. 0.5 GHz). However, if the operating frequency is increased to 2.5 GHz, the calibration curves for the samples treated with the distilled water and 29‰ saline water are almost identical, with the relative difference with the respect to FSO of less than 1.78%. The calibration curve for 70‰ saline water is still different, since the operating frequency is not sufficiently high (i.e. it is below 3.23 GHz).

As predicted analytically, the measurement results have clearly showed that the conductivity influence on calibration curves is more pronounced at lower frequencies. On the other hand, if the sensor is operated at sufficiently high frequency, the calibration curves converge to one curve, thus allowing unique characterisation of different types of soil.

It can be noted that the calibration curves do not start from the same point, although the first measurement is always done for the dry sand sample. This is a consequence of the fitting procedure, since the calibration curves represent the best fit for all measurements and therefore can result in different starting points. The effect of fitting is clearly seen in Figure 2 where calibration curve does not intersect the calibration point obtained for a dry sample.

The proposed sensor, based on the measurement of the phase shift, offers certain advantages over other methods. Unlike, for example, the time domain reflectometry (TDR) probes which measure the amplitude of the reflected wave, sensors based on the estimation of the phase shift detected the phase of the signal which is less susceptible to

noise. Furthermore, the combination of high conductivity and water content represents a great obstacle for TDR probes (Dalton, 1992), not prominent in the case when the phase shift based method is used.

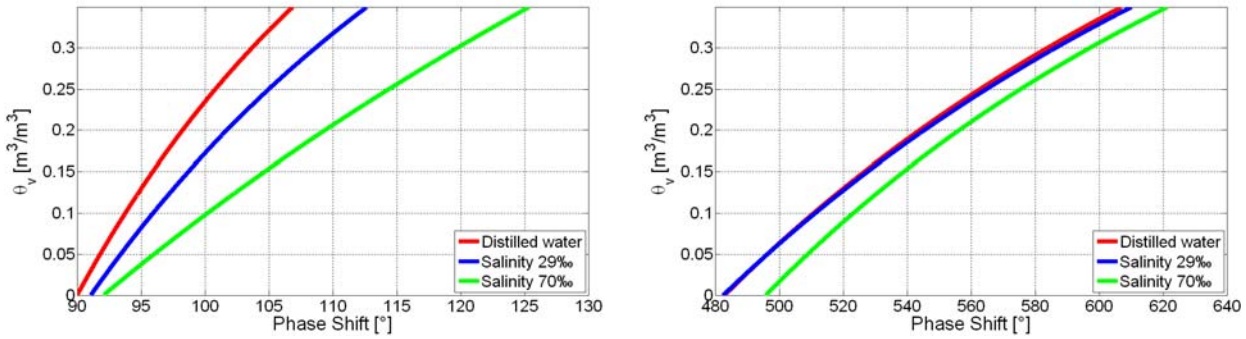

Figure 3. Calibration curves at a) 0.5 GHz and b) 2.5 GHz.

4 Conclusions

The influence of the conductivity on the microstrip soil moisture sensors output is investigated by performing the measurements with test samples moisturized with water of different salinities. Calibration curves were obtained by fitting the TPMM to the measurement results. It was confirmed that if the operating frequency is sufficiently high, the influence of soil conductivity on the calibration curves based on the mixing-model can be neglected. The relative difference between the calibration curves obtained for the samples treated with distilled water and 29‰ saline water with the respect to FSO was only 1.78%. These results represent one step closer to the final goal of designing the miniature soil independent soil moisture sensor for applications in wireless sensor networks.

5 References

DALTON, F.N., VAN GENUCHTEN, M. TH. 1986. The time-domain reflectometry method for measuring soil water content and salinity. Geoderma, **38** pp. 237-250.

DALTON, F.N. 1992. Development of time-domain reflectometry for measuring soil water content and bulk soil electrical conductivity. In: Advances in Measurement of Soil Physical Properties: Bringing Theory into Practice (editors: Topp, G.C., Reynolds, W.D. and Green, R.E.), pp. 143-168.

GEORGE, B.H. 1999. Comparison of techniques for measuring the water content of soil and other porous media. BScAgr. Department of Agricultural Chemistry & Soil Science, University of Sydney, 13 pp.

KITIĆ, G., RADONIĆ, V. , JANKOVIĆ, N., CRNOJEVIĆ-BENGIN, V. 2010. Senzor vlažnosti zemljišta baziran na metodi faznog pomeraja (Soil moisture sensor based on phase shift mehtod),In: Etran 2010: Proceedings of Etran, Donji Milanovac, Serbia

KRAMER, J.H., CULLEN, S.J., EVERETT, L.G. 1992. Vadose zone monitoring with the neutron moisture probe. Groundwater Monitoring & Remediation, **12** (3) pp. 177-187.

NUSSBERGER, M. 2005. Soil moisture determination with TDR: single-rod probes and profile reconstruction algorithms. Ph.D. thesis. Swiss Federal Institute of Technology Zurich, 5-6.

RADONIĆ, V., KITIĆ, G., CRNOJEVIĆ-BENGIN, V. 2010. Novel Hilbert soil-moisture sensor based on the phase shift method. In: MMS 2010: Proceedings of Mediterranean Microwave Symposium (MMS), pp. 377-380.

ROTH, K., SCHULIN, R., FLUHLER, H., ATTINGER, W. 1990. Calibration of time domain reflectometry for water content measurement using a composite dielectric approach. Water Resources Research, **26** (10) pp. 2267-2273.

TOPP, G.C., DAVIS, J.L., ANNAN, A.P. 1980. Electromagnetic determination of soil water content: measurements in coaxial transmission lines. Water Resources Research, **16** pp. 574-582.

WHALLEY, W,R., DEAN, T.J., IZZARD, P. 1992. Evaluation of the capacitance technique as a method for dynamically measuring soil water content. Journal of Agricultural Engineering Research, **52** pp. 147-155.

Spatial variation in Swedish field experiments

K. Piikki[1*], M. Söderström[1], M. Stenberg[1], J. Forkman[2], J. Roland[1]

[1]SLU, Swedish University of Agricultural Sciences, Department of Soil and Environment, Precision agriculture and pedometrics, P.O. Box 234, SE-532 23 Skara, Sweden
[2]SLU, Swedish University of Agricultural Sciences, Field Research Unit, P.O. Box 7043, SE-750 07, Uppsala, Sweden
[*]E-mail: kristin.piikki@slu.se

Abstract

Spatial variation in seven randomly selected Swedish field experiments were investigated by use of two non-invasive on-the-go proximal soil sensors, one gamma spectroscopy sensor and one electromagnetic induction sensor. It was concluded that there can be substantial spatial variation in soil properties, even though a site appears to be homogeneous by visual inspection. The experimental residual error was related to the magnitude of variation in apparent electrical conductivity (ECa) and to use an ECa map as decision support for site selection would be a good approach. To account for spatial variation by including proximally sensed covariates only improved the statistical modelling in one experiment out of seven.

Keywords: Gamma-ray spectroscopy, electromagnetic induction, field experiments.

1 Introduction

Field trials have for many years been the accepted method to investigate agricultural research questions. The selection of experimental sites is an issue that has a great influence on the outcome of the studies. Many trials are carried out at farm sites, to provide the agricultural society with scientifically based knowledge on different soils and under different climatic conditions. The farm sites are often less well known than experimental sites on research stations.

In a field experiment, the experimental response variable may vary between the experimental plots due to the experimental treatment, but there is always some degree of additional variation caused by other factors, e.g. spatial variation in soil properties of importance for the crop. If the experimental residual variation is large, the experiment may have to be discarded, which means unnecessary costs and delayed research projects. Spatial variation in soil properties may be handled in different ways:

1. It can be avoided by selecting homogeneous experimental sites.
2. Its effects on treatment comparisons can be made random by using randomization.
3. Its effects on treatment comparisons can be reduced by using blocks.

4. It can be accounted for in the statistical analysis, by *i*) modelling autocorrelation among plots, *ii*) nearest-neighbour analysis, or *iii*) including spatial covariates, such as proximally sensed data, in the statistical model.

Today, unwanted variation is avoided by selection of homogeneous test sites, as judged from visual inspection, and by using randomized complete block designs, to prevent spatial variation in growth conditions to have a systematic effect on the experimental treatments. Lück et al (2011) performed proximal sensor measurements of soil apparent electrical conductivity (ECa) in Swedish field experiments and found that the spatial variation patterns in ECa often corresponded with the spatial variation patterns of soil texture. They proposed to include ECa as a covariate in the statistical analysis. The present study investigates if proximal sensors can be useful tools for the first and the fourth of the strategies listed above.

2 Objectives

The project aimed to quantify the soil variation in seven Swedish field trials and to propose strategies to deal with this background variation.

3 Materials and methods

3.1 Field experiments

Seven nitrogen fertilization experiments with randomized complete block designs (7-14 nitrogen levels × 4 blocks) on the Västergötland plain in Sweden were selected with no prior expectation of whether the spatial variation would be large or small. The crops were winter and spring barley (*Hordeum vulgare* L.), winter wheat (*Triticum aestivum* L.) and oats (*Avena sativa* L.). The response variables were grain yield and protein content.

3.2 Proximal sensor measurements and data preparation

Two different sensors were used to quantify the spatial soil variation, one gamma spectrometer (The Mole, The Soil Company), which measured the natural gamma ray emissions from the topsoil and one electromagnetic induction sensor (EM38 MK-2, Geonics Ltd.). The radioactive isotope ^{232}Th, measured by the gamma sensor, and ECa with an effective measurement depth of 0.8 m, measured by the EM38, were used in the present study. Both sensors were used to log values in transects across the experiments (103-639 observations per site) after the harvest in September 2010. The proximal measurements and the experimental plots were positioned using an RTK-GPS (Chamelion, DataGrid) with about ± 2 cm accuracy in the horizontal plane. The point measurements of ECa and ^{232}Th emissions were interpolated by ordinary point kriging to a 0.2 m × 0.2 m grid (ArcGIS 9.3, ESRI Inc.) and average values were formed for each experimental plot. Values of grain yield at 15% water content and grain protein content were

extracted from the Swedish field trial database (Field Research Unit, Swedish University of Agricultural Sciences)

3.3 Data analyses.

For the investigation of the magnitude of variation, ^{232}Th were approximated to the more easily apprehensible variable clay content using a regional linear pedotransfer function parameterized by Söderström & Stadig (2012). In all other analyses ^{232}Th values were used. For the investigation of whether it would be useful to include the proximal sensor values as covariates in the statistical analyses, seven different models for grain yield were fitted by maximum likelihood (ML) and evaluated with the small-sample corrected Akaike Information Criterion AICC (Hurvich & Tsai, 1989). The SAS 9.2 software (SAS Institute Inc.) was used. The AICC information criterion makes possible comparisons of non-nested models. It was chosen based on a simulation study of 200 field trials without any actual effects of covariates. This simulation study showed that AICC could correctly identify the correct model in 95% of the cases (not shown). In addition, the significance of the last term of each model was tested.

4 Results

At the experimental site with the largest soil variation, the plot average clay content values ranged between 12 % clay and 35 % clay and in the least variable experiment it ranged between 28 % clay and 35 % clay. The ECa ranges (Figure 1) was of comparable level to six of the experiments investigated by Lück et al. (2011), where 95% of the measured values were <10 mS m^{-1} but in the other six experiments in that study larger variation ranges (< 20 mS m^{-1}) were observed.

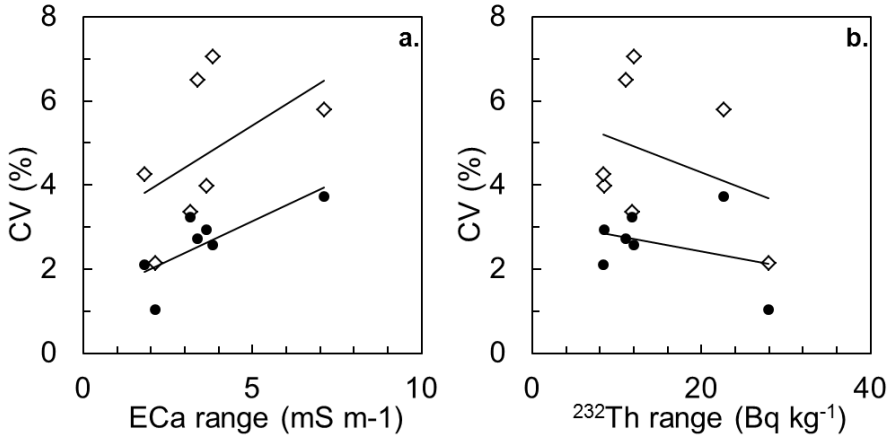

Figure 1. Residual coefficient of variation (CV) of grain yield and protein content in relation to the ranges of a) apparent electrical conductivity (ECa) and b) ^{232}Th in the seven field experiments. Open diamonds = grain yield, closed circles = protein content.

Note, however, that the studies were not exacly similar. The depth of exploration was shallower in the present study and the ranges were calculated from plot-wise averages. From Figure 1 it can also be inferred that sites with a large variation in ECa also tended to have a large experimental error. The residual coefficients of variation (CV) of the response variables and the variation ranges of ECa were correlated (R^2 = 0.24 for grain yield and R^2 = 0.58 for grain protein content). There were no similar relationships between the two CVs and the ranges of ^{232}Th (R^2 = 0.11 for both response variabels). In the present study, it was most often not useful to include the proximally sensed covariates in the statistical model (Table 1).

Table 1. The small-sample corrected Akaike information criterion (AICC, smaller is better) of models parameterized by maximum likelihood. Values that are smaller than for the baseline-model are indicated with a star. B = block, N = nitrogen treatment, ECa = apparent electrical conductivity, Th = ^{232}Th. In addition, all models also included an intercept and a residual error term.

Model	Börjesgården	Forshall	Koberg	Lunden	Malma	Russelbacka	Skofteby
B + N (baseline)	816	537	497	354	404	424	615
B + N + ECa	821	542	502	359	409	**422***	619
B + N + ECa + ECa^2	824	548	508	369	415	425	621
B + N + ECa × N	903	598	549	526	497	481	667
B + N + Th	820	537	502	356	411	**420***	617
B + N + Th + Th^2	824	542	508	359	420	426	622
B + N + Th + Th × N	904	592	559	476	503	469	657

5 Discussion

The spatial variation in soil properties was not entirely avoided even though sites that appeared as homogeneous by visual inspection were selected. The soil variation was considerable in some cases and the maximum difference in calculated clay content between plots was as large as 22 % clay in one of the experiments. However, the magnitude of variation in ECa was correlated to the magnitude of the experimental residual errors and the selection of homogeneous sites may be improved by using an ECa map as decision support, instead of mere visual inspection.

There may be several explanations for why the proximal measurements often did not improve models, the variation in the measured soil properties was not large enough, the measured soil properties did not have a large enough impact on the response variable, and the variation was already accounted for by the blocks. The latter explanation is probably the most important since the variation was quite considerable and the magnitude of variation in ECa was related to experimental error, which indicates a direct or indirect impact of soil properties influencing ECa on grain yield.

6 Conclusions

In seven randomly selected -nitrogen fertilization experiments performed at the Västergötland plain in Sweden 2010, it was found that:

- Variation in clay content can be large even though a site appears to be homogeneous.
- ECa maps may constitute a good decision support for the placement of experiments on homogeneous soil.
- To take spatial variation into account by including ECa or ^{232}Th as a covariate in the statistical model only improved the results in one experiment out of seven, most likely because a large portion of the spatial variation was accounted for by using blocks.

Acknowledgements

Thanks are due to The Swedish Farmers' Foundation for Agricultural Research for funding of the project and to Amelie Lindgren for conducting the field measurements.

References

HURVICH, C. M., TSAI, C.-L. 1989. Regression and time series model selection in small samples. Biometrika **76** 297–307.

LÜCK, E., RÜHLMANN, J., KIRCHMANN, H. 2011. Properties of soils from the Swedish longterm fertility experiments: VI. Mapping soil electrical conductivity with different geophysical methods. Acta Agriculturae Scandinavica, Section B - Soil & Plant Science **61** 438-447.

SÖDERSTRÖM, M., STADIG, H. 2012. Local and regional soil clay mapping using gamma ray spectrometry. 11th International Conference on Precision Agriculture, July 15-18, 2012, Indianapolis, USA. Poster paper published on CD, 2 pp.

Mapping soil horizon change in the viticultural region of the Hunter Valley in NSW, Australia, employing a DUALEM-421 induction probe

U. Stockmann[1*], J. Triantafilis[2], B. Minasny[1], A. McBratney[1]

[1]*Department of Environmental Sciences, Faculty of Agriculture and Environment, The University of Sydney, Biomedical Building C81, 1 Central Avenue, Australian Technology Park, Eveleigh, NSW, 2015, Australia*

[2]*School of Biological, Earth and Environmental Sciences, Faculty of Science, The University of New South Wales, Biological Sciences Building, Gate 9 High Street, Randwick, NSW, 2052, Australia*

[*]*E-mail: uta.stockmann@sydney.edu.au*

Abstract

Electromagnetic instruments which measure the soil's apparent electrical conductivity (EC_a) have been used widely in proximal soil sensing to map the areal variation of soil properties. However, soil also varies with depth owing to the interaction of various soil-forming factors. Here, we collect EC_a data from a DUALEM-421 along a toposequence in the viticultural region of the Hunter Valley, Australia. We subsequently invert this data using EM4Soil and compare 2-d models of the true electrical conductivity (σ) against measured soil morphological as well as chemical and physical properties. Preliminary results suggest that the model of σ can be used to identify differences in soil based on parent materials and that the topography influences the distribution of soil properties.

Keywords: soil horizon mapping, soil apparent electrical conductivity, inversion modelling.

1 Introduction

Proximal soil sensing techniques have been used extensively in digital soil mapping to identify and map the areal variations of soil properties across the landscape and therefore to make inferences about the quality of the studied soils (McBratney et al., 2003). One of the most popular has been electromagnetic (EM) instruments (Corwin and Lesch, 2005). This is because they measure the soil's apparent electrical conductivity (EC_a – mS/m), which is influenced by soil porosity, moisture content, salinity, temperature and the amount and composition of colloids (McNeill, 1980). For the most part this has been done for average soil properties. However, soil varies with depth (i.e. A and B horizons) owing to the action of various soil forming factors (e.g. parent material and topography).

Recently, inversion software (EM4Soil) has been developed, which enables a user to generate models of the spatial variation of the true electrical conductivity (σ – mS/m) of

soil with depth (Monteiro Santos et al., 2010). In addition, advances in instrumentation have led to the development of single-frequency and multiple coil devices (i.e. DUALEM-421).

Here, we employed a multiconfiguration EM instrument to potentially estimate and map soil horizon depths along a toposequence in a small catchment in the viticultural region of Pokolbin in the Hunter Valley in NSW, Australia, to subsequently investigate soil horizon as well as soil parent material change in this managed agricultural system.

2 Materials and methods

Surveying took place in a small catchment in the viticultural region of Pokolbin in the Hunter Valley in NSW, Australia. The soil-landscape of the survey region resulted from a variety of parent rocks including lithic sandstone, mudstone, shale and marl (a form of limestone) (Kovac and Lawrie, 1991), with alluvium and colluvium forming the soil parent materials at the lower elevations of the site. Soil types in the study area range from well-drained Red Chromosols to more poorly drained Brown Dermosols to a small number of Supracalcic Calcarosols (Australian Soil Classification system; Isbell et al., 1997).

We collected EC_a data from a DUALEM-421 (Dualem Inc., Milton, Ontario, Canada) along a toposequence in the survey area. We based our hillslope transect selection on maps of the areal distribution of EC_a to capture a wide range of EC_a along the toposequence. The advantage of the DUALEM-421 is that it operates at a single frequency of about 9 kHz and takes readings at multiple coil spacings (4 m, 2 m and 1 m) and orientations (horizontal co planar and perpendicular arrays) simultaneously. The EM data stream was recorded together with positioning information from an Omnistar High Precision DGPS. The DUALEM-421 was mounted on a plastic sled which was pulled by a John Deere Gator six-wheel-drive mode field vehicle.

Figure 1. Field vehicle and instrument setup.

We invert the transect EC_a data using EM4Soil to estimate the spatial variation of the true electrical conductivity (σ – mS/m) of the soil with depth. EM4Soil is a software based on a one-dimension laterally constrained inversion algorithm with two-dimensional smoothness constraints between adjacent one-dimensional models (Monteiro Santos et al., 2010).

In order to validate inversion results, we selected 12 sampling sites along the toposequence, based on the range of σ. At each sampling site soil samples were taken to a depth of 1 m, to analyse soil chemical (e.g. $EC_{1:5}$ – mS/m) and physical properties (e.g. particle size analysis) in the laboratory.

3 Results and discussion

Figure 2 shows a contour plot of estimated electrical conductivity (σ – mS/m) using a damping factor (lambda, λ) value of 2.4. We subsequently compare our 2-d model of σ against measured soil morphological (e.g. depth of horizons) and soil chemical (EC1:5) and physical properties (particle size fractions).

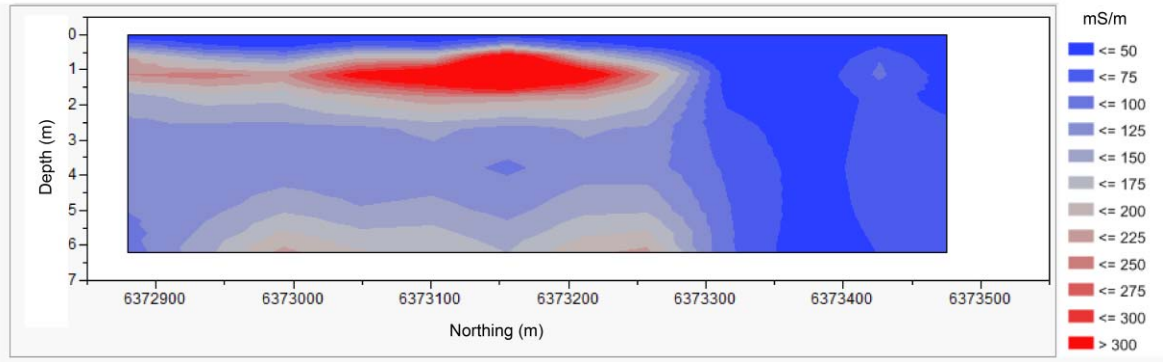

Figure 2. Contour plot of estimated electrical conductivity (σ – mS/m) employing a lambda (λ) value of 2.4 using EM4Soil and DUALEM-421 data (ECa – mS/m).

Preliminary interpretations suggest to us that the model of σ can be used to identify differences in soil based on parent material (i.e. marl present at the hilltop sites is less conductive than shale present at the lower elevations of the toposequence) and that the topography influences the distribution of soil properties (i.e. salts mobilised into lower landscape positions which are generally more conductive).

4 Conclusion and future work

We believe that observations from this study will enable a better understanding of soil formation processes at the studied site and allow us to improve our knowledge of how the soil landscape has been altered due to agricultural production. This work is ongoing.

References

CORWIN, D.L., LESCH, S.M. 2005. Apparent soil electrical conductivity measurements in agriculture. Computers and Electronics in Agriculture **46**(1–3) 11-43.

ISBELL, R.F., MCDONALD, W.S., ASHTON, L.J. 1997. Concepts and Rationale of the Australian Soil Classification. ACLEP, CSIRO Land and Water, Canberra.

KOVAC, M., LAWRIE, J.W. 1991. Soil Landscapes of the Singleton 1:250.000 Sheet. Soil Conservation Service of NSW, Sydney.

MCBRATNEY, A.B., MENDONCA SANTOS, M.L., MINASNY, B. 2003. On digital soil mapping. Geoderma **117**(1-2) 3-52.

MCNEILL, J.D. 1980. Electrical conductivity of soils and rocks. Technical Note TN-5 Geonics Limited, Mississauga, Ontario, Canada.

MONTEIRO SANTOS, F.A., TRIANTAFILIS, J., BRUZGULIS, K.E., ROE, J.A.E. 2010. Inversion of multiconfiguration electromagnetic (DUALEM-421) profiling data using a one-dimensional laterally constrained algorithm. Vadose Zone Journal **9**(1) 117-125.

Response of EMI based proximal soil sensor in two contrasting tropical landscapes

U.W.A. Vitharana[1*], M. Van Meirvenne[2], A. Verdoodt[2], H.Lenoir[2], T. Saey[2], T. Haputanthri[1]

[1]*Department of Soil Science, Faculty of Agriculture, University of Peradeniya, Sri Lanka*
[2]*Research Group Soil Spatial Inventory Techniques, Department of Soil Management, Ghent University, Belgium.*
[*]*E-mail: uvithara@pdn.ac.lk*

Abstract

Detailed soil information is a pre-requisite to improve the present level of crop productivity in many developing countries in the tropical belt. This study was conducted in Sri Lanka to investigate the potential of proximally sensed apparent electrical conductivity (ECa) measurements to predict soil properties in two sites with two levels of soil formation. The Electromagnetic induction (EMI) based proximal sensor showed a high response (range 1 - 40 mS/m) in moderately weathered Alfisols soil-scape. Principal component analysis indicated a strong correlation between ECa and topsoil clay, pH and CEC. However, the response of the sensor was low in highly weathered Ulitsols soil-scape (range 1-13 mS/m) and those measurement were highly correlated with top and subsoil electrical conductivity (r = 0.8). This study revealed that the response by EMI based ECa sensing in two tropical soil-scapes is useful as a basis for the prediction of primary soil properties and also for the delineation of potential management zones for site-specific soil management.

Keywords: Soil apparent electrical conductivity, tropical soils, Alfisols, Ultisoils.

1 Introduction

Highly weathered tropical soils bear a limited potential for crop production (Jao and Franzluebbers, 2003). Rapid growth of the population in the tropical region itself causes a tremendous pressure on the presently available arable lands. Nevertheless, the present blanket recommendations based intensive soil management practices have posed a great danger for the environmental integrity. Therefore, there is a need for a gradual shift from present soil management practices to practices those ensure increased crop production with a favourable environmental balance (Dobermann et al, 2002). Site-specific soil management is one of the viable approaches to optimize the crop production capacity of soils (Plant, 2001). Key steps of planning such as identification of uniform within-field areas (potential management zones) and site-specific management of inputs require priory detailed soil information. However, detailed soil information are not available in many countries hence that act as one of the major obstacles for the adop-

tion of Site Specific Soil Management. Generation of detailed soil information through classical soil survey approaches is costly and time consuming. Alternative cost-effective methods to generate detailed digital soil maps e.g. proximal soil sensing, have been explored elsewhere (Vitharana et al, 2008). However, there is a need to investigate the adaptability of these novel technologies in tropical soil environments. Current study focuses on the suitability of proximal sensed apparent electrical conductivity (ECa) measurements to infer the soil variability of two tropical soils those at different degree of soil formations.

2 Materials and methods

This study was conducted at two agricultural sites in Sri Lanka (Figure 1), one located on an Alfisols soil-scape (1.6 ha paddy land: 7^0 53.458'N, 80^0 40.400'E) in Palwehera area of the dry zone (annual precipitation <1750 mm)) and the other located on an Ultisols soil-scape (1 ha tea plantation: 7^0 16.475'N, 80^0 32.734'E) in the Peradeniya area of the wet zone (Annual precipitation >2500 mm).

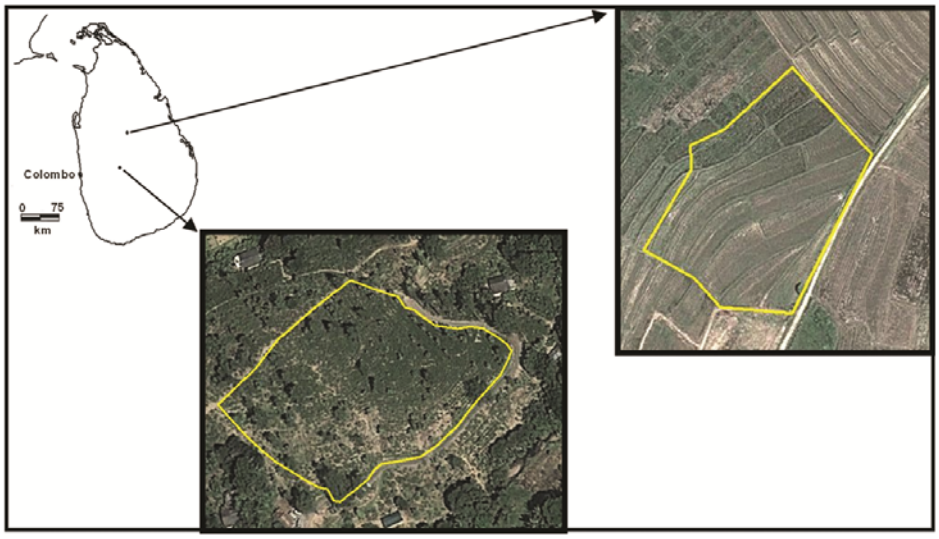

Figure 1. Satellite images of the paddy field in the Alfisols soil-scape (top) and Tea cultivated field in the Ultisols soil-scape (yellow lines show the boundaries).

A grid combined random sampling scheme was used to obtain a total of 26 topsoil samples (0 – 30 cm) from the Alfisols field. Half of the sampling points were located on each grid node of a 25 m regular grid and the remaining sampling points were assigned as random samples within each grid cell. Samples were analysed for soil texture using pipette method, EC (1:5 soil:water), pH (1:2.5 soil:water), available P, K, cation exchange capacity (CEC) and micronutrients. In both fields, an ECa survey was conducted by manually dragging the vertical dipole mode of the EM38 sensor (ECa-V). The Ultisols land was surveyed more densely (4460 measurements) in comparison to the Alfisols land (2680 measurements). The spatial variability of ECa-V measurements was used as the basis for the soil sampling scheme in the Ultisol land. and Ten top (0-

30 cm) and subsoil (30-60 cm) samples were taken. These were analysed for soil texture, EC (1:5 soil:water), pH (1:2.5 soil:water), organic matter content and CEC. Exploratory data analysis was performed for all measured soil properties. Principal component analysis (PCA) was used to investigate the key soil variables representing the spatial variability of the field and their relationships with ECa-V in the Alfisol field. Due to the limited number of soil observations, correlation analysis was done for the Ultisol field to explore the relationships of soil properties with ECa-V.

3 Results and discussion

Table 1 shows the descriptive statistics of the soil properties measured in both fields. The Alfisols field showed a considerable variability in soil texture. Corresponding to the variability of the clay content, the CEC also showed a large variability within the study area.

Table 1. Descriptive statistics of the topsoil properties measured in the Alfisols and Ultisols fields (*SD = standard deviation).

Property	Alfisols field				Ultisols field			
	Min	Max	Mean	SD*	Min	Max	Mean	SD*
Clay (%)	1.5	31.7	13.2	7.6	16.4	41.3	27.2	9.3
Sand (%)	58.0	91.0	74	8.5	45.8	55.3	50.2	3.22
Silt (%)	7.0	16.2	12.0	2.2	6.5	33.5	22.6	10.5
pH	5.3	6.8	5.9	0.3	4.2	5.3	4.5	0.3
CEC (cmol+/kg)	3.1	12.1	6.9	2.7	4.0	26.8	16.7	8.4
EC (mS/m)	2.1	9.9	1.6	8.8	3.6	7.8	5.9	1.5
ECa-V (mS/m)	1	40	14.6	7.1	1	13	6.2	1.9
P (mg/kg)	2.0	35.0	11.04	7.3				
K (mg/kg)	28.4	292.8	99.5	49.8				
Ca (mg/kg)	353.5	1905.2	878.8	409.8				
Zn (mg/kg)	0.80	2.4	1.3	0.38				
Cu (mg/kg)	1.0	6.9	3.1	1.7				
Organicmatter(%)					1.4	1.9	1.7	0.2
Gravel (%)					0.3	5.8	3.6	1.7

The range of soil EC values indicated that the studied soil was not affected by salt accumulation (Brady, 1998). Further, soil pH and macro and micro nutrient contents also largely varied within the field. Importantly, observed large range of ECa-V values (1 to 40 mS/m) indicated a considerable sensitivity of the EMI based sensor for the soil variability in the Alfisols field (Figure 2).

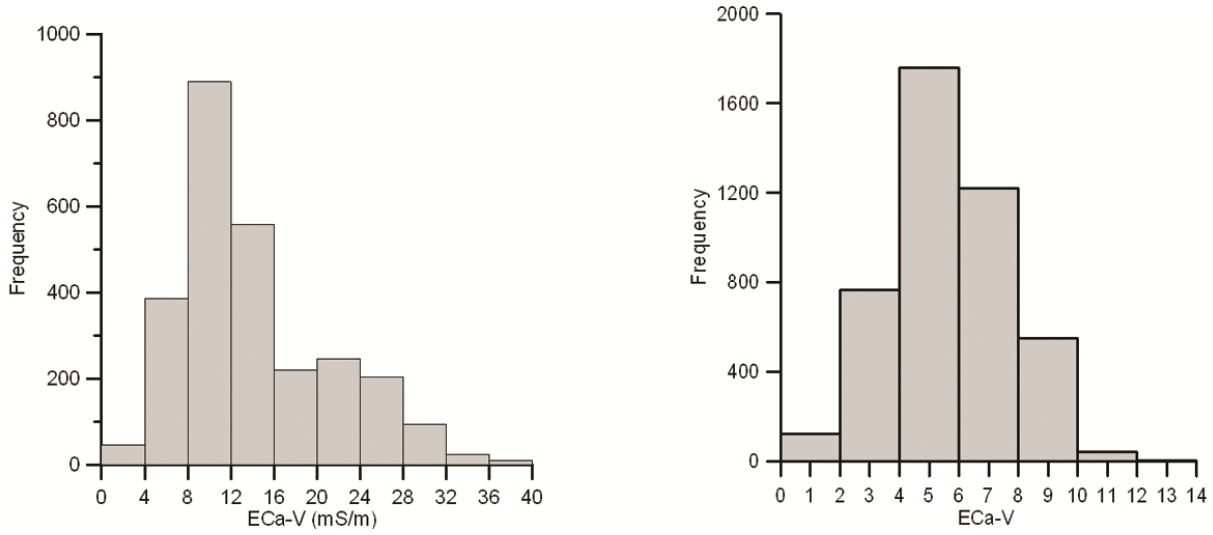

Figure 2. Histograms of ECa-V measured in the Alfisols field (left) and the Ultisols field (right).

A linear model (nugget = 3.1, slope = 0.7) showed the best fit for the variogram calculated for the ECa-V measured in the Alfisols field. The interpolated ECa-V measurements divided the field into two major areas with high and low ECa-V values (Figure 3 (left)). The North-East part of the field was distributed with larger ECa-V values (20 -35 mS/m) and the South-West part contained lower values (1 – 20 mS/m) Two principal components (PCs) were identified and those accounted for 76% of the variance of the data set. PC1 explained 57.8% of the total variance and which was dominated by clay, pH, CEC and ECa-V. PC2 explained 18% of the total variance and which was related to Zn and P contents of the field. Importantly, soil EC did not show a strong relationship with ECa-V (r =0.1). Topsoil clay content showed a significant correlation (r =0.7) with ECa-V values.

Descriptive statistics of the Ultisols field also showed a strong variability of all measured soil properties (Table 1, only the statistics of the topsoil is presented). Compared to the Alfisols, an enrichment of topsoil clay was observed. Subsoil also showed a similar variability in the clay content (20 -41 %). Consequently, a higher range of CEC was also observed both in the top and subsoil. Compared to the Alfisols, the soil electrical conductivity, both in the top (3.6 -7.8 mS/m) and subsoil (2.5 -9.1 mS/m) showed smaller values. However, ECa-V values were surprisingly low (1 to 13 mS/m) which can be attributed probably to the presence of low active clay minerals. Besides, distinct patterns of smaller (southern part) and comparatively larger (Northern part) ECa-V values could be observed (Figure 3 (right)). According to the correlations between the top and subsoil properties and ECa-V (Table 2), the relationships between ECa-V and soil textural fractions were not as strong as in the Alfisols field . However, ECa-V showed a strong correlation with the top and subsoil EC (r=0.6 and 0.8, respectively). Topsoil organic matter also strongly correlated (r=0.8) with ECa-V. Contrary to the findings of Vitharana et al. (2006) the ECa-V values measured in the Ultisols field showed a moderate nega-

tive correlation with top and subsoil (r=-0.5) clay contents. All other properties showed rather poor correlations (r<0.3) with ECa-V. In both fields, the interpolated ECa-V showed contiguous areas of high and low values indicating a strong potential for the use of ECa measurements to delineate potential management zones.

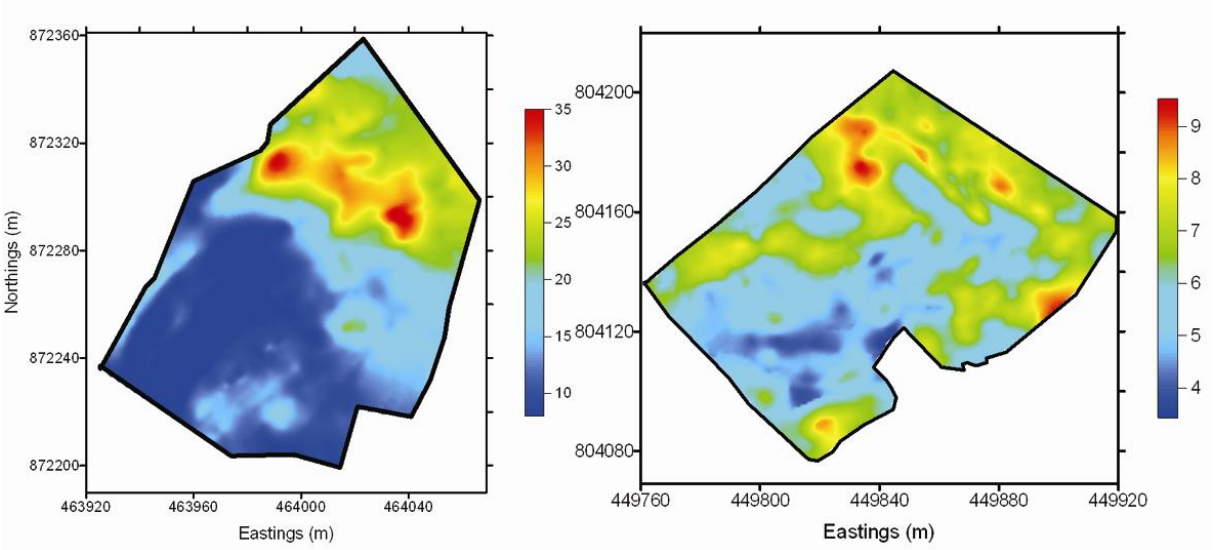

Figure 3. Ordinary krigged maps of ECa-V (mS/m) of (left) Alfisols paddy field and (right) Ultisols tea field

4 Conclusion

Response by EMI based ECa sensing in two tropical soilscapes is useful as a basis for the prediction of primary soil properties representing the soil spatial variability and subsequent delineation of potential management zones. However, absolute ECa values were found to be very low on the Ultisols field reflecting possibly the presence of low-activity clay minerals.

Acknowledgement

Authors acknowledge Vlir-UOS University development cooperation (Belgium) for funding. The CIC Agribusiness and Giragama Tea Estate in Sri Lanka are acknoweldged for providing access to the study fields.

References

DOBERMANN, A., WITT, C. DAVE, D. ET. AL. 2002. Site-specific nutrient management for intensive rice cropping systems in Asia. Field Crop Research **74** 36-77.

BRADY, N. C. AND WEIL, R. R. 1998. The nature and properties of soils: R.R. Weil (ed.). A Simon and Schuster company, Prentice Hall, New Jersey.

JUO, A.S.R., FRANZLUEBBERS, K. 2003. Tropical Soils: Properties and Management for Sustainable Agriculture. Oxford University Press.

PLANT, R. E. 2001. Site-specific management: the application of information technology to crop production. Computers and Electronics in Agriculture **30** 9-29.

VITHARANA, U.W.A., M. VAN MEIRVENNE, L. COCKX, J. BOURGEOIS. 2006. Identifying potential management zones in a layered soil using multiple sources of ancillary information. Soil Use and Management **22** 405-413.

VITHARANA, U.W.A., SAEY, T. COCKX, L. SIMPSON, D. VERMEERSCH, H., VAN MEIRVENNE. M. 2008. Upgrading a 1/20000 soil map with an apparent electrical conductivity survey. Geoderma **148** 107-112.

Accurate electromagnetic measurement of apparent conductivity: issues and applications

R.S. Taylor[1*], J.S. Holladay[2]

[1]*Dualem Inc., Milton, ON, Canada*
[2]*Geosensors Inc., Toronto, ON, Canada*
[*]*E-mail: inbox@dualem.com*

Abstract

Accurate measurement of the apparent electrical conductivity (ECa) of soils by electromagnetic induction is limited by instrumentation error and environmental noise. For applications that require measurements that are comparable over days to years, such as the monitoring of soil status, long-term variation in zero-level ("offset") is typically the critical factor in accuracy. Variation over shorter time-scales ("drift"), such as during a day of surveying, can also produce observable error. Environment noise occurs at the timescale of seconds or less. Drift and noise are readily identifiable in survey data, while offset can be quantified by specialized tests.

Keywords: Electromagnetic Induction, Apparent Conductivity, Stability.

1 Introduction

Reviews of instrument operation and test data inform an assessment of the sources and characteristics of measurement error. The development of practical tests allows surveyors to quantify significant errors in a given set of measurements. Four such tests are the noise test, the drift test, the roll test and the vertical sounding. Systematic measurements at a test site enable an evaluation of (i) test effectiveness and (ii) the relative amplitudes of conductivity fluctuation attributable to instrumental error and variability in soil conductivity.

2 Materials and methods

Instruments with dual horizontal-coplanar (HCP) and perpendicular (PRP) arrays, with array lengths of 1- and 2-m, were used for data acquisition. Test data were acquired at various survey sites by the authors and/or by commercial users of the instruments. A grape-research centre was one such site, at which measurements for a set of traverses and vertical soundings were repeated on sixteen days between May 26, 2012 and October 10, 2012.

3 Results

The general source of environmental noise is atmospheric discharge; nearby electrical equipment can also produce noise. Measurements made with a sensor with dual 1-m arrays (D-1S) provide examples of noise from discharge which, characteristically, has duration of a fraction of a second. For a noise test, the D-1S was positioned about 0.3 m above moderately conductive soil in Milton, ON, at about 2 a.m. on June 24, 2004, and set for the measurement period of 10 s. Figure 1 shows temperature and ECa recorded until about 8 a.m. D-1S temperature shows a very brief initial rise, as the sensor adjusted to outdoor conditions. The sensor then recorded diurnal cooling until a little before 3 a.m., until a warm pulse of air made temperature rise until about 3:30 a.m. A 25 mS/m spike, in both HCP- and PRP-ECa, occurred in a single measurement at about this time. After renewed cooling, a second atmospheric pulse warmed temperature from 5 a.m. until about 6:45 a.m. Several single-measurement spikes accompanied this pulse, with spike amplitude (to 100 mS/m) in PRP ECa generally exceeding that in HCP ECa. Following the pulse, temperature dropped to its lowest level of the session just after 8 a.m., even as the sun rose. Just before temperature reached its minimum, there was a minor rise in temperature at about 8 am, with a coincident spike in HCP ECa.

Noise from nearby devices that transport or use electrical power can range in amplitude from insignificant to unmanageable. Such noise tends to be incoherent in terrain with low conductivity. Where conductivity is generally higher, or has structure in the ground, harmonic fields around devices can interact complexly with the ground, showing variable coherence with certain structures, or causing interference at distances exceeding 100 m.

An example of noise characteristic of a nearby electrical-power line was captured in measurements made with a D-1S in 2004 at the Waterman Farm site of Ohio State University. An overhead power-line borders the southern edge of the site, along with a road and, likely, buried municipal infrastructure. The site itself has drainage tiles and buried pipes for irrigation. Figure 2 shows 1-s D-1S measurements along a profile that began nearly below the power line, and extended 100 m to the north. The profile was traversed at walking speed, with the D-1S within 0.1 m of the surface in a sled. Noise of at least a few mS/m appears to affect measurements within 40 m of the power line. Noise in PRP ECa appears to be relatively greater within 20 m of the power line.

Figure 3 shows measurements that followed those of Figure 1, i.e. after 8 a.m. on June 24, 2004. The atmospheric-noise spike that occurred just after 8 am appears again in Figure 3 (although at different scale), along with another spike at 15.25 h (3:15 p.m.).

Prior to starting this drift test, the D-1S was wrapped in black polyethylene to maximize solar heating. This contributed to the rise in D-1S temperature from about 15 ^{o}C shortly after 8 a.m. to about 37 ^{o}C at the end of the test. Throughout this 22 ^{o}C change in sen-

sor temperature, there was no discernable change in PRP ECa. HCP ECa was about 27 mS/m at 8 a.m., and stayed closest to that value until the sensor started its period of most-rapid warming slightly after 12 p.m. During the afternoon, as clouds caused some irregularity in warming from from 20 °C to 37 °C, HCP ECa fluctuated though a range from slightly less than 26 mS/m to 29 mS/m.

The roll test is a convenient means of testing for the development of quasi-stable offset in the zero-level of an array. Figure 4 shows the results (Precision Agronomics Australia, personal communication, 2011) of a roll test of a sensor that incorporates dual arrays of both 1-m and 2-m length (D-21S). The sensor has been in service since 2008.

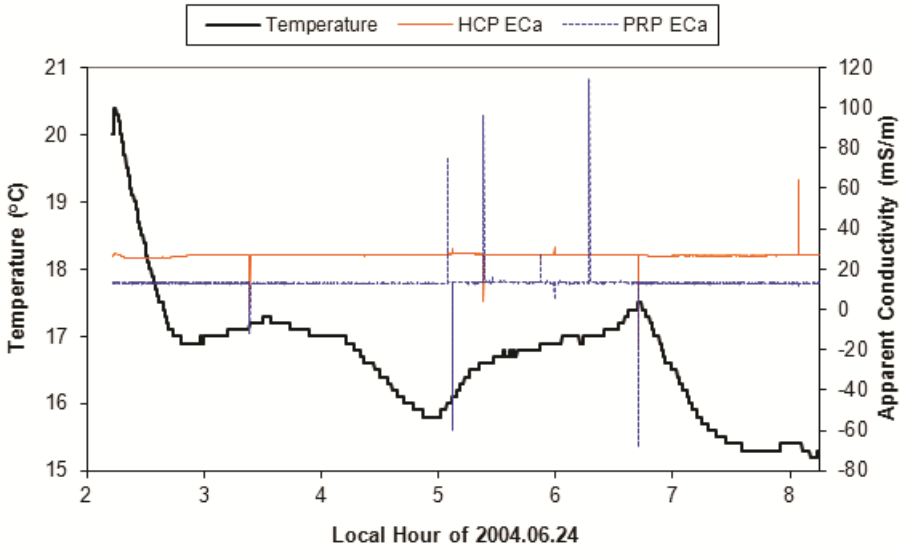

Figure 1. Examples of atmospheric noise with a 1-m dual-array sensor.

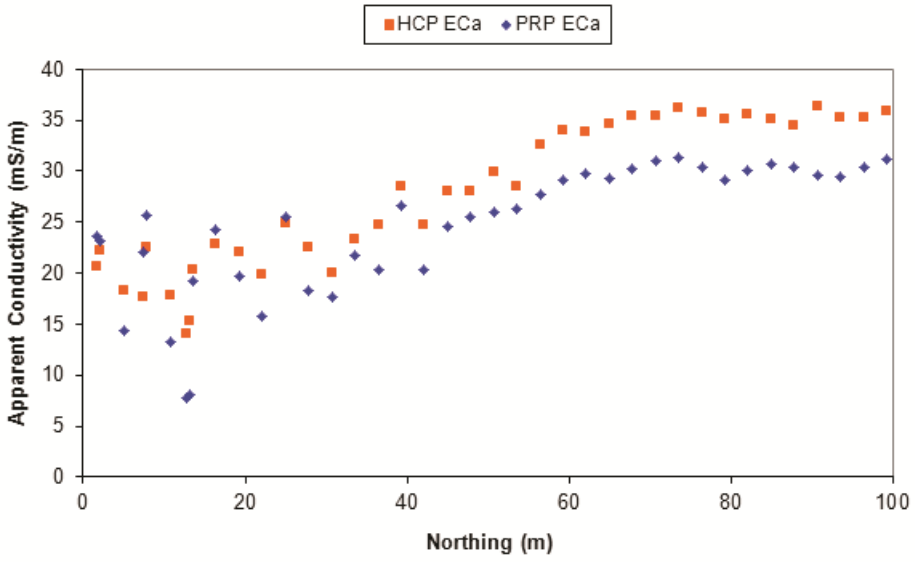

Figure 2. An example of electrical-power noise with a 1-m dual-array sensor.

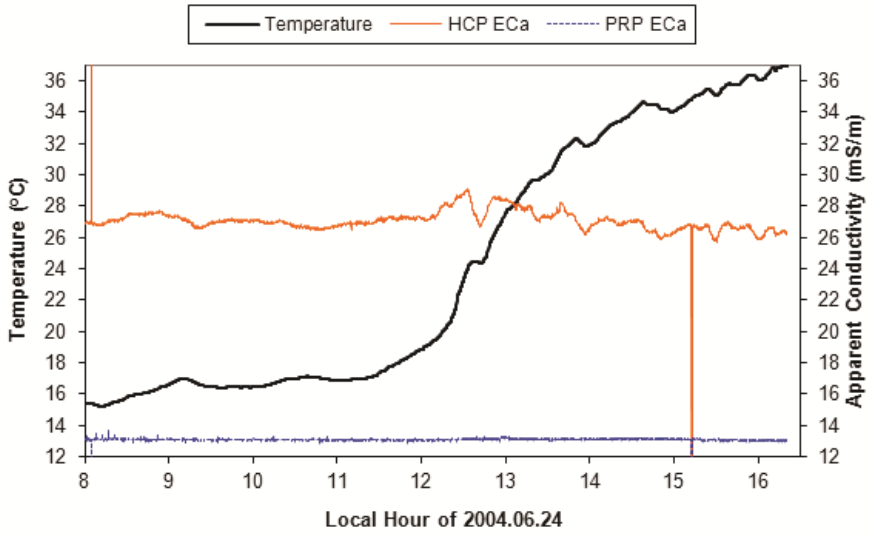

Figure 3. Example of thermal drift in a 1-m dual-array sensor.

If a PRP array is rotated 180 degrees about its long axis from its customary position, its measurement will be equal in amplitude but opposite in sign. If an HCP array is raised at least 2 array lengths above the surface and rotated 90 degrees about its long axis from its customary position, its measurement will be reduced by half (Frischknecht, et al., 1991); a further 90-degree rotation will restore full amplitude, etc. The roll-test results of Figure 4 show measurements from a complete long-axis rotation of a D-21S, where the D-21S was held overhead at about 2.2-m height.

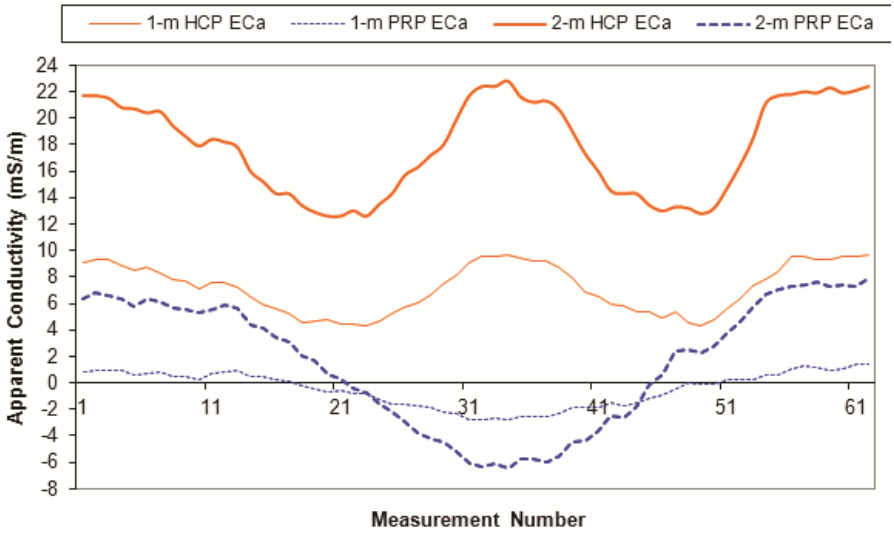

Figure 4. Roll test of a D-21S to test for zero-level offsets.

1-m PRP ECa measurements range from +1 mS/m to –3 mS/m, indicating that there is a zero-level offset of +1 mS/m for this array (i.e. this offset should be added to all measurements). 2-m PRP ECa measurements range from +7 mS/m to –7 mS/m,

indicating that this array has no evident offset. 1-m HCP ECa measurements range from about 9.5 mS/m to 4.5 mS/m, indicating an offset of +0.5 mS/m (which is less than thermal drift of at least 1 mS/m that can be expected with the 1-m HCP array). For an HCP array less than 2 array lengths above the surface, the range of measurements with rotation depends on conductive layering in the earth; however, the range never exceeds the 2:1 ratio. The range of 2-m HCP ECa is from 22 mS/m to 13 mS/m (a ratio slightly less than 2:1) but test does not permit a quantitative estimate of offset.

The vertical-sounding test (e.g., http://www.dualem.com/vertsnd.htm), where ECa is measured through a range of heights from surface to as-high-as-is-convenient, is the standard procedure for calibrating zero-levels, as it enables calibration of longer arrays through robust discrimination between the effects of offset and of layered conductivity in the earth.

Monitoring applications require zero-level stability throughout their duration, so that trends and fluctuations in ECa can be discerned with confidence. Repeated surveys of a test line at the University of Guelph Grape Research Centre (GRC) near Vineland, ON, Canada show fluctuations in ECa that can occur during a growing season.

Measurements were made with a sensor with dual 2-m arrays (D-2S) placed at stations along the east-west test line. Station interval was 0.25 m. The measurement period at each station was 1 s. The D-2S was aligned with the line, with the receiver end to the east. The easting of the measurement indicates the centre-point of the D-2S. The line was located by wooden stakes at eastings 1 and 26. Drain tiles are known to pass beneath the line, at 2.4-m (8-foot) intervals.

The earliest measurements were made on day 147 (May 26) of 2012. The measurements were repeated at roughly two-week intervals. Measurements made on day 220 (August 7) showed the lowest overall conductivity. Measurements made on day 268 (September 24) showed the highest overall conductivity. The latest measurements were made on day 284 (October 10).

Figure 5 shows HCP ECa measurements. Average HCP ECa in mS/m was 34.3 for day 147, 27.9 for day 220, 41.1 for day 268 and 39.3 for day 284; thus, the observed range in average HCP ECa was about 13 mS/m.

Measurements for all days show pronounced minima at stations 1 and 26. Except for day 220, when average ECa was at a minimum, there were local minima of amplitude up to 5 mS/m at about 2.4-m intervals between eastings 3.25 and 23.25. The spacing of the local minima and their disappearance when the soil was driest in early August suggest that they are related to the effect on HCP ECa of soil drainage by the drain tiles.

The pronounced minima at eastings 1 and 26 persist with amplitude greater than 5 mS/m even in the driest conditions. These minima might have a drainage component, but they might also represent in part the negative portion of an HCP response over a conductor that is narrow and shallow relative to the array length of 2 m.

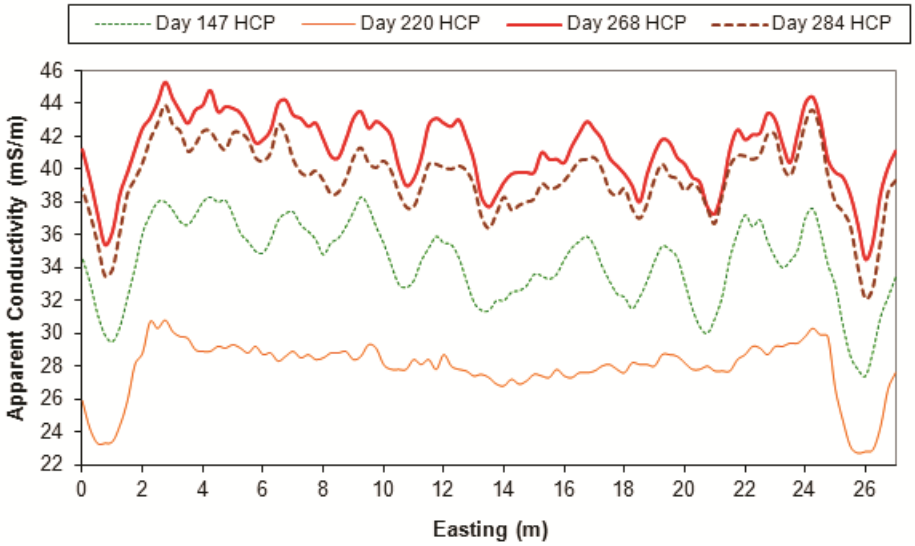

Figure 5. D-2S HCP ECa for GRC Test Line.

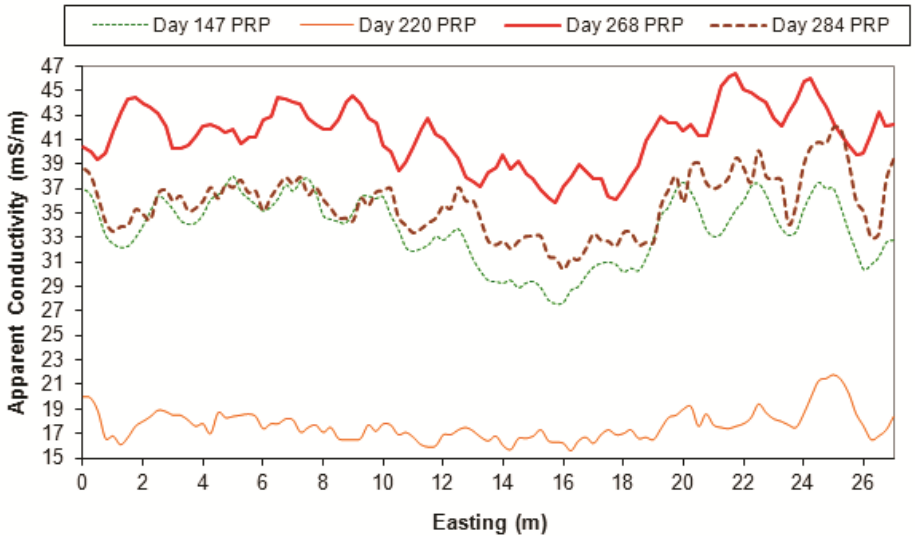

Figure 6. D-2S PRP ECa for GRC Test Line.

Figure 6 shows PRP ECa measurements. Average PRP ECa in mS/m was 33.7 for day 147, 17.7 for day 220, 41.3 for day 268 and 35.7 for day 284; thus, the observed range in average PRP ECa was about 24 mS/m. The PRP measurements show local minima similar in spacing but smaller in amplitude than the local HCP minima. The fluctuations around eastings 1 and 26 are suggestive of the PRP crossover response over a narrow-and-shallow conductor.

Foregoing comments about soil-moisture conditions are based on (i) visual observation during surveying and (ii) a cursory review of meteorological data for the nearby Vineland station (http://www.weatheroffice.gc.ca/city/pages/on-109_metric_e.html). The data include precipitation- and temperature-records. Temperatures were assumed to indicate roughly the loss of moisture due to evaporation.

4 Discussion

Atmospheric noise tends to be polarized into the horizontal plane, so noise can be stronger in arrays that use a horizontal dipole antenna, such as the PRP array. Environmental noise is typically less than 1 mS/m, except for strong and/or nearby electrical discharge or power devices. Where the feature of interest has conductive amplitude of at least 10 mS/m, environmental noise is generally minor, but surveyors should inspect data for the effect of strong sources that might not be visually evident.

Drift is primarily related to changes in ambient temperature, as some components of instrumentation are temperature sensitive. Instruments that are temperature compensated may exhibit drift during temperature change, but typically return to their calibrated zero-levels as temperature stabilizes. Instruments lacking compensation may exhibit different zero-levels at different stable temperatures.

Offset can arise from the aging of instrumentation, and may be precipitated by shock or strong vibration. Roll tests and vertical soundings are used to assess offset. Such tests are sensitive to errors in array positioning, as well as lateral conductivity variations. Such sensitivities are most evident where ambient conductivities are high, whereas offset is distinct where ambient conductivity is negligible. Reorienting the arrays can reveal the presence of lateral conductivity variation. Vertical conductivity variations can introduce ambiguity in HCP roll-test data (while PRP data remain definitive). Quantitative interpretation of HCP vertical sounding data can distinguish offset from the effect of vertical conductivity variation.

The repeated surveys at the GRC show that the ECa of vineyard soil can vary by more than 20 mS/m through the growing season. The effect of drainage structures in the soil was evident when apparent conductivity was relatively high. A multi-year study in somewhat different conditions (Eigenberg, et al., 2006) identified changes in soil wetness and dissolved solids as the major factors of conductivity fluctuation.

5 Conclusions

Error in the measurement of apparent conductivity using best practices with state-of-the art electromagnetic instrumentation is on the order of 1 mS/m. Thus, such measurements can be used to monitor the status of agricultural soils, where status changes cause conductivity fluctuations greater than about 10 mS/m, as at the grape-research centre. Research continues in improving the zero-level stability of such instruments, which should increase the range of applications in the future.

Acknowledgements

The authors thank Dr. Barry Allred of the USDA-ARS for assistance with measurements at Ohio State University, Precision Agronomics Australia for the D-21S roll test, the Uni-

versity of Guelph for making the GRC available for measurements, and Dr. Tony Endres, Cameron Toy and Alicia Beynon of the University of Waterloo for assistance with measurements at the GRC.

References

EIGENBERG, R.A., NIENABER, J.A., WOODBURY, B.L., FERGUSON, R.B. 2006. Soil Conductivity as a Measure of Soil and Crop Status – A Four-Year Summary. SSSA Journal, **70** 1600-1611.

FRISCHKNECHT, F.C., LABSON, V.F., SPIES, B.R., ANDERSON, W.L. 1991. Profiling Methods Using Small Sources. In: Electromagnetic Methods in Applied Geophysics, edited by M.N. Nabighian, Society of Exploration Geophysicists, Tulsa, USA, pp. 105-252.

Heterogeneity of paddy soil characterized by mid-infrared photoacoustic spectroscopy combining RGB-imaging

D. Changwen*, Z. Jianmin, Z. Yongcun

The National Key Laboratory of Soil and Sustainable Agriculture, Institute of Soil Science Chinese Academy of Sciences, Nanjing 210008, China
**E-Mail: chwdu@issas.ac.cn*

Abstract

Fourier transform infrared photoacoustic spectroscopy (FTIR-PAS), as an alternative technique, was applied to characterize paddy soil. The results showed that there was a main cluster for paddy using FTIR-PAS spectra based principal components distribution; however, there also existed variance in paddy soils. The first three principal components (PCA1, PCA2 and PCA3) were used to represent red, green and blue color, respectively, and this RGB color based soil mapping directly demonstrated that paddy soils were very heterogeneous in the space, and could be differentiated into numerous sub-types, which will be useful in soil management.

Keywords: Paddy soil, photoacoustic spectroscopy, principal component analysis, RGB, heterogeneity.

1 Introduction

Paddy soil is one of the typical arable soils in China for rice production, and it not only provides food but also plays role in climatic change (Cao et al., 2006). At the same time, paddy soils are the largest anthropogenic wetlands on earth, and they may originate from any type of soil in pedological terms, but are highly modified by anthropogenic activities (Kögel-Knabner et al., 2010), thus it received considerable studies. Soil properties are inherently variable in nature mainly due to pedogenetical factors (e.g. parental material, vegetation, climate), but heterogeneity can be also induced by farmers' management, especially for the paddy soil with high frequency of alteration of wetting and drying. Recognizing heterogeneity in soils is important as this knowledge can be used for enhancing natural resource management (Liu, et al., 2004), predicting soil properties (Du et al., 2009) and improving sampling designs in future agro-ecological studies (Rossi et al., 2009).

Conventional agro-chemical analysis were usually used to express the soil heterogeneity, but single or limited soil properties is far from enough to reach the purpose, and multiple soil properties are needed. However, the determination of agro-chemical properties is cost and time consuming. Further more, base on soil agro-chemical properties paddy soil can only be identified into limited sub-types; therefore, paddy soils are totally homogeneity due to the similar component. However, paddy soils in different locations took

on significant variance in soil fertility or soil quality, and agro-chemical analysis is difficult to fully characterize the variance even use multiple soil parameters. Thus, an alternative method, infrared spectroscopy (FTIR), has been developed for fast capturing soil information. Infrared spectroscopy is able to detect the different molecular vibrations due to the stretching and binding of the different compounds of a sample when illuminated by an infrared beam (McBratney et al., 2006). In recent years, FTIR-PAS offered an alternative option in monitoring soil, which demonstrated that it was very suitable for high absorbed soil samples with varied morphology and particle size (Du et al., 2009), and more promisingly, its unique feature, i.e. depth profiling function (Du et al., 2010), allows *in situ* three dimension investigating of soil sample, which yielded a infrared spectra with containing more soil information.

The objectives of this study are to fast characterize the heterogeneity of paddy soil using the technique of FTIR-PAS.

2 Materials and methods

2.1 Soil samples

The study area is located in the South east of China (Taihu Lake area). 740 top soil samples (0-20 cm) from this study area (rice field) were collected. As comparison. All the soil samples were air-dried at room temperature, and passed through a 2 mm sieve for use.

2.2 Determination of soil agro-chemical properties

Nine soil agro-chemical properties (pH, SOM, CEC, TN, TP, TK, AP, AK, clay) were determined using routine chemical method, and the statistics of results are demonstrated in Table 1.

Table 1. The statistics of agro-chemical properties of used paddy soil samples (*n* = 740).

	pH	OM (g kg^{-1})	CEC (cmol kg^{-1})	TN (g kg^{-1})	TP (g kg^{-1})	TK (g kg^{-1})	AP (mg kg^{-1})	AK (mg kg^{-1})	Clay (%)
Min	4.61	7.75	4.31	0.36	0.00	6.92	0.93	31.00	5.80
Max	8.42	62.79	32.45	3.14	1.59	24.81	89.37	236.00	41.40
Mean	6.22	29.82	17.28	1.62	0.61	15.01	8.55	83.14	23.05
Std	0.89	7.18	3.95	0.36	0.18	2.55	7.58	24.97	6.45

2.3 Determination of soil FTIR-PAS spectra

Soil FTIR-PAS spectra were recorded using an infrared spectrophotometer (Nicolet 6700, USA) equipped with a photoacoustic cell (Model 300, MTEC, USA); the scans were conducted in the wavenumber region of 500-4000 cm^{-1} with a resolution of 4 cm^{-1}

and a mirror velocity of 0.32 cm s^{-1}, and 32 successive scans were recorded and averaged.

2.4 Data processing

Photoacoustic spectra were pre-processed with a smoothing filter (first-order Savitzky-Golay filter). Soil spectral data and agro-chemical properties data reduction were achieved by the principal component analysis (PCA), and the PCA scores were used to differentiate paddy soils. Matlab was used to do the analysis of the spectral data. A specific color can be obtained by mixing three primary colors (red, green and blue) (Fig.1). The red, green and blue color are represented by the first three principal scores (PCA1, PCA2 and PCA3) from FTIR-PAS spectra based principal component analysis. Therefore, the soil sample in each site can be represented by a specific RGB color, and then spatial interpolation (Kriging method) was applied in the soil mapping to obtain a RGB image.

3 Results and discussion

3.1 Characterization of paddy soils and black soils using FTIR-PAS

Figure 1 shows the FTIR-PAS spectra of paddy soils and black soils. Totally 10 visible absorption bands were obtained in the FTIR-PAS spectra of paddy soils (Fig. 2 a). The absorption bands were located in the wavenumber range of 2800-3700 cm^{-1} (O-H, N-H, C-H vibration), 1800-2100 cm^{-1} (C≡C, C=C-C=C vibration), 1500-1700 cm^{-1} (C=C, C=O, C=N vibration), 1300-1500 cm^{-1} (N-O, N-H, C-H vibration), 900-1200 cm^{-1} (C-O, Si-O vibration), and 600-900 cm-1 (C-C,O-H, C-H vibration).

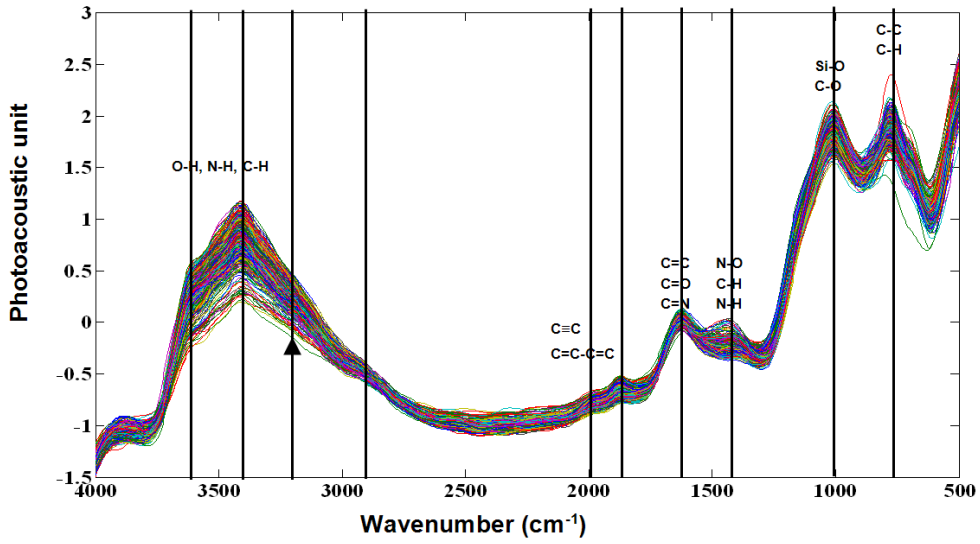

Figure 1. FTIR PAS spectra of paddy soil (*n* = 740).

The spectra of black soils show similar absorption bands as that of paddy soils , however, the relative absorption intensity significantly varied. The absorption around 3600-3650 cm^{-1} was assigned as O-H vibration deprived from 1:1 type kaolin mineral, and it contributed to the spectra of paddy soils; There were significant differences in the absorption around 1800-2100 cm^{-1}, and the absorption bands in the spectra of paddy soils were stronger, and might caused by the anaerobic conditions in paddy soil. In the absorption around 1300-1500 cm^{-1} in the spectra of paddy soils, the absorption peaks in this region were not uniform, which implied the differences in the dynamics of SOM due to the influence of climate and human being. Great differences were also observed from the FTIR-PAS spectra within paddy soils, such as the absorption intensities around 3400 cm^{-1}, it varied from 0.24 to 1.15.

3.2 Heterogeneity of paddy soil using FTIR-PAS

Single or limited agro-chemical property was far from enough to discriminate soil since usually there was large variance in each property, and it was needed to combing multiple agro-chemical properties for meeting this purpose. The determined 9 soil agro-chemical properties were used in the principal component analysis to reduce the dimension to 3, and the explained variances of the first three principal components were 43.41%, 25.47% and 19.32%, respectively. The same analysis was also conducted using FTIR-PAS spectra, and variances of the first three principal components were 57.61%, 19.33% and 6.33%, respectively. Then, three dimension distributions of principal components were plotted (Fig. 2).

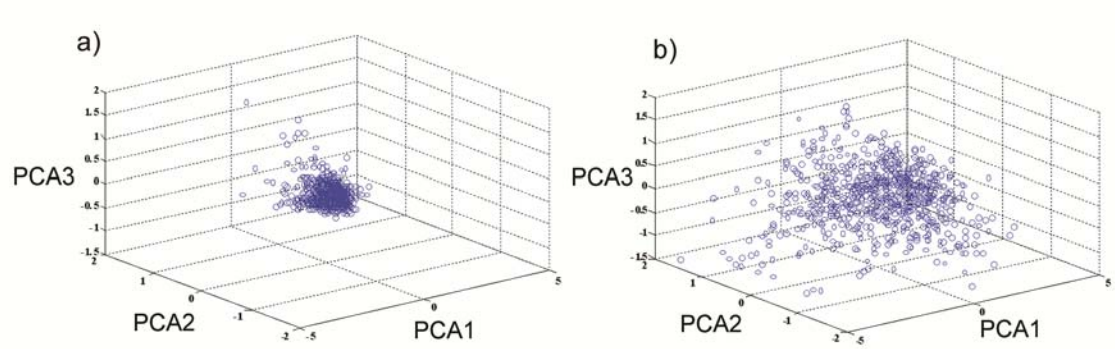

Figure 2. Three dimension distributions of principal components from chemical properties (a) and FTIR-PAS spectra (b) of paddy soil (n = 740).

The cluster density from agro-chemical properties based distribution (Fig. 2a) was significantly higher than that from FTIR-PAS spectra (Fig. 2b), which meant that the heterogeneity of paddy soil expressed by FTIR-PAS was larger than that by agro-chemical properties, and this distribution difference resulted from the information from source data. The soil FTIR-PAS spectra were significantly related with many soil agro-chemical properties, such soil pH, SOM, CEC, clay, TN etc., thus, soil FTIR-PAS spectra could be well presentation of soil components; in addition, the information of soil

components' structures was also hidden in the FTIR-PAS spectra. Therefore, the FTIR-PAS spectra contained the information of both components and structures, and soil FTIR-PAS spectra based distribution was more reliable and accurate.

3.3 Mapping of paddy soil based on FTIR-PAS

Since the heterogeneity was very large with paddy soil, it was needed to further express the heterogeneity in the soil managements; the three components from FTIR-PAS spectra were thereof used to characterize the heterogeneity of paddy soil.

The Euclidean distances were firstly calculated based on the three principal components, and was then in soil mapping through technique of spatial interpolation; soil variances were obvious indicated (Fig. 5a), which showed paddy soils were totally homogeneous, and the main heterogeneity was indicated in the upper middle area. Since the calculation of Euclidean distance only considered the value of principal components, and ignored the vector direction, thereof the large bias might occur in this kind of mapping. Three primary color principle (RGB) was further applied in the soil heterogeneity characterization, which could cover more spectral information. Since the first three principal component occupied enough variance (more 80%), the first three principal components (PCA1, PCA2 and PCA3) were used to represent the red, green and blue colors, respectively, then the color of a specific soil was the superposition of the three colors, and the final RGB color represented a specific soil type. Comparing with the Fig. 5a, strong heterogeneity of paddy soils was directly observed in this soil mapping (Fig. 5b). Red color accounted for big percentage in the North West area, while the rest were dominated by blue and green colors.

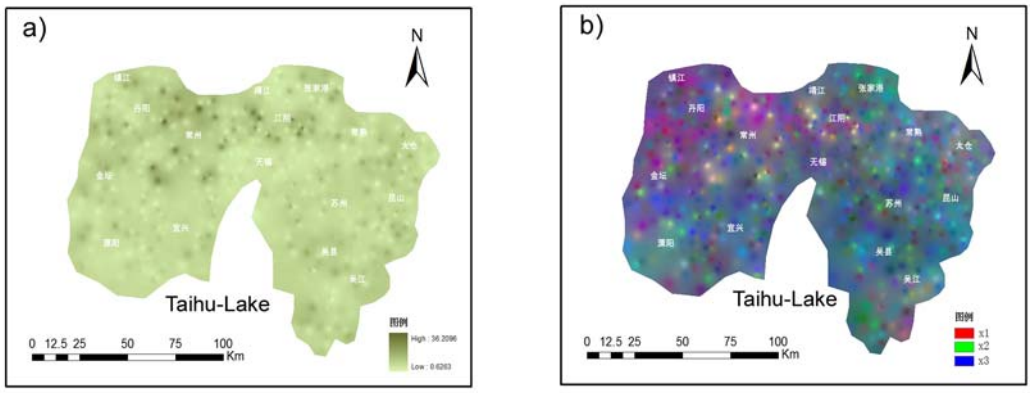

Figure 5. Spatial interpolation soil mapping using Euclidean distances (*n* = 740). (a) Euclidean distance method (b) FTIR-PAS spectra and RGB methods.

The heterogeneity of paddy soils might be the result from climate and varied farming systems, and the inner mechanism needs further exploration considering natural and man-made factors. However, this heterogeneity should be closely related with soil

physical, chemical and biological properties, which showed great potential in the soil management, such as soil fertility evaluation, soil classification and soil digitalization.

4 Conclusions

Paddy soil is significant different from black soil, but single soil agro-chemical property is far from enough to characterize soil type. The technique of FTIR-PAS is a strong sensing tool to characterize paddy soil due to more recorded information including components and their structures. There exists overlapping between paddy soil and black soil, and no absolute boundary can be obtained. FTIR-PAS spectra and RGB imaging based soil mapping demonstrated that paddy soils were very heterogeneous, and could be differentiated into numerous sub-types.

Acknowledgements

This research was supported by the National Natural Science Foundation of China (41130749) and the Knowledge Innovation Program of the Chinese Academy of Sciences (KZCX2-YW-QN411)

References

CAO, Z. H., DING, J. L., HU, Z. Y., KNICKER, H., KÖGEL-KNABNER, I. 2006. Ancient paddy soils from the Neolithic age in China's Yangtze River Delta. Naturwissenschaften, **93** 232-236.

DU, C. W., ZHOU, J. M., WANG, H. W., CHEN, X. Q. 2010. Depth profiling of clay-xanthan complexes using step-scan mid-infrared photoacoustic spectroscopy. Journal of Soils and Sediments, **10** 855-862.

DU C. W., ZHOU, J. M., WANG, H. W., CHEN, X. Q., ZHU, A. N., ZHANG, J. B. 2009. Determination of soil properties using Fourier transform mid-infrared photoacoustic spectroscopy. Vibrational Spectroscopy, **49** 32-37.

KÖGEL-KNABNER, I., AMELUNG, W., CAO, Z. H., FIEDLER, S., FRENZEL, P. 2010. Biogeochemistry of paddy soils. Geoderma, **157** 1-14.

LIU, X., XU, J., ZHANG, M., ZHOU, B. 2004. Effects of land management change on spatial variability of organic matter and nutrients in paddy field: a case study of Pinghu, China. Environmental Management, **34** 691-700.

MCBRATNEY, A. B., MINASNY, B., ROSSEL, R. V. 2006. Spectral soil analysis and inferencesystems: a powerful combination for solving the soil data crisis. Geoderma, **136** 272-278.

ROSSI, J., GOVAERTS, A., VOS, B.D., VERBIST, B., VERVOORT, A., POESEN, J., MUYS, B., DECKERS, J. 2009. Spatial structures of soil organic carbon in tropical forests — a case study ofSoutheastern Tanzania. Catena, **77** 19-27.

Fusion of proximal soil sensing and crop data for fertility zone delineation

G. Halcro, R. Corstanje, A. M. Mouazen*

Environmental Science and Technology Department, Cranfield University, Bedfordshire, MK43 0AL, UK

**E-mail: a.mouazen@cranfield.ac.uk*

Abstract

Management zone (MZ) delineation can be improved by acquiring high-resolution data on soil and crop properties. This hypothesis was tested in this work by directly comparing three nitrogen (N) fertiliser application schemas - each derived from different MZ delineation approaches. A uniform-rate (UR) scheme was used alongside two variable-rate methods. One replicated the traditional mapping of fertility-based MZ (VR1), the other employed soil property maps derived from a visible near-infrared (vis-NIR) on-line sensor (VR2) together with crop data . Results showed that VR2 produced higher yields of oil-seed rape (OSR) per hectare than both the traditional and uniform application in the same study field for the 2012 crop. This method also used less N fertiliser than the UR, indicating that this approach to fertility zone delineation has both economic and environmental benefits.

Keywords: management zones, delineation, sensor, variable-rate, fertiliser.

1 Introduction

Better characterisation of within-field variation of soil properties offers the potential to delineate management zones (MZ), which better reflect their actual variation. Traditional soil sampling and laboratory analysis is currently not cost effective. Recent research has used various sensors to measure single soil chemical and physical attributes in order to reduce costs and improve MZ delineation. However, the soil-water-crop system is too complex to be characterised well by single property sensors (Adamchuk et al., 2004).

Lab-based studies have shown that soil reflectance spectra from visible and near infrared (vis-NIR) wavelength range can provide both direct and proxy measurements of several yield-limiting factors (Kuang et al., 2012) This success has led to research into mobile vis-NIR sensors which could collect soil reflectance *in situ* (Christy, 2008; Mouazen et al., 2005; Shibusawa et al., 2001). These on-line soil sensors provide high resolution data on soil. Prediction models made by correlating reflectance spectra with lab-tested soil samples taken from the survey trench can produce site-specific prediction maps of individual soil properties (Kuang & Mouazen, 2011). These maps can be useful for managing the remediation of soil macro- and micro-nutrients through variable-rate

applications (VRA). However, traditional VRA is based on 1 to 3 samples per hectare. In addition, data fusion techniques can be used to combine multiple layers of yield-limiting soil properties, with maps of in-season crop growth and historical yield from existing sensor systems. The result is a fertility map which can be delineated into MZ and used for managing a fertiliser VRA.

This study seeks to fuse multi-layer data on soil and crop cover, collected at high sampling resolution with proximal sensors, to delineate management zones and determine the improvement on the effectiveness of VR fertiliser applications.

2 Materials and methods

An analysis of three MZ delineation approaches were employed on a 22 ha field of winter oil-seed rape (OSR) in Bedfordshire, U.K (2011-12 season). The following steps were taken to investigate the variation of yield-limiting factors and derive fertility-based MZ.

2.1 Uniform rate (UR) - MZ delineation based on the farmer's usual method

The field was treated as a single MZ with a uniform rate of fertiliser applied in accordance with the UK Department of Environment, Food and Rural Affairs (DEFRA) recommendations for the specific crop, soil type and off-take strategy (i.e. a total of 220 kg ha^{-1} nitrogen).

2.2 Traditional variable rate (VR1) - MZ delineation based on the standard commercial approach

An EMI survey was conducted in 2011 using a Dualem 2S (Dualem, Canada) proximal sensor. The apparent electrical conductivity (EC_A) data were imported into ArcGIS (Esri, USA) and mapped to indicate the spatial variation of soil texture. A total of 30 soil samples were taken from the study field. Chemical analysis was carried out to measure levels of pH, phosphorous (P), potassium (K) and magnesium (Mg). Map layers for each soil property and EC_A were produced by inverse distance weighting (IDW) interpolation. Data fusion of the layers was performed using k-means clustering (Statistica - StatSoft, USA) to group areas of similar fertility. The output was exported into ArcGIS software for visualisation and spatial analysis. Small and irregular-shaped clusters were merged with neighbours of similar fertility to comply with the capabilities of the spreader technology. This resulted in three classes and the delineation of three fertility-based MZ.

2.3 Innovative variable rate (VR2) - MZ delineation based on proximal sensor surveys

A spectral reflectance survey using the on-line vis-NIR sensor platform (Mouazen, 2005) was performed after the 2011 harvest. This used an AgroSpec mobile, fibre type, vis-NIR spectrophotometer (Tec5 Technology for Spectroscopy, Germany) with a

measurement range of 305-2200 nm. A total of 60 soil samples were collected from the bottom of the survey trench opened by the subsoiler to provide lab-tested levels of selected yield-limiting properties (i.e. pH, P, K, Mg, organic carbon (OC), moisture content (MC), total nitrogen (TN), cat-ion exchange capacity (CEC), calcium (Ca). Soil reflectance spectra and chemical analysis values were subjected to partial least squares (PLS) regression analysis to develop soil property prediction models. Each model was applied to the on-line survey data to provide point predictions.

Geostatistical analysis of the prediction results allowed the creation of appropriate variograms. These variograms enabled the production of prediction maps through interpolation by kriging. A survey of the active canopy reflectance was collected using a boom-mounted ACS-210 Crop Circle system (Holland Scientific Inc., USA). NDVI was calculated for each point and mapped using IDW interpolation in ArcGIS. Yield data collected from the previous harvest was interpolated by IDW to provide a further map layer indicating past field fertility variation. All interpolated map layers, representing the variations of nine yield-limiting soil properties, were combined with interpolated maps of in-season crop cover and historical yield data. Clustering and MZ delineation were performed in the manner described for VR1 (above). This resulted in five classes and nine fertility-based MZ.

2.4 Fertiliser Application

The MZ maps provided the basis for the fertiliser recommendation map. The relative fertility of each zone was determined by analysis of the cluster means of the input properties, together with the variations seen in historical yield and NDVI maps. The fertiliser application rates for each MZ class were based on the uniform rate recommended by DEFRA for the crop and soil type. Increments of 12% higher and lower were chosen which reflected the fertility of the MZ. Most fertiliser was applied to the least fertile areas. Variable-rate application of fertiliser was conducted in alternate strips of the same field according to each of the two application maps (e.g. VR1 and VR2). A third strip of UR N fertiliser was added in order to replicate the farmer’s normal application.

2.5 Yield measurement

Yield data from each treatment was collected from a combined-harvester mounted sensor. Two 7.35 m wide strips were cut from each treatment. Care was taken to ensure the harvester had a full header for the entire length of the study area cuts. This enabled accurate calculations of yield per harvested area. The cuts were positioned to avoid the bare earth of the tramlines and the area of overlap at treatment borders.

3 Results and discussion

Interpolated map layers of soil and crop properties were successfully created and merged to produce fertility zones which were used as a basis for VR N application. The yield gained and the fertiliser applied to each cut were calculated (Table 1). A comparison of the cost of the fertiliser input and financial gain from the crop is shown in Table (2). The traditional VR1 approach used less fertiliser than the UR or VR2 and led to a similar yield to that of UR. The highest yield per hectare was achieved using the VR2 approach which would have provided the farmer with the most profit, if it had been used over the whole field.

Table 1. Comparison of fertiliser-used and yield-gained for each delineation approach.

Field (5 Plots)	Area (ha)	Yield (t ha^{-1})	Yield (t)	Fertiliser Input (t)
UR	2.983	5.023	14.990	2.246
VR1	2.981	5.021	14.967	2.091
VR2	2.990	5.174	15.475	2.235
Per ha	Area (ha)	Yield (t ha^{-1})		Fertiliser Input (t ha^{-1})
UR	21.99	5.023		0.785
VR1	21.99	5.021		0.701
VR2	21.99	5.174		0.765

Table 2. Margin calculations; costs were £0.33 $kg^{-1}$for nitrate / sulphur fertiliser and £0.37 kg^{-1} for nitrate fertiliser product and the selling price for the OSR crop was £390 t^{-1}.

Field (5 plots)	Input cost fertiliser £	Yield price £	Margin £
UR	834	5621	4787
VR1	741	5613	4871
VR2	829	5802	4974
Per hectare	Input cost fertiliser £	Yield price £	Margin £
UR	280	1884	1604
VR1	249	1883	1634
VR2	277	1941	1663

Interpolated map layers of soil and crop properties were successfully created and merged to produce fertility zones which were used as a basis for VR N application. The yield gained and the fertiliser applied to each cut were calculated (Table 1). A comparison of the cost of the fertiliser input and financial gain from the crop is shown in Table (2). The traditional VR1 approach used less fertiliser than the UR or VR2 and led to a similar yield to that of UR. The highest yield per hectare was achieved using the

VR2 approach which would have provided the farmer with the most profit, if it had been used over the whole field.

4 Conclusions

The results of this study showed that the innovative VR2 N fertilisation based on site-specific MZ delineated using proximal sensors, including an on-line vis-NIR soil survey, can increase the overall yield of this OSR crop when compared to both UR and traditional VR1 N fertilisation. The innovative approach adopted in this study is an alternative method of producing maps of multiple yield-limiting soil and crop properties which characterises their fine-grained spatial variations. These maps can be used for VR soil fertilisation, such as N, phosphate or lime. In addition, farm efficiency and yield can be increased by improved management zone delineation through the fusion of high resolution data on crop growth and yield-limiting soil properties.

References

ADAMCHUK, V. I., HUMMEL, J. W., MORGAN, M. T.,UPADHYAYA, S. K. 2004. "On-the-go soil sensors for precision agriculture", In: Computers and Electronics in Agriculture, vol. 44, no. 1, pp. 71-91.

CHRISTY, C. D. 2008. "Real-time measurement of soil attributes using on-the-go near infrared reflectance spectroscopy", In: Computers and Electronics in Agriculture, vol. 61, no. 1, pp. 10-19.

KUANG, B., MAHMOOD, H. S., QURAISHI, M. Z., HOOGMOED, W. B., MOUAZEN, A. M., VAN HENTEN, E. J. 2012. "Chapter four - sensing soil properties in the laboratory, in situ, and on-line: a review", In: Donald Sparks, editor: Advances in Agronomy, vol. 114, Academic Press, 30 Corporate Drive, Burlington, MA 01803, USA , pp. 155-223.

KUANG, B., MOUAZEN, A. M. 2011. "Calibration of visible and near infrared spectroscopy for soil analysis at the field scale on three European farms", In: European Journal of Soil Science, vol. 62, no. 4, pp. 629-636.

MOUAZEN, A. M., DE BAERDEMAEKER, J., RAMON, H. 2005. "Towards development of on-line soil moisture content sensor using a fibre-type NIR spectrophotometer", In: Soil and Tillage Research, vol. 80, no. 1-2, pp. 171-183.

SHIBUSAWA, S., ANOM, S. W. I., SATO, S., SASAO, A., HIRAKO, S. 2001. "Soil mapping using the real-time soil spectrophotometer", Proceedings of the 3rd European Conference on Precision Agriculture, (on CD-ROM), pp. 18.

A cost comparison of soil C measurement methods

C. Waring[1*], B. Whelan[2]

[1]*Australian Nuclear Science & Technology Organisation*
[2]*Precision Agriculture Laboratory, University of Sydney*
[*]*E-mail: chris.waring@ansto.gov.au*

Abstract

The high cost of accurately measuring soil carbon mass by soil sampling and laboratory analysis at farm scale has impeded the adoption of carbon farming methods and generation of carbon credits for soil carbon sequestration. Proximal soil sensing methods such as visible - Near Infra Red (vis-NIR) and Fast Neutron Activation Analysis (FNAA) provide a lower cost alternative to standard soil sampling. At the sample rate of 1 / ha soil sampling and laboratory analysis costs A$124 / measure, vis-NIR A$23 – A$37 / measure, and stop & go mode FNAA scanning A$2 / measure. At higher sample rates (22 / ha) with 5m long integrated samples, continuous mode FNAA scanning offers the prospect of affordable (A$0.32 / measure or A$7.27 / ha) soil carbon mapping.

Keywords: cost, soil carbon, soil sampling, vis-NIR, FNAA.

1 Introduction

An ability to cost effectively and accurately measure soil carbon (C) mass at the farm scale is becoming an important international issue for agronomic, economic and environmental reasons. However, using standard soil sampling and laboratory analysis to accurately measure soil C mass at a farm scale is expensive. This is due to the high cost of each individual measurement using standard techniques whilst maintaining a low measurement error requires a large sample set to reflect the full variability of the soil C mass across a farm.

Proximal soil sensing offers an alternate strategy for reducing the cost to accurately measure soil C pools by decreasing the cost per measurement. New C measurement technologies such as vis-NIR reflectance spectroscopy and FNAA scanning can measure C in the field. Consequently the efficacy of farm scale soil C manipulation for agronomic, economic and environmental outcomes requires a full assessment of the impact, measurement error and associated C measurement costs.

The principal objective of this paper is to assess and compare the costs of conventional soil sampling and laboratory analysis with vis-NIR and FNAA proximal soil sensing methods for accurately assessing the mass of soil carbon at the farm scale.

2 Materials and methods

Vis-NIR field equipment is commercially available (eg. Veris P4000 soil probe). A proof-of-concept FNAA scanner has been built and operated in the field by Brookhaven National Laboratory (Wielopolski et al. 2008, 2011a, 2011b). Each FNAA measurement with the BNL instrument takes approximately 60mins. ANSTO is developing a ~100x faster FNAA scanner with otherwise similar performance to the BNL instrument.

2.1 Cost analysis assumptions:

- Farm area is approximately equi-dimensional.
- A nominal farm area of 1,000 ha is used.
- The number of samples taken or measured on the farm is the sampling rate (1,000 samples / 1,000 ha farm = 1 sample/ha).
- An approximation of the distance to the next sample is calculated by assuming samples are evenly distributed over the farm area.
- Costs in Australian dollars (A$ = US$1.04 on 27/3/2013).
- Measurement of soil composition assumes a consultant will drive (average 2 hrs each way) to the farm from a regional centre bringing the necessary sampling (auger) or measurement (FNAA scanning) equipment.
- For work duration > 1 day, overnight accommodation at the local hotel plus a transit time (15 mins each way) to the farm is expected.
- Expensive field instruments are amortized over 7 years, 10% discount rate and 10 operational days per month.

Significant differences in the operational characteristics of the proximal soil sensing C measurement methods (Table 1) results in different field practices. The vis-NIR method is a point measurement of an exposed soil surface. There is a significant difference in the time taken to insert the vis-NIR spectrometer into soft soil (1.5mins) compared to drilling a hole in compacted soil (10mins) and lowering the spectrometer (1.5mins) to obtain a depth profile. Two separate cost cases are prepared for vis-NIR measurement in soft or compacted soil.

FNAA scanning automatically measures a relatively large soil volume (~262,000cm^3 or ~1m dia, ~50 cm deep footprint) beneath the active scanner compared with a 5cm diameter 50cm soil core which has a ~981cm^3 volume. In conventional lab analysis the soil core volume and mass is measured for bulk density, then dried, sieved and subsampled to produce a ~1g sample that is introduced to an analytical instrument for measurement. Each stage is done manually with little potential to reduce labour cost and numerous points for error to be introduced.

Table 1. Comparison of characteristics of soil C measurement techniques

	Soil sampling & laboratory analysis	Vis-NIR & 10% sampled for lab analysis	Fast Neutron Activation Analysis
Depth of measurement	~100cm	~100cm	~50cm
Measured soil volume to ~100cm or 50cm for FNAA	~1962cm^3 sub-sampled to ~1g	~1962cm^3 represented by 100cm line	~262,000cm^3
Ground penetration	yes	yes	no
Measurement Accuracy	high	variable	high
Requires EM zone stratification	yes	yes	no
Total field time / sample	~30mins	~3mins soft soil ~15mins hard soil	~60mins BNL ~0.5mins ANSTO
Measures bulk density in-situ	no	no	yes
Measures soil moisture H_2O in-situ	no	no	yes
Measures other elements / minerals in-situ	no	yes	yes
Time to results	2-6wks	2-6wks	Immediate
Requires post-processing	yes	yes	no
Scope for further automation	small	moderate	Full automation

3 Results

Variograms of soil C distribution from 4 field research sites are used to estimate the relationship between sampling error and sampling rate. Farm scale soil C mass measurement cost may be calculated and optimised for a specific soil C distribution, sampling rate, measurement method and the measurement uncertainty quantified.

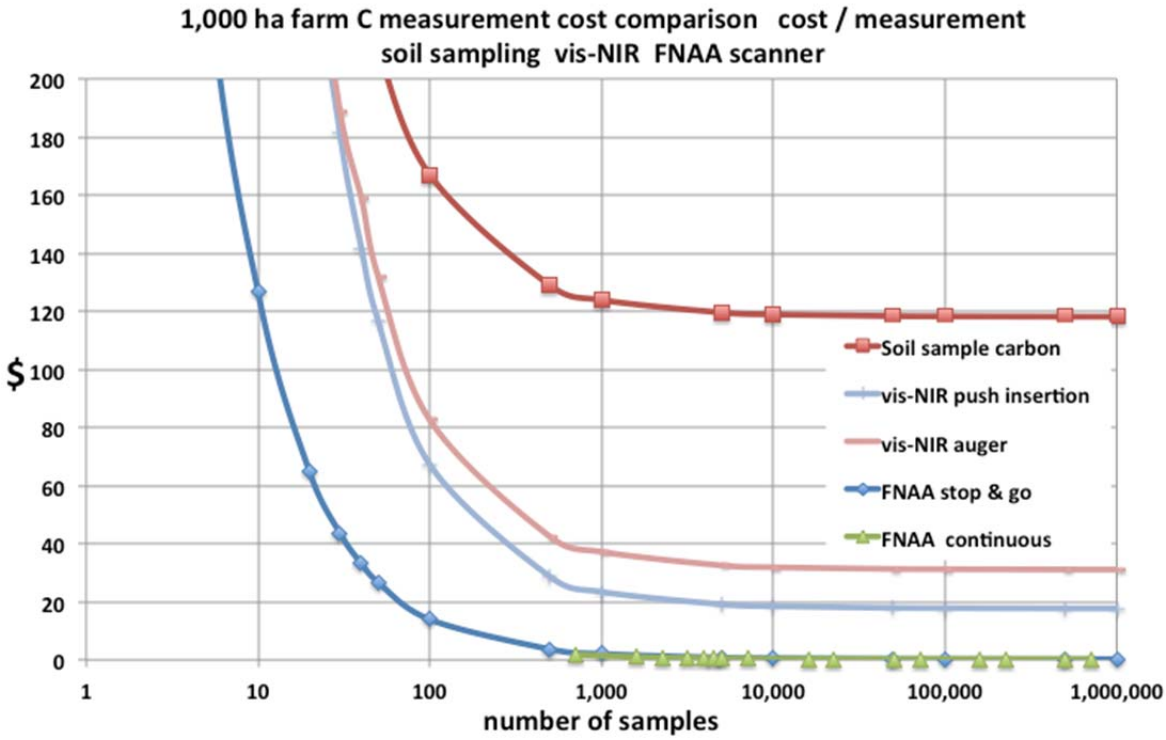

Figure 1. Comparison of cost / measurement for soil C measurement techniques (log scale x-axis is equivalent to sampling rate, ie 1,000 samples = 1 sample / ha).

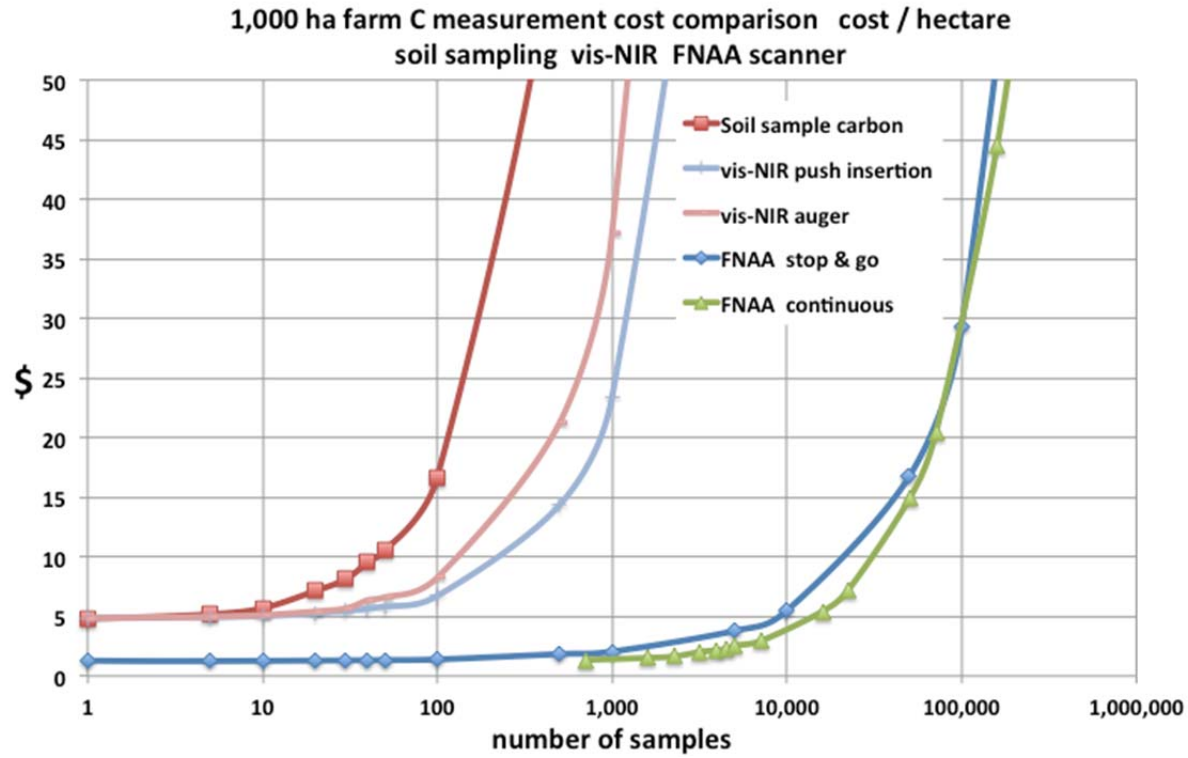

Figure 2. Comparison of cost / hectare for soil C measurement techniques (log scale x-axis is equivalent to sampling rate, ie 1,000 samples = 1 sample / ha).

4 Discussion and conclusions

FNAA scanning measurement differs from traditional soil sampling by requiring one field operator rather than two and excludes the cost of laboratory soil analysis. However, FNAA scanning operational expense does include an amortised FNAA equipment cost. For stop and go FNAA scanning the same number of samples are measured as soil sampling, however the time spent at each sample site is much shorter (30 sec) compared with soil sampling (32 min). Continuous FNAA scanning requires a low speed (1 - 2 km/hr).

Current soil sampling and analysis techniques have little scope for cost reduction because of the fixed labour component and the time taken for reliable field sampling (~A$60). Manual handling of samples in the laboratory for determining bulk density, moisture, and sub-sampling means C analysis cost (~A$13) is small compared to the total lab cost (~A$64). For high sampling rates >1 / ha the total cost / sample is ~A$120 / sample. For low sampling rates the cost / sample escalates with consequent increases in associated sampling error. The estimated comparable cost per sample for measurement by in-situ vis-NIR is A$23 – A$37 and stop & go mode FNAA scanning is between A$2.05 / measure. At higher sample rates (22 / ha) with 5m long integrated samples, continuous mode FNAA scanning offers the prospect of affordable (A$0.32 / measure or A$7.27 / ha) soil carbon mapping.

References

WIELOPOLSKI, L., HENDREY, G., JOHNSEN, K.H., MITRA, S., PRIOR, S.A., ROGERS, H.H., TORBERT, H.A. 2008. Nondestructive system for analyzing carbon in the soil. Soil Science Society of America Journal, 72, 1269-1277.

WIELOPOLSKI L., A. CHATTERJEE, S. MITRA, R. LAL. 2011A. *In situ* Determination of Soil Carbon Pool by Inelastic Neutron Scattering: Comparison with Dry Combustion. Geoderma, 160:394-399.

WIELOPOLSKI L. 2011B. Nuclear Methodology for Non-destructive Multi-elemental Analysis of Large Volumes of Soil. In “Planet Earth 2011 - Global Warming Challenges and Opportunities for Policy and Practice”, Elias G. Carayannis (Ed.), ISBN: 978-953-307-733-8, InTech, Chapter 21:467-492.

Coupling imaging O_2 dynamics with greenhouse gas emissions in soil amended with animal manure

K. Zhu[1*], S. Bruun[1], M. Larsen[2], R. N. Glud[2], L. Stoumann Jensen[1]

[1]*Department of Plant and Environmental Sciences, University of Copenhagen*
[2]*Nordic Center for Earth Evolution, University of Southern Denmark*
[*]*E-mail: kunzhu@life.ku.dk*

Abstract

A laboratory study was carried out to image O_2 dynamics in soil amended with animal manure. An O_2-specific planar optode was mounted on a flank of a chamber filled with soil. Manure was either homogeneously mixed into soil or placed as a layer in the soil. The spatial distribution of O_2 in soil was monitored by planar optode, and fluxes of N_2O and CO_2 were routinely measured. This work documented that the planar optode was an excellent tool for visualizing and quantifying O_2 dynamics in soil, and demonstrated the importance of O_2 dynamics for the greenhouse gas emissions following manure application.

Keywords: O_2, planar optode, manure, N_2O.

1 Introduction

O_2 is a key parameter for the biogeochemistry of soil; however, its spatial distribution in soil has rarely been reported in detail. Single ectrochemical and optical sensor has been used to quantify soil O_2 concentrations both in the laboratory and in situ (Richelt *et al.*, in press). Planar optodes have proven to be a versatile and powerful analytical tool to resolve the O_2 dynamics in complex substrates such as soil (Askaer *et al.*, 2010, Blossfeld *et al.*, 2011). This has provided novel insights into the dynamics and interlink between O_2 and other soil gases (Elberling *et al.*, 2011). O_2 availability is one of key factors influencing N_2O emissions from nitrification and denitrification processes in soil; therefore we followed O_2 dynamics and N_2O emission after manure addition in agriculture soil.

2 Materials and methods

2.1 Planar optode sensor

The measuring principle of planar O_2 optodes has previously been described in detail (Larsen *et al.*, 2011). Briefly, the planar optode sensor of the present study consisted of an O_2 quenchable luminophore, Pt(II)-tetrakis(pentafluorophenyl)porphyrin (PtTFPP), which was combined with an antenna dye (the coumarin dye Macrolex® fluorescence yellow 10GN). The platinum (II) complex, the antenna dye and polystyrene were dis-

solved in a 4% wt/wt polystyrene matrix, using chloroform as solvent, and then coated onto a 125-um thick polyester support foil. The excitation light was supplied by seven blue light-emitting diodes, λ-peak= 447.5 nm (Luxeonstar, SR-02-R0500, Canada), equipped with short-pass filters (475 nm) (TECHSPEC, USA). The ratio between the red and green luminescence emitted from indicator and antenna dye, respectively, was used to quantify the O_2 concentration by means of a digital single-lens reflex camera (Canon EOS 1100D). The camera was equipped with a quality prime macro lens (Sigma 50 mm F2.8 EX DG Macro) covered by a long-pass emission filter (OG 530, Schott) to remove any reflected blue light from the excitation source. The camera chip consisted of 2145 ×1428 pixels, which, at the given optical configuration and with a pixel binning of 2, covered an effective area of 12 × 8 cm with a theoretical spatial resolution of 112 × 112 µm pixel^{-1}. Each image was obtained from the average of 3 images taken within 2 second.

2.2 Experimental setup

The experimental mesocosm consisted of a transparent glass aquarium (200 × 100 × 50 mm), equipped with the O_2 optode sensor on one side (Figure 1). Solid fraction of pig manure was either homogeneously mixed with soil (SOL_M) or placed as a layer in the soil (SOL_L). Soil without any amendments (CON) was included as a control in this set-up. The soil water potential was set to -5 KPa (94.5% of water-filled pore space), and temperature was 25 °C. N_2O samples was manually taken from headspace and analysed by gas chromatography.

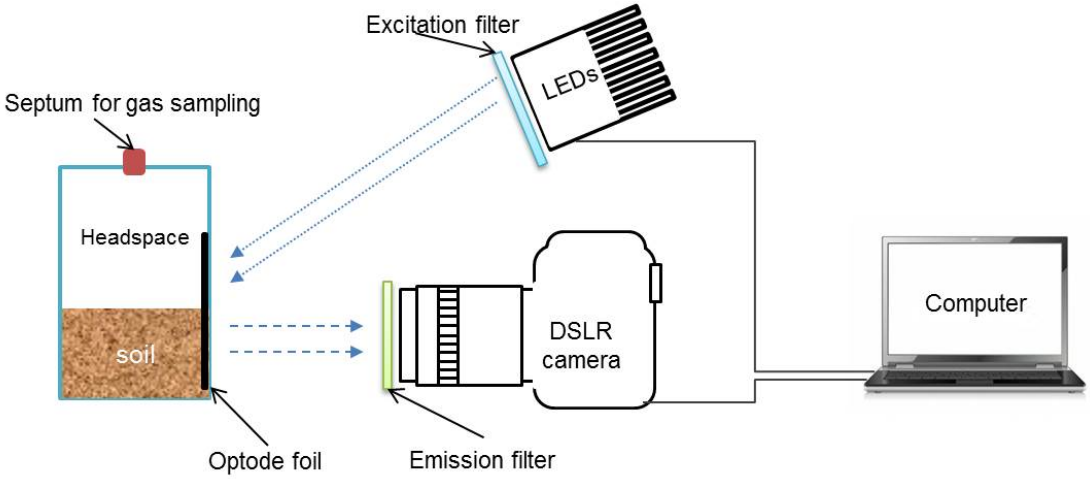

Figure 1. Illustration of the experimental setup used for O_2 measurement (not to scale). Excitation filter: 475 nm short-pass filter; Emission filter: 530 nm long-pass filter. Adapted from Larsen *et al.* (2011).

3 Results and discussions

For each treatment, a series of 48 optode images were recorded with a 30 minutes interval between each image. During the image series, no drift was observed in the signal. Five images from each treatment were presented in Figure 2 and reflected the dynamics of O_2 in soil. Around 50% of O_2 was consumed in CON after 5 hours (Figure 2), In contrast, anoxia quickly developed in soil with manure addition. For SOL_M, anoxia developed more or less homogenously, while in SOL_L, anoxia gradually spread from the centerline where manure was added.

N_2O emissions were quite low (less than 5 µg kg^{-1} soil h^{-1}) both at SOL_L and SOL_M during the first 4 hours (Figure 3). Then N_2O emission exponentially increased as anoxia developed in both of the treatments, although the patterns of O_2 consumption in the two treatments were different. CO_2 emission rates in SOL_M gradually increased during the first 12 hours, and they were a little higher than that from SOL_L, where O_2 availability for organic matter in manure was more limited.

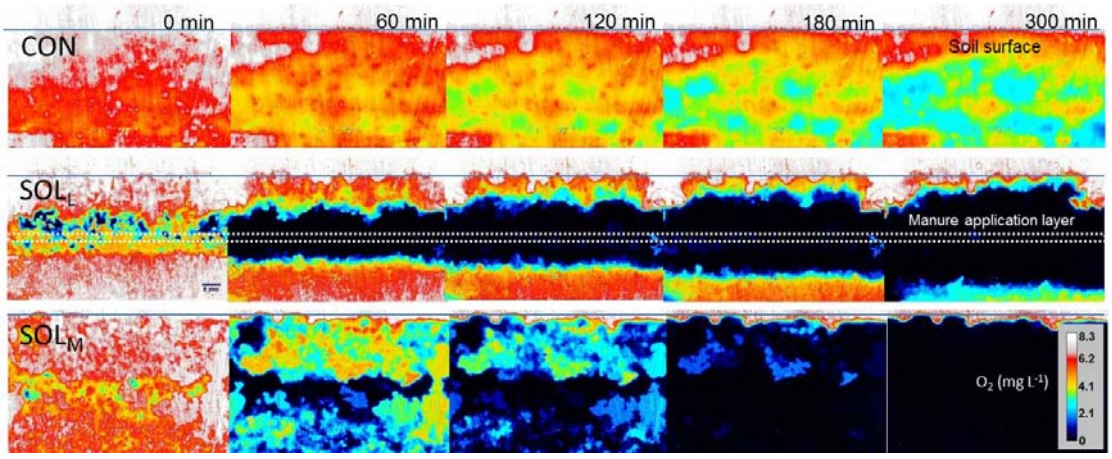

Figure 2. Images of O_2 contents in soil profiles. CON: soil without amendment; SOL_L: soil amended with a manure layer; SOL_M: soil mixed with manure.

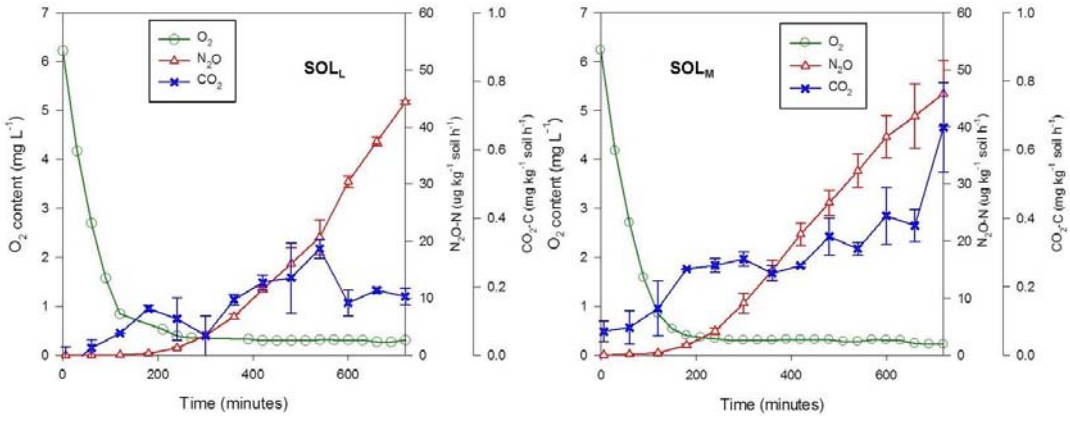

Figure 3. Average O_2 content and N_2O, CO_2 emission in SOL_L and SOL_M.

Evidently the N_2O emission rates were stimulated by the gradual development of anoxia. Nitrous oxide is primarily formed in two processes, nitrification and denitrification (Khalil *et al.*, 2004; Mørkved *et al.*, 2006). Nitrification requires O_2 and will prevail along the oxic interphases (for instance at the soil-air interphase). In absence of O_2, denitrification in soil trends to progress all the way to N_2 with little N_2O loss (Stevenson 1982). Therefore, if the N_2O is formed from denitrification, it is also likely to occur in the oxic-anoxic interphases.

4 Potential and limitations

The advantage of the optode in studying O_2 dynamics in soil is that it is a non-destructive method, with possibilities for a good time-resolution. It also provides information on 2D spatial variation with a sub-millimeter resolution. As pointed out by Glud (2008), planar optode imaging is always preformed along a wall, and the optode sensor acts as an impermeable wall, which might distort the three-dimensional O_2 distribution, therefore, interpreting 2D O_2 images and deriving quantitative estimates should always be done with caution.

5 Conclusion

The O_2 optode was proved to be useful for measuring O_2 distribution in soil with manure addition. It also shows the potential to link soil O_2 status and emissions of greenhouse gases and improve our understanding on the spatial dynamics of the processes leading to the formation of important greenhouse gases. With layered manure in soil, the anoxic layer was formed rapidly around the manure site. With mixed distribution, anoxic conditions developed more broadly, and both treatments subsequently resulted in N_2O emission with similar patterns. Homogeneously distributed manure enhanced more CO_2 emissions than that of layering-added manure. The formation of N_2O is likely to occur in the soil regions under sub- or low oxic conditions, which are favoured for N_2O producing processes.

References

ASKAER, L., ELBERLING, B., GLUD, R. N., KÜHL, M., LAURITSEN, F. R.,JOENSEN, H. P. 2010. Soil heterogeneity effects on O2 distribution and CH4 emissions from wetlands: In situ and mesocosm studies with planar O2 optodes and membrane inlet mass spectrometry. *Soil Biology and Biochemistry* 42(12): 2254-2265

BAKKEN, L., DÖRSCH, P. 2007. Nitrous Oxide Emission and Global Changes: Modeling Approaches. In *Biology of the Nitrogen Cycle*, 381-395 (Eds B. Hermann, J. F. Stuart, S. J. F. William E. NewtonA2 - Hermann Bothe and E. N. William). Amsterdam: Elsevier.

BLOSSFELD, S., GANSERT, D., THIELE, B., KUHN, A. J., LOSCH, R. 2011. The dynamics of oxygen concentration, pH value, and organic acids in the rhizosphere of Juncus spp. *Soil Biology & Biochemistry* 43(6): 1186-1197.

CHEN, D., LI, Y., GRACE, P., MOSIER, A. 2008. N_2O emissions from agricultural lands: a synthesis

of simulation approaches. *Plant and Soil* 309(1): 169-189.

ELBERLING, B., ASKAER, L., JORGENSEN, C. J., JOENSEN, H. P., KUHL, M., GLUD, R. N., LAURITSEN, F. R. 2011. Linking Soil O(2), CO(2), and CH(4) Concentrations in a Wetland Soil: Implications for CO(2) and CH(4) Fluxes. *Environmental Science & Technology* 45(8): 3393-3399.

GLUD, R. N. 2008. Oxygen dynamics of marine sediments. *Marine Biology Research* 4(4): 243-289.

KHALIL, K., MARY, B., RENAULT, P. 2004. Nitrous oxide production by nitrification and denitrification in soil aggregates as affected by O2 concentration. *Soil Biology and Biochemistry* 36(4): 687-699.

LARSEN, M., BORISOV, S. M., GRUNWALD, B., KLIMANT, I., GLUD, R. N. 2011. A simple and inexpensive high resolution color ratiometric planar optode imaging approach: application to oxygen and pH sensing. *Limnology and Oceanography-Methods* 9: 348-360.

MØRKVED, P. T., DÖRSCH, P., HENRIKSEN, T. M., BAKKEN, L. R. 2006. N2O emissions and product ratios of nitrification and denitrification as affected by freezing and thawing. *Soil Biology and Biochemistry* 38(12): 3411-3420.

RICKELT, L. F.; ASKAER, L.; WALPERSDORF, E.; ELBERLING, B.; GLUD, R. N.; KÜHL, M. (IN PRESS). An optode sensor array for long term in situ O2 measurements in soil and sediment. *J Environ Quality.*

STEVENSON F. J. 1982. Nitrogen in agricultural soils. American Society of Agronomy. Madison, Wisconsin, USA.

Measurements of soil water storage at field scale via Cosmic Ray neutron Sensing

G. Baroni*, C. A. Rivera Villarreyes, S. E. Oswald

Institute of Earth and Environmental Science, University of Potsdam, Karl-Liebknecht-Strasse 24-25, 14476, Potsdam, Germany
**E-mail: baroni@uni-potsdam.de*

Abstract

Cosmic Ray neutron Sensing (CRS) is a novel, non-invasive land-surface methodology used for the measurement of soil moisture. This method has been tested at two agricultural sites in Germany. The results show that integral soil moisture derived from CRS compared quantitatively with mean values derived from a network of classical devices. However, the natural fast neutrons were affected also by water stored within snow and biomass. These results suggest that CRS can be a valuable ground-truthing option to detect integral water storage at intermediate scale, though corrections have to be introduced to separate the contribution of the different compartments.

Keywords: cosmic ray neutron sensing, soil moisture, water biomass, snow.

1 Introduction

Soil moisture is a key variable controlling hydrological and energy fluxes at different spatio-temporal scales. Characterization of its variability is still one of the major challenges within the soil and hydrological sciences (Vereecken et al., 2007). During the last few decades, an increasing number of studies have focused on the estimation of soil moisture using different approaches (Robinson et al., 2008). These studies have covered mainly relatively small scales using point measurements (Western et al., 2002), or larger scales (large catchments and whole planet) using remote sensing observations (Kerr et al., 2001). Few methodologies have aimed to detect soil moisture at an intermediate scale (Christiansen et al., 2011). Recently, integral quantifications of seasonal soil moisture in the root zone at the field scale have become also possible with a novel methodology introduced by Zreda et al. (2008) named Cosmic Ray Neutron Sensing. Indeed, the Cosmic Ray Neutron Sensing shows a lot of potential for covering data requirements for large-scale studies, e.g. calibration and validation of both land surface models and satellite-based soil moisture retrievals (Zreda et al., 2012). However, there are still some open questions on this methodology that have to be evaluated with further research. Overall, our research has focused on (i) testing the Cosmic Ray Neutron Sensing in different conditions and (ii) evaluating its integration into hydrological models. In the present contribution, results from studies conducted at two experimental sites

are presented. Implications for soil and hydrological applications are discussed in the final conclusions.

2 Materials and methods

2.1 Cosmic ray neutron sensing method

Fast neutrons are generated naturally at the air-ground interface by the interactions between secondary of cosmic rays and land surface materials. These neutron fluxes are mainly influenced by hydrogen, providing the possibility to measure water stored at the land surface via neutron data alone. Based on these interactions, Zreda et al. (2008) showed that neutron detectors, i.e. specific proportional counters, installed in the field are able to measure the soil moisture over an area of ca. 30 ha and down to a depth from 10 to 70 cm. This represents a unique passive and non-invasive method for measurements of soil moisture at intermediate spatial scale ideal for many soil and hydrological applications.

2.2 Experimental sites and experimental design

The research is conducted at two experimental sites in Germany: (i) a cropped field close to Potsdam (Bornim, Brandenburg) since 2010 (Figure 1, left) and (ii) a mountainous agricultural catchment (Schaefertal, Harz Mountains) since middle of 2011 (Figure 1, right). Classical FDR soil moisture devices (Frequency Domain Reflectometry, MR2 probes Delta-T Devices Ltd., Cambridge, UK) and meteorological data are used for calibration and validation of the CRS approach.

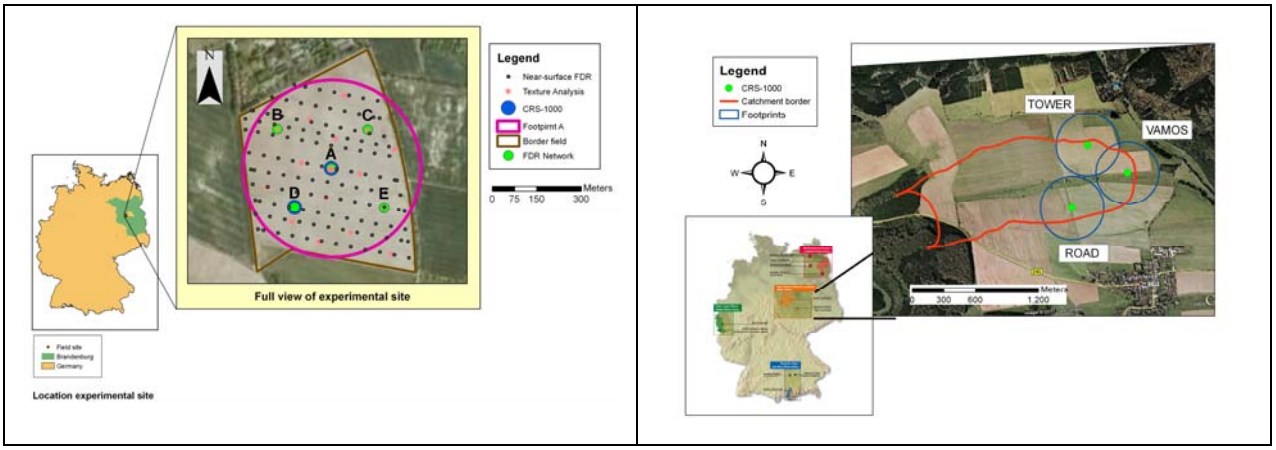

Figure 1. Experimental sites in Bornim (left) and Schaefertal (right, part of the TERRENO observatory, http://teodoor.icg.kfa-juelich.de/overview-de). Positions and footprint of the Cosmic Ray probes (CRS) are reported together with the FDR soil moisture network.

The cosmic-ray fast neutron detector, CRS-1000 (Hydroinnova, Albuquerque, USA), was mounted on a pole at a height of 1.5 m above-ground. The neutron counter of the CRS probes was set-up to record counts every 20 min; neutron counts were

subsequently integrated into one-hour time intervals. FDR probes were distributed in different locations and three depths (5 cm, 20 cm and 40 cm). Before installation of FDR sensors, soil cores were extracted at same locations for calibration. During the crop seasons, measurements of crop height were taken. This information was used to distinguish major crop growing stages during the monitoring period.

2.3 Calibration/validation methods

Previous to the calibration of the CRS probe, fast neutrons were corrected by changes of local atmospheric pressure (Rivera Villarreyes et al., 2011), incoming cosmic radiation (Zreda et al., 2012) and atmospheric water vapor (Franz et al., 2012). In the case of incoming cosmic-rays, the neutron monitoring station Jungfraujoch in Switzerland (www.nmdb.eu) was chosen as reference station.

According to the literature (Desilets et al., 2010), the relation between the soil moisture neutron counts can be defined as follow:

$$\theta_{CRS} = \frac{0.0808}{N / N_o - 0.372} - 0.115 \quad (1)$$

where θ_{CRS} is the volumetric soil moisture [m^3 m^{-3}], N is the counting rate [cph] and N_o [cph] is the counting rate in dry conditions. One approach for calibration is then to consider the value of soil moisture measured during a sampling campaign inside the footprint to fit the value of N_0 (Zreda et al., 2012). In the present study, instead of a sampling campaign, part of the soil moisture detected by the FDR network is considered as the basis for calibration and the rest of the time series is considered for validation.

3 Results and discussion

Figure 2 shows as example the results obtained in Bornim site in two different seasons. It has to be noted that the calibration period (defined by the arrow) corresponds to the initial stage of the sunflower period when the biomass was low. The results show that soil moisture derived from Cosmic-ray probes (~30 ha and below 40 cm) compared quantitatively with mean values derived from a network of classical devices. However, neutrons were affected also by water stored in snow and partly by biomass. In particular, CRS overestimates soil moisture during the crop growing season. The deviations from the FDR fits well the crop height, used as a simple proxy for the water biomass dynamics. In winter period, the snow dynamics shows to be the dominant hydrogen contribution and the CRS strongly deviates from real soil moisture values (i.e., values nominally higher than saturation).

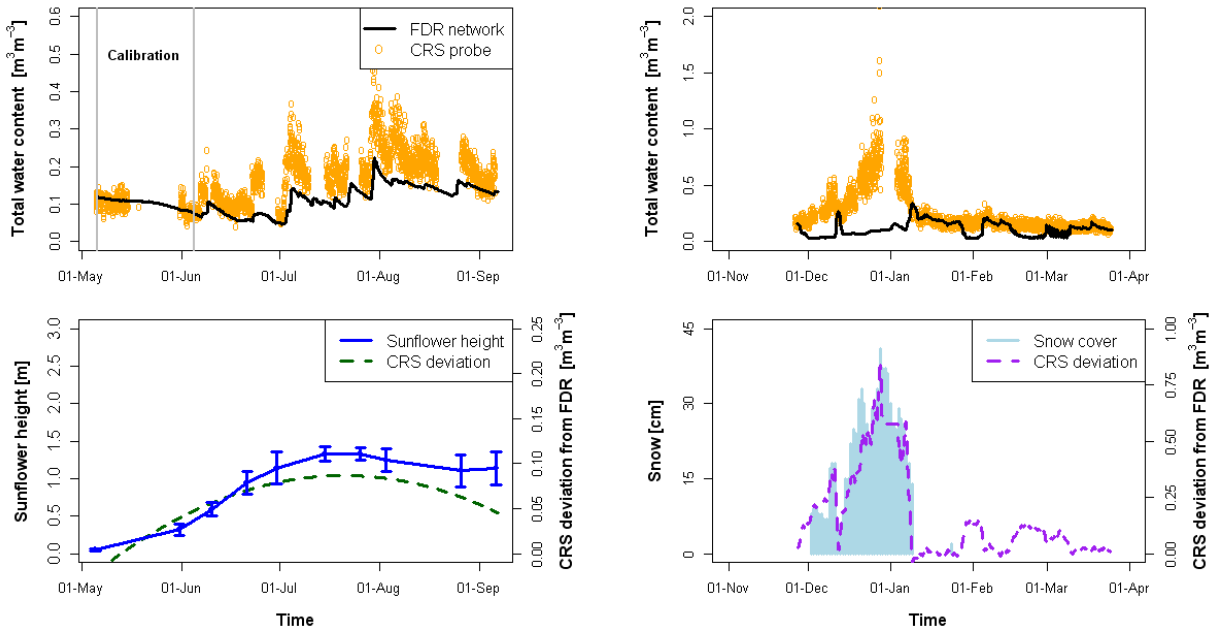

Figure 2. Soil moisture measured by CRS (dots) and by FDR (line) in summer (a) and winter season (b). Lower graphs show the deviations between CRS and FDR in comparison to the crop height (c) and to the snow (d).

4 Conclusions

The results suggest that the Cosmic Ray Neutron Sensing can be a reliable land-surface methodology to detect integral soil water storage at intermediate scale. This methodology can be then applied in different contexts, from ground-truthing of remote sensing products to validation of hydrological modeling and improvement of agricultural water management. Combinations with other geophysical methods (e.g., gamma ray) are also possible with bigger detectors mounted on a vehicle for specific soil mapping.

However, as expected, the neutrons are affected by all H pools, therefore corrections have to be introduced to separate contribution from different compartments (e.g., soil moisture, intercepted water, snow, biomass, etc.). Limitations in its applicability can arise when complex variability of hydrogen pools in time and space is present for the specific experimental site. Further research is expected to contribute in this direction.

Acknowledgements

The research was supported by the Helmholtz Centre for Environmental Research (UFZ) and TERENO (Terrestrial Environmental Observatories) by providing the Cosmic ray probes. Furthermore, we thank Dr. Robin Gebbers of the Leibniz Institute for Agricultural Engineering Potsdam-Bornim (ATB) for conveying the experimental site and supporting our field work in Bornim.

References

CHRISTIANSEN, L., LUND, S., ANDERSEN, O.B., BINNING, P.J., ROSBJERG, D., BAUER-GOTTWEIN, P. 2011. Measuring gravity change caused by water storage variations: Performance assessment under controlled conditions. Journal of Hydrology 402, 60–70.

DESILETS, D., ZREDA, M., FERRÉ, T.P.A. 2010. Nature's neutron probe: Land surface hydrology at an elusive scale with cosmic rays. Water Resources Research 46.

FRANZ, T.E., ZREDA, M., FERRE, T.P.A., ROSOLEM, R., ZWECK, C., STILLMAN, S., ZENG, X., SHUTTLEWORTH, W.J. 2012. Measurement depth of the cosmic ray soil moisture probe affected by hydrogen from various sources. Water Resources Research 48.

KERR, Y.H., WALDTEUFEL, P., WIGNERON, J.-P., MARTINUZZI, J., FONT, J., BERGER, M. 2001. Soil moisture retrieval from space: the Soil Moisture and Ocean Salinity (SMOS) mission. IEEE Transactions on Geoscience and Remote Sensing 39, 1729–1735.

RIVERA VILLARREYES, C.A., BARONI, G., OSWALD, S.E. 2011. Integral quantification of seasonal soil moisture changes in farmland by cosmic-ray neutrons. Hydrology and Earth System Sciences 15, 3843–3859.

ROBINSON, D.A., CAMPBELL, C.S., HOPMANS, J.W., HORNBUCKLE, B.K., JONES, S.B., KNIGHT, R., OGDEN, F., SELKER, J., WENDROTH, O. 2008. Soil Moisture Measurement for Ecological and Hydrological Watershed-Scale Observatories: A Review. Vadose Zone Journal 7, 358.

VEREECKEN, H., KASTEEL, R., VANDERBORGHT, J., HARTER, T. 2007. Upscaling Hydraulic Properties and Soil Water Flow Processes in Heterogeneous Soils. Vadose Zone Journal 6, 1.

WESTERN, A.W., GRAYSON, R.B., BLÖSCHL, G. 2002. Scaling of soil moisture: a Hydrologic Perspective. Annual Review of Earth and Planetary Sciences 30, 149–180.

ZREDA, M., DESILETS, D., FERRÉ, T.P.A., SCOTT, R.L. 2008. Measuring soil moisture content non-invasively at intermediate spatial scale using cosmic-ray neutrons. Geophysical Research Letters 35.

ZREDA, M., SHUTTLEWORTH, W.J., ZENG, X., ZWECK, C., DESILETS, D., FRANZ, T., ROSOLEM, R. 2012. COSMOS: the COsmic-ray Soil Moisture Observing System. Hydrology and Earth System Sciences 16, 4079–4099.

Validation of an on-the-go soil pH sensing system to derive pH maps for variable lime application

H.-W. Olfs*, A. Borchert, D. Trautz

Faculty of Agricultural Science and Landscape Architecture, University of Applied Sciences Osnabrueck, Am Kruempel 31, D-49090 Osnabrueck, Germany
**E-mail: h-w.olfs@hs-osnabrueck.de*

Abstract

To evaluate on-the-go soil pH sensing as basis for variable lime applications under German soil and weather conditions 30 arable fields (2 to 45 ha) were scanned and a lime application experiment was carried out (no lime/lime rate based on field average pH/lime rate adjusted to zone specific pH). Substantial in-field soil pH variability was revealed irrespective of field size. Both liming strategies resulted in higher soil pH, but pH variability was lower for the site-specific treatment. A precise liming strategy will result in a more homogeneous soil pH status within a field and lead to better growing conditions for crops.

Keywords: in-field variability, precision lime application, soil pH mapping, Veris MSP.

1 Introduction

It is well-known that soil pH affects soil nutrient availability as well as plant growth. Furthermore substantial in-field variability exists for soil pH (Bianchini and Mallarino, 2002; McBratney and Pringle, 1997). However, due to related costs for manual soil sampling and for analysing huge amounts of samples in the lab the required density of soil pH measurements per field to derive reliable soil pH maps could not be achieved in the past. To overcome these constraints a fully automated on-the-go soil pH mapping system (Veris MSP) has been developed (e.g. Adamchuk et al., 1999; Lund et al., 2005¸ Viscarra Rossel and McBratney, 1997). Using this pH sensing system it is possible to obtain spatial information on soil pH at the required high resolution. This online pH sensor has been extensively validated under US farming conditions. To evaluate the use of Veris MSP data for decisions on lime application rates under German soil and weather conditions lab and field trials were conducted.

2 Materials and methods

From 2009 to 2011 a series of 30 arable fields (2 to 45 ha; sandy to loamy soil texture) located in north-western Germany was scanned using the Veris MSP equipped with a pH and an EC unit (Olfs et al., 2012). The sampling density ranged from 30 to 90 samples per hectare (working speed 5 - 13 km/h; spacing between passes 7.5 - 30 m). On

17 fields reference samples were collected from the topsoil layer (0 - 30 cm) in zones with low, medium and high pH values for lab pH analysis. The transformation of Veris MSP pH values into German standard pH values was either done based on pH data from all 17 selected fields or by only taking the three reference samples from each individual field into account.

To evaluate the effect of liming strategies based on soil pH maps a lime application experiment was carried out on a 7.1 ha field (soil texture loamy sand). Before sowing maize this heterogeneous field was scanned with the Veris MSP sensor. Based on the soil pH map five zones were identified with different pH status (pH ranging from 5.1 to 5.8). In each zone three treatments were installed: (1) no lime, (2) lime rate based on field average or (3) lime rate adjusted to the pH in the specific zone. At tasseling leaf samples were taken for nutrient analysis using standard lab protocols. After harvest soil samples were taken from the 0 to 30 cm soil layer in each plot and pH was measured after air drying and sieving (< 2mm mesh) in a 0.01 molar $CaCl_2$ solution at a 1 : 2.5 ratio.

3 Results and discussion

Substantial in-field variability for soil pH (0.9 - 3.1 Veris MSP pH units) was found for the 30 fields studied in this series irrespective of the field size indicating that it is reasonable to adapt liming rates within a field. In agreement with results reported from surveys conducted *in North America* (e.g. Bianchini and Mallarino, 2002; *Brouder et al., 2005; Lauzon et al., 2005) soil pH can vary* even within small distances revealing that a high sampling density is necessary to derive reliable lime application maps (Olfs et al., 2010).

Due to differences between lab and on-the-go pH measurement procedures (i.e. 2 hours reaction period and use of a 0.01 molar $CaCl_2$ solution cause an increased desorption of H^+ ions from soil particles resulting in lower pH value under lab conditions) Veris MSP pH values have to be converted before pH data can be used for the lime recommendation scheme utilized by the German advisory service. For this transformation using pH values from the 3 individual reference samples per field was considerably better compared to a generalized regression based on data sets obtained from all fields of the study (mean difference 0.08 vs. 0.26 pH units). The procedure based on field individual referencing also takes into account that other interference factors (e.g. changes in the signal strength from the electrodes due to abrasion/deterioration, water quality, temperature) might alter on-the-go pH measurement under field conditions (Olfs et al., 2012).

At tasseling growth stage maize leaf concentrations for most nutrients (N, P, K, S, and Mg) were not affected by the 3 different liming strategies (data not shown). However, for micro nutrients like Mn and Zn, which are considered as particular relevant for maize growth, significantly higher leaf concentrations were found in the “no lime” treatment

(Fig. 1). As availability of these micro nutrients is controlled by soil pH, an excessive lime rate might decrease soil solution concentrations and as a consequence plant uptake will be considerably hindered.

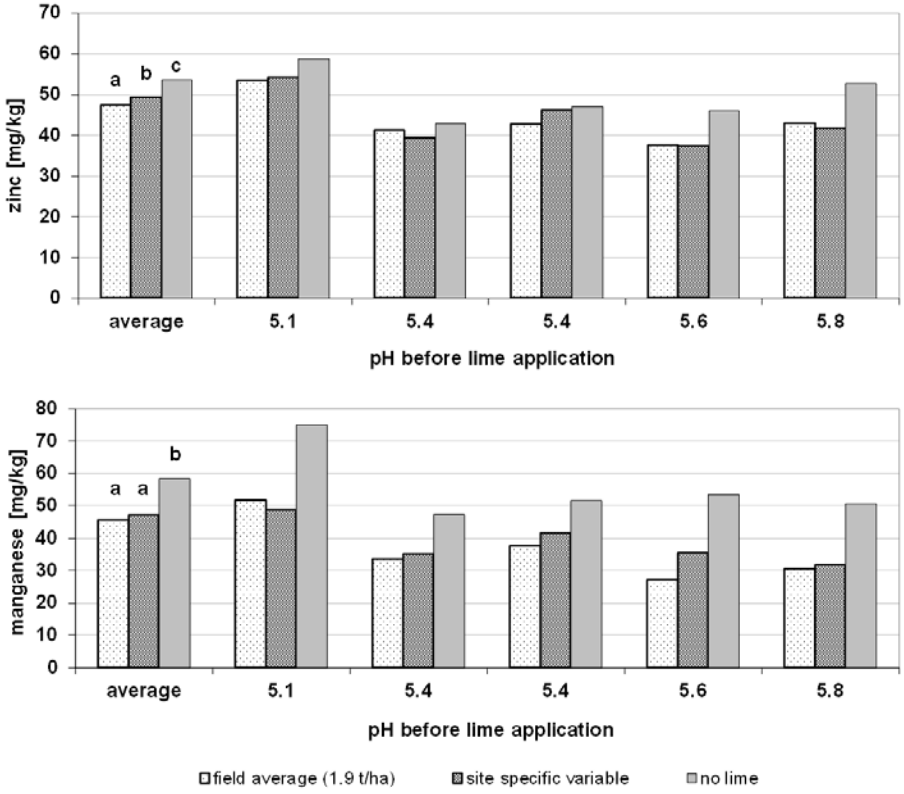

Figure 1. Zinc (top) and manganese (bottom) concentrations in maize leaves at tasseling growth stage for 3 different lime application strategies (different letters above columns indicate significant differences at the 5% level)

As expected both liming strategies resulted in significantly higher soil pH values compared to the no lime control (Fig. 2). Although average pH values for the “field average” and the “site specific variable” lime treatments do not show significant differences between each other, it has to be emphasized that pH variability between the 5 subplots was much lower for the site-specific adapted liming treatment (pH range 5.9 - 6.1) compared to the “field average lime rate” (pH range 5.6 - 6.2). For one subplot the target range for the pH values (5.5 - 6.2) is not achieved and for one subplot the pH value is at the upper limit.

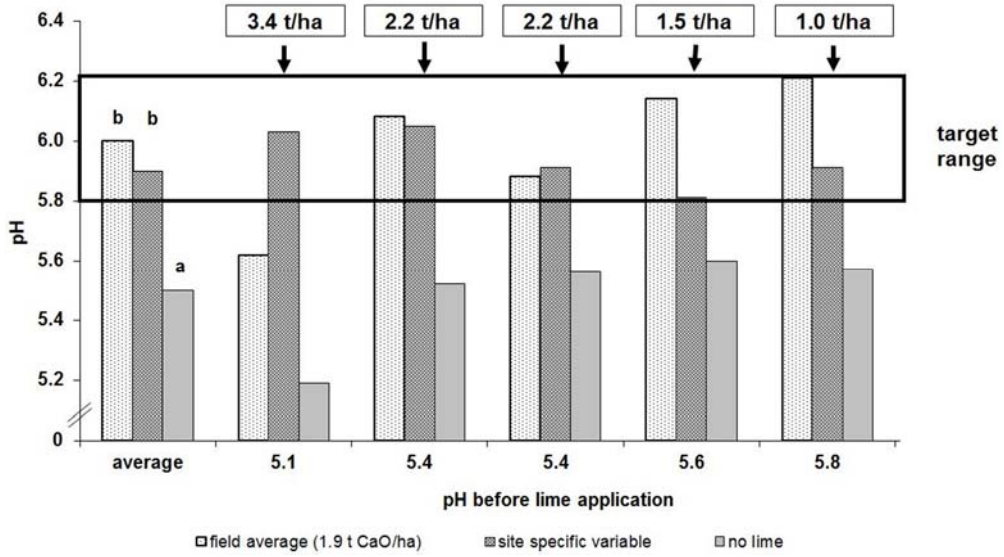

Figure 2. Soil pH at harvest (average of 5 selected zones and form each zone) for 3 different lime application strategies (different letters above columns indicate significant differences at the 5% level)

4 Conclusions

Data on soil pH in-field heterogeneity obtained with the Veris MSP on-the-go system reveal that it is reasonable to adopt liming rates for arable fields in north-western Germany. However, Veris MSP pH values have to be converted into pH data conform to the German lime recommendation system. Such a precise liming strategy will result in a more homogeneous soil pH status within a field compared with standard farm practice and finally improve soil nutritional status and crop growing conditions.

Acknowledgements

This research project was funded by grants from the NBank (Hannover, Germany) in the framework of the European Fond for Regional Development. Thanks to the farmers for allowing us to do the on-the-go pH-measurement and to our colleague Herbert Pralle for developing software tools to enable routine data management at field level to localize zones for reference sampling and for data exploration and visualization at office level.

References

ADAMCHUK, V.I., MORGAN, M.T., ESS, D.R. 1999. An automated sampling system for measuring soil pH. Trans. ASAE **42** 885-891.

BIANCHINI, A.A., MALLARINO, A.P. 2002. Soil-sampling alternatives and variable-rate liming for a soybean-corn rotation. Agron. J. **94** 1355-1366.

BROUDER, S.M., HOFMANN, B.S., MORRIS, D.K. 2005. Mapping soil pH: Accuracy of common soil sampling strategies and estimation techniques. Soil Science Society of America Journal **69**

427-441.

LAUZON, J.D., O'HALLORAN, I.P., FALLOW, D.J. VON BERTOLDI, A.P., ASPINALL, D. 2005. Spatial variability of soil test phosphorus, potassium, and pH of Ontario soils. Agronomy Journal **97** 524-532.

LUND, E.D., ADAMCHUK, V.I., COLLINGS, K.L., DRUMMOND, P.E., CHRISTY, C.D. 2005. Development of soil pH and lime requirement maps using on-the-go soil sensors. In: Precision Agriculture 2005, edited by J.V. Stafford, Wageningen Academic Publishers, Wageningen, The Netherlands, pp. 457-464.

MCBRATNEY, A., PRINGLE, M. 1997. Spatial variability in soil - implications for precision agriculture. In: Precision Agriculture ´97: Proceedings of the 1st European Conference on Precision Agriculture, edited by J.V. Stafford, BIOS Scientific Publishers Ltd, Oxford, UK, pp. 3-31.

OLFS, H.-W., BORCHERT, A., TRAUTZ, D. 2010. Validation of on-the-go soil pH-measurements – primary results from Germany. In: Proceedings of the 10th International Conference on Precision Agriculture, edited by R. Khosla, Colorado State University, Denver, CO, USA, [CD].

OLFS, H.-W., BORCHERT, A., TRAUTZ, D. 2012. SOIL pH maps derived from on-the-go pH-measurements as basis for variable lime application under German conditions: Concept development and evaluation in field trials. In: Proceedings of the 12th International Conference on Precision Agriculture, edited by R. Khosla, [CD-Rom].

VISCARRA ROSSEL, R.A., MCBRATNEY, A.B. 1997. Preliminary experiments towards the evaluation of a suitable soil sensor for continuous 'on-the-go' field pH measurements. In: Precision Agriculture ´97: Proceedings of the 1st European Conference on Precision Agriculture, edited by J.V. Stafford, BIOS Scientific Publishers Ltd, Oxford, UK, pp. 493-502.

Comparison of soil pH measurement in a non tilled vineyard: conventional laboratory values vs. 3100 Veris soil pH sensor readings

J.R. Marques[1], J.M. Terrón[2], J. Blanco[2], F. Pérez[2], F. Galea[2], F.J. Moral[3*], C. Alexandre[1], J. Serrano[1], L.L. Silva[1]

[1]Universidade de Évora, Departamento de Engenharia Rural, Instituto de Ciências Agrárias e Ambientais Mediterrãneas (ICAAM), Portugal
[2]Centro de Investigación "La Orden - Valdesequera", Gobierno de Extremadura, Spain
[3]Universidad de Extremadura, Departamento de Expresión Gráfica, Badajoz, 06006, Spain
[*]E-mail: fjmoral@unex.es

Abstract

This work pretends to compare the soil pH measured by the 3100 Veris sensor with the conventional soil sampling in a specific soil condition of a non tilled vineyard. Whereas high density data was obtained with the soil pH sensor, which were used to delineate a pH surface using a geostatistical algorithm, conventional laboratory values were divided in two sets, depending on their location in a 3 or a 12 years non tilled vineyards. Comparison leads to some differences, but varibility was minor when the area not mobilized for 12 years was considered.

Keywords: soil pH, vineyard, proximal sensing.

1 Introduction

Some physical and chemical soil properties, as pH or organic matter content, can have an important influence on the vegetative development of crops. These properties can affect grapevine root system; a decrease in soil acidity, combined with a low water infiltration and an increase of bulk density, can cause a reduction in the root density (Morlat et al., 1993). Thus, the soil acidity is a basic property in the dynamic of biochemical balance and, if the soil is far from the neutrality, the vegetative growth of plants can be limited. In general, the range of soil pH in vineyards presents different values, finding productive crops on soils with pH from 4.5 to 8.5, as in calcareous soils (Ribérau-Gayon, 1982).

Soil pH affects decisively the vineyard nutrition, so it is important to know its spatial variation. Effects of a low pH on the soil lead to a lower availability of basic nutrients, such as phosphorous or potassium, and an increase in zinc, iron, and aluminium toxicity, among others, in addition to a less availability of organic matter due to a lower decomposition rate. Contrarily, a high soil pH can lead to similar effects in the availability of nutrients and toxicity, and is able to modify the structural stability and increase the or-

ganic matter consumption due to the higher microbiological activity (Hidalgo-Togores, 2006).

Precision agriculture utilizes rapidly evolving electronic information technologies to modify land management in a site-specific manner as conditions change spatially and temporally. During the last years, a diversity of several soil sensors has become an invaluable tool for identifying soil physicochemical properties influencing crop yield. Nevertheless, one must be aware that in some particular conditions these types of sensors must be tested and their data must be validated. Thus, the objective of this case study is compare, in non tilled vineyards, the soil pH on-the-go readings measured by the 3100 Veris sensor with the soil pH data obtained by standard methods of soil pH assessment.

2 Material and methods

The field research was conducted at a farm called Herdade de Pinheiros, in the proximity of Évora city, Portugal. The study area is approximately 66 ha and soil pH was sampled using two different methodologies: i) 1627 measurements were taken with the 3100 Veris pH sensor Manager (Veris Technologies Inc., Salina, KS, USA), and ii) 58 samples were taken from the top layer (0-20 cm) using a stratified sampling scheme (17 and 41 samples from a 3 and a 12 years non-tilled vineyard area respectively). Conventional soil sampling occurred in 2011 spring and Veris pH sensor sampling occurred in 2012 autumn. The 66 ha site is occupied with a non-tilled vineyard and, consequently, in the top layer there was a high concentration of vineyard roots. The 3100 Veris sensor works on-the-go mode. Sampled lines are 15 m average spaced and the Veris soil samples, in each line, are 20 m averaged spaced. Each sample is collected by a device located in the rear of the platform, which is raised and get in contact with two antimony pH electrodes. The pH values are obtained considering the average voltage outputs of the two electrodes. Each measurement is followed by an electrodes wash cycle.

3 Results and discussion

After the sampling process, the 3100 Veris pH values were 10 m grid interpolated, using the ordinary kriging algorithm, and a pH surface was obtained. To compare the two methodologies (low density conventional pH sampling and high density 3100 Veris pH sampling), a database was constructed considering the 58 conventional soil pH values and, for the same positions, 58 pH values obtained through pH surface. The last values were computed considering the averaged pH of a 60 m diameter circle centered in the 58 conventional soil sampling positions (Fig 1).

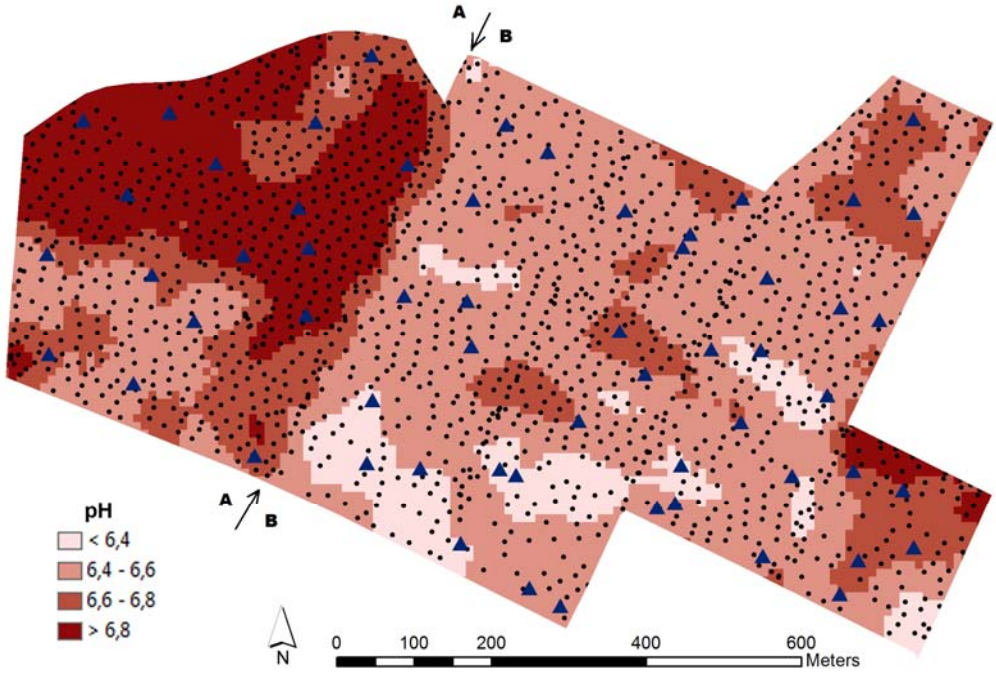

Figure 1. Soil pH samples (triangles) and 3100 Veris pH sensor readings (dots) in the vineyard not mobilized for 3 years (A) and the vineyard not mobilized for 12 years (B). Kriged surface from soil pH sensor data is also shown.

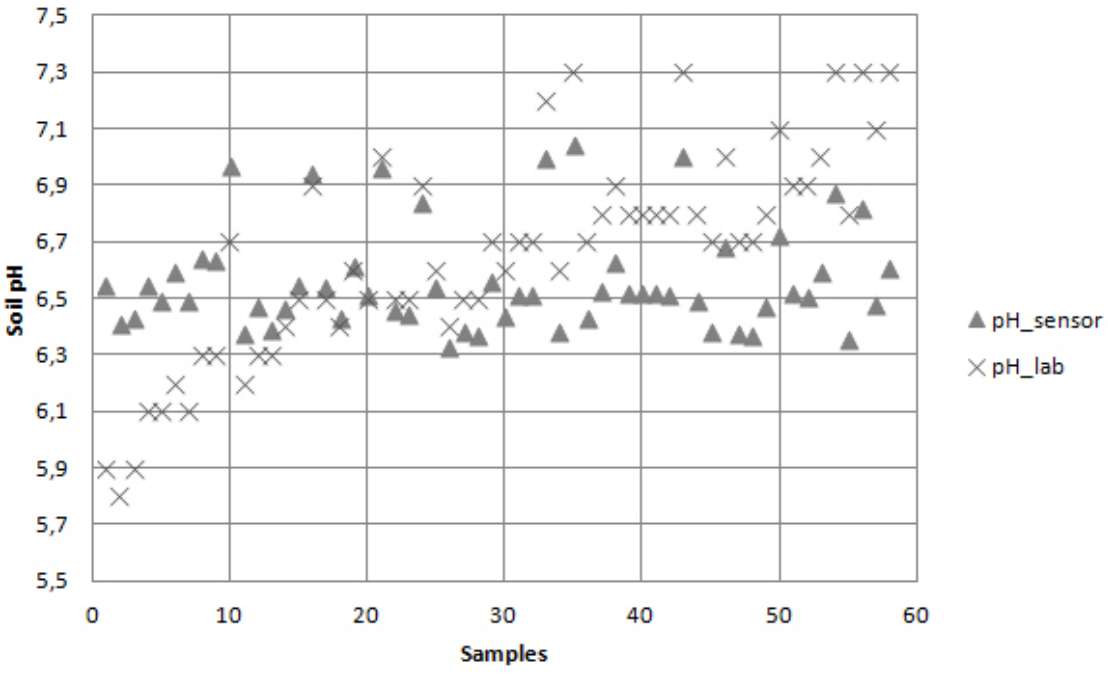

Figure 2. pH values measured by standard laboratory methods (pH_lab) and by 3100 Veris pH sensor (pH_sensor) at the same sampling location.

Some differences (|~10%|) in the pH measurement behaviour for the two used methodologies were obtained. In some cases, the Veris measurements when compared

with analytical laboratory pH values overestimate or underestimate the soil pH value (Fig. 2). It was also found that there are areas in the experimental field where the pH spatial variability is greater than others (Fig. 1). The pH variability measured by Veris sensor is usually minor in the areas that were not mobilized for 12 years when compared to the areas that were not mobilized for 3 years. Apparently the number of years that the soil was not mobilized influences the local pH spatial stability measured by the Veris platform and this may be related to the organic matter content in the soil.

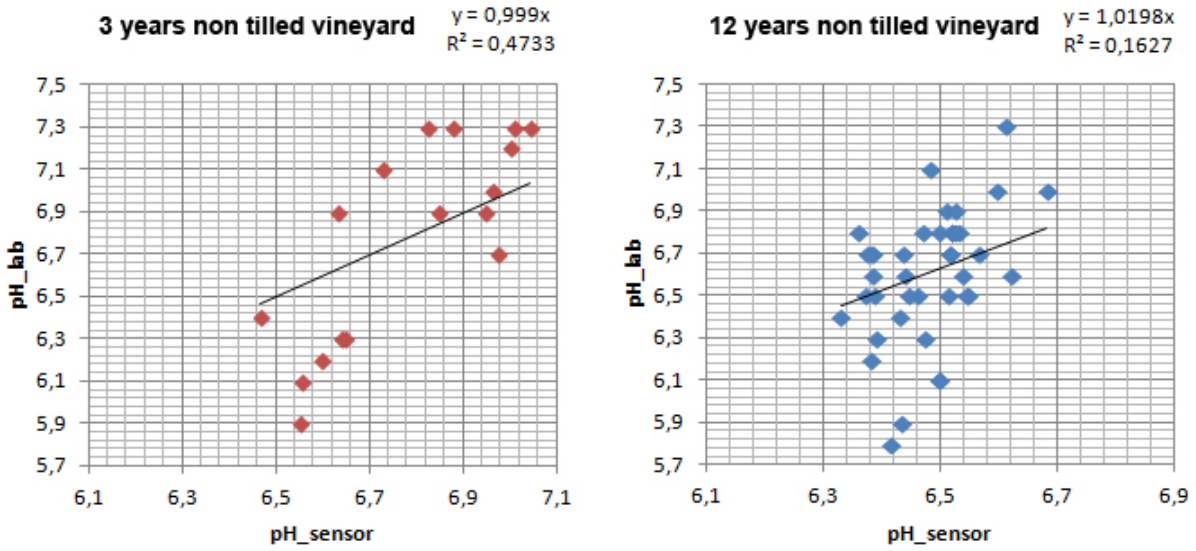

Figure 3. Scatter plot of pH values measured by standard laboratory methods (pH_lab) and by 3100 Veris pH sensor (pH_sensor) for the 3 years non tilled vineyard and for the 12 years non tilled vineyard. The regression model is also shown.

Fig. 3 shows the relationships between pH values obtained in laboratory and average values from pH surface. Higher coefficient of determination was computed when the 3 years non tilled vineyard data were considered, whereas a very low correlation was apparent for the 12 years non tilled vineyard data. In both cases, correlations were lower that those reported in other works (e.g., Schirrmann et al., 2011).

Given the obtained results the questions that can be raised are whether the observed maladjustment are due to a misbehaviour with the Veris pH sensor, problems with the laboratory measurements, or the difficulties in the comparison itself, because, although we are analyzing nearby sites, we cannot compare low density conventional pH sampling, not sensible to pH spatial variation, with high density 3100 Veris pH sampling, sensible to pH spatial variation.

4 Conclusions

Soil pH mapping using high density data provided by the 3100 Veris soil pH sensor is necessary to accurately delineate the spatial pattern of this key variable in vineyards.

However, data must be validated. Thus, apparently, there are pH values measured in the laboratory that are confirmed by the Veris sensor in the field but, however, others do not coincide. Such variability should be examined and the discrepancy between the two measuring methods should be confirmed, or if the pH local variability, undetected by point method, is responsible for the found differences.

Further research is necessary to clarify the error level of soil pH on-the-go readings in non-tilled soils, particularly in those not mobilized for a long time, and to improve the calibration using additional information as soil apparent electrical conductivity, which is simultaneously measured with the device located on the same platform.

Acknowledgements

This work was carried out with funding the RITECA Project, Transboundary Research Network Extremadura, Center and Alentejo, co-financed by the European Regional Development Fund (FEDER) by the Spain-Portugal Border Cooperation Operational Programme (POCTEP) 2007-2013.

This research was also co-financed by the Gobierno de Extremadura and the European Regional Development Fund (ERDF) through the project GR10038 (Research Group TIC008).

References

HIDALGO-TOGORES, J. 2006. La calidad del vino desde el viñedo. Ed. Mundi-Prensa Libros. Madrid.

MORLAT, R., JACQUET, A., ASSELIN, C. 1993. Principaux effets de l'enherbement permanent contrôlé du sol, dans un essai de longue durée en Anjou. Progr. Agric. Vitic., **110** 406-410.

RIBÉREAU-GAYON, Y. 1982. Ciencia y técnicas de la viña. Tomo 2º: Biología de la viña. Suelos de viñedo. Ed. Hemisferio Sur S.A. Buenos Aires.

SCHIRRMANN, M., GEBBERS, R., KRAMER, E., SEIDEL, J. 2011. Soil pH Mapping with an On-The-Go Sensor. Sensors, **11** 573-598.

Keynote: Proximal sensing for soil functions

M. Van Meirvenne*, T. Saey, P. De Smedt, E. Van de Vijver, M. M. Islam, S. Delefortrie, E. Meerschman

Universiteit Gent, Department of Soil Management, Coupure links 653, Gent, Belgium
**E-mail: marc.vanmeirvenne@ugent.be*

Abstract

Soil fulfills a number of distinct functions to man and the environment, such as the production of food and biomass, protection against environmental threats, support for human activities, source of raw materials and safeguarding geogenic and cultural heritage (Blum, 2005). Increasingly, our society expects soil scientists to provide detailed information on these functions, including spatial assessments. This paper discusses how proximal soil sensing can help in providing such information. In taking up this challenge soil scientist can improve their contribution to the discussions on our changing environment and the central role of soil. Several case studies will be discussed in which different applications of proximal soil sensors were used to address a variety of objectives related to several soil functions and their treats.

References

BLUM W. 2005. Functions of soil for society and the environment. Reviews in Environmental Science and Bio/Technology 4:75-79.

Can γ-radiometrics predict soil textural data in different parent materials?

S. Priori*, N. Bianconi, E.A.C. Costantini

Consiglio per la Ricerca e la Sperimentazione in Agricoltura, CRA-ABP (Research Center of Agrobiology and Pedology), Firenze, Italy.
**E-mail: simone.priori@entecra.it*

Abstract

The use of γ-radiometrics for soil proximal sensing is strongly site specific, because of the strong influence of parent material mineralogy on the γ-rays emitted from the soil. The work wants to propose a multivariate statistics approach to predict soil textural data from γ-radiometrics measured in heterogeneous soils in terms of parent material, pedogenesis, morphology, coarse material and moisture content.

Keywords: PCA, Geographically Weighted Regression, geostatistics, survey, vineyards.

1 Introduction

In soil surveying, γ-rays spectra are mainly influenced by the mineralogy of bedrock and parent material, but also by soil weathering. Numerous studies (Cook et al., 1996; Pracilio et al., 2006) using airborne γ-rays spectrometry surveys showed strong relationships between γ-rays counts, nuclide concentrations (^{40}K, ^{238}U, ^{232}Th) and soil features. Other authors report strong correlation of γ-rays ground-based measurements, namely between ^{40}K and soil available potassium (Wong and Harper, 1999), ^{232}Th and organic carbon (Dierke and Werban, in press), ^{232}Th and clay content (Mahmood et al., 2011). Most of the authors concluded that the use of γ-radiometrics for soil mapping is strongly site-specific (Rawlins et al., 2007; Dierke and Werban, in press), because of greater weight of the parent material mineralogy, respect to the soil features. Therefore, soil properties prediction/mapping by γ-radiometrics needs to be calibrated in each surveyed area.

The aim of this work is to propose a multivariate spatial statistics approach to predict soil textural data from γ-rays data measured in heterogeneous soils in terms of bedrock, parent material, pedogenetic development, morphology, gravels and moisture content.

2 Materials and methods

The study was conducted in 7 vineyards of the "*Barone Ricasoli*" farm, Gaiole in Chianti (Central Italy). The total area of the surveyed vineyards was 30.7 hectares and the vineyards were situated on different bedrocks (fig. 1): calcareous flysch (Cretaceous-

Paleogene), marly-shales (Cretaceous-Paleogene), feldspatic sandstone (Oligocene), sandy and silty-clayey marine deposits with gravel lenses (Early Pliocene), ancient fluvial deposits (Plio-Pleistocene).

The vineyards were surveyed by “The Mole” γ-rays sensor, conceived by “The Soil Company” (van Egmond et al., 2008). The survey was conducted during 4 consecutive days and the sensor was placed behind a tractor at a constant height of 40 cm from the surface. The sensing swaths were spaced about 20 m apart, every 8-9 vine rows. The γ-rays spectrum was analysed by a Full Spectrum Analysis (FSA) to convert the γ-rays spectrum into individual nuclide concentrations (^{40}K, ^{238}U, ^{232}Th) and total counts, using “The Gamman, Medusa” software. The nuclide concentrations and the total counts were interpolated by ordinary kriging, after a filtering of the outliers to obtain grid maps at 1 m spacing. The maps of soil moisture content of the vineyards, calculated for other purposes, were used to correct the γ-rays data by the equation of Beamish (2013):

$$\mu_d = \frac{\mu_w}{1+1.11w} \quad (1)$$

where μ_d and μ_w were the γ-rays in the dry and wet soil, respectively, and w was the soil moisture content (g g^{-1}).

A digital elevation model of the vineyards at 1 m was used to estimate elevation.

A total of 77 soil samples were taken from the topsoil (0-40 cm) for the laboratory textural analysis. This analysis was performed by the X-rays Sedigraph-III 5120 (Micromeritics) following the method of Andrenelli et al. (2013).

An exploratory Principal Component Analysis (PCA) was performed to detect the multivariate correlations between variables and between cases, using the nuclide concentrations, the total counts and the elevation (h). The exploratory PCA allowed us to detect three distinct groups of cases (fig. 2) that corresponded to the three main groups of lithologies: 1) sandstone; 2) calcareous flysch, and 3) others lithologies.

For this reason, a k-means clustering of the counts, the nuclides concentrations and the altitude was performed by SAGA-Gis software, which formed 3 groups reflecting the 3 lithotypes. To predict the soil texture, another PCA was performed on all the maps of γ-rays data, including the nuclides ratios (K/U, K/Th and U/Th) and the grid maps of the main lithologies (used as dummy binary variables), derived from the previous clustering. To predict the maps of clay and sand, a geographically weighted multiple regression (GWMR) was performed by SAGA-Gis software, using the most important PCA factors as predictors. GWMR is a spatial statistics method to estimate non-stationary data, calculating a spatial weighting function in the regression models (Brunsdon et al., 1996).

The data of other independent 20 soil profiles were used for the validation.

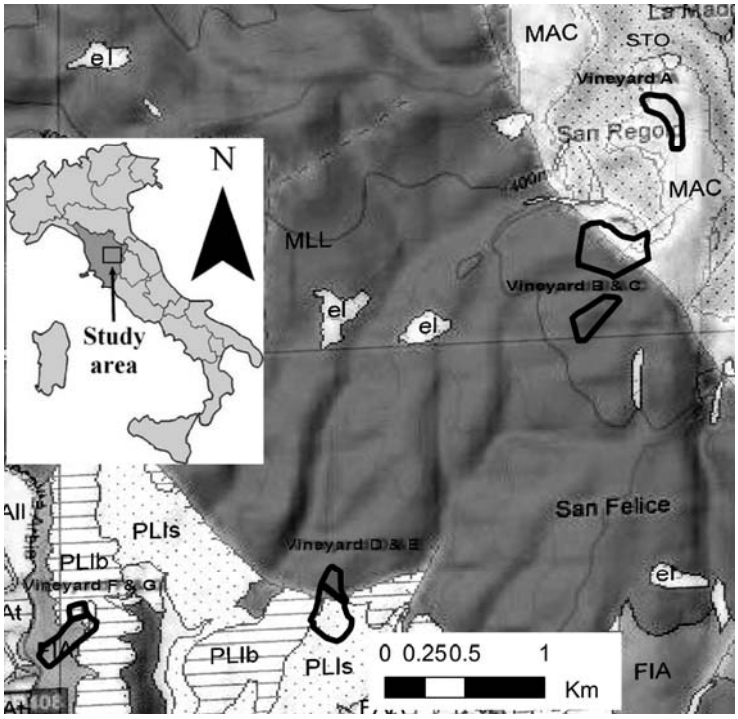

Figure 1. Extract of the geological map (1:25,000), with the studied vineyards (in black). Legend: MAC-Macigno Fm., sandstone; STO: shales; MLL: Calcareous flysch; FIA: marly-shales; PLI: sandy (PLs) and silty-clay (PLb) marine deposits.

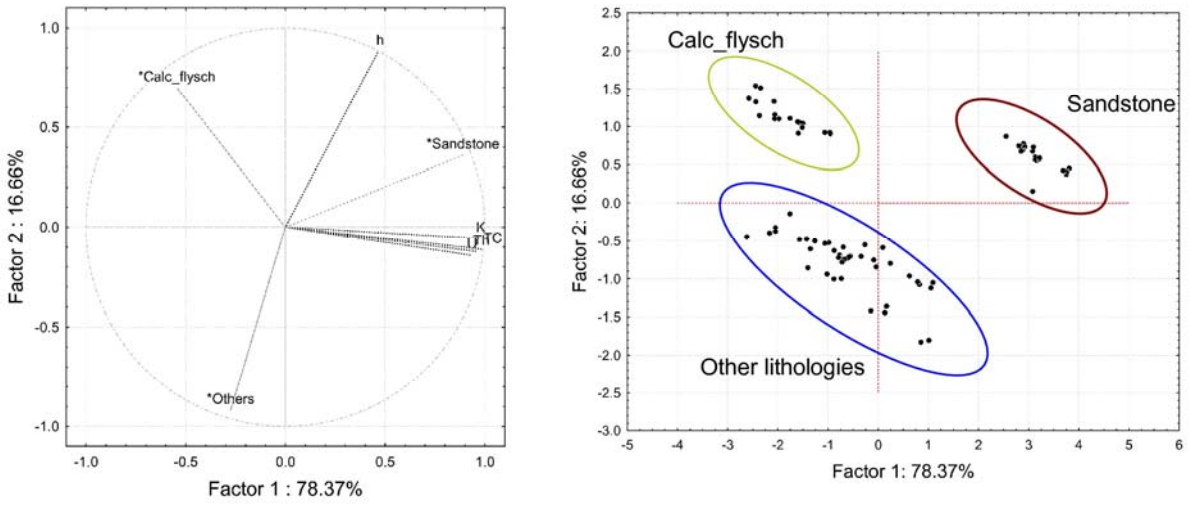

Figure 2. PCA, factor loadings (variables), on the left, and factor scores (cases), on the right. *: supplementary variables (Calc_flysch, Sandstone, Others) not entered in the PCA.

3 Results and discussion

The γ-rays total counts of the studied fields varied between 210 and 735 counts sec^{-1} (tab. 1) and were strongly correlated with ^{40}K nuclide concentration (tab. 2). The ratios

between the nuclides concentrations were poorly correlated to the counts and to the nuclides (tab. 2).

The k-means cluster analysis defined three groups, which represented the main lithologies. The clustering map fitted very well the lithological discontinuities between sandstone, calcareous flysch, and the others lithologies observed in the geological map and in the field.

Table1. Descriptive statistics of the γ-rays data

	n	Counts counts sec^{-1}	^{40}K	^{238}U	^{232}Th	$^{40}K/^{238}U$	$^{40}K/^{232}Th$	$^{238}U/^{232}Th$
			Bq Kg^{-1}					
Mean	24383	418	52.2	5.2	5.5	11.7	9.8	1.1
Min		210	3.3	0.5	0.6	0.5	0.8	0.1
Max		735	148.0	15.2	14.3	170.8	65.3	12.6
CV %		31.2	49.1	42.0	38.5	73.0	40.4	60.1

Table 2. Pearson's correlations coefficients between γ-rays data

	Counts	**^{40}K**	**^{238}U**	**^{232}Th**	**$^{40}K/^{238}U$**	**$^{40}K/^{232}Th$**	**$^{238}U/^{232}Th$**
Counts	1.00	0.88	0.65	0.81	0.13	0.21	-0.11
	^{40}K	1.00	0.42	0.68	0.37	0.48	-0.18
		^{238}U	1.00	0.23	-0.46	0.26	0.52
			^{232}Th	1.00	0.32	-0.23	-0.54
				$^{40}K/^{238}U$	1.00	0.13	-0.50
					$^{40}K/^{232}Th$	1.00	0.48
						$^{238}U/^{232}Th$	1.00

The second PCA, performed on the three lithological maps (calcareous flysch, sandstone, other lithologies) and all the γ-rays data (counts, nuclides and ratios between nuclides), showed that the first two factors, PC1 and the PC2 explained the 52.7% and the 41.4% of the variance, respectively (tab. 3). These factors were used as predictors in the GWMR, to calculate the maps of clay and sand content (fig. 3). Since the best variogram model of the sand and clay measured points was the polynomial of 3rd order (R^2= 59.3%), the distance weighting used in the GWMR was the inverse distance to a power of 3rd order.

The validation of clay and sand content on the profiles had a R^2 of 0.60 and 0.82 ($p < 0.01$), respectively, whereas the RMSE was 6.3 g $100g^{-1}$ and 8 g $100g^{-1}$ (fig. 3).

Table 3. Explained variance and factor loadings of the first two PCA factors.

Factors	Explained variance	Cumulative variance	Factor loadings									
			Counts	^{40}K	^{238}U	^{232}Th	$^{40}K/^{238}U$	$^{40}K/^{232}Th$	$^{238}U/^{232}Th$	Flysch	Sandstone	Others
PC1	52.7	52.7	0.33	0.32	0.21	0.23	0.10	0.11	-0.02	-0.66	0.42	0.24
PC2	41.4	94.1	-0.19	-0.19	-0.12	-0.14	-0.03	-0.04	0.02	-0.30	-0.46	0.76

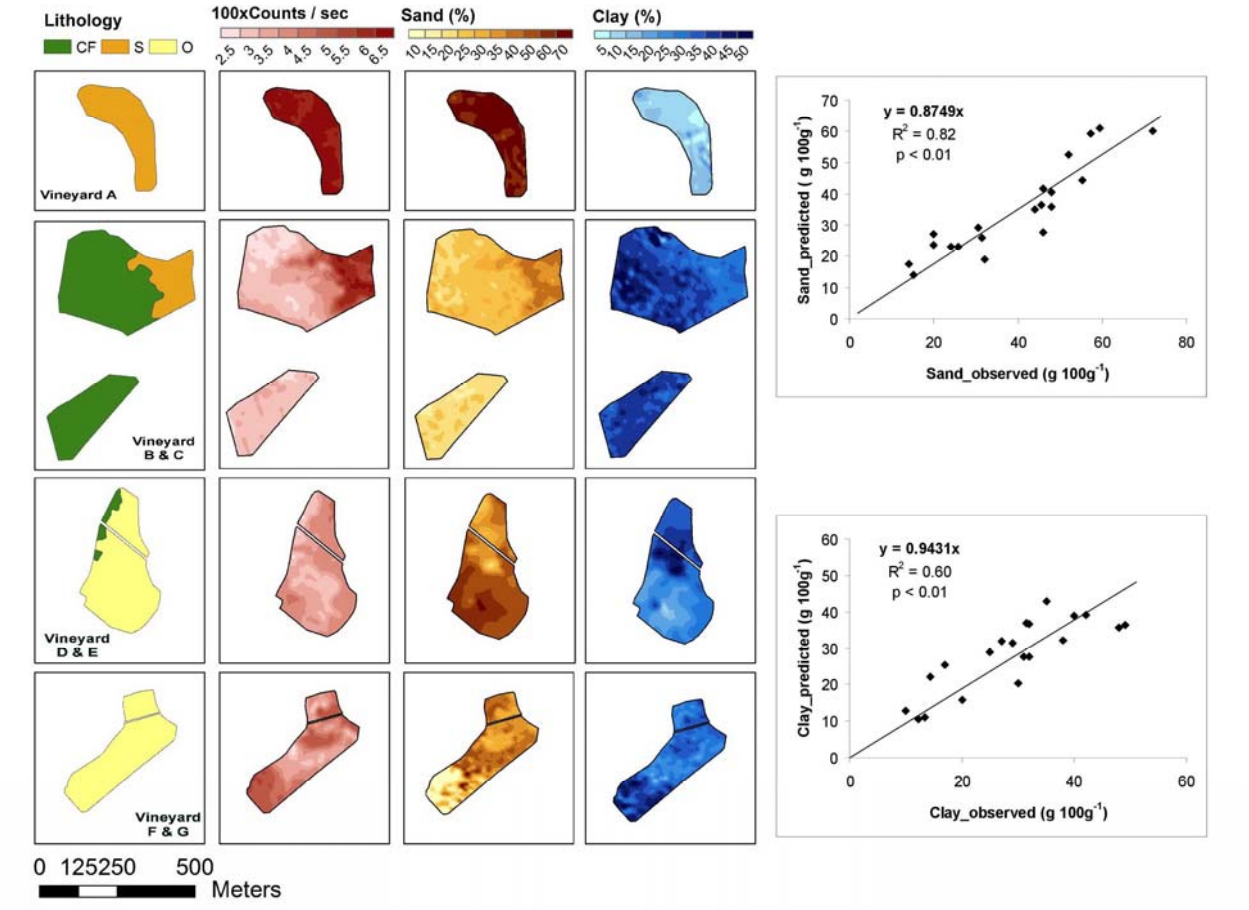

Figure 3. Maps of the lithology (obtained by the clustering), total γ-rays counts, sand predicted and clay predicted (by GWR). On the right, the validation graphs of sand and clay predicted.

4 Conclusions

Proximal soil sensing with γ-radiometrics is strongly site-specific and influenced by parent material. A general prediction model of a soil feature by γ-radiometrics data, such as texture, needs to include parent material. A multivariate approach, which takes into account all the γ-radiometrics data (total counts, nuclide concentrations, ratios between nuclides) and the main lithologies can strongly improve the previsional model.

Acknowledgements

This work was supported by the “Barone Ricasoli” s.p.a. farm (VignaCRU project). The authors wish to thank the agricultural manager of the farm Massimiliano Biagi and their co-workers for their support in the field operations.

References

ANDRENELLI M.C., FIORI V., PELLEGRINI S. 2013. Soil particle-size analysis up to 250 µm by X-ray granulometer: Device set-up and regressions for data conversion into pipette-equivalent values. Geoderma, **192**, 380–393.

BEAMISH D. 2013. Gamma ray attenuation in the soils of Northern Ireland, with special reference to peat. Journal of Environmental Radioactivity, 115, 13-27.

BRUNSDON C., FOTHERINGHAM A.S., CHARLTON. 1996. Geographically weighted regression: a method for exploring spatial nonstationarity. Geographical Analysis, **28** (4), 281-298.

COOK, S.E., CORNER, R.J., GROVES, P.R., GREALISH G.J. 1996. Use of airborne gamma radiometric data for soil mapping. Australian Journal of Soil Research, **34** (1): 183-194.

DIERKE C., WERBAN U. (IN PRESS). Relationships between gamma-ray data and soil properties at an agricultural test site. Geoderma.

MAHMOOD, H.S., HOOGMOED, W.B., VAN HENTEN, E.J. 2011. Estimating soil properties with a proximal gamma-ray spectrometer using windows and full-spectrum analysis methods. 2nd Global Workshop on Proximal Soil Sensing, 15-18 May 2011, Montreal, Quebec, Canada.

PRACILIO, G., ADAMS, M.L., SMETTEM, K.R.J., HARPER, R.J. 2006. Determination of spatial distribution patterns of clay and plant available potassium contents in surface soils at the farm scale using high resolution gamma ray spectrometry. Plant and Soil, **282**(1-2), 67-82.

RAWLINS, B.G., LARK, R.M., WEBSTER, R. 2007. Understanding airborne radiometric survey signals across part of eastern England. Earth Surface Processes and Landforms, **32**(10), 1503-1515.

VAN EGMOND, F.M., LOONSTRA, E.H., LIMBURG J. 2008. Gamma-ray sensor for topsoil mapping: The Mole. 1st Global workshop on High Resolution Digital Soil Sensing & Mapping, 5-8 February 2008, Sydney, Australia.

WONG M.T.F., HARPER R.J. 1999. Use of on-ground gamma-ray spectrometry to measure plant-available potassium and other topsoil attributes. Australian Journal of Soil Research, **37**, 2, 267-277.

Data fusion of different geophysical measurements for estimating soil water content after an irrigation event

D. De Benedetto[1,2*], A. Castrignanò[2], R. Quarto[1], A. D. Palumbo[2]

[1]*Università degli Studi "Aldo Moro", Bari, Italy*

[2]*Consiglio per la ricerca e la sperimentazione in agricoltura, SCA, Bari, Italy*

[*]*E-mail: daniela.debenedetto@virgilio.it*

Abstract

The objective of this study was to fuse different geophysical data for SWC estimation. The measurements with EMI and GPR sensors were carried out in a test site under wet soil conditions. Soil samples were collected to measure SWC with gravimetric method. SWC data and geophysical estimates at the sample locations were jointly processed using multicollocated cokriging (MCCOK). Cross-validation was used to assess goodness of the estimates and compare MCCOK with ordinary cokriging (OK).

The results showed that MCCOK was effective to fuse EMI and GPR sensor information in SWC estimation reducing error mean and variance.

Keywords: EMI, GPR, data fusion, multicollocated cokriging.

1 Introduction

The importance of accurate soil moisture characterization at various temporal and spatial scales for agriculture applications has boosted the development of different soil moisture sensing techniques. In particular rapid large-scale data collection techniques of soil moisture are required because of the limited possibilities of conventional methods based on direct sampling. In the last years geophysical methods, such as Ground Penetrating Radar (GPR) and Electromagnetic Induction (EMI), have shown promise for estimating soil water content at field scale. EMI was widely used for repetitive monitoring of a large number of sites, over an extended period, in soil at field and landscape scales (Corwin & Lesch, 2003; De Benedetto et al., 2011). A review of GPR applications for soil moisture sensing was given by Huisman et al. (2003) and numerous studies used the GPR techniques for soil moisture determination (Grote et al., 2010). The drawbacks of these sensors stem from the complexity of the relation between sensor outcomes and soil water content, because the observations are affected not by a single physical parameter, which leads to an ambiguity in interpretation. This problem can be partially solved through a complementary use of different sensors to obtain a more comprehensive representation of the area under analysis (sensor fusion system) (Adamchuck et al., 2011). With the profusion and wide diversification of data sources provided by modern technology of proximal sensing, sensor datasets could then be used as auxiliary information to supplement a sparsely sampled target variable. However, this is not with-

out difficulties, because proximal sensing data are often massive, taken on different spatial and temporal scales, and subject to measurement error biases. Geostatistics offers a set of linear multivariate (cokriging) estimators for merging multiple data sets and yields a statistical best estimate of the spatial distribution of the target variable, together with a quantification of the associated uncertainty.

The paper applies a multivariate geostatistical data-fusion technique to different geophysical sensor data, in particular GPR and EMI, for stationary estimation of soil water content in an agricultural field under wet conditions.

2 Material and methods

2.1 Study area and data collection

The surveys were carried out in an uncropped plot (40x20m) at the agricultural experimental farm of CRA-SCA, located in south-eastern Italy (40°59′48.25″ N, 17°02′02.06″ E). Soil is classified as fine, mixed, superactive, thermic Typic Haploxeralfs according to the Soil Taxonomy. Soil texture is mainly clayey with the clay content ranging from 30% to 60% by weight and basically increasing in depth.

The plot was monitored with an EMI sensor (EM38DD, Geonics Limited, Mississauga, Ontario, Canada), carried across the plot, which simultaneously measures apparent electrical conductivity (EC_a) in the horizontal (EC_{aH}) and vertical (EC_{aV}) orientations. EC_a measurements were geo-referenced using a Differential Global Positioning System (HiPer® 27 Pro, TOPCON) with planimetric and altimetric centimeter accuracies. The surveys were conducted along longitudinal and transversal transects about 1 m apart and data were recorded every second with a spatial resolution of 0.5 m on average along the transect. A GPR system (IDS Ing-manufactured, RIS 2k-MF Multifrequency Array Radar-System), with two antennas of different (600 and 1600 MHz) frequencies and operating in mono-static mode, was carried on the same transects. The GPR system worked with a time window of 60ns and a sampling interval of 0.05ns; successive traces were collected every 0.024m. In order to assess propagation velocity profiles in the subsoil, some profile measurements were made with the technique of Common Mid Point (CMP), using a bistatic GPR system with central frequency of 450 MHz (pulseEKKO 1000, Sensors & Software Inc, Mississauga, Ontario, Canada). In all cases sixteen pulses for each measurement point were sent in the soil, for obtaining stacked traces less affected by noises.

One hundred and sixteen samples were collected up to 0.30-m depth to measure SWC with gravimetric method in October 2012, after the plot was irrigated (drip irrigation) for a week until the saturation, and the water surplus was lost for gravitation.

2.2 Data analysis

The GPR data pre-processing was performed with REFLEX Software, including the set zero time correction, “dewow” filter and trapezoidal bandpass filter. No amplitude gain functions were applied to the data. After processing, the instantaneous amplitude or envelope of data was calculated using a quadrature filter (Hilbert transformation), which gives an estimation of the attenuation of radar signal, possibly caused by moisture conditions. Amplitude maps (time slices) were built by averaging the amplitude of the radar signal within consecutive time windows of 2ns and 1ns for 600 and 1600MHz antennas, respectively. The time slices were then transformed in depth slice maps using the velocity of the radar waves determined through the analysis of Common-Mid Point measurements (not reported). To eliminate the noise due to variable energy of the transmitted signal at different points, a normalization of the amplitudes was performed using the first time slice, mainly related to the radar waves in air, as a reference.

To create the geophysical-moisture point data set of coregionalisation, the selected geophysical variables through stepwise regression were estimated at the soil sample locations. SWC sample data, EMI and GPR estimates were then jointly processed using multi collocated cokriging, which is a way of integrating secondary finer-resolution information in primary sparse variable modelling. The spatial dependence among soil water data and the selected geophysical data was then explored by fitting a linear model of coregionalization (LMC) and a multicollocated cokriging map of soil moisture was finally produced.

3 Results

The OK SCW map (Fig. 1a) could be roughly split into two main areas with the northern area characterized by higher water content. The high degree of smoothness in this map is due to the coarser sampling scale.

The EC_{aH} map (Fig. 2a) showed a large area of the plot characterized by higher values. The same spatial structures roughly appeared in the EC_{aV} map (Fig. 2b), through with lower values in the northern area, denoting some discontinuity within about 1-m depth. The area of the plot with higher values of EC_{aH} corresponded approximately to the zones characterized by higher SWC. The maps of the estimated amplitude for 600 MHz antenna at the different depths (not shown) looked quite similar, revealing some consistency within the 0.30-m depth, with tendentially higher values of amplitude in the northern part of the plot. The maps of the estimated amplitude for 1600MHz antenna (not shown) up to 0.165-m depth looked noisier compared with the previous ones. Nevertheless, the northern area was characterised by higher amplitude values for both antennas, at least up to 0.165-m depth. Some inconsistencies were detectable between the 0.18-m map of 600 MHz antenna and the 0.165-m map of 1600 MHz antenna, quite likely due to the finer spatial resolution of the latter.

The stepwise regression selected EC_a in horizontal polarization, the slices at 0.06-m, 0.18-m and 0.30-m depth for the antenna of 600MHz and the slices at 0.03-m, 0.09-m and 0.165-m depth for the 1600MHz antenna with R^2= 0.55. A correlation analysis showed that the strongest correlation occurred between soil water content and EC_{aH}, therefore the latter was chosen as the collocated variable. These results show that EMI sensor was a useful indicator of shallow SWC whereas only some GPR slices of the two antennas were affecting its estimation.

An intrinsic stationarity was assumed for all variables and an isotropic LMC was then fitted to model all the experimental variograms. The model included a nugget effect and a spherical model with a range of 21.35 m. The results of cross-validation test showed that the overall performances of OK and MCCOK were quite similar, though MCCOK realized lower error mean and variance.

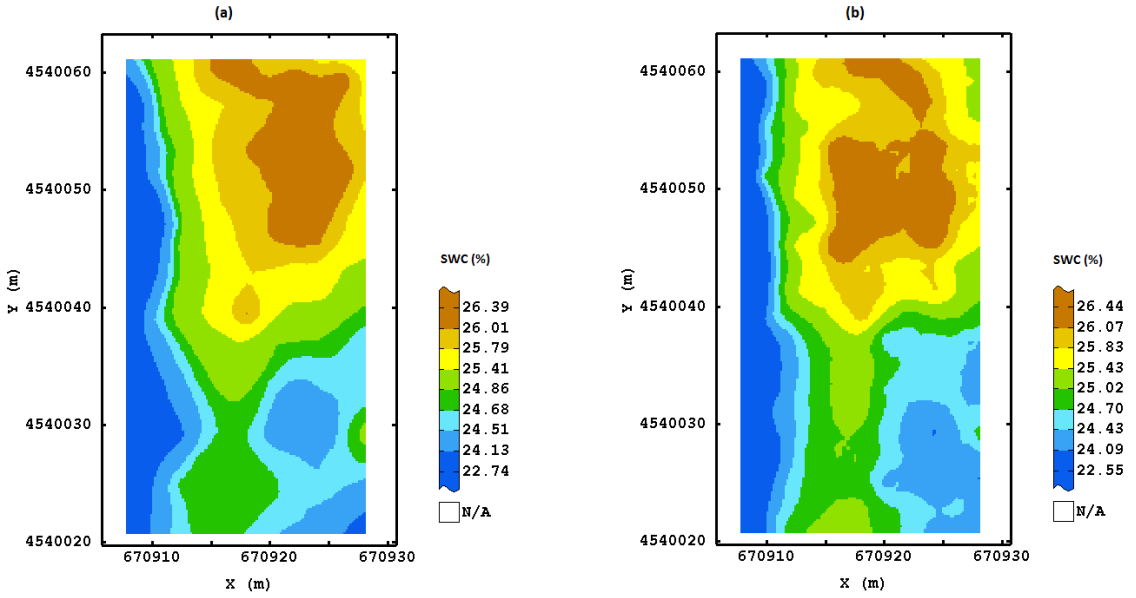

Figure 1. Spatial estimate of SWC obtained with OK (a) and CCK (b).

Comparing the maps of SWC obtained with MCCOK (Fig. 1b) with the one obtained with OK (Fig. 1a), the two types of maps seemed to reproduce the same main structures of spatial dependence, even if the MCCKO map looked more variable. All the maps revealed a wide northern area of higher values, though the MCCOK map looked more locally changeable in the southern area. This increase of GPR signal amplitude is ascribable to higher clay content (data not reported).

The increased variability, observed in the MCCOK map, can be explained since the sub-metre scale information in the geophysical images was used to downscale the SWC variation. However, it still has to be proved that such variability corresponded to actual variation in SWC.

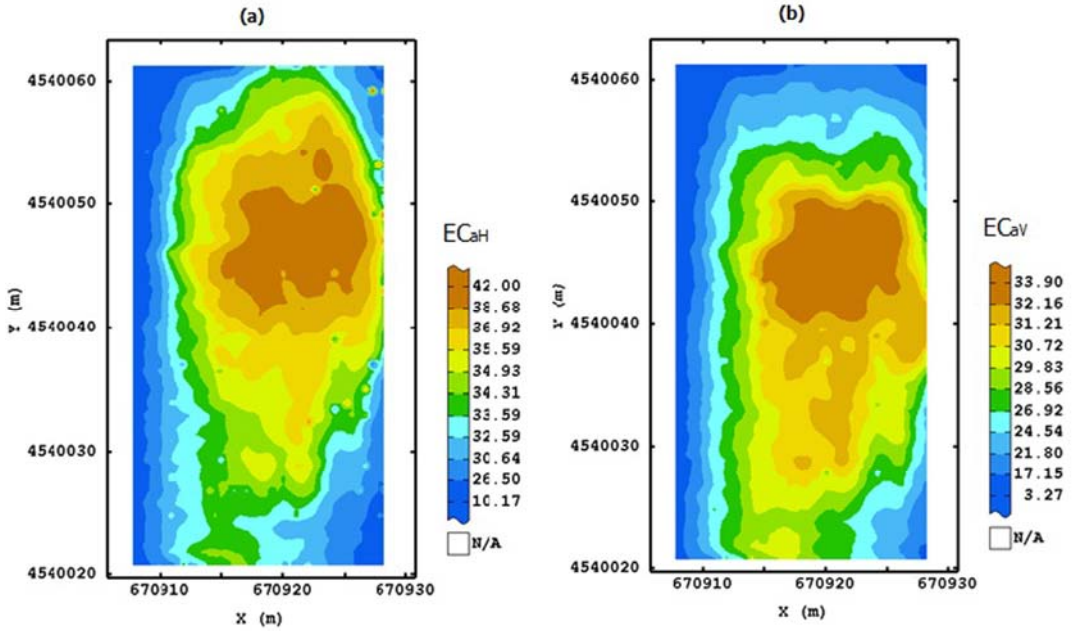

Figure 2. Spatial estimate of EC_a in horizontal (a) and vertical (b) polarization (in milli-Simens per meter).

4 Conclusion

This research focused on a combination of GPR and EMI data and it has proved that a multivariate geostatistical approach is effective to fuse sensor information to estimate soil water content. Further investigation in sensor data fusion is strongly recommended in the light of the current proliferation of data from different sources.

References

ADAMCHUK, V.I., VISCARRA ROSSEL, R.A., SUDDUTH, K.A., SCHULZE LAMMERS, P. 2011. Sensor fusion for precision agriculture. In: Thomas, C., editor. Sensor Fusion - Foundation and Applications. Croatia:In-Tech. p. 27-40.

CORWIN, D.L., LESCH, S.M. 2003. Application of soil electrical conductivity to precision agriculture: theory, principles, and guidelines. Agronomy Journal, 95 pp. 455–471.

DE BENEDETTO, D., CASTRIGNANO`, A., SOLLITTO, D., MODUGNO, F., BUTTAFUOCO, G., LO PAPA, G. 2011. Integrating geophysical and geostatistical techniques to map the spatial variation of clay. Geoderma, 171-172 pp. 53–63.

GROTE, K., ANGER, C., KELLY, B., HUBBARD, S., RUBIN, Y. 2010. Characterization of Soil Water Content Variability and Soil Texture using GPR Groundwave Techniques. Journal of Environmental and Engineering Geophysics, 15 (3, Sp. Iss. SI) pp.93-110.

HUISMAN, J.A., HUBBARD, S.S., REDMAN, J.D., ANNAN, A.P. 2003. Measuring Soil Water Content with Ground Penetrating Radar: A Review. Vadose Zone Journal, 2 pp. 476–491.

Use of gamma-ray emission for mapping topsoil clay content in various Mediterranean landscapes

G. Coulouma[1*], E.H. Loonstra[2], P. Lagacherie[1]

[1]*NRA – UMR LISAH, 2 place Viala 34060 MONTPELLIER CEDEX 2*

[2]*The Soil Company – Leonard Springerlaan 9 9727 KB Groningen, The Netherlands*

[*]*E-mail: coulouma@supagro.inra.fr*

Abstract

In mediterranean areas, cultivated areas are mainly encountered on sedimentary areas. The use of gamma-ray emission for soil sensing can be hampered by low contents of radio-active minerals. On-the-go gamma-rays measurements and 96 clay content analysis were carried out over nine vineyard blocks representative of the geopedological units of the Languedoc. This work showed that i) the different units revealed significant differences in 40K and 232Th content ii) Clay content can be predicted from gamma-ray by calibrating a function at the little region scale and iii) gamma-ray predicted clay field maps exhibited realistic soil patterns. These results suggested that gamma-ray could be also efficient in mediterranean sedimentary contexts with however some severe limitations for specific parent materials.

1 Introduction

The natural gamma ray measurements are often used in igneous or metamorphic geological context to map soil properties at a regional scale (Wilford, 2012) or to delineate iso-management zones at the farm scale (Pracilio et al., 2006). The presence of radionuclides in the tilled layer are detected in relation to the amount of minerals and to the weathering products of these minerals, which are partially adsorbed onto the surface of clay particles. Most of the Mediterranean soils highly depend on the parent materials according to the preponderant morphopedogenesis processes. A large part of the parent materials in cultivated Mediterranean areas are derived from marine sediments. The lack of the minerals associated with plutonic rocks and the preponderant morphopedogenesis may disturb the prediction of soil properties from natural gamma ray surveys. The aims are to compare the gamma ray signals measured in various Mediterranean landscapes and to propose a clay content prediction in a very low contrasted area without igneous rocks and old pedogenesis.

2 Material and methods

The study was undertaken over nine vineyard blocks representative of the various types of parent materials and soils in Languedoc Mediterranean area. The main characteristics of the blocks are detailed in the table 1. This blocks were studied in

previous works with classical soil survey, boreholes and geophysical transects (Coulouma et al., 2013). The different geo-pedological situations were detailed according to the WRB : class I) very shallow soils developed over micritic limestone without igneous minerals and weathering products – Calcisols (skeletic), class II) deep soils with sediments from the slopes in the same environment – Cambisols (calcaric), class III) soils over recent marine sediments – plaggic Cambisols, class IV) soils over marine sedimentary sandstones with a lot of micas – Calcisols (siltic), class V) soils over tertiary sediments with different origins – Calcisols (clayic), class VI) soils over the old colluvial deposits – Cambisols (clayic) and class VII) soils over the old alluvial deposits with a lot of micas and highly weathered igneous rock fragments – Fluvisols (skeletic). A proximal gamma-ray survey was performed with the Soil Company "The Mole" sensor and a DGPS. Each site was mapped with lines 5 m spaced, resulting in high resolution gamma ray maps of Total Counts, Potassium-40, Thorium-232, Uranium-238 and Cesium-137. Geophysical measurements were calibrated from 96 additional soil samples within the tilled layer of the set of vineyard. The sampling strategy were chosen to cover the entire plots according to a grid cell randomly sampled. The predicted model was tested with a "leave one plot out cross validation" (Christy, 2008). The given RMSE of each block correspond to the errors calculated on the block with the model calibrated with the other blocks.

Table 1. Description of the main soil properties of the 9 studied blocks

Block	Size (m^2)	Geopedological context	Topsoil properties				
			Clay(g/kg)	Silt (g/kg)	Sand(g/kg)	pH	Pebbles (g/kg)
P1	17140	Class VI	234(54)	227(39)	539(92)	8.2(0.5)	101(71)
P2	5729	Class VI	262(31)	225(33)	513(80)	8.5(0.1)	79(41)
P3	32315	Class VII	335(41)	278(43)	387(95)	7.2(0.7)	102(99)
P4*	8000	Class V	274	385	341	-	-
P5	5634	Class II	242(55)	438(30)	330(47)	8.6(0.1)	441
P6*	8500	Class III	-	-	-	-	-
P7	7880	Class I/Class II	153(39)	206(17)	641(90)	8.7(0.1)	382
P8*	1200	Class I/Class II	-	-	-	-	-
P9	7000	Class IV	175(21)	288(51)	537(55)	8.6(0.1)	4(5)

*The soil analysis of the P4, P6 and P8 are still working.

3 Results

Figure 1 revealed significant differences in 40K and 232Th content between the studied situations. However, the 40K and 232Th content correspond to low values compared to

other Mediterranean regions with old weathered soils (Laubestein & Magaldi, 2008). Three main groups were distinguished: i) class I and class II with low 40K and 232Th content, ii) class VII with the highest contents, and iii) the other class with medium 40K and various 232Th content. These differences were due to the presence of igneous minerals with or without clay particles in the soil. The 232Th is generally fixed on the clay particles during the weathering of igneous minerals and this nucleide is often used for a prediction of clay content in the soil (Van Egmond et al., 2010).

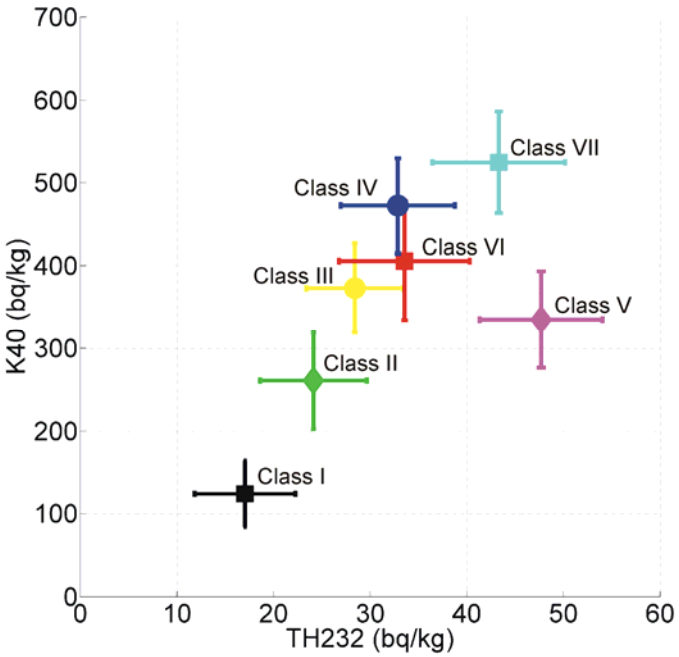

Figure 1. Correlation diagram between K40 and Th232 according to each geopedological context (the lines represent the standard deviation of each nucleide)

Figure 2 show the relation between the 232Th and the measured clay content of the samples. It exhibits a moderate correlation (R2 = 0.5). However, the relation is strongly perturbed by the sites with soils developed over marine sandstone (class IV in blue on figure 2) whose clay content is systematically overestimated. This can be explained by a large amount of micas in the soils over this old marine sandstone from the Pyrenees, which significantly increases the Th232 measurements. After removing class IV, a much more satisfactory relation was computed (R2 = 0.66). To test if the previous calibrated function can be used to predict clay content across the geopedological units of the vineyard plain – except class IV- we applied a leave-one-plot cross validation. 60 % of the variance was explained with this regional model and the resulting RMSE (49 g/kg) on the clay content was satisfactory. Moreover the clay content maps for each plot are given in the figure 3. The spatial patterns of the clay content correspond for each plot to the field observations. For example, the increase of clay content on the bottom part of the block P1 correspond to a old alluvial deposit with an increase of weathered clay

particles. The low clay content on the top of the block P7 correspond to an outcrop of limestone destructured after the vineyard establishment.

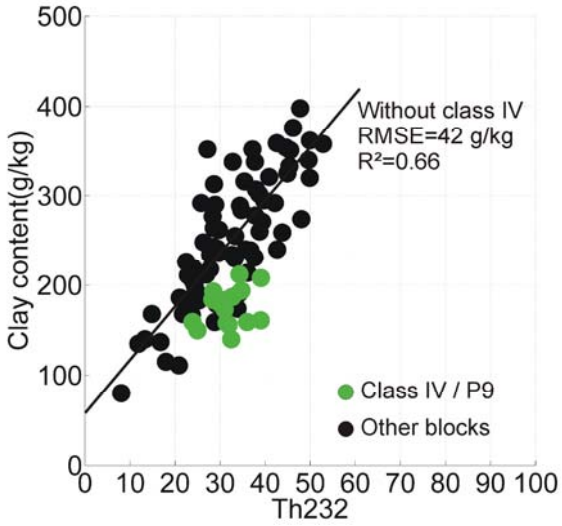

Figure 2. Correlation diagram between measured clay content (g/kg) and Th232

4 Conclusion

These results suggest that Gamma-ray measurements can improve the knowledge and delineations of Mediterranean geopedological contexts characterized by a very low contrasted area without igneous rocks and old pedogenesis. Except the soils developed over marine sandstones, a calibration of prediction from 232Th was possible for this studied region. This use for mapping clay content at the plot scale in such contexts is still questioned. However, a “regional” calibration may be used for the plot scale without large amount of soil analysis.

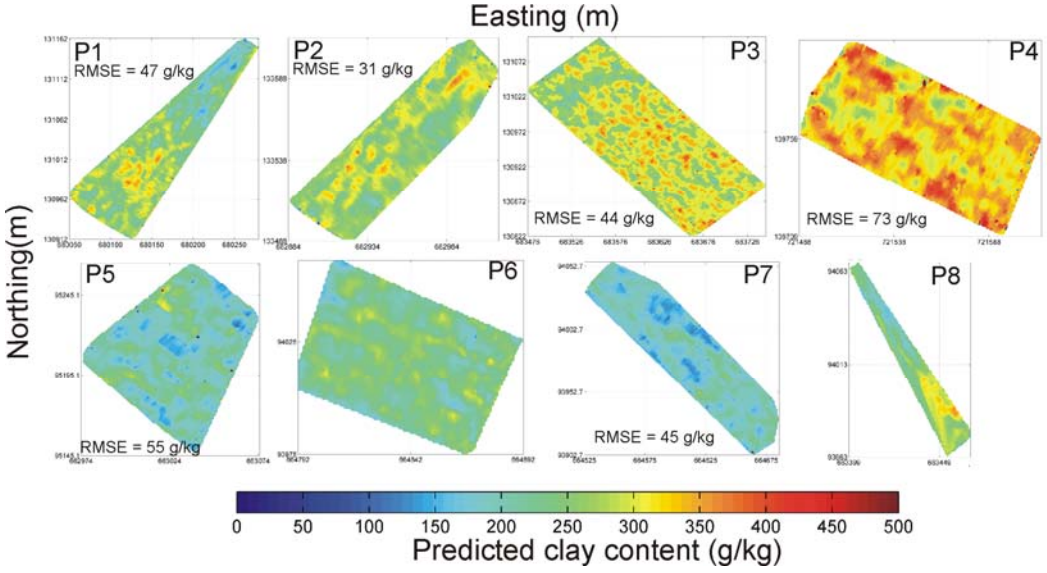

Figure 3. Predicted clay content for each plot from the Th232 based regional model

Acknowledgements

This study was funded by the FP7-DIGISOIL project (FP7-ENV-2007-1 N°211523) financed by the EC under the 7th Framework Programme for Research and Technological Development, Area "Environment", Activity 6.3 "Environmental Technologies". The authors thank particularly J.L. Belotti for this help in soil analysis.

References

COULOUMA, G., LAGACHERIE, P., SAMYN, K., GRANDJEAN, G. 2013. Comparisons of dry ERT, diachronic ERT and the spectral analysis of surface waves for estimating bedrock depth in various Mediterranean landscapes. Geoderma, **199** 128-134.

CRISTY, C.D. 2008. Real time measurements of soil attributes using on-the-go near infrared reflectance spectroscopy. Computers and Electronics in Agriculture, **61** 10-19.

LAUBESTEIN, M., MAGALDI, D. 2008. Natural radioactivity of some red Mediterranean soils. Catena, **76** 22-26

PRACILIO, G., ADAMS, M.L., SMETTEM, K.R.J., HARPER, R.J. 2006. Determination of spatial distribution patterns of clay and plant available potassium contents in surface soils at the farm scale using high resolution gamma ray spectrometry. Plant and Soil, **282** 67-82.

VAN EGMOND, F.M., LOONSTRA, E.H., LIMBURG, J. 2010. Gamma ray sensor for topsoil mapping: The Mole. In " Proximal Soil Sensing" Viscarra Rossel, R.A., McBratney, A., and Minasny, B. (Eds). Progress in Soil Science series. Springer.

WILFORD, J. 2012. A weathering intensity index for the Australian continent using airborne gamma-ray spectrometry and digital terrain analysis. Geoderma, **183-184** 124-142.

Visualizing small scale variability of clay content on soils at Mt. Kilimanjaro by VIS-NIR spectroscopy

A. Kühnel[1*], C. Bogner[2], H. Pabst[3], B. Huwe[1]

[1]*Soil Physics Group, BayCEER, University of Bayreuth, Germany*
[2]*Ecological Modelling, BayCEER, University of Bayreuth, Germany*
[3]*Department of Soil Science of Temperate Ecosystems, University of Göttingen, Germany*
[*]*E-Mail: anna.kuehnel@uni-bayreuth.de*

Abstract

We investigated the feasibility of VIS-NIR reflectance spectra to predict clay content for different land-use forms in situ. We used partial least square regression on an independent validation dataset and root mean squared error and the Akaike information criterion to evaluate our model. With this model we predicted clay content in four soil profiles on a 3 x 3 cm scale. Models performed well for spectra taken in the laboratory (RPD > 2; R^2 > 0.76). The accuracy for in situ predictions however varies between the land-use forms and predictions are preliminary.

Keywords: agricultural soils, diffuse reflectance spectroscopy, spatial variation, clay.

1 Introduction

The conversion of natural or semi-natural ecosystems to anthropogenic land-use forms often results in degradation of soil quality and alterated ecosystem functions like water and carbon storage or erosion control. To infer the implications of these changes, fast and accurate predictions are required. This is especially important for the sub-Saharan ecosystems where information on soil properties is still rather scarce. Visible (VIS) and near-infrared (NIR) spectroscopy is a fast method to predict various soil properties simultaneously at comparatively low costs and has been widely used under laboratory conditions (Chang et al., 2001; Viscarra Rossel et al., 2006; Awiti et al., 2008). Using VIS-NIR spectroscopy directly in the field is not yet as reliable (Morgan et al., 2009; Nocita et al., 2011). However, it provides a direct and non-destructive method, if stable models can be developed. The goal of this study is to visualize the small scale variability of clay content, in situ. We use VIS-NIR reflectance spectra of soil to build a model based on partial least square regression (PLSR) to predict clay content for different land-use forms.

2 Materials and methods

2.1 Study site

The study was conducted on the southern slopes of Mt. Kilimanjaro, Tanzania (3°4'33"S, 37°21'12"E). The natural ecosystem of the lowlands around Mt. Kilimanjaro

(up to 1100m a.s.l) is savannah that developed on superficial deposits from the volcano. Mean annual rainfall fluctuates between 400–900mm (Soini, 2005), the main soil type is Vertisol and the vegetation is dominated by *Balanitis aegyptiaca* and different Acacia species. The savannah ecosystem is threatened by the transformation into fields, as the increasing population needs arable land, where maize and sunflowers are grown.

The submontane zone, an area between 1100–1800m a.s.l. on the southern slopes of Mt. Kilimanjaro is mainly covered by homegarden ecosystems, a traditional agroforestry system, where banana (*Musa* spp.) and coffee (*Coffea arabica*) trees are grown together with a variety of smaller crops (Fernandes et al., 1985) and coffee plantations. Mean annual rainfall is between 1200 and 2000mm (Soini, 2005), the main soil types of the higher elevations are Andosols, more weathered soils develop into Vertisols. We have selected four of the typical ecosystems, namely natural savannah, maize field, homegarden and coffee plantation. Soil under coffee plantation was described as Haplic Vertisol, soil under homegarden and savannah as Sodic Vertisol and soil under maize field as Thephric Cambisol (FAO, IUSS Working Group, WRB, 2007).

2.2 Soil sampling and laboratory analysis

In each of the four selected ecosystems a soil pit was dug to a depth of at least 100cm or until continuous rock was reached. One profile wall was carefully cleaned of roots and debris and a frame of 0.5 x 1m with 3 x 3cm segments was put on it. Each segment was then scanned with the contact probe attached to an Agrispec portable spectrometer (ASD, Boulder Colorado) in the spectral range of 350–2500nm in 1nm intervals. Small soil core samples (diameter 2.5cm) were taken for validation. For the model calibration, soil samples were collected from 25 different sites with a soil auger and different soil horizons were separated, resulting in 146 samples. All samples were oven-dried at 45° for 24h and sieved <2 mm. Clay content was measured using a Master Sizer S particle size analyzer.

2.3 Spectral measurements and model calibration

For spectral measurements a well-mixed aliquot of the dried sample was scanned with the same device as used in the field. The instrument was calibrated with a Spectralon® white tile prior to measurements. For each sample as well as for the calibration with the white reference 30 reflectance spectra were averaged to reduce the noise.

Each spectrum was corrected for the ASD offset between the detectors with the additive method (Becvar et al., (2006 - 2008)). Then, a wavelet transformation was performed and the spectra were transformed into absorbance values. Afterwards, noisy portions of the spectra were removed and only the range from 500 nm to 2400 nm was kept. The dataset was split into a calibration and a validation dataset by randomly choosing 3/4 for calibration. The number of components for the optimal PLSR model was chosen based on the leave-one-out cross validation. The root mean squared error of prediction

$$RMSE = \sqrt{\frac{1}{N}\sum_{i=1}^{N}(x_i - y_i)^2} \quad (1)$$

the Akaike Information Criterion,

$$AIC = N \log\ RMSE\ +\ 2m \quad (2)$$

the coefficient of determination

$$R^2 = 1 - \frac{\sum_{i=1}^{N}(x_i - y_i)^2}{\sum_{i=1}^{N}(y_i - y_i)^2} \quad (3)$$

and the ratio of percent deviation

$$RPD = \frac{\sqrt{\frac{1}{N-1}\sum_{i=1}^{N}(y_i - \hat{y}_i)^2}}{RMSE} \quad (4)$$

were calculated, where N is the number of samples, m is the number of model parameters, x_i is the predicted value, y_i is the observed value and y_i is the mean of the observed values. The model with the lowest AIC was chosen, as AIC helps to select a model that represents the variability in the data without causing it to overfit (Viscarra Rossel, 2008). All analyses were performed in R (R Development Core Team, 2011).

3 Results and discussion

3.1 Model calibration

We have chosen a model with 10 components. The means and the range of clay content in calibration and validation datasets were similar, with the validation dataset covering the whole range of measurements (Table 1).

Table 1. Parameter of the PLSR model

Clay	Mean	Range	R^2	RMSE	RPD
Calibration	51.2	20.0 - 85.0	0.84	8.0	2.04
Validation	50.8	21.0 - 76.0	0.80	7.1	2.26

Other studies predicting the clay content showed slightly better R^2 and RMSE values. Stenberg (2010), for example, analysed the effect of different pre-treatments of the samples on clay content and found $R^2 > 0.86$. Considering the classification of RPD values by Viscarra Rossel et al., 2006, our models performed well and quantitative predictions are very good (RPD > 2.0).

3.2 Model validation

Correlations between a) the air-dried spectra taken in the laboratory and b) the spectra taken in the field and the measured values were calculated (Figure 1). When looking at all plots, the PLSR model for the prediction of clay content with the air dried spectra performed quite well (R^2 = 0.75; RPD = 2.02), whereas predicting clay with field spectra resulted only in R^2 of 0.27 and a RPD value of 1.18 (Table 2).

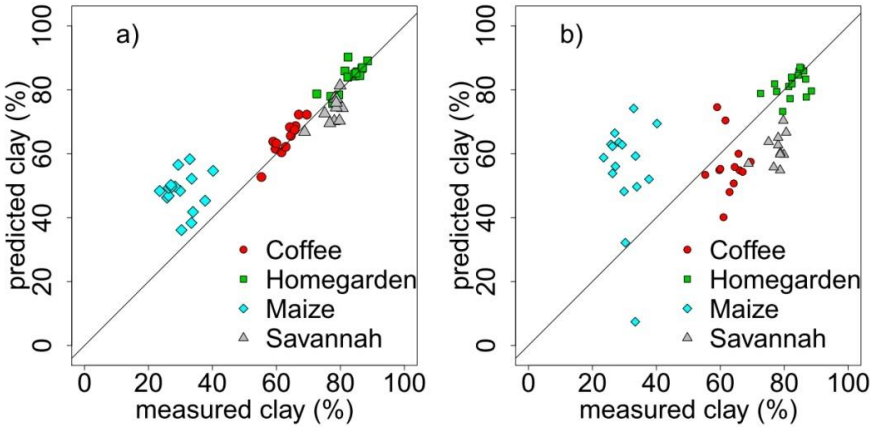

Figure 1. Predicted versus measured clay content for a) spectra taken under laboratory conditions and b) field spectra

Table 2. Validation parameters for laboratory and field predictions of clay content

	Air-dried spectra			Field spectra		
Plot	RMSE	RPD	R^2	RMSE	RPD	R^2
Homegarden	3.0	1.48	0.51	4.4	0.96	0.15
Coffee plantation	3.0	1.33	0.38	11.6	0.33	-8.8
Savannah	5.1	0.65	-1.64	16.7	0.2	-27.6
Maize field	19.3	0.24	-17.8	29.7	0.15	-43.6
All Plots	11.0	2.02	0.75	18.5	1.18	0.27

There are, however, large differences between the individual plots. The clay content of the homegarden, coffee and savannah profiles could be predicted quite accurately from air dried spectra. In contrast, the clay content in the maize field was poorly predicted. This could be due to a high amount of volcanic material in the soil. In our study we had only few samples of this material, so that it is probably under-represented in our calibration dataset.

Due to the fact that scanning was conducted during the rainy season, field spectra were probably affected by the moisture content of the soil. As soil moisture has a strong influence on the reflectance spectra (Lobell et al., 2002), spectra taken under field conditions are often not reliable. Other factors influencing the spectra are the size and shape

of the particles and the distribution of voids (Chang et al., 2001), thus smearing of clay during surface preparation or differences in bulk density could have an effect.

3.3 Small scale variability in the field

For each 3 x 3cm segment of the profiles clay content was predicted from field spectra with the respective model (Figure 2). Differences between the ecosystems are clearly visible. Soil in the homegarden ecosystem showed high clay content throughout the profile. In the maize profile the starting of the Cv-horizon at about −30cm was clearly visible. The accuracy of these predictions however is not yet satisfying and interpretations are preliminary.

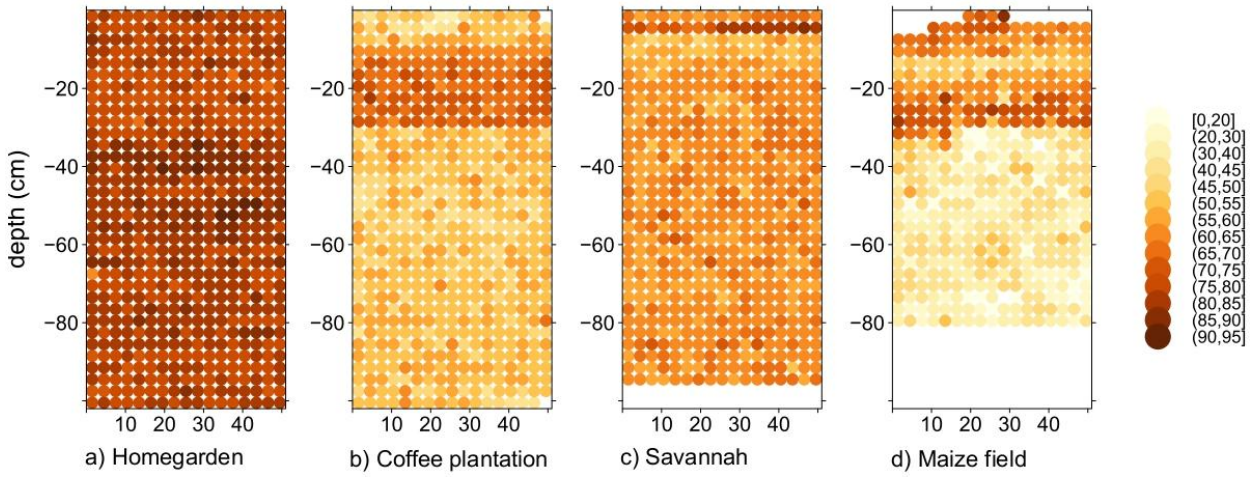

Figure 2. Small scale variability of clay content (%) in the different ecosystems

4 Conclusions

VIS-NIR spectroscopy is a fast and promising tool, but not yet applicable for detecting small scale differences in the field. Moisture content in the field and the different structure of the soil in situ compared to sieved samples needs to be taken into account. Possible solutions are preprocessing the calibration dataset with external parameter orthogonalisation, as suggested by Minasny et al., 2011 or to consider the difference between field and laboratory spectra. Whenever predictions are more accurate however, VIS-NIR spectroscopy can be used to assess the spatial organisation of soils rapidly and helps to understand the functioning of the soil within the ecosystem.

Acknowledgements

This study was funded by the German Research Foundation (DFG) within the Research-Unit 1246 (KiLi) and supported by the Tanzanian Commission for Science and Technology (COSTECH), the Tanzania Wildlife Research Institute (TAWIRI) and the Mount Kilimanjaro National Park (KINAPA). Additionally we want to thank Johannes Hepp for assistance in the field and laboratory.

References

AWITI, A. O., WALSH, M. G., SHEPHERD, K. D., KINYAMARIO J. 2008. “Soil condition classi-fication using infrared spectroscopy: A proposition for assessment of soil condition along a tropical forest-cropland chronosequence”. In: Geoderma 143.1-2, pp. 73–84

BECVAR, M., HIRNER, A., HEIDEN, U. 2006 - 2008. DLR Spectral Archive. url: http://cocoon.caf.dlr.de/intro_en.html

CHANG, C.-W., LAIRD, D. A., MAUSBACH, M. J., HURBURGH, C. R. 2001. “Near-Infra-red Reflectance Spectroscopy – Principal Components Regression Analyses of Soil Properties”. In: Soil Sci. Soc. Am. J. 65.2, pp. 480–490

FAO, IUSS WORKING GROUP, WRB 2007. World Reference Base for Soil Resources, first update 2007. World Soil Resources Report 103. Rome, Italy.

FERNANDES, E. C. M., OKTINGATI, A., MAGHEMBE, J. 1985. “The Chagga homegardens: a multistoried agroforestry cropping system on Mt. Kilimanjaro (Northern Tanzania)”. In: Agroforestry Systems 2, pp. 73–86

LOBELL, D. B., ASNER, G. P. 2002. Moisture Effects on Soil Reflectance.

MINASNY, B., MCBRATNEY, A. B., BELLON-MAUREL, V., ROGER, J.-M., GOBRECHT, A., FERRAND, L., JOALLAND, S. 2011. “Removing the effect of soil moisture from NIR diffuse reflectance spectra for the prediction of soil organic carbon”. In: Geoderma 167-168, pp. 118-124

MORGAN, C. L., WAISER, T. H., BROWN, D. J., HALLMARK, C. T. 2009. “Simulated in situ characterization of soil organic and inorganic carbon with visible near-infrared diffuse reflectance spectroscopy”. In: Geoderma 151.3-4, pp. 249 –256

NOCITA, M., KOOISTRA, L., BACHMANN, M., MÜLLER, A., POWELL, M., WEEL, S. 2011. “Predictions of soil surface and topsoil organic carbon content through the use of laboratory and field spectroscopy in the Albany Thicket Biome of Eastern Cape Province of South Africa”. In: Geoderma 167-168, pp. 295–302

R DEVELOPMENT CORE TEAM. 2011. R: A Language and Environment for Statistical Compo-ting. ISBN 3-900051-07-0. R Foundation for Statistical Computing. Vienna, Austria.

SOINI, E. 2005. “Changing livelihoods on the slopes of Mt. Kilimanjaro, Tanzania: Challenges and opportunities in the Chagga homegarden system”. In: Agroforestry Systems 64.2, pp. 157–167

STENBERG, B. 2010. “Effects of soil sample pretreatments and standardised rewetting as interacted with sand classes on Vis-NIR predictions of clay and soil organic carbon”. In: Geoderma 158.1-2. Diffuse reflectance spectroscopy in soil science and land resource assessment, pp. 15 –22

VISCARRA ROSSEL, R., MCGLYNN, R., MCBRATNEY, A. 2006. “Determining the composition of mineral-organic mixes using UV–vis–NIR diffuse reflectance spectroscopy”. In: Geoderma 137.1-2, pp. 70–82

VISCARRA ROSSEL, R. 2008. “ParLeS: Software for chemometric analysis of spectroscopic data”. In: Chemometrics and Intelligent Laboratory Systems 90.1, pp. 72–83

Comparison of soil property prediction ability of two VIS-NIR spectrometers

T. Mannschatz[1*], K.-H. Feger[2], P. Dietrich[1]

[1] Helmholtz Centre of Environmental Research - UFZ, Department of Monitoring and Exploration Technologies, Leipzig, Germany and University of Tübingen, Germany
[2]Dresden University of Technology, Institute of Soil Science and Site Ecology, Tharandt, Germany
[*]E-mail: theresa.mannschatz@ufz.de

Abstract

Novel approaches are required to perform soil mapping of physical and chemical properties since traditional methods are both time and cost intensive. We compared two different mobile VIS-NIR spectroscopy instruments in order to investigate and compare their soil property prediction abilities.

Keywords: VIS-NIR spectroscopy, soil science, PLSR, instrument comparison, soil mapping.

1 Introduction

Traditional soil sampling methods for soil mapping or monitoring are not very cost effective and are time consuming. An alternative approach that allows for fast and more cost-effective (and thus quasi-continuous soil investigation) is visible near-infrared (VIS-NIR) spectroscopy (Reeves 2010, Shepherd & Walsh 2002, Viscarra Rossel et al. 2010). Nowadays, several mobile VIS-NIR spectroscopy instruments are commercially available which possess different characteristics and can operate at diverse modalities.

This study evaluates the prediction performance of two commercially available mobile VIS-NIR spectrometers. The prediction results obtained from the devices are compared for several soil properties. The motivation for this research is to identify and to compare the prediction abilities of both spectrometers for a distinct soil property. In the case that both spectrometers perform similarly, the user could select the instrument according to their budget and application objective. Taking the research objective into account, we investigated two mobile spectrometers, namely the VERIS (Veris Technologies, Inc., Salina KS, USA, www.veristech.com) and ASD Fieldspec3 (Analytical Spectral Devices, Boulder, CO) devices, to analyze if sensor data obtained are comparable. Firstly, we studied: (i) the spectral differences and (ii) the predictive performance based on calibration models of selected soil properties of each spectrometer.

2 Materials and methods

To ensure that the results obtained remained generally valid, soil samples from two different climatic regions were analyzed (semi-arid NW Jordan and humid-tropical NE Brazil). Soil samples were collected from two different climate regions: humid tropical Northeastern Brazil and subtropical-Mediterranean to semi-arid Northern Jordan. The predominant soil type at both sites is Vertisol. In Jordan, both vertic Cambisols and Vertisols are present. The Brazilian sampling site is located 4 km south of Santo Amaro in Northeastern Brazil (Bahia state) and is characterized by flat terrain with elevations ranging from 0 to 70 m above sea level (Jarvis et al. 2008). Vegetation onsite is comprised of a bamboo (*Bambusa vulgaris*) plantation and a secondary forest consisting of native forest and agricultural species, such as cacao. The sampling area is approximately 10 km². The region receives a mean annual precipitation of about 1600 mm (1945-2011) with a rainy season from March to August and a dry season from September to February. Mean annual temperature is 24°C (CEPLAC & CEPEC 2012). In contrast, the Jordan study site is located in NW-Jordan in the Wadi Al-Arab catchment, which is ca. 300 km² in size. The Mediterranean climate is characterized by a yearly mean air temperature of approximately 24°C and mean annual precipitation of 400 mm.

In total, 148 soil samples were randomly collected and analyzed from both study sites. The soil sample pool is formed by 61 Brazilian composite soil samples from 0-30 cm depth and 34 single samples originating from different depths (0-10, 10-30, 30-70, 70-100 cm) and 53 Jordan composite soil samples. All soil samples were removed from their roots, air dried (35-40°C) and sieved to 2 mm. The samples were analyzed in the laboratory for soil texture, nitrogen (N), total (TC), inorganic (TIC) and organic carbon (TOC) (Table 1).

The fine fractions of all samples were scanned in the laboratory with an ASD FieldSpec3 (Analytical Spectral Devices, ASD Inc., Boulder, CO, USA) and a VERIS (Veris Technologies, Salina, KS) spectrometer. For FieldSpec3 measurements, the fine soil sample (ca. 50g) was placed in a 10 cm diameter Petri dish and illuminated by a halogen quartz lamp (Kaiser, 1000W). A Spectralon ‘white reference’ was used every 10 scans to calibrate the system. For measurements with VERIS, a smaller soil sample (ca. 5 g) is required. The instrument is calibrated before the measurement based on gray references. For each soil sub-sample, 20 measured spectra are averaged in total to obtain one spectrum. In order to improve the understanding of collected soil sample homogeneity and the consistency of repeated spectral measurements, each soil sample was measured twice at 90° rotations (Fieldspec3) or using a sub-sample (VERIS).

Noise reduction was achieved in original spectra wavelength by omitting any such ‘noisy bands’ from Fieldspec3 and VERIS spectra data. Both raw spectral datasets were then re-sampled to 5nm by interpolating between every 5th nm wavelength to fit with the native resolution of both instruments, thereby assuring comparability. For our comparison

of model results, the spectral range used (400-1000 nm and 1100-2220 nm) was the same for both instruments. Furthermore, the (1) reflectance, (2) absorbance, (3) 1st and (4) 2nd derivate (both polynome of 3rd order) as well as (5) MSC and (6) Range Normalization were applied to raw spectral data.

Table 1. Soil sample analysis methods and soil properties

Site	n	Method	Property	Max	Min	Mean	Median	Range	SD
Brazil (total 95)	62	Pipette method	Clay %	81.9	7.2	**60.7**	67.7	74.7	32.8
			Silt %	84.5	11.0	**23.8**	21.8	73.4	14.7
			Sand %	78.8	1.0	**12.8**	5.3	77.7	15.1
	95	Leco RC-412	TOC %	5.20	0.41	**2.54**	2.74	4.79	1.10
			TIC %	2.44	0.04	**0.19**	0.11	2.41	0.30
			TC %	5.44	0.87	**2.73**	2.91	4.57	1.07
	48	TrueSpec CHN	N %	0.40	0.02	**0.21**	0.24	0.39	0.13
Jordan (total 98)	29	Pipette method	Clay %	55.2	9.8	**33.4**	33.1	45.4	16.8
			Silt %	60.0	16.5	**45.9**	46.0	43.5	21.8
			Sand %	39.4	0.4	**9.1**	7.6	38.9	6.8
	55	Leco RC-412	TOC %	3.97	0.45	**1.71**	1.59	3.50	1.11
			TIC %	10.02	0.09	**5.22**	6.41	9.90	3.40
			TC %	11.47	0.79	**6.93**	8.11	10.70	4.17
		TrueSpec CHN	N %	0.24	0.00	**0.04**	0.01	0.20	0.06

PLS-Regression was used for the development of a calibration model for each instrument, soil property and study site. Sample outliers were removed prior to regression. Validation was performed as 'one-leave-out' cross-validation and as test-set validation. The performance quality indicators used are root mean square error of prediction (RMSEP), coefficient of determination of validation (Q^2), bias between predicted and measured (bias) and ratio of performance to deviation (RPD). For test set-validation, prediction quality is also investigated using a bootstrapped regression between predicted Fieldspec3 and VERIS values. This yields the requisite confidence intervals. Bootstrapping is based on resampling algorithms that allow the calculation of a confidence interval even if the sample population is not perfectly 'normally distributed' or small (Efron & Tibshirani 1994).

3 Results and Discussion

With the intention to obtain a representative spectrum of a soil sample, two soil subsamples from a single soil sample are averaged to a mean spectrum that is then used

to construct the calibration model (PLSR). However, because of the averaging important soil information may be lost. For that reason it is helpful to understand the uncertainty introduced by averaging of soil spectra and the potential effect of soil sample heterogeneity on the calibration model results. In order to evaluate the influence of soil heterogeneity, two different calibration models are constructed for each soil property. One model is based on the highest and one model is based on lowest measured spectrum of both sub-sample measurements. Sequentially, the percentage difference of the soil property prediction value and corresponding RMSEP of both calibration models are compared. The soil sample heterogeneity test shows that the percentage variability of model prediction (RMSEP) varies for mean percentage variability of carbon and N prediction by about 0.1% (1.7%) for VERIS and 0.1% (4.8%) for Fieldspec3. For mean texture variability, the percentage model prediction (RMSEP) varies by about 0.9% (6.9%) for VERIS and 0.4% (4.0%) for Fieldspec3.

In order to clarify whether the information content encoded within the spectra of both instruments is similar, the 1st derivative spectra of reflectance is analyzed for both sets of soil samples from Jordan and Brazil. The spectral heterogeneity between VERIS and Fieldspec3 of the normalized 1st derivative reflectance range is higher for VIS measurements than for the NIR spectral range. Nevertheless, the overall shape of the spectral information is comparable between both instruments (Figure 1).

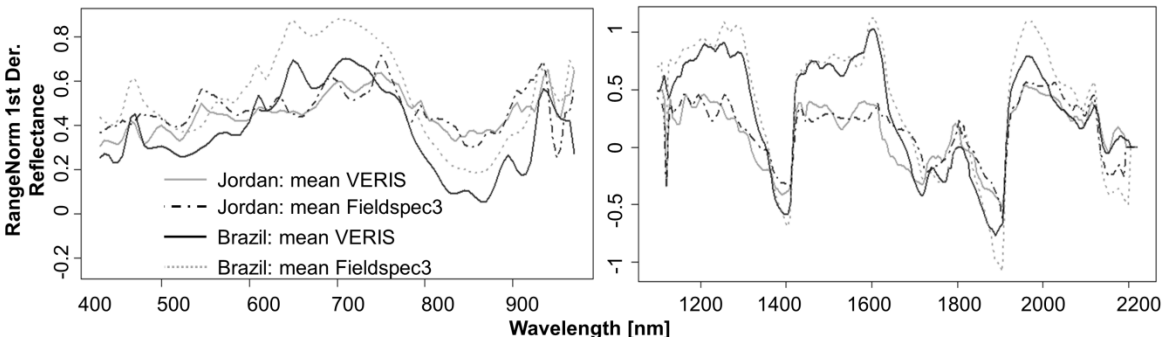

Figure 1. Range normalized mean of 1st derivative spectra of reflectance is calculated over all soil samples at each wavelength for Fielspec3 and VERIS at each study site for (left) visible and (right) NIR range.

When we performed a cross-validation, the PLSR calibration models generally achieved similar results for both instruments and independently of study site for TOC, TIC, TC, N, clay, silt, and sand. For the Jordan study site, we obtained good cross-Q^2 validation (Q^2) results for TC (0.93), TIC (0.89), Sand (0.88) and Clay (0.83). Sufficient Q^2 results were obtained for Silt (0.74) and TOC (0.72) and low Q^2 for N (0.51). For the Brazilian site, good Q^2 values were achieved for clay (0.86), N (0.86), TOC (0.82) and sufficient Q^2 results for Sand (0.78) and TC (0.76). Low results were realized for TIC (0.54) and silt (0.29).

The predictive ability of both instruments was additionally tested using test set-validation for the Brazilian samples. The test set-validation results are generally inferior to the cross-validation results due to a smaller dataset being used than for the calibration models. However, prediction performance of both instruments was still similar in most cases with the exception of clay and sand prediction (Figure 2), where Fieldspec3 outperformed VERIS. The linear regression between the predicted test set-samples of VERIS and Fieldspec3 shows low R^2 for Silt% (0.40) and Sand% (0.36), moderate R^2 for TIC% (0.69), N% (0.65) and Clay% (0.50). A very good accordance between predicted values from the VERIS and Fieldspec3 devices is obtained for TOC% (0.87).

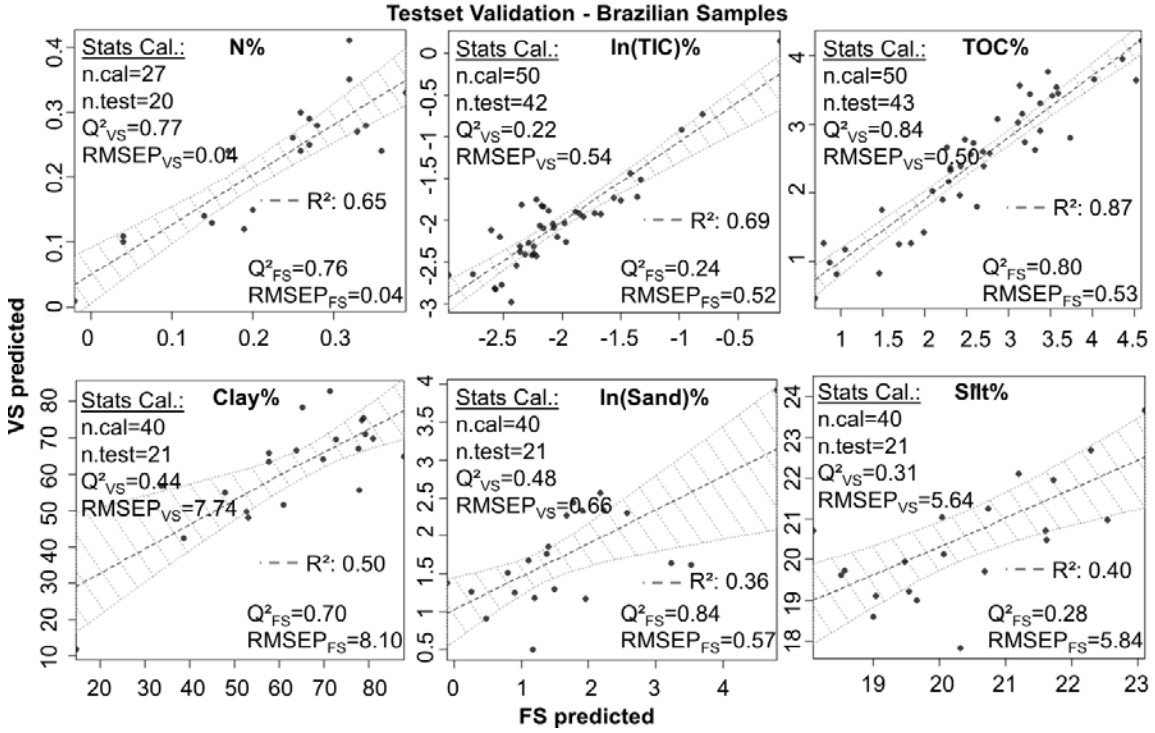

Figure 2. Bootstrapped regression of test set-validation results for the Brazilian soil samples as predicted vs. predicted of a) VERIS (VS) and b) Fieldspec3 (FS). R^2 (Spearman) corresponds to the regression result between predicted vs. predicted and the "stats cal." summarizes the validation results of the corresponding calibration models calculated based on VERIS or Fieldspec3., Q^2 (Spearman) is calculated to validate results using predicted and measured values for each calibration model.

4 Conclusion

When constructing the calibration models, it was not possible to identify a specific spectral data pre-processing method based on all available soil samples that yields the best prediction performance results for a specific soil property. Hence, we suggest that it is advantageous to experiment with different data pre-treatment methods in order to obtain the best prediction performance and uncertainties. The results of the cross-validation of calibration models reveal that predictive ability is similar for both instruments. However, the comparison of range normalized 1st derivative reflectance between VERIS and

Fieldspec3 shows that spectral information from both instruments is comparable, but not identical. This becomes apparent when the calibration models are based on smaller datasets and evaluated using a defined test set. The single soil sample heterogeneity test showed that soil samples are homogeneous, leading to mean variations of model prediction (RMSEP) smaller than 1% (6%). However, the VERIS device seems to be more sensitive to influences caused by texture than to carbon and N predictions. Fieldspec3 show similar sensitivities for texture, carbon and N predictions and prediction variability is higher than for the VERIS device – even sub-measurements could be captured from the same sub-sample by simply rotating the sample by 90°.

Acknowledgement

This research was funded by the IPSWAT scholarship program, an initiative of BMBF. Furthermore, this work was kindly supported by Helmholtz Impulse and Networking Fund through Helmholtz Interdisciplinary Graduate School for Environmental Research (HIGRADE) (Bissinger & Kolditz 2008). We sincerely thank Stephan Schulz and Sabine Kraushaar for providing the Jordan soil samples. We thank Stefan Burkhardt, Dr. Angela Lausch, Gundula Schulz and Steffen Lehmann for the measurement support. Special thanks to native English speaker Christopher Higgins for proofreading this text.

References

CEPLAC & CEPEC. 2012. Climate Data of ESOMI (Experimental station Sósthenes de Miranda). climate data. Retrieved (http://www.ceplac.gov.br).

EFRON, B., TIBSHIRANI, R.J. 1994. An introduction to the Bootstrap - Monographs on Statistics and Applied Probability. CRC Press.

JARVIS, A., REUTER, H. I., NELSON, A., GUEVARA, E. 2008. Hole-filled seamless SRTM data V4. International Centre for Tropical Agriculture (CIAT), USGS/NASA Retrieved (http://srtm.csi.cgiar.org).

REEVES, J. B. 2010. Near- versus mid-infrared diffuse reflectance spectroscopy for soil analysis emphasizing carbon and laboratory versus on-site analysis: Where are we and what needs to be done?" Geoderma 158(1-2):3–14.

SHEPHERD, K. D., WALSH, M. G.. 2002. Development of Reflectance Spectral Libraries for Characterization of Soil Properties. Soil Science Soc. Am. Journal (66):988–998.

VISCARRA ROSSEL, R. A., STENBERG B., MOUAZEN A. M., WETTERLIND, J. 2010. Visible and near infrared spectroscopy in soil science. p. 163–215 in Advances in Agronomy, vol. 107, edited by Donald L. Sparks. Burlington: Academic Press.

Towards an on-the-go assessment of soil organic carbon using VIS-NIR diffuse reflectance spectroscopy using a tractor-driven chamber

A. Rodionov[1], G. Welp[1], L. Damerow[2], T. Berg[2], W. Amelung[1], S. Pätzold[1*]

[1]*University of Bonn, Institute of Crop Science and Resource Conservation (INRES), Soil Science, Nussallee 13, 53115 Bonn, Germany*

[2]*University of Bonn, Institute of Agricultural Engineering, Nussallee 5, 53115 Bonn, Germany*

[*]*E-mail: s.paetzold@uni-bonn.de*

Abstract

High resolution estimation of soil organic carbon (SOC) contents in the field is requested for Precision Farming purposes. Diffuse reflectance spectroscopy (VIS-NIRS) is a promising tool for SOC prediction. However, spectra acquisition in the field is restricted by several factors. The project presented here aimed at developing a universal prediction model which allows SOC prediction on moist and rough soil surfaces. Further, a mobile measuring chamber was constructed for spectra acquisition in the field, but under controlled conditions. First tests on arable fields with heterogeneous SOC contents yielded very promising prediction quality and mapping results.

Keywords: soil organic matter prediction estimation, on-the-go spectra acquisition.

1 Introduction

High-resolution field estimation of soil organic carbon (SOC) content and its spatial pattern on arable land are requested for, e.g., precision agriculture purposes (Patzold et al., 2008). Such measurements could be conducted via VIS-NIR diffuse reflectance spectroscopy (VIS-NIRS). In the past years the optical sensing of SOC has made considerable progress; however, most studies were conducted under laboratory conditions. Field studies are scarce, because illumination, soil moisture and surface roughness vary and diminish the quality of SOC prediction via Partial Least Square Regression (PLSR) models. We hypothesized that an on-the-go field measurement should be possible given an adequate minimization of these disturbing influences. Thus, our project aimed at (i) quantifying the influence of disturbance factors, (ii) testing correction possibilities, and (iii) preparing a system for reliable on-the-go SOC measurements for Precision Farming purposes.

2 Experimental approach

We chose two long-term fertilizing experiments at the University of Bonn (homogeneous substrate and soil texture, heterogeneous SOC contents) as study sites. First, undis-

turbed soil samples were taken to the lab and VIS-NIRS spectra (410-2300 nm) were acquired at difference moisture and roughness conditions in order to build a model for field conditions. For the on-the-go measurements, a closed chamber to be mounted to a tractor was constructed. The chamber is equipped with a generator, allowing an artificial illumination with six halogen lamps with a defined quality (Fig. 1). An ASD AgriSpec spectrometer (350-2500 nm) was used in the lab as well as mounted to the mobile chamber.

Figure 1. Novel mobile measuring VIS-NIRS chamber during field survey of SOC contents.

3 Results and discussion

We successfully developed a universal procedure to predict at first soil moisture content, which allows in a second step deriving moisture-specific SOC predictions. Thereby, roughness reduced reflectance, but did not disturb moisture prediction. Thus, we derived soil moisture from the spectra and annotated the actual field conditions to one of three moisture classes. For each moisture class, a separate SOC model was applied. Again, roughness did not disturb the SOC prediction. This approach does not require spectra transformation as proposed by McBratney et al. (2011). Yet, it proved to yield sufficiently precise moisture prediction for applying the correct SOC model. The newly constructed measuring chamber offered weather-independent illumination conditions and a measuring geometry which resulted in a prediction quality comparable to laboratory conditions.

Stop-and-go measurements as well as on-the-go measurements at 3 km h^{-1} were conducted on all plots of both field trials. Plant debris and gravel on the soil surface resulted in erratic extremes of SOC contents. Most often, negative SOC contents were predicted in such situations. In this stage of the project, we manually eliminated these data as outliers. Anyway, only approx. 2.5 % of the data points were eliminated, because the soil had been ploughed and tilled; moreover, gravels seldom disturbed the spectra because the soils were almost free of stones (loess and fluvial sediment,

respectively). After connecting the predicted SOC contents with the GPS coordinates in ArcGIS software, SOC maps were created. Fig. 2 shows the predicted SOC contents as estimated on-the-go for the Dikopshof trial. The variation of SOC contents derived from a 100 years experimental period with varying input of manure and mineral fertilizer. The plots in the north-eastern part of the trial did not receive manure, resulting in relatively low SOC contents. With a coefficient of determination of R^2 = 0.53 to 0.67 and a standard error of estimation of 1.4 g SOC kg^{-1}, the results are promising, but require further optimization.

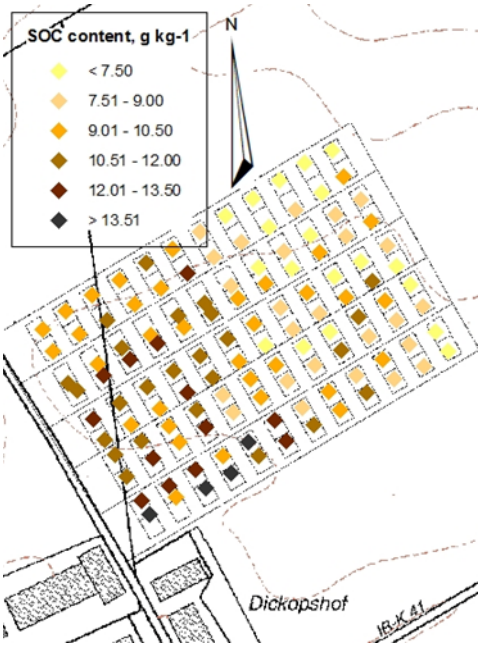

Figure 2. Map of predicted SOC contents in 120 plots (each of 18.5 * 7 m size) of the long-term trial at Dikopshof research station. Related spectra were acquired on-the-go using the novel measuring chamber.

Our approach requires some efforts for the preparation of the soil surface. Ploughing and tilling were carried out to create a surface which was mostly free of plant debris and fine-structured. However, other systems which are less dependent from surface conditions have been presented. Mouazen et al. (2005, 2007, 2009), for example, used a VIS-NIR fiber system in combination with a subsoiler chisel which acquired the spectra under the soil surface. Though, other problems occurred such as geometrical variation of the subsoiler position, soil-to-sensor distance variation, or contact problems between sensor unit and soil. These problems do not play a role using our measuring chamber.

4 Conclusions

Reliable on-the-go field estimation of SOC contents is possible at a satisfying precision following the approach presented here. Spectra acquisition in the field using the novel

measuring chamber and SOC prediction with the developed universal model makes VIS-NIRS application mostly independent of weather and soil surface conditions. Automated algorithms for choosing the appropriate moisture-adapted SOC model as well as for outlier identification will further improve the performance of the procedure. Alternatively, other moisture correction approaches such as proposed by McBratney et al. (2011) could be tested. Mapping SOC on-the-go for Precision Agriculture applications seems possible in the near future.

Acknowledgements

The project was funded by the German Federal Ministry of Education and Research (BMBF) and the State Ministry of Innovation, Science, Research and Technology of North Rhine-Westphalia (Germany) as part of the CROP.SENSe.net network.

References

McBratney, A.B., Minasny, B., Bellon-Maurel, V., Gobrecht, A., Roger, J-M., Ferrand, L., Joalland, S. 2011. Removing the effect of soil moisture from NIR diffuse reflectance spectra for prediction of soil carbon. The Second Global Workshop on Proximal Soil Sensing – Montreal 2011, 108-111.

Mouazen, A.M., De Baerdemaeker, J., Ramon, H. 2005. Towards development of on-line soil moisture content sensor using a fibre-type NIR spectrophotometer. Soil Till. Res. 80 (1–2), 171–183.

Mouazen, A.M., Maleki, M.R., De Baerdemaeker, J., Ramon, H. 2007. On-line measurement of some selected soil properties using a VIS-NIR sensor. Soil Till. Res. 93, 13-27.

Mouazen, A.M., Maleki, M.R., Cockx, L., Van Meirvenne, M., Van Holm, L.H.J., Merckx, R., De Baerdemaeker, J., Ramon, H. 2009. Optimum three-point link set up for optimal quality of soil spectra collected during on-line measurement. Soil Till. Res. 103 (1), 144–152.

Pätzold, S., Mertens, F.M., Bornemann, L., Koleczek, B., Franke, J., Feilhauer, H., Welp, G. 2008. Soil heterogeneity at the field scale: a challenge for precision crop protection. Prec. Agric. 9, 367–390.

Removing the effects of water from proximally sensed vis-NIR spectra of paddy soil

W. Ji[1,2*], R. A. Viscarra Rossel[2], Z. Shi[1]

[1]*Institute of Agricultural Remote Sensing and Information Technology Application, College of Environmental and Resource Sciences, Zhejiang University, Hangzhou, China, 310058*
[2]*CSIRO Land and Water, Bruce E. Butler Laboratory, PO Box 1666, Canberra, ACT 2601, Australia*
[*]*E-mail: 30239000@qq.com*

Abstract

In-situ and air-dried ground spectroscopic measurements were separately completed for one hundred and four samples from paddy fields in Zhejiang province, China. All samples were divided into calibration and validation set. A subset of the calibration set, known as transfer set, was selected to obtain the transfer parameters. Validation set was transferred and validated by PLSR model developed using the lab-collected spectra of calibration samples. The prediction improved greatly when comparing to that predicting with original field-collected spectra. China soil spectral library were used to further test the spectral transferability of the direct standardization (DS) algorithm and met with success. This research shows the great transferability of DS algorithm in correcting the effect of water content on field-based spectroscopic measurements.

Keywords: direct standardization (DS), visible and near-infrared (vis-NIR), water effect, paddy soil.

1 Introduction

Proximal soil vis–NIR sensing is currently receiving attention because it is an effective approach to collect soil information rapidly and cheaply (Viscarra Rossel et al. 2011). While some studies have shown that proximally sensed spectra can be used to predict soil properties (Waiser *et al.*, 2007; Morgan *et al.*, 2009; Viscarra Rossel *et al.*, 2009; Kusumo *et al.*, 2010), there are also unsuccessful reports (e.g. Udelhoven *et al.*, 2003). Spectra recorded in the field are affected by environmental factors such as the amount of water in the soil, ambient light, temperature and the condition of the soil surface. soil water has the most obvious effect on spectra, causing the depth and width of the water absorptions near 1400 nm and 1900 nm to increase but generally producing an overall decrease in reflectance (Bowers & Hanks, 1965; Viscarra Rossel & McBratney, 1998). The effects of environmental factors on field-recorded vis–NIR spectra and their effects on the accuracies of spectroscopic models to predict soil properties need further research.

A number of strategies that aim to account for the effects that the environment has on spectra to improve the spectroscopic calibrations of soil have been reported. They may be characterized as strategies to (i) improve the leverage of multivariate calibrations by 'spiking', (ii) improve the similarity between spectra using spectroscopic preprocessing and/or transfer algorithms and (iii) to remove the effects of 'unwanted' spectral parameters from the calibrations.

As is recognized, substantial efforts (i.e. time and cost) have been paid to build a robust calibration model with lab-based spectra. However, the existing calibrations will become invalid when the soils to be predicted are measured under different environmental factors (in field condition). It would be a waste not to use the existing calibrations but to build a new model for spectra measured in new situation. This paper investigated direct standardization (DS) to correct the external environmental effects on field spectroscopic measurements and met with success. The DS algorithm directly relates the field-based spectra to the spectra measured in lab condition. Comparing to other algorithm on spectral transformation, the benefit of DS is the original calibration models could be kept after correcting those differences affected by external parameters on field-based spectra. Initially proposed by Wang et al (Wang *et al.*, 1991), DS was first used for NIR spectroscopy calibration transfer of gasoline samples when response variations exist between instruments. This algorithm was initially used to correct the spectra from the secondary spectrometer to match the ones measured on the primary instrument without the need of recalibrations. It has great abilities enabling not only to handle differences between two or over three instruments, the variation over time of one instrument or the different samples batches (Swierenga *et al.*, 1998; Li *et al.*, 2007), but also spectral corrections when physical modifications of soil samples occur (Bouveresse *et al.*, 1996) or measuring environment changes. In this study we presume that the external environmental effects on soil samples measured in field conditions, comparing to measurement in the lab, could be regarded as the measuring environmental change or samples physical modifications and therefore DS algorithms could be performed. To keep these models, DS algorithm is more practical than other method.

The aim of this study is focus on removing the effect of soil moisture on spectra measured in field conditions using DS algorithm for quantification of soil organic matter content (SOM). Calibration strategies were also carried out to make a comparison of the prediction results. All in all, the research procedures were threefold: 1) to compare the spectra obtained in field and in the laboratory; 2) to estimate the ability of SOM prediction using spectra measured in field conditions; 3) to apply DS algorithm on removing the water effects from the field in situ spectra and access its transferability.

2 Materials and methods

2.1 Soil sampling and spectra measuring experiment

One hundred and four surface soil samples (0-20cm) were collected at several paddy fields in seven cities of Zhejiang province, N29°03′~30°10′ , E119°10′~122°48′, before harvest in November, 2011. Soil samples were scanned firstly in situ using ASD field-spec Pro FR vis-NIR spectrometer (Analytical Spectral Devices, Boulder, CO, USA) equipped with a high intensity contact probe, with a performance of spectral range from 350 nm to 2500 nm. Meanwhile, water content was measured twice by TDR-300 (Spectrum Technologies Inc., USA) and averaged. After in situ spectra measuring, samples were collected and brought back to laboratory for lab-based spectral measurement. Soils were air-dried, ground and sieved to be smaller than 2 mm in size to measure lab-based spectra, using the same contact probe, and meanwhile to do “wet” chemical analysis of soil properties.

2.2 China soil spectral library

In the past several decades, more than 1552 soil samples have been accumulated to build a China soil spectral library. These soil samples were collected from different locations in Zhejiang, Heilongjiang, Sichuan, Henan and Xinjiang and other provinces in China, derived from different parent materials. They represent paddy soil, purple soil, phaeozem, Seashore solonchak and Fluvo-aquic soil and others and were taken from varies depth down to 1m from surface. The same vis-NIR spectrometer was used to measure the spectra. However, the difference is that here we used bare fibre and tungsten lamp instead of high intensity contact probe.

2.3 Soil organic matter content prediction

Soil organic matter was measured using dichromate oxidation method. Soil organic matter values were transformed into sqrt (OM) to get a lower skew and follow normal distribution. The spectral region with wavelength between 350-399 nm and 2451-2500 nm was deleted as noisy edges before soil statistics analysis. Reflectance spectra were sampled into 10 nm intervals.

Calibration separately with field- and lab-based spectra. In this study, 70 samples were selected from 104 experimental samples by Kennard-Stone method for the calibration set and the remaining samples were used in validation set (n=34). PLSR algorithms were performed on the calibration set with field- and lab-based spectra respectively with the optical number factors decided by leave-one-out cross validation, and the validation dataset were used to validate the PLSR model independently.

China soil spectral library used for organic matter predictions. For the China soil spectral library, 1552 samples were sorted by values from small to large sqrt (OM), odd rows

selected into training dataset (n=776) and even rows in test dataset (n=776). A model was conducted using training dataset by PLSR algorithm, the number factors of which were decided by leave-one-out cross validation, and independently tested by 776 test dataset samples. Before modeling, reflectance spectra from the library were transformed into absorbance (log 1/ reflectance), mean centred, and smoothed by Savitzky-Golay algorithm with polynomial of order 2 and window size of 11. To remove baseline effect, spectra were corrected by Standard Normal Variate (SNV). The library PLSR model were used to predict the organic matter content of 104 samples using lab-based spectra and field-based spectra, respectively, and the prediction accuracies were compared. The spectral transfer ability of DS algorithm was also further tested by validating with the library PLSR model, as well as the EPO algorithm.

2.4 Spectral transfer with DS

Direct standardization (DS) algorithm is a spectra transfer method available not only in different instruments or measurement modes standardization, but also in spectral correction resulted from instrument drift, changes in measurement or sample conditions (Tormod Naes et al, 2002). In this study, we employed multivariate DS techniques, using reflectance data at each wavelength in 10nm intervals in the full range between 400nm and 2450nm to calibrate field-based spectra. Hereafter, lab-based spectra were treated as master spectra and field-based spectra were slave spectra. After DS algorithm application, field-based spectra were transformed and looked more “similar” to lab-based spectra.

The aim of DS algorithm is to find the relation function between lab-based spectra $\mathrm{X_{lab}}$ and field-based spectra $\mathrm{X_{field}}$,

$$\boldsymbol{X}_{lab} = f(\mathrm{X_{field}}) \tag{1}$$

According to formula 1, $\mathrm{X_{field}}$ could be transferred to $\mathrm{X'_{field}}$ and thus the environmental effect such as water content, particle size, temperature and others could be removed.

The procedure of DS algorithm application is following:

Let $\mathrm{X_{lab}}$ be the spectra matrix of lab-based samples, $\mathrm{X_{field}}$ be the spectra matrix of field-based samples, the dimension of both of them are m*p, m is the number of soil samples and p is the number of wavelength. Then the multivariate DS approach assumes the model

$$\boldsymbol{X}_{\mathrm{lab}} = \boldsymbol{X}_{\mathrm{field}}\mathrm{B} + \mathrm{E} \tag{2}$$

Here B is the transfer matrix (p*p) of unknown parameters;

E is the residual matrix, which could be written as

$$\mathrm{E} = \mathrm{ld}_{\mathrm{s}}^{\mathrm{T}} \tag{3}$$

Where d_s is a p by 1 matrix produced by baseline difference and l is a column vector with all elements being 1. Then function 2 could be written as

$$\boldsymbol{X}_{lab} = \boldsymbol{X}_{field}B + l\mathrm{d}_s^{\mathrm{T}} \quad (4)$$

To compute the unknown B transfer matrix, a mean centered matrix Cm (m*m) was defined as,

$$\mathrm{C_m} = \mathrm{I_m} - (1/\mathrm{m})\mathrm{ll}^{\mathrm{T}} \quad (5)$$

Where $\mathrm{I_m}$is an m by m identity matrix.

We multiply $\mathrm{C_m}$ at both sides of formula 4, after which $\mathrm{C_mE}$ is equal to 0, $\mathrm{C_mX_{lab}}$ and $\mathrm{C_mX_{field}}$ were both mean centered spectra matrix of $\mathrm{X_{lab}}$ and $\mathrm{X_{field}}$, written as $\bar{\mathrm{x}}_{\mathrm{lab}}$ and $\bar{\mathrm{x}}_{\mathrm{field}}$. Thus, formula 4 was transformed to

$$\bar{\mathrm{x}}_{\mathrm{lab}} = \bar{\mathrm{x}}_{\mathrm{field}}\mathrm{B} \quad (6)$$

Further,

$$\mathrm{B} = \bar{\mathrm{x}}_{\mathrm{field}}{}^{+}\ \bar{\mathrm{x}}_{\mathrm{lab}} \quad (7)$$

Where "+"represent the generalized inverse of a matrix.

After getting transfer matrix B, we then started to calculate the residual matrix E. We multiplied $(1/\mathrm{m})\mathrm{l}^{\mathrm{T}}$ on both sides of formula 4, getting $\mathrm{d_s}$

$$\mathrm{d_s} = \mathrm{x}_{\mathrm{lab}}^{\mathrm{T}} - \mathrm{B}^{\mathrm{T}}\mathrm{x}_{\mathrm{field}}^{\mathrm{T}} \quad (8)$$

Where $\mathrm{x_{lab}}$ and $\mathrm{x_{field}}$ were row vectors (p*1) which consist of the averaged column elements of $\mathrm{X_{lab}}$ and $\mathrm{X_{field}}$.

In our study, $\mathrm{X_{lab}}$ was the matrix of lab-based spectra and $\mathrm{X_{field}}$ was the matrix of field-based spectra originating from the transfer set selected by KS algorithm as before, both of them were reflectance spectra. $\bar{\mathrm{x}}_{\mathrm{lab}}$ and $\bar{\mathrm{x}}_{\mathrm{field}}$ were mean centred reflectance spectra of $\mathrm{X_{lab}}$ and $\mathrm{X_{field}}$, m was the number of transfer samples and p was 206 (10 nm intervals).

After getting B and $\mathrm{d_s}$, the 34 field-based spectra from validation set could be transferred using:

$$\mathrm{X}'_{\mathrm{field34}} = \mathrm{X_{field34}B} + \mathrm{E} \quad (9)$$

In a nutshell, the DS algorithm application in this paper was as follows:

1. Apply DS algorithm on the transfer set (n=5, 10, 15, 20…65, 70), to get the transfer matrix B and the residual matrix E using formula 7 , 8 and 3;

2. Using B and E, transform 34 field-based spectra from the validation set to 34 transformed field spectra;
3. The 34 transformed field spectra were mean centered and transformed into absorbance to validate PLSR model built with 70 lab-based spectra from the calibration set.
4. R^2 , RMSE and RPD were calculated respectively in a series of transfer samples to help decide the optimal number of transfer samples.

All processing of data analysis and algorithms application were developed in R 2.15.0 and ParLes 3.1.

3 Results

3.1 Comparisons between field-moist in situ spectra and lab air-dried ground spectra

Figure 1 shows the differences between field-based spectra and lab-based spectra. It is obvious that field-based spectra were much higher than air-dried ground spectra in absorbance, and larger in width and depth in water absorbance band at 1450nm and 1940nm. The result is similar to what Minasny et al., 2011 reported but without SNV normalization. However, there are differences for their experiments only aimed to simulate field moisture condition that they produced air-dried soil samples with different moisture levels in the lab condition while our study was carried out under in situ field condition. The spectral differences at other wavelengths may be caused by other soil properties other than water content in soils. For example, the small peaks at 1700 nm and the several waves around 2300 nm show the combined influence of CH3, CH2 and CH (Weyer and Lo, 2002; Workman, 2000).

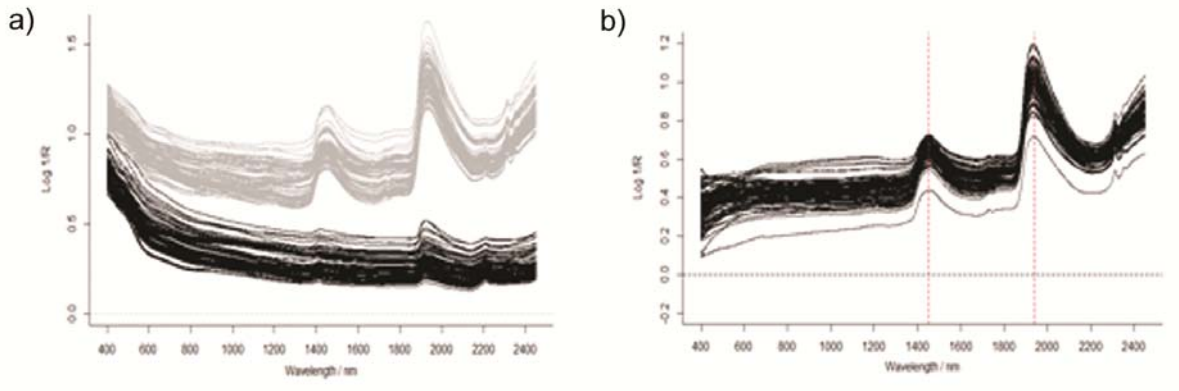

Figure 1. Comparison of 104 paddy soil spectra measured in field- and lab-based conditions. (a)Black curves are field-based spectra while grey curves are lab-based spectra. (b) The difference spectra of 104 paddy soil field- and lab-based spectra.

The first two principal components of the distribution of field-based, lab-based spectra and the 1552 spectra from the China soil spectral library were scatter plotted in Figure 2. In Figure 2(a), the first principal component occupied 86% of the variance, represen-

ting the largest differences between field-based spectra and air-dried ground spectra, while the second PC accounted for 10%. It is obvious that field-based spectra were separated with all other spectra including the lab-based spectra and 1552 spectra from the China soil spectral library. However, air-dried ground spectra were more similar with spectra from 1552 China library spectra. The differences between field-based spectra and air-dried ground spectra or library spectra were mainly caused by the soil water in the field, but some other effects such as particle size as well.

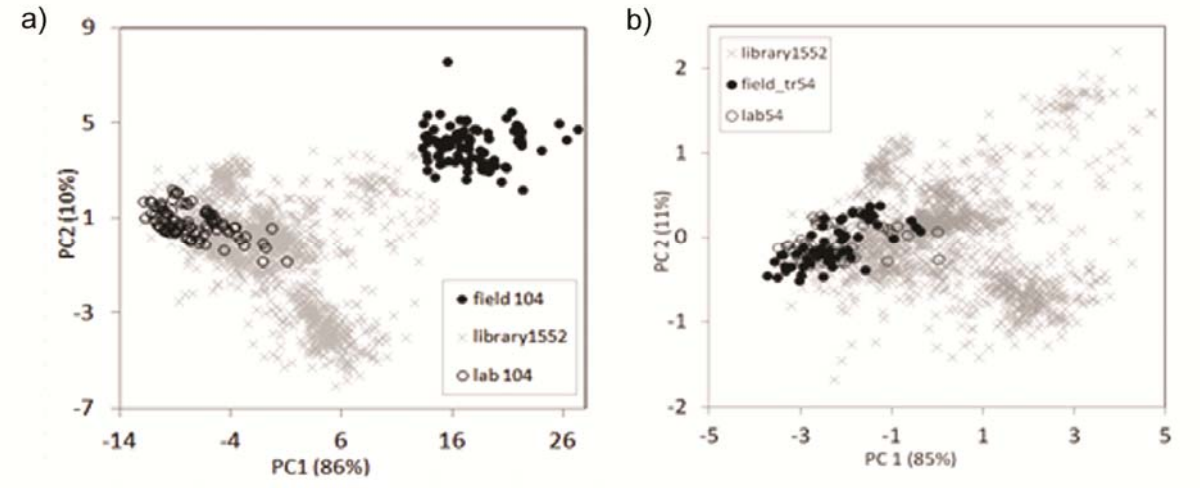

Figure 2. Principal component analyses of 104 field-based spectra, 104 lab-based spectra and 1552 spectra from the China soil spectral library. Black closed circles are field-based spectra, black open circles are lab-based spectra and light grey crosses are spectra from China soil spectra library. (a)PCA results of original 104 field-based spectra, 104 lab-based spectra and 1552 China library spectra; (b) after DS algorithm application, 54 field spectra were transformed to transformed field spectra (field_tr54). PCA results for 54 transformed field spectra, 54 corresponding lab-based spectra and 1552 spectra from the China soil spectral library.

3.2 DS for SOM prediction

The statistics of SOM content are listed below in Table 1. Soil organic matter were transformed into sqrt(OM) to decrease skews of data distribution.

3.2.1 Selection of standardization samples

Kennard-Stone algorithm was used to select samples for the transfer set, calculated from the PC scores of 70 field spectra in calibration set. The field- and lab-collected spectra of the transfer set samples were then used to compute the transfer matrix by the steps described in section *Materials and methods*. To decide the optimal number of transfer samples needed in DS algorithm, different size of transfer sets (n_{tr}=5, 10, 15, 20, 25…65, 70) were arranged from calibration dataset. To get comparable results, the same 34 samples from the validation set were then transferred by a series of transfer matrixes obtained from different transfer sets respectively. At last, the 34 transformed

field spectra were validated by PLSR model built with 70 lab-based spectra and prediction accuracies were plotted (Figure 3).

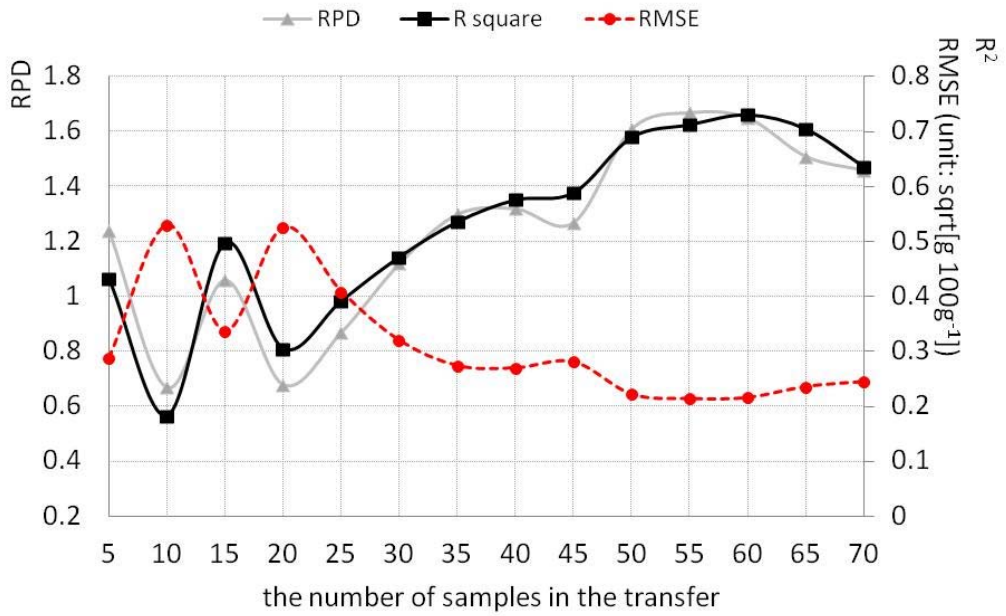

Figure 3. Prediction accuracies of different number of transfer samples. The RPD, R^2 and RMSE change with the number of samples selected in the transfer set.

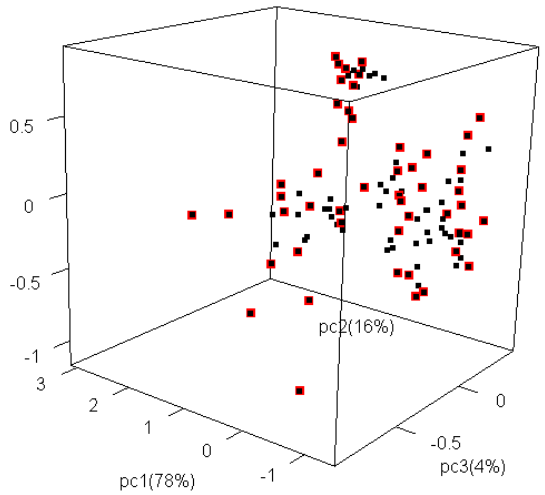

Figure 4. The distribution of 50 selected samples in transfer set by KS method. Black points are PC scores of 104 field-based spectra while the ones covered with red circles represent the 50 chosen samples by KS. It shows the 50 transfer samples PCs spread quite well in the environmental domain and have good representativeness of prediction samples.

Variable prediction results were obtained when the number of transfer samples was in the range of 5 to 25. The RMSE was high at 10 and 20 but low when 15 samples were used. Prediction accuracies became stable after using more than 25 samples, RPD and R^2 were increased overall and RMSE decreased after 25 samples, and all values stayed almost flat within small variations between 50 and 70 samples. RPD and R^2

remained at a high range (RPD>1.4, R^2>0.6) when the transfer samples number exceeded 50 and RMSE was lower than 0.3(unit: sqrt (OM %)), all predictions did not get remarkably better results after that. As a result, we conclude that at least 50 samples should be selected for the transfer set using KS method to develop the DS algorithm in our study.

Table 1. SOM (%) statistics of 104 paddy soil samples and 1552 library samples. SOM values were transformed into sqrt (OM) for their original values were not in normal distribution.

category	n	mean	St.d	min	med	max	Skew
China soil spectral library	1552	2.31	1.14	0.17	2.24	7.48	1.02
In this study	104	2.91	1.37	0.69	2.59	6.05	0.76

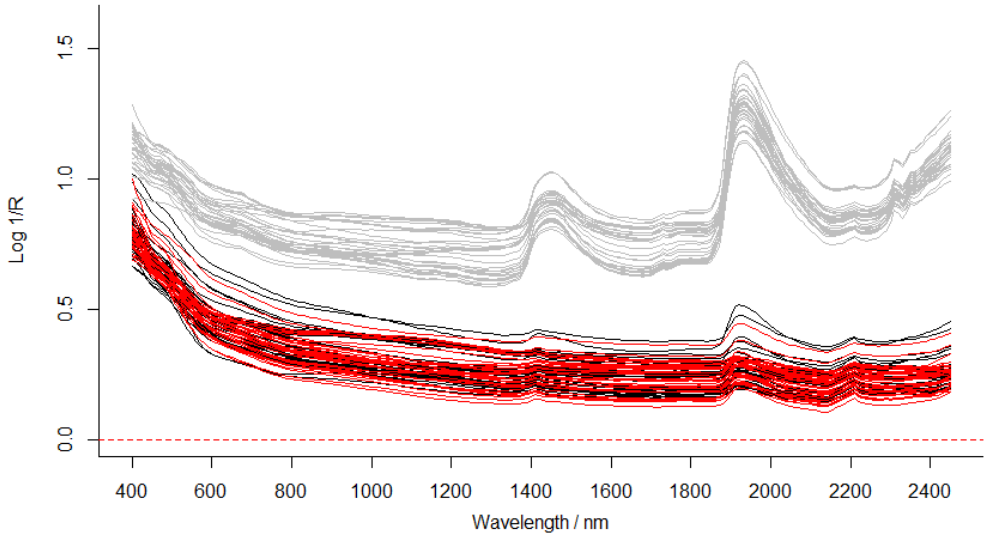

Figure 5. Spectral comparison of original field-based spectra, lab-based spectra and transformed field spectra after DS of 34 samples in validation set. The light grey curves were of original field-based spectra, black were lab-based spectra and red were transformed field spectra.

We also tested the other two ways to choose samples in transfer set: one was still based on the spectra features using KS method, but calculated from the PC scores of 70 lab-based spectra; the other was based on their response values (SOM values), which means, to select one sample at certain distances between intervals after sorting SOM content from smallest to largest. It is pleasing to see that both of the two selecting methods gave similar results.

3.2.2 DS algorithm for spectral transfer

The 50 selected transfer samples scattered at the entire space of the 104 field-based spectra PC scores created in figure 4, showing their excellent representativeness of the validation set. The relationship could be then built between lab-based spectra and field-based spectra using DS algorithm to get transfer parameters, and after which the 34

field-based spectra can be transformed to 34 transformed field spectra. The 34 transformed field spectra look quite similar to corresponding 34 lab-based spectra (Figure 5), almost coinciding, showing the success in spectral transferability of DS algorithm on field-based spectroscopic measurement.

Table 2. PLSR prediction accuracies of SOM content using field-based spectra and lab-based spectra, respectively.

Calibration dataset					Test prediction			
dataset	NO. factors	R2	RMSE	RPD	Dataset	R2	RMSE	RPD
Lab 70	10	0.92	0.13	3.46	Lab 34	0.81	0.17	2.05
Lab 70	10	0.92	0.13	3.46	Field 34	0.25	1.03	0.35
Field 70	10	0.87	0.16	2.79	Field 34	0.79	0.18	1.94
Lab 70	10	0.92	0.13	3.46	Transformed field 34	0.69	0.22	1.61

Prediction accuracies among the following three situations were compared: (i) 34 field-based spectra were validated by PLSR models built with 70 field-based spectra; (ii) 34 lab-based spectra were validated by PLSR models built with 70 lab-based spectra; (iii) 34 transformed field spectra were validated by PLSR models by 70 lab-based spectra. Samples were first split into calibration dataset (n=70) by KS algorithms and validation dataset (n=34). Good predictions could be performed with both field-based spectra and lab-based spectra for SOM estimation (Table 2) for both their R^2 around 0.8 and RPD around 2. This should be due to the direct spectral responses of carbon in the visible and near infrared range, which are the overtones and combinations of CH+CH and CH+CC whose fundamental vibrations occur in the mid-IR region (Viscarra Rossel & Behrens, 2010). However, prediction with lab-based spectra is slightly better than that with field-based spectra for its pre-treatments. Cross predictions were also produced between the two different measurement situations, but bad results were obtained. Calibrations built with 70 lab-based spectra cannot be used to predict with 34 field-based spectra from validation set (R^2=0.25, RMSE=1.03 sqrt(OM %) and RPD=0.35), and vice versa. After spectral transfer by DS algorithm, 34 transformed field spectra were estimate by PLSR model built with 70 lab-based spectra. The results were improved greatly compared with the validation using original field-based spectra: R^2 increased from 0.25 to 0.69 and RPD from 0.35 to 1.61 while RMSE decreased from 1.03 to 0.22 (unit: sqrt (OM %)). Figure 6 shows the predicted values of SOM against the observations. The predictions with 34 transformed field spectra were distributed around the 1:1 line and the prediction accuracy (RPD=1.61) was comparable with that of separately calibrating predictions (RPD_{lab}=2.05, RPD_{field}=1.94).

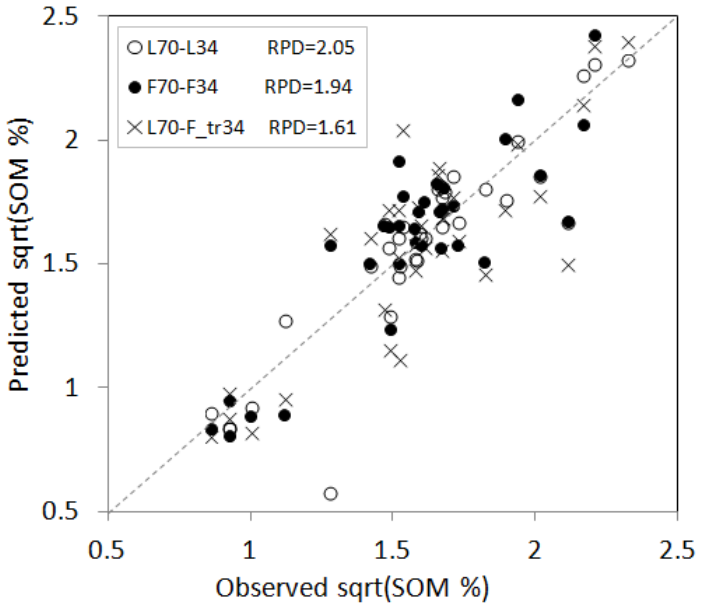

Figure 6. Scatter graph of predicted values against observed values of SOM. Black closed circles represent the predictions with 34 original field-based spectra by PLSR models built with 70 field-based spectra (F70-F34). Black open circles and black crosses were predictions with 34 lab-based spectra (L70-L34) and 34 transformed field spectra (L70-F_tr34) both validated by PLSR models built with 70 lab-based spectra.

3.3 Using the China soil spectral library to test spectral transferability of DS

The data for the China soil spectral library were used for further testing the practical applicability of DS algorithm. 50 transfer samples were selected in the same way as before and the remaining 54 samples were transformed. The principle component analysis of 54 transformed field spectra, 54 corresponding lab-based spectra and 1552 spectra from the China soil spectral library were scatter plotted in Figure 3(b). It shows the 54 transformed field spectra were quite close to those of lab-based spectra and occupied similar places in the area of library spectra scores in comparison to Figure 3(a). However, there remains a systematic difference in the scores between lab-based and field-based spectral PC scores. Some chemically relevant variance might have been lost in the spectral transfer.

According to leave-one-out cross validation, a PLSR model with 15 number factors was built using 776 spectra of the China soil spectral library calibration dataset. We used this model to predict SOM of 104 samples with lab-based spectra and field-based spectra (original), respectively, but the prediction accuracies were quite different, with a quite good prediction with lab air-dried spectra but bad result with field-based spectra (for lab-based: R^2=0.81, RMSE=0.19 sqrt (OM %), and RPD=2.24; for field-based: R^2=0.06, RMSE=2.79 sqrt (OM %), and RPD=0.15). This could be interpreted by the principal component analysis results in figure 3(a) that field-based spectra were far away from library spectra while lab-based spectra came within the library range.

This library calibrated PLSR model is also used to predict SOM of the remaining 54 samples with transformed field spectra, getting a prediction of R^2=0.70, RMSE=0.21 sqrt (OM %) units, and RPD=1.79 (DS method). The prediction improved greatly compared with the 104 original field-based spectra validation.

3.4 Comparison with EPO algorithm and "spiking"

For EPO algorithm, here we used the same method and parameters referred to Minasny (2011). The purpose of conducting EPO transformed here is to check if our field-collected data is suitable for EPO transformation.

Table 3. comparisons of PLSR prediction results: a) original: calibrate models using 776 library samples and validate with the original 104 lab- and field-based spectra; b) spiking: a new library model was built using 776 library spectra spiked with 50 representative field-based spectra; c) DS: transformed field-based spectra by DS algorithm were validated by the same library PLSR model as in original method; d)EPO: 54 transformed field-based spectra and 54 transformed lab-based spectra were validated by the PLSR model built by 776 transformed lab-based spectra from China soil spectral library.

method	Calibration dataset	NO. factors	Validation dataset	R^2	RMSE	RPD
original	Library776	13	Lab104	0.83	0.20	2.04
			Field104	0.09	4.558	0.09
spiking	Library776 +Field50	14	Lab104	0.85	0.24	1.77
			Field54	0.67	0.27	1.44
DS	Library776	13	Lab104	0.83	0.20	2.04
			DS transformed Field54	0.70	0.21	1.79
EPO	Transformed library776	15	EPO transformed Lab54	0.68	0.30	1.41
			EPO transformed Field54	0.63	0.256	1.49

To avoid confusion that there are too many dataset in this study, for EPO transformation, we will not separate our data again. In our study, we regarded a) the transfer set of DS consist of 50 samples as EPO transfer dataset(dataset A), which have both field-collected spectra and lab-collected spectra; b) the rest 54 samples with field-collected spectra as the validation dataset(dataset B), which were transformed by EPO transfer parameters to validate the new model using transformed lab-based spectra from the China soil spectral library; c) the training dataset of China soil spectral library (n=776) as the model calibration dataset(dataset C).

The number of EPO dimensions (i.e. parameter c), is defined as 4 according to their research. After getting the projection matrix P, transformed spectra of dataset B were used to validate the model built by transformed spectra of dataset C. The organic matter content prediction of the 54 samples with the transformed field-based spectra was im-

proved obviously to 1.49 from 0.09. However, the prediction with the 54 transformed lab-based spectra decreased by a large margin to 1.41 from 2.04 when comparing with the original predictions.

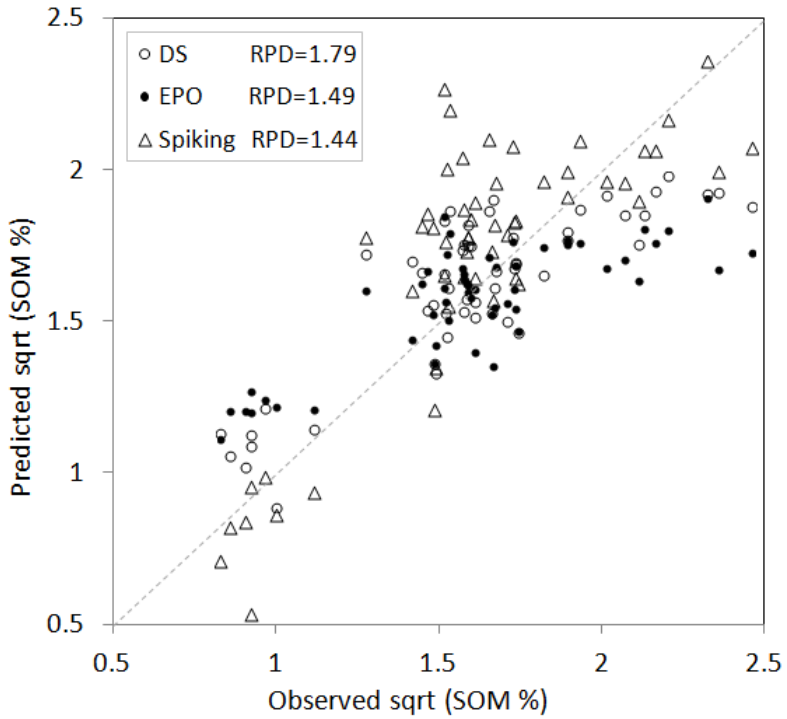

Figure 7. Scatter plot of predicted values against observations of SOM. Black open circles were prediction results after DS algorithm application using the model with 776 spectra from the China soil spectral library calibration dataset. Black closed circles were validations of transformed field-based spectra to 776 transformed lab-based spectra model, using EPO algorithm. Open triangles were predictions with original 54 field spectra using the PLSR model built with 776 library spectra combined with 50 well-chosen field-based spectra from transfer set.

Meanwhile, 776 library spectra were combined with the same 50 field-based spectra from transfer set to build a new library model with 15 factors (spiking method). The predictions with the remaining 54 field-based spectra also improved obviously but did not arrive at a satisfactory extent since its RPD was lower than 1.4. What is worse, the RPD of 104 lab-based spectra prediction decreased from 2.04 to 1.77 when original situation was compared against the spiking method.

Prediction accuracy with transformed field spectra by original library PLSR model was better than using “spiking” models to predict with untransformed field spectra.

The comparison of prediction accuracies of the three algorithms were shown in figure 7. DS algorithm works better than EPO and “spiking” method when using 50 samples in transfer set. More transfer samples (to 70) were also applied for EPO algorithm in this study, however, no better prediction accuracies were obtained. EPO performs better than “spiking” method when predicting with the transformed field-based spectra, but it decreased the prediction accuracies when predicting with the transformed lab-based

spectra obviously. Without the need of recalibration, DS algorithm shows better transferability with less transfer samples.

4 Discussion and conclusions

4.1 Water effects on spectra measurement

Water content is recognized as one of the most important factors of changes in the shape of spectra for two main reasons. One is its modification of soil colour. Wet soils always look darker than dry soil because water, as a replacement of air in the surrounding medium of soil, increases the degree of forward scattering before the light reemerges from soils (Lobell & Asner, 2002). In another words, the water in soil results in an overall increase in light absorbance (Figure 1(a)). Yet, it will be another matter when exceeding the soil moisture content exceeds field water limits. The other reason is the strong water absorption bands in the near infrared region which influence in the spectral features of other soil properties (Stenberg et al, 2010). Lobell and Asner (2002) found that increasing moisture in soil reduced the spectral feature of clay minerals at 2200nm, which affected the accuracy of calibration model.

In our study, water content seems to be the most affected parameter than other environmental effects such as surface soil condition. The effect of surface soil condition could be avoided in field-based spectral measurements when performed on well-chosen flat area without plant root using the high intensity contact probe with a quite small viewing area (2-cm-diameter circle). However, the transferability for the field-moist in-situ spectra with different moisture levels and different surface soil conditions to the lab-based spectra using DS algorithm, as well as the predictions on other soil properties, need to be tested.

4.2 The selection of transfer samples in DS algorithm

The application of the DS algorithm to spectral transformation requires a few well-chosen samples, the spectra of which need to be measured in both field-based and lab-based conditions before the transfer matrix could be computed. After examining the validation results of a series of transfer samples, we decide at least 50 samples to be the optimal number in transfer set. Compared with researches on calibration transfer only using quite a small subset of samples in transfer set, soil spectral transfer need quite a larger transfer set in this study for its complex and large amount of information contained in vis-NIR spectra.

When comparing to EPO algorithm and “spiking” method, DS algorithm is a valid step to avoid time-consuming recalibration procedures. It shows in our study that it has the ability to correct not just the complex instrumental response differences but also changes in spectra under different water contents in the soil. However, some shortcomings do exist with this approach that significantly large amount of chemical information might be lost

(Formula 2 & Figure 2(b)) in the procedure of computing transfer parameters for it assumed that any change in spectra is due to the external environmental effects, and thus the transfer matrix will not truly represent the environmental difference between field- and lab-based spectral measurements.

4.3 DS application in field-based spectral measurement

In situ field vis-NIR spectral measurement has a promising and bright future because of its time-efficiency for the soil properties prediction. However, external environmental parameter effects should be removed first from the field-based spectra to improve the prediction of soil properties. We propose to use the following procedures for field-based spectroscopic predictions: firstly, field-based spectral measurements were carried out in situ with careful attention avoiding rough surface condition, plant root and scatter light (pressing tightly against contact probe). Secondly, at least 50 samples were chosen by KS method from the PC scores of field-based spectra for DS transfer set. And then the 50 samples were air-dried and ground and measured in the lab condition. Thirdly, transfer parameters were calculated from the transfer samples with both field- and lab-based spectra using DS algorithm. The remaining field-based spectra were then transformed and validate the existing calibrations built with lab-based spectra. In this way, only a few (50) samples need to be pre-treated for air-dried and ground so that a lot of time, money and efforts could be saved.

Compared to those studies just concentrating on lab experiment simulating field-moist conditions, our study is a step forward because its focus is on direct field-moist in situ spectra. Although after spectral transfer by DS algorithm, transformed field spectra does not perform as well as the lab-based spectra prediction or recalibration results, with about 1.2 times larger error for transformed field spectra prediction in RMSE. It does improve the predictions obviously comparing to using untransformed field-based spectra. What is more, only a few subset of samples need to be measured again in lab condition, which makes the prediction accuracy satisfactory acceptable in real applications.

Acknowledgements

Our work is supported by Zhejiang university 985 project for Ph.D scholarship (Wenjun Ji).

Reference

BOUVERESSE, E., C. HARTMANN, D.L. MASSART, I.R. LAST, K.A. PREBBLE. 1996. Standardization of Near-Infrared Spectrometric Instruments. *Analytical Chemistry*, **68,** 982-990.

BOWERS, S.A., R.J. HANKS. 1965. reflection of radiant energy from soils. *Soil Science*, **100,** 130-138.

DE GROOT, P.J., G.J. POSTMA, W.J. MELSSEN, L.M.C. BUYDENS. 1999. Selecting a representative training set for the classification of demolition waste using remote NIR sensing. *Analytica Chimica Acta*, **392,** 67-75.

FEUDALE, R.N., N.A. WOODY, H. TAN, A.J. MYLES, S.D. BROWN, J. FERRÉ. 2002. Transfer of multivariate calibration models: a review. *Chemometrics and Intelligent Laboratory Systems*, **64,** 181-192.

GUERRERO, C., R. ZORNOZA, I. GÓMEZ , J. MATAIX-BENEYTO. 2010. Spiking of NIR regional models using samples from target sites: Effect of model size on prediction accuracy. *Geoderma*, **158,** 66-77.

KENNARD, R.W., L.A. STONE. 1969. Computer Aided Design of Experiments. *Technometrics*, **11,** 137-148.

KUSUMO, B.H., M.J. HEDLEY, M.P. TUOHY, C.B. HEDLEY, G.C. ARNOLD. 2010. Predicting Soil Carbon and Nitrogen Concentrations and Pasture Root Densities from Proximally Sensed Soil Spectral Reflectance. 177-190.

LI, Q.B., G.J. ZHANG, K.X. XU, Y. WANG. 2007. Application of DS Algorithm to the Calibration Transfer in Near-Infrared Spectroscopy (Chinese). *Spectroscopy and Spectral Analysis*, **27,** 873-876.

LOBELL, D.B., G.P. ASNER. 2002. Moisture Effects on Soil Reflectance. *Soil Sci. Soc. Am. J.*, **66,** 722-727.

MINASNY, B., A.B. MCBRATNEY, V. BELLON-MAUREL, J.-M. ROGER, A. GOBRECHT, L. FERRAND, S. JOALLAND. 2011. Removing the effect of soil moisture from NIR diffuse reflectance spectra for the prediction of soil organic carbon. *Geoderma*, **167-168,** 118-124.

MORGAN, C.L.S., T.H. WAISER, D.J. BROWN, C.T. HALLMARK. 2009. Simulated in situ characterization of soil organic and inorganic carbon with visible near-infrared diffuse reflectance spectroscopy. *Geoderma*, **151,** 249-256.

NÆS, T., ISAKSSON, T., FEAM, T., DAVIES, T. 2002. A user-friendly guide to multivariate calibration and classification. NIR publications

ROGER, J.-M., F. CHAUCHARD, V. BELLON-MAUREL. 2003. EPO–PLS external parameter orthogonalisation of PLS application to temperature-independent measurement of sugar content of intact fruits. *Chemometrics and Intelligent Laboratory Systems*, **66,** 191-204.

STENBERG, B., R.A. VISCARRA ROSSEL, A.M. MOUAZEN, J. WETTERLIND. 2010. Visible and Near Infrared Spectroscopy in Soil Science. **107,** 163-215.

SWIERENGA, H., W.G. HAANSTRA, A.P.D. WEIJER, L.M.C. BUYDENS. 1998. Comparison of Two Different Approaches toward Model Transferability in NIR Spectroscopy. *Appl. Spectrosc.*, **52,** 7-16.

UDELHOVEN, T., C. EMMERLING, T. JARMER. 2003. Quantitative analysis of soil chemical properties with diffuse reflectance spectrometry and partial least-square regression: A feasibility study. *Plant and Soil*, **251,** 319-329.

VISCARRA ROSSEL, R.A., T. BEHRENS. 2010. Using data mining to model and interpret soil diffuse reflectance spectra. *Geoderma*, **158,** 46-54.

VISCARRA ROSSEL, R.A., S.R. CATTLE, A. ORTEGA, Y. FOUAD. 2009. In situ measurements of soil colour, mineral composition and clay content by vis–NIR spectroscopy. *Geoderma*, **150,** 253-266.

WAISER, T.H., C.L.S. MORGAN, D.J. BROWN, C.T. HALLMARK. 2007. In Situ Characterization of Soil Clay Content with Visible Near-Infrared Diffuse Reflectance Spectroscopy. *Soil Science Society of America Journal*, **71,** 389.

WANG, Y., D.J. VELTKAMP, B.R. KOWALSKI. 1991. Multivariate instrument standardization. *Analytical Chemistry*, **63,** 2750-2756.

WU, C.Y., A.R. JACOBSON, M. LABA, P.C. BAVEYE. 2009. Alleviating Moisture Content Effects on the Visible Near-Infrared Diffuse-Reflectance Sensing of Soils. *Soil Science*, **174,** 456-465.

NIR PUBLICATIONS. 2002. Tormod Næs, Tomas isaksson, Tom Feam, Tony Davies, *A user-friendly guide to multivariate calibration and classification*.

Optimised on-line vis-NIR measurement of soil organic carbon using artificial neural network in a Danish farm

B. Kuang[1*] , Y. Tekin[2], A. M. Mouazen[1]

[1]*Department of Environmental Science and Technology, Cranfield University, Cranfield, MK43 0AL, UK.*

[2]*Vocational School of Technical Sciences, Uludag University, Bursa, Turkey*

[*]*E-mail: b.kuang@cranfield.ac.uk*

Abstract

The on-line measurement of soil organic carbon (OC) is needed for the management of soil carbon stock and for variable rate lime application. This paper reports on the application of the visible and near infrared (vis-NIR) spectroscopy for the on-line measurement of OC. Partial least squares (PLS) regression and artificial neural network (ANN) modelling techniques were compared in two fields in Denmark. Results based on statistical evaluation of root mean square error (RMSEP) and map comparison with laboratory measurement showed that ANN (RMSEP = 1.25 & 1.70 %) out-performed PLS (RMSEP = 1.45 & 2.01 %) for on-line prediction of soil OC.

1 Introduction

Recent advancement in proximal soil sensing techniques indicates that on-line sensors are capable to provide trustful and high resolution data on soil properties including soil organic carbon (OC). Among available techniques, the visible and near infrared (vis-NIR) spectroscopy proved to be the most capable technology for on-line characterisation and quantification of within field variation in soil properties (Shibusawa et al, 2001; Mouazen et al, 2007; Bricklemyer & Brown 2010; Kuang & Mouazen, 2013). Having proven on-line vis-NIR soil sensors encourages the on-line measurement of OC, as to provide useful information for the management of soil carbon stock. Also, the detailed within field OC maps is a valuable data for accurate variable rate lime application. Although the on-line vis-NIR sensors are proven to provide accurate data on OC measurement, accuracy may improve further. So far modelling of on-line collected data has been carried out with linear algorithms, e.g. with partial least squares (PLS) regression. But, literature proved the non-linear behaviour of vis-NIR prediction for OC (Stenberg et al, 2010).Therefore, it is expected that the use of non-linear analysis technique e.g. artificial neural network will result in improving the prediction accuracy of OC based on on-line collected spectra. This paper aims to apply ANN algorithm to improve the prediction accuracy of on-line vis-NIR measurement of soil OC in two fields in a Danish farm.

2 Materials and methods

2.1 Experimental site and on-line measurement

Two fields (Table 1) were measured in Vindumovergaard Farm, Denmark, using the on-line vis-NIR sensor (Fig.1) developed by Mouazen (2006). Lime application is planned in both fields in spring, 2013. During the field measurement, the on-line sensor was pulled through adjacent lines of 20 m intervals at a travel speed of 2 km/h, setting the subsoiler at 15 cm depth. About 5 to 14 soil samples were collected from each line from the bottom of trenches, and the sampling positions were carefully recorded with a DGPS. Each of those samples was equally divided into two parts.

Figure 1. The on-line visible and near (vis-NIR) soil sensor (Mouazen, 2006).

One half used to carry out the laboratory reference measurement of soil OC, whereas the other half was used for optical scanning using a mobile, fibre type, vis-NIR spectrophotometer (AgroSpec from tec5 Technology for Spectroscopy, Germany).

Table 1. Information about two experimental fields in Vindumovergaard Farm, Denmark.

Field	Area, ha	Crop	Sample Nr	Texture type	Sand, %	Silt, %	Clay, %	Year
Field1	20	Wheat	132	Sandy loam	70.58	24.56	4.86	2012
Field2	35	Wheat	80	Sandy loam	68.57	21.96	9.48	2012

2.2 Laboratory analysis

Soil OC was measured by a TrusSpecCNS spectrometer (LECO Corporation, St. Joseph, MI, USA) using the Dumas combustion method.

2.3 Optical measurement in the laboratory

Each soil sample was dumped into a glass container and mixed well. Big stones and plant residue were excluded. Then each soil sample was placed into three Petri dishes, which were 2 cm in depth and 2 cm in diameter. The soil in the Petri dish was shaken and pressed gently before levelling with a spatula. A smooth soil surface ensures maximum light reflection and high signal to noise ratio. The soil samples were scanned by the same spectrophotometer used during the on-line measurement. A 100 % white reference was used before scanning. A total of 10 scans were collected from each cup, and these were averaged in one spectrum.

2.4 Model development

A total of 132 and 80 samples were collected from the field 1 and field 2, respectively. Out of those samples, 32 and 28 samples were pooled together in one matrix with other 187 samples collected previously from other European farms (Table 2). The remaining samples were used for validation of on-line measurement in both fields. PLS regression and artificial neural network (ANN) were used to develop OC models. PLS calibration was carried out using the Unscrambler 7.8 software (Camo Inc.; Oslo, Norway). STATISTLCA 10 (StatSoft, Inc. USA) software was used to perform ANN calculation, including network choose, training and validation.

Table 2. Sample statistics of samples used for OC model development and validation.

		Model				On-line validation			
		Min	Max	Mean	SD	Min	Max	Mean	SD
Field 1	OC (%)	0.73	17.85	4.52	4.57	0.92	11.4	2.32	2.85
Field 2	OC (%)	0.73	17.85	4.52	4.57	1.01	13.38	4.64	3.96

3 Results and discussion

3.1 Model accuracy in calibration and on-line validation

Models established for OC using PLS regression shows good calibration accuracy in cross-validation (ration of prediction deviation (RPD) = 2.29 and root mean square error of prediction (RMSEP) = 1.99 %, whereas ANN clearly over-performs PLS (RPD = 3.01 and RMSEP = 1.5 %). In line with the calibration accuracy, the ANN over-performs the PLS for on-line measurement of OC in both fields. In field 1 and field 2, the RPD value increases from 1.93 to 2.28 and from 1.97 to 2.33, whereas RMSEP value decreases from 1.48 % to 1.25 % and from 2.01 % to 1.70 %, respectively.

Table 3. Summary of OC model calibration and on-line validation results.

		PLS			ANN		
	Field	R^2	RMSEP, %	RPD	R^2	RMSEP, %	RPD
Calibration	NA	0.81	1.99	2.29	0.9	1.50	3.01
On-line validation	1	0.71	1.48	1.93	0.83	1.25	2.28
	2	0.75	2.01	1.97	0.86	1.70	2.33

3.2 Mapping

A comparison between maps of measured and predicted soil OC shows large spatial similarity, with high and low values zones match well, for both PLSR-based and ANN-based maps (Figure 2). This proves the high quality of on-line measured spectra, which reflects the sensor stability and robustness during on-line measurement. However, better correlation can be observed for ANN maps, as compared to PLS maps, which is further confirmation for ANN to perform better than PLS for on-line measurement of OC.

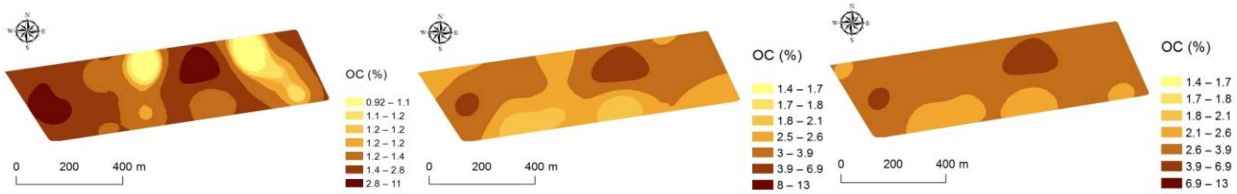

Figure 2. Comparison maps of OC for laboratory reference measurement (left), ANN on-line predicted (middle) and PLS on-line predicted (right), shown for field 1.

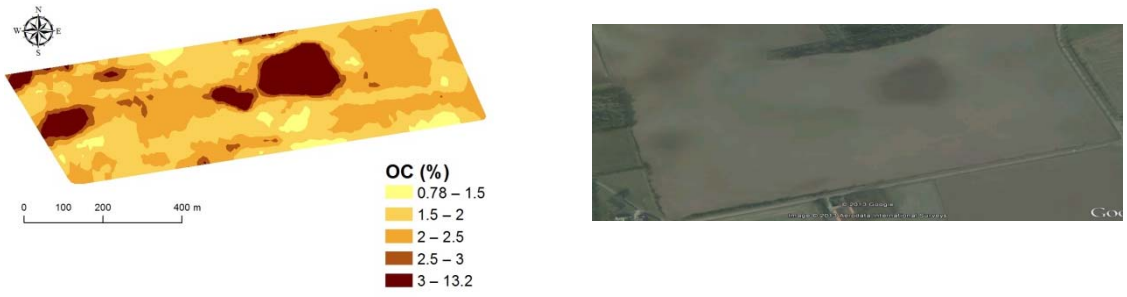

Figure 3. Map of on-line ANN predicted OC based on entire data points (left), as compared to satellite image (right) of field 1.

Comparing the on-line OC map based on full-point measurement with satellite imagery of the same field, shows high spatial similarity. The high OC areas shown by the on-line map match the corresponding areas where soil received high manure application (manure reservoirs) (Figure 3).

4 Conclusions

The results obtained in this study confirmed ANN calibration technique of vis-NIR spectra to provide a better accuracy for on-line prediction on soil OC, as compared to the PLS analysis. ANN-based soil OC maps are recommended for management zones development for variable rate lime application. .

Acknowledgement

The research leading to these results has received funding from the European Space Agency under the FarmingTruth project. Authors also acknowledge the knowledge Centre of Agriculture in Denmark, for providing the experimental fields and facilitating measurement.

References

BRICKLEMYER, R. S., BROWN, D. J. 2010. On-the-go VisNIR: Potential and limitations for mapping soil clay and organic carbon. Computers and Electronics in Agriculture, **70**, p. 209-216.

KUANG, B., MOUAZEN, A.M. 2013. Effect of spiking strategy and ratio on calibration of on-line visible and near infrared soil sensor for measurement in European farms. Soil & Tillage Research, **128** 125–136.

MOUAZEN, A.M. 2006. Soil Survey Device. International publication published under the patent cooperation treaty (PCT). World Intellectual Property Organization, International Bureau. International Publication Number: WO2006/015463; PCT/BE2005/000129; IPC: G01N21/00; G01N21/00.

MOUAZEN, A. M., MALEKI, M. R., DE BAERDEMAEKER, J., RAMON, H. 2007. On-line measurement of some selected soil properties using a VIS-NIR sensor. Soil and Tillage Research, **93** 13-27.

SHIBUSAWA, S., IMADE ANOM, S.W., SATO, S., SASAO, A., HIRAKO, S. 2001. Soil mapping using the real-time soil spectrophotometer. In: G. Grenier and S. Blackmore (Editors), ECPA 2001, Third European Conference on Precision Agriculture vol. 1, Agro Montpellier, Montpellier, France, pp. 497–508.

STENBERG, B., VISCARRA ROSSEL, R., MOUAZEN, A.M., WETTERLIND, J. 2010. Visible and near infrared spectroscopy in soil science. Advances in Agronomy, **107** 163-215.

Analysis of the repeatability of soil spectral data obtained using different measurement techniques

N. Dhawale[1], V. Adamchuk[1*], S. Prasher[1], A. Ismail[2], R.A. Viscarra Rossel[3]

[1]*Department of Bioresource Engineering, McGill University, Ste-Anne-de-Bellevue, QC, H9X 3V9, Canada*

[2]*Department of Food Science and Agricultural Chemistry, McGill University, Ste-Anne-de-Bellevue, QC, H9X 3V9, Canada*

[3]*CSIRO Land and Water, Bruce E. Butler Laboratory, GPO Box 1666, Canberra ACT 2601, Australia*

[*]*E-mail: viacheslav.adamchuk@mcgill.ca*

Abstract

Soil reflectance spectroscopy (SRS) shows promise for the rapid assessment of a number of physical and chemical soils attributes when used to perform both in-situ, and ex-situ, measurements. Many soil properties can be predicted indirectly, using the soil reflectance measurement transformed by means of a data-specific transformation model. To understand the modelling uncertainties, it is important to assess the repeatability of raw data and any derived parameters when measuring the same soil samples several times. The objective of this study was to evaluate the repeatability of the soil diffuse reflectance measurements collected using visible-near-infrared (Vis-NIR) and mid-infrared (MIR) spectrometers. The Vis-NIR measurements were performed in the field and in the laboratory. Twenty locations in three agricultural fields were selected to represent an extensive range of crop growing conditions, varying from sand to clay loam soils. Air-dried soil samples representing each of the 20 locations were measured in the laboratory using both Vis-NIR and MIR instruments. In addition, 0-0.2 m soil reflectance profiles, obtained within a distance of less than 0.5 m from each other, were used to evaluate the repeatability of the in-situ measurements. All measurements were repeated three times and evaluated in terms of the spread over error ratio (RSE). The most repeatable measurements with the greatest ability to distinguish among samples were found for filtered DR-MIR measurements. In the case of the Vis-NIR measurements, the highest RSEs were found for the second derivative data. Naturally, in-situ measurements were less repeatable than those performed indoors.

Keywords: Proximal soil sensing, soil reflectance spectroscopy, spectral data stability.

1 Introduction

Visible and near-infrared reflectance spectroscopy is an indirect analytical method based on the development of empirical models that can predict the concentration of a soil constituent from complex spectral data (Couteaux et al. 2003). Malley et al. (2004)

and Viscarra Rossel et al. (2006) summarized the published applications of near-infrared spectroscopy (NIRS) in soil analysis for the determination of primary and secondary properties. The primary properties, for which NIRS predictions have a theoretical basis for (Chang et al. 2001), include: particle size distribution, soil water content, organic carbon and total nitrogen. Secondary properties include: pH, electrical conductivity (EC), cation-exchange capacity (CEC), potentially mineralizable N, specific surface area, wet aggregate stability, enzyme activities, microbial respiration, and microbial biomass. Secondary properties are NIRS predictable because of their correlation with certain primary properties (Chang et al. 2001). Published research results frequently reveal that variability in the homogeneity of soil samples, soil texture, quality of the reference methods and soil spectra, and the calibration methods may lead to differences in the performance of NIRS techniques (Chodak et al. 2002; Couteaux et al. 2003; Udelhoven et al. 2003; Madari et al. 2006). The objective of this project was to assess the repeatability of unprocessed visible, near-infrared, and mid-infrared spectra as well as their most common derivatives when the same soil samples were measured repeatedly in the lab or directly in the field.

2 Materials and methods

A combined, dual type spectrophotometer instrument, operating in the visible and near-infrared regions of the spectrum, as well as a portable diffuse reflectance MIR variable-filter-array (VFA) spectrometer were used in this project (Figure 1). The Vis-NIR instrument (P4000, Veris Tehcnologies, Inc., Salina, Kansas, USA) was ready for both in-situ and ex-situ measurements. One of the two spectrometers was used to collect soil reflectance data between 350 and 1000 nm, and the other spectrometer measured between 1100 and 2200 nm. The MIR VFA system (prototype spectrometer, Wilks Enterprise, Inc., East Norwalk, Connecticut, USA) was used to obtain soil reflectance spectra between 2780 and 5033 nm. Both instruments included their own light source and were capable of maintaining a constant distance between measured soil surfaces and detectors.

A total of 20 composite soil samples were collected from three non-uniform agricultural fields (Macdonald Farm, McGill University, Ste-Anne-de-Bellevue, Quebec, Canada). Each sample represented a specific field location, 0-20 cm depth, and was air-dried and sieved (2-mm mesh) prior to the measurements. In-situ measurements were obtained in the same locations within a 0.5 m radius. Each raw spectral response was filtered (median of three consecutive wavelengths) to remove outliers. In addition, the first and the second derivatives (11 consecutive wavelengths) were taken to characterize the local dynamics of the spectral behaviour at each wavelength. A second-order polynomial fit was used to represent the overall trend with data around 1400 and 1900 nm removed prior to the fitting. Principal component analysis (PCA) was implemented to define the

orthogonal linear transformation of the filtered spectral response to reduce the dimensionality of the spectral data while preserving the spectral information value.

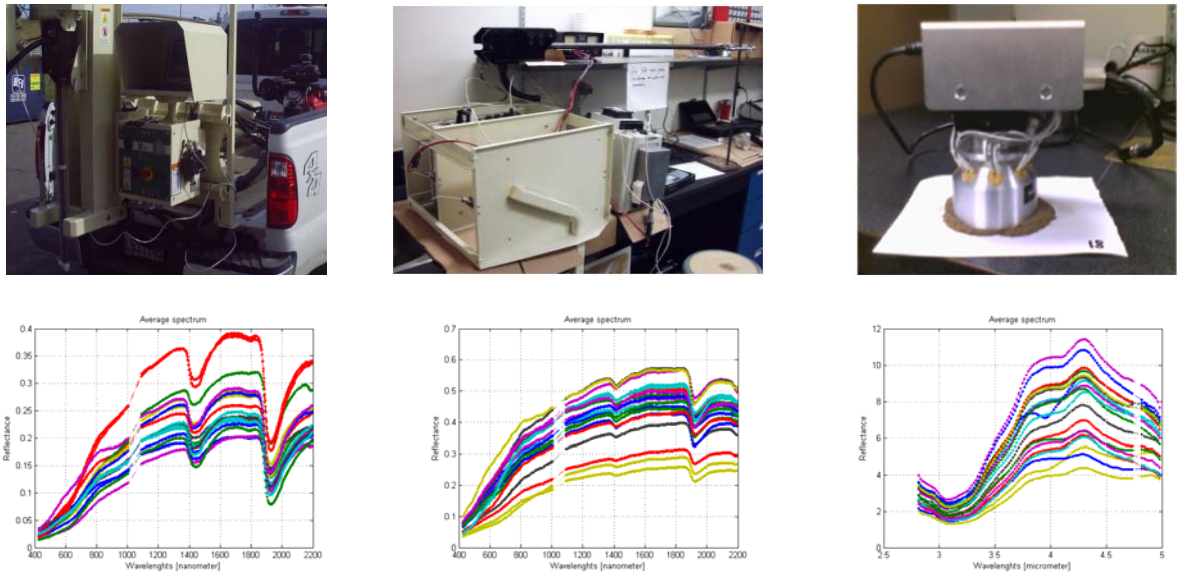

Vis-NIR in field | Vis-NIR in laboratory | DR-MIR in laboratory

Figure 1. Instruments, setup and raw spectra collected in this project.

Each in-situ measurement was repeated three times in a randomized order during a two-week time period to maximize the possible temporal signal drift when re-measuring the same sample. Each laboratory Vis-NIR measurement represented an average of 15 spectral scans obtained within 6 s, and each MIR measurement was an average of 32 consecutive scans obtained within 20 s. During the in-situ measurements, short-distance soil variability was an additional factor affecting the measurement's reproducibility. Among the different statistics considered for this analysis, the ratio of spread over error (RSE) appeared to be the most convenient:

$$RSE = \frac{SD_{SA}}{RMSE} \quad (1)$$

where SD_{SA} is the standard deviation of 20 sample average values, and RMSE is the root mean squared error calculated based on three replicated measurements for each of the 20 samples.

Similar to the frequently used ratio of prediction over deviation (RPD), high RSE means a relatively strong ability of a given measurement to distinguish different soil samples and is directly related to ANOVA F-statistics used to compare the means of three repeated measurements. Based on the degrees of freedom involved, the difference among the soil samples (means of three measurements) can be detected at α=0.05 when RSE is greater than 0.79 ($\sqrt{\frac{1}{3}F_{stat}}$). This analysis evaluated measurement preci-

sion with the underlying hypothesis that a particular parameter that does not change when measuring the same soil sample and the change is at its maximum when measuring different samples should be considered reliable.

3 Results and conclusions

Table 1 summarises the distributions of the RSE values for each measurement instrument, type of measurement and data transformation method. For the polynomial fit, prediction values were evaluated at each wavelength. It is clear that the filtered DR-MIR measurements had the highest relative reproducibility across the entire spectrum, while RSE for the first derivative was dependent on the wavelength. In terms of Vis-NIR data, as one might expect, ex-situ measurements were more reproducible than those conducted in natural soil conditions within a 0.5 m distance from each other. However, in both cases, the second derivative (spectral inflection data) yielded data that had the highest relative reproducibility in certain parts of the spectrum. Other types of data transformation did not yield a substantially higher RSE, which in every case would have at least several wavelengths with the ability to separate the means of the three replicated measurements (RSE>0.79).

Table 1. RSE comparison of transformed data for each equipment and method

Equipment and Method	Data Transformation	RSE				
		Min	25 %	Median	75 %	Max
VIS NIR *In-situ*	Filtered	1.01	1.39	1.49	1.54	1.56
	Polynomial fit	1.84	1.86	1.93	2.08	2.13
	First derivative	0.92	1.84	2.00	2.90	1.56
	Second derivative	1.04	1.83	2.36	3.19	5.93
	Principal components	0.29	0.48	1.15	1.24	1.80
VIS NIR *Ex-situ*	Filtered	1.72	1.76	1.78	1.85	2.24
	Polynomial fit	1.85	1.86	1.91	2.12	2.19
	First derivative	0.92	1.63	2.03	2.40	2.24
	Second derivative	0.47	1.20	1.68	2.25	8.07
	Principal components	1.52	1.64	2.21	2.98	3.00
DR-MIR *Ex-situ*	Filtered	11.28	15.70	17.84	18.80	21.41
	Polynomial fit	11.70	13.00	12.85	13.50	13.81
	First derivative	1.64	4.11	6.88	10.80	21.41
	Second derivative	0.68	2.23	4.18	6.82	11.58
	Principal components	0.33	0.39	2.61	7.83	13.67

It is also noticeable that the PCA method failed to produce a linear spectral transformation that would have substantially greater value when measuring different soils (different level of soil organic matter) versus the same soil sample. The next step in this research is to expand a similar analysis to a greater number of datasets involving more soil samples and additional instruments. Furthermore, we intend to compare precision (reproducibility) and accuracy (predictability) of spectral soil measurements.

4 References

CHANG, C.W., LAIRD, D.A., MAUSBACH, M.J., HURBURGH, C.R. 2001. Near-infrared reflectance spectroscopy - principal components regression analyses of soil properties. *Soil Sci. Soc. Am. J.* 65: 480-490.

CHODAK, M., LUDWIG, B., KHANNA, P., BEESE, F. 2002. Use of near infrared spectroscopy to determine biological and chemical characteristics of organic layers under spruce and beech stands. *J. Plant Nutr. Soil Sci.* 165: 27-33.

COUTEAUX, M.M., BERG, B., ROVIRA, P. 2003. Near infrared reflectance spectroscopy for determination of organic matter fractions including microbial biomass in coniferous forest soils. *Soil Biol. Biochem.* 35: 1587-1600.

MADARI, B.E., REEVES, J.B., MACHADO, P.L.O.A., GUIMARAES, C.M., TORRES, E., MCCARTY, G.W. 2006. Mid and near-infrared spectroscopic assessment of soil compositional parameters and structural indices in two Ferralsols. *Geoderma* 136: 245-59.

MALLEY, D.F., MARTIN, P.D., BEN-DOR, E. 2004. Application in analysis of soils. In: *Near-infrared spectroscopy in agriculture*, Roberts, C.A., Workman J., and Reeves J.B., eds. Agronomy 44, ASA, CSSA, SSSA, Madison, Wisconsin, USA, pp.729-784.

UDELHOVEN, T., EMMERLING, C., JARMER, T. 2003. Quantitative analysis of soil chemical properties with diffuse reflectance spectrometry and partial least-square regression: A feasibility study. *J.Plant Soil* 251: 319-329.

VISCARRA ROSSEL, R.A., WALVOORT, D.J.J., MCBRATNEY, A.B., JANIK, L.J., SKJEMSTAD J.O. 2006. Visible, near infrared, mid infrared or combined diffuse reflectance spectroscopy for simultaneous assessment of various soil properties. *Geoderma* 131: 59–75.

Soil spectroscopy as a method to monitor Total Petroleum Hydrocarbon (TPH) contamination in soil

G. Schwartz[1,2*], E. Ben-Dor[2], G. Eshel[3]

[1]*The Porter School of Environmental Studies, Tel Aviv University, Tel Aviv, Israel*
[2]*Remote Sensing Laboratory, Tel Aviv University, Tel Aviv, Israel*
[3]*Soil Erosion Research Station, Ruppin Inst., Emeck-Hefer, Israel*
[*]*E-mail: guy.rslab@gmail.com*

Abstract

Contamination of soil with Petroleum hydrocarbons plays an important role in recent environmental deterioration. The commonly used analytic method for assessing Total Petroleum Hydrocarbons (TPH) in soil samples, is based on extraction with 1,1,2-Trichlorotrifluoroethane (Freon 113), a substance prohibited to use by the EPA. The current paper assembles the use of reflectance radiation across the VNIR-SWIR region (400-2500 nm) to monitor TPH concentration in soil. This technology is environmental friendly and permits rapid and cost-effective measurements of large number of samples. Artificial contaminated samples were analyzed chemically and spectrally to form a data-base of 5 soils contaminated with 3 types of TPH, creating 15 datasets of 48 samples each at contamination levels of 50 – 5000 wt% ppm. A brute force preprocessing approach was used by combining 8 different preprocessing techniques at “all possibilities”, resulting in 120 different mutations for each dataset. The brute force was done based on an innovative computing system developed for this study termed “all possibilities” approach. The use of the “all possibilities” system proved to be effective and efficient for optimal spectral modeling in soil in general and assessing TPH contamination in soil in particular.

Keyword: Soil Spectroscopy, TPH, Best Spectral Model.

1 Introduction

Petroleum hydrocarbons (PHC) is a potential contaminator of both water and soil with significant effects on human health and environment vitality (Hutcheson et al., 1996). For both the diagnosis of suspected areas and the possibility of controlling the rehabilitation process, there is a great need to develop and implement a method to rapidly detect and assess PHC in soils. Due to the complex nature and structure of PHC ingredients, a general measurement index "Total PHC" (TPH) was defined and is the common measurement index for quantifying environmental contamination originated by PHC. The TPH level is determined by the ratio of IR absorption measured sample extraction, relative to the IR absorption of the EPA standard consisting of 31.5% isooctane, 35% hexadecane and 33.5% chlorobenzene. The common method for assessing TPH in soil

samples is based on the no longer approved Environment Protection Agency (EPA) method 418.1 due to the use of Freon 113 in the analysis. This adds to the fact that the method needs skilled operators, it requires a long analytical process, needs to transport the samples to the laboratory and is relatively an expensive one. A comprehensive review on the attempt to use reflectance information across the VIS-NIR-SWIR spectral region was given by Schwartz et al., 2013 who pointed out that only concentration levels above 0.1% TPH can be detectable by the spectral method. Totay's environmental regulations require identification levels that are an order of magnitude lower. As most of the spectral studies were performed with high concentration of PHC at laboratory-prepared samples and just a few were used natural field samples it was concluded that further study has to be conducted on this issue. This study needs to concentrate on real quantitative operation model that will enable real-life applications in situ (low concentration and high power). The purpose of this study is thus, to develop an effective analytical tool to assess hydrocarbon contamination in soils rapidly, accurately, and cost effectively way solely from reflectance spectroscopy.

2 Materials and methods

2.1 Soils and hydrocarbons

Five soils were selected for this study (defined according to local definition system) as well as the USDA key[27]) – Loess (Tipic Xerofluvent), Hamra (Tipic Xerocherept), Gromosol (Typic Chromoxerert), Rendenzina (Lithic Haploxeroll) and Terra Rosa (Lithic ruptic Xerochrept). The soils were contaminated artificially by PHC by mixing a known weight of several PHC types including: Octane Fuel, Diesel and Kerosene with known quantities of soil. Each of the prepared sample was placed in an amber glass vial, capped with a PTFE lined cap at and kept 4^{o}C. Tables I describes the samples properties.

Table 1. Soil Properties

Israeli Classification	USDA Classification	HM	Sand	Silt	Clay	SOC	SIC	TotalN	pH[1]	EC[1]	SSA
		%		volume %			g kg^{-1}			mS m^{-1}	m^2 g^{-1}
Loess	Tipic Xerofluvent	4.14	38.6	49.4	12	5.4	22.5	0.9	8.22	5.44	167
Hamra	Tipic Xerocherept	1.44	97.37	1.73	0.9	1.5	2.1	0.5	8.57	0.08	83
Gromosol	Typic Chromoxerert	5.23	46.46	38.98	14.56	7.6	12.5	1.3	8.68	0.55	238
Terra Rosa	Lithic ruptic Xerochrept	9.14	19.89	57.14	22.97	20.9	15.5	2.6	7.71	0.36	380
Rendzina	Lithic Haploxeroll	5.63	2.19	77.61	20.2	11.5	70.5	1.7	7.79	0.45	262

2.2 Spectroscopy measurements

All samples were measured spectrally using an ASD Field spec PRO spectrometer (ASD Inc., Boulder, CO.), each measurement included 2150 wavelengths between 350 and 2500nm at 1nm intervals. A Spectralon (Labsphere, NH, USA.) surface was used for the calibration of the spectrometer and as a relative target. Each sample was measured 3 times using a self-illuminated contact probe (ASD Inc., Boulder, CO.). An average spectrum was calculated as the representative spectrum for each sample, as the standard deviation was negligible. The first 100 (350 – 450 nm) and last 50 (2450 – 2500 nm) bands were removed due to noisy signal; the remaining 2000 bands (450 – 2450 nm) were used as the spectral data for the chemometric analysis.

2.3 TPH chemical analysis

We used the method for TPH measurements in soil that is based on the adjusted EPA 418.1 method that was originally designed for waste water (Okparanma and Mouazen 2013) . In general the process includs extracting the hydrocarbons from 3g of soil sample in 15ml of 1,1,2-TrichloroTrifluoroethane (Freon 113, PESTI-S) and measuring the extraction the non polar solvent by an Infra Red TPH analyzer (Buck scientific Inc. model HC-404) calibrated by standard TPH solutions (Buck scientific Inc. EPA method 418.1 reference standard part # 404-11).

2.4 Preprocessing the spectral data

Each of the 15 data sets (5 soils and 3 PHC types) was preprocessed by the following preprocessing techniques and all of their possible combinations:

1.Initial Smoothing for spectral noise elimination 2. Multiplicative Scatter Correction (MSC) for spectral normalization–3. Standard Normal Variate (SNV) for scatter correction and normalization 4. Conversion to Absorptance log (1/R) (where R= reflectance) 5. Continuum Removal for normalization 6. First Derivative for albedo correction after applying Savitzky-Golay algorithm (Savitzky and Golay 1964), 7. Second Derivative for correcting both additive and multiplicative effects after) and 8. Final Smoothing for eliminating noise that were amplified during previous process. To extract the best model out of the abovementioned all possible combinations of the pre-process techniques is recommended (Ben Dor and Banin 1994). While using the “all possible combinations” approach could potentially yield 256 different “mutations” of the dataset, only 120 mutations were used due to some unreasonable combinations, i.e: using both MSC and SNV, using both first and second derivatives and combining SNV (that results in negative values) with transformation to absorbance that would results with complex numbers with imaginary parts that cannot be modeled in PLS.

2.5 Modeling process

Before the modeling process, we divided each dataset into three groups: training, validation and test. The relationship between the chemistry and the spectroscopy data was found via the training group and was simultaneously cross-validated by the validation group. Finally, the model was applied to the test group, independently of the training and validation process. Samples were divided in the following manner: 75% (36 samples) for training and validation (validation was done by the leave one out method) and 25% (12 samples) for test. For reliable results that represent the entire dataset as best as possible the Conditioned Latin Hypercube Sampling (cLHS) method was used to select the samples in each the abovementioned groups.

2.6 “All possibilities” approach: the Paracuda system

Managing and deploying thousands of chemometric models and preprocessing methods combinations requires an automated system and distributed computing, whereas manual management and deployment of these tasks is impossible manually. *Paracuda* is a specially designed modeling and data mining software developed by *Novospec ltd* (http://www.novospec.com/). and the Remote sensing laboratory at the Tel Aviv University, for exploring very large datasets and finding the hidden patterns and relationships within the data. *Paracuda* excels especially in handling spectroscopy data and modeling spectroscopy measurements against chemical constitutes, for creation of robust prediction models. The *Paracuda* system is based on finding the most important variables (or wavelengths when dealing with spectroscopy data) and thus minimizing the amount of data needed to be analyzed. *Paracuda* is utilizing the parsimony concept for avoiding situations where models that have good calibration results are in fact over-fitted and produce poor results when the test data is presented. *Paracuda* also tries to employ pretreatment of the data presented using several preprocessing methods and their combinations as described in the materials and methods section. Due to the vast world of data mining algorithms *Paracuda* employs the " all possibilities" approach; this approach is applying all state-of-the art linear and non linear algorithms combined with preprocessing methods for modeling the data: Artificial Neural Networks (ANN), Genetic Algorithms (GA), Support Vector Machines (SVMs), Fuzzy Logic (FL), Partial Least Squares (PLS), Multiple Linear Regression (MLR), Principle Component Regression (PCR) etc. This "all possibilities" approach which includes testing multiple preprocessing methods and their combinations, dimension reduction and different modeling techniques is extremely processing power consuming, therefore *Paracuda* in running on a grid based supercomputer with many processing cores for rapid analysis. The system is easy to operate via an excel plug-in and a web interface that enables easy and fast data transfers to the *Paracuda* servers, changing modeling parameters for advanced users (a full automatic mode is the default) as well as controlling your current jobs and monitoring their progress. The server side architecture of the *Paracuda* system consists of

many components: Job Manager, Job Generator, Shared file system, Workers and various other modules (Dimension Reduction, Data Division, Preprocessing, Excel Generator etc.).

3 Results and discussion

3.1 Modeling performances and soil properties

Fig 2 shows that Hamra and Loess soils contaminated with diesel and kerosene are the datasets with best performing models with average RPD values of over 20 and 10 respectively. All other soils and PHC perform also quite well with the best model with RPD over 4. In our study we found that coarse soil particles presented by low Specific Surface Area (SSA) of the soil reduce albedo levels, and finer soil particles presented by higher SSA yields higher albedo levels. The soil matrix reflectance is equivalent to the background and the contaminant reflectance is the target we are trying to model. We hypothesis that when we try to quantify the contaminant in the soil matrix, the relative reflectance contribution of the matrix with high SSA relative to the contribution of the contaminant is much higher making the modeling more difficult. Therefore, the low SSA of the Hamra and Loess soils can explain the better performing models. As the soil brightness affects the Signal to Noise Ratio by producing a better signal, the brighter soils yields better performing models. Taking into consideration both brightness and SSA, Hamra soil models perform better than Rendzina or Loess soils models although the latter are brighter. Rendzina soil models did not perform as well as Hamra and Loess soils due to its high SSA even though the Rendzina is a very bright soil.

3.2 Optimal model selection

RPD is commonly used as a parameter for evaluating the performance of chemometric models, as it incorporate both the modeling error and the Y variables value range. Table II shows that modeling efficiency depends on both soil type as well as PHC type. In general the brighter the soil and the heavier the PHC, the easier it is to model. The resulting models from these datasets yields the best performances that could reach i.e. an average RPD of ~23 and average RMSEP of ~73 (hamra soil contaminated with kerosene dataset). Nevertheless, dark soils and lighter PHC also yields fair results with average RPD of ~4 and average RMSEP of ~400. The effect of preprocessing on the modeling outcome is critical and could mean the difference between a non-working model to an excellent model. I.e. the loess contaminated with diesel dataset showed results ranging from RPD of 4 to RPD of 14, or even RPD of under 1 in some cases, as shown in the distribution of the average RPD results in Fig. 1. The score distribution of the loess contaminated with diesel dataset shows almost the same distribution indicating the validity of the results and the importance of the preprocessing methods employed on the modeling process results. The best preprocessing method varies from dataset to dataset as shown in Table II, indicating of how important is using the “all pos-

sibilities" approach in the modeling process for achieving the best results. Interesting to note is that in all datasets, the best preprocessing method almost always included some sort of spectral normalization procedure; in a limited resource modeling situation (lack of proper modeling software or high performance computing) a normalizing preprocessing procedure should be always employed for improved performances.

Table 2. Datasets and best pretreatment mutation by RPD and MPS

Soil	PHC	Datase #	Best RPD Mutation	Best MPS Mutation
Gromosol	95	1	FDCrfS	sD
	Diesel	2	Cr	SFDCrfS
	Kerosene	3	Cr	fDCr
Hamra	95	4	AfD	AsDCr
	Diesel	5	SfDCrfS	SSNVfDfS
	Kerosene	6	Cr	SSNVfDfS
Loess	95	7	**FDCr**	**fDCr**
	Diesel	8	**SfD**	**SfD**
	Kerosene	9	S	SSNVfS
Rendzina	95	10	SafD	SfDCr
	Diesel	11	Cr	SNVfDfS
	Kerosene	12	**SfDCr**	**SfDCr**
Terra Rosa	95	13	MSC	SafD
	Diesel	14	**AfD**	**AfD**
	Kerosene	15	SDCr	sD

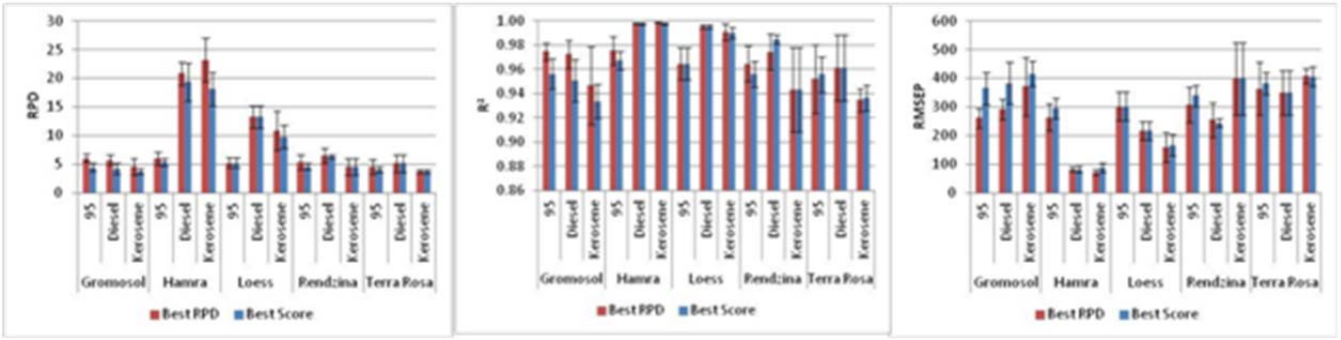

Figure 1. Comparison of the Best RPD models (alongside with R2 and RMSEP) and the Best Score Models

Due to the 10 different repetitions of the division into training/validation and test groups process that was done for each mutation, we can have a better understanding of the modeling process of a certain dataset. Instead of a single RPD (or any other statistical parameter) value based on a specific division, even when based on a well-known smart algorithm and not random, we now have two parameters: average RPD and RPD

standard deviation. Based on these values we can understand much better the modeling capabilities of our dataset and its future performances. We can see in Fig. 1 by the distribution of the RPD values for the loess contaminated with diesel dataset, difference between models can reach up to 50% based on the division into the training/validation and test groups alone.

4 Summery and conclusions

The results of this study clearly shows that predicting TPH levels at low concentrations in selected soils at high precision levels is viable. Modeling performance results ranged with average RPD of 4 to over 20. Each time we divide a dataset into training, validation and test groups, although these groups represent the dataset very well, slightly different groups can be created, thus affecting the modeling process to some extent. Different preprocessing methods or their combinations needs to be selected based on soil type and PHC type. Therefore, Paracuda, a new interface for the “all possibilities” modeling approach was developed especially for this task. The latest review of spectroscopic and non-spectroscopic techniques for TPH and PAH determination by Okparanma and Mouazen, 2013 preformed a comprehensive comparative study that concluded that the reflectance spectroscopy method is cheap, fast, safe, environmental friendly and with good accuracy. In summery, reflectance spectroscopy can be used as a viable, rapid, cost effective, environmental friendly tool to determine TPH contamination in soils. A preliminary study in the field shows that the use of the presented technology permits environmental friendly, rapid and cost-effective measurements of many samples. It suggests that further study to establish the spectral measurement as a practical (and may be even commercial) too is very important.

References

Ben-Dor E., Banin, A. 1995. Near infrared analysis (NIRA) as a simultaneously method to evaluate spectral featureless constituents in soils., *Soil Science,* 159:259-269

Hutcheson, M. S., Pedersen, D., Anastas, N. D., Fitzgerald, J., H. Silverman, D. 1996. ‘‘Beyond TPH: Health-Based Evaluation of Petroleum Hydrocarbon Exposures’’. Regul. Toxicol. Pharm. 24: 85–101.

Okparanma, R. N., Mouazen, A. M. 2013. ‘‘Determination of total petroleum hydrocarbon (TPH) and polycyclic aromatic hydrocarbon (PAH) in soils: a review of spectroscopic and non-spectroscopic techniques’’. Appl. Spectrosc. Rev.. doi:10.1080/05704928.2012.736048.

Savitzky, A., Golay, M. J. E. 1964. ‘‘Smoothing and Differentiation of Data by Simplified Least Squares Procedures.’’ Anal. Chem. 1964. 36: 1627–1639.

Prediction of soil organic matter using cluster-local regression and national Vis-NIR soil spectral library in China

Z. Shi[1*], Q. L. Wang[1], R. A. Viscarra Rossel[2] , W. J. Ji[1,2], L.Q. Zhou[1] , S.C. Chen[1]

[1]Institute of Agricultural Remote Sensing and Information Technology Application, Zhejiang University, Hangzhou, 310058, China

[2]CSIRO Land and Water, Bruce E. Butler Laboratory, PO Box 1666, Canberra, ACT2601, Australia

[*]E-mail: shizhou@zju.edu.cn

Abstract

With the development of soil spectral libraries (SSL) at regional, national and global scale, we should confront with a question how to use SSL for predicting local soil samplings and even serving for site-specific practice within field. In this study, we used a China soil Vis-NIR spectral library (CSSL) which including 2808 soil samples collected from 20 provinces in China to test an cluster-local regression (CLR) method which combining with spectral-regionally classification and local weighted regression (LWR). The method includes two key steps: (i) All the continuum-removed spectra were compressed by a principal components analysis (PCA), and the resulting PC scores were used to classify all soil spectra into four spectral clusters using a K-mean classifier, then each spectral cluster were continually divided into five sub-clusters according to the soil geographic-zoning; (ii) The new test set were projected into a PCA space and identified the optimal sub-cluster it belongs. Within this sub-cluster, 50 similar spectra were selected for build a calibration model of soil organic matter using LWR method. The results showed that the prediction accuracy of CLR method has been significantly improved in comparison to the conventional PLSR methods without classification: R^2 increased from 0.498 to 0.879 and RPD from1.41 to 2.88, respectively. In addition we provide an idea how to build the suitable spectroscopic calibrations of soils from the national scale for local estimation, and this calibration model will be embedded flexibly into the rapid Vis-NIR sensors in laboratory or in situ conditions.

Keywords: VisNIR, Soil organic matter, Soil-spectral library, local regression, China.

1 Introduction

Over the last two decade, proximal visible near-infrared (Vis-NIR) diffuse reflectance spectroscopy (DRS) technology has developed as a major tool for rapid, inexpensive predictions of a range of soil properties. However, how to build the robust and widely-used Vis-NIR soil predicting models with accepted accuracy is still a changeling task. Due to the soil diversity across different region or spatial variability of the site, we should collect the sufficient samples that can adequately describe this complexity of soil prop-

erties for modeling (Viscarra Rossel et al, 2008). During the last ten years, therefore, several large soil-spectral libraries at global or national scale have been constructed or are continually building, which could facilitate the wider use of VNIR-DRS by reducing the number of calibration samples required for local applications (Shepherd & Walsh, 2002; Brown et al, 2006; Sankey et al, 2008; Knadel et al, 2012; Viscarra Rossel & Webster, 2012; Ji et al, 2012).

On the other hand, the accuracy of the models usually decreased when the larger dataset contains very diverse samples in terms of geographical origin, mineralogy, parent material, environmental conditions, etc (Ramirez-Lopez et al, 2013). Recently some studies try to use soil spectral libraries (with lager number of samples) to estimate the local samples in very heterogeneous regions (in term of pedodiversity). The central ideal of these researchers are reducing the complexity of a given soil calibration dataset and finding out the relatively homogeneous partitions or clusters based on spectral or geographical information. For instance, some reported the use of spectral variability such as the spiking of the spectral libraries to recalibrate models before prediction (Brown, 2007; Guerrero et al. 2010), or directly use of local modeling such as locally weighted partial least squares regression (LWR, Christy & Dyer, 2006; Igne et al, 2010) and LOCAL algorithm (Gogé et al. 2012). Several studies demonstrated the geographical partition with agro-geological regions (Stevens et al, 2010), or spatial region (Wetterlind & Stenberg, 2010) . But there is lack of research about the use of the combining spectral and geographical information for partitioning the lager spectral library into local calibration dataset.

In this context, the objectives of this research were: (i) to develop a national soil spectral library in China, (ii) to find out the classification rules for partitioning the whole soil spectra into several clusters with the homogenous of soil spectra and soil geographical conditions, and (iii) to build a cluster-based calibration model for predicting soil organic matter (SOM) using local regression method.

2 Materials and methods

2.1 China soil spectral library

A China soil Vis-NIR spectral library (CSSL) which including 2782 soil samples collected from 20 provinces in China, representing 10 orders (China Soil Taxonomy) (see Figure 1). Soil sampling was collected from 0-20 cm surface soil. After air-drying and sieving (<2 mm), the diffuse reflectance spectra with a range of 350nm to 2500nm were measured using an ASD vis-NIR spectrometer (Analytical Spectral Devices) under laboratory condition. After removing the noisy portions between 350 and 400 nm and 2451-2500 nm, the leaving spectra in the range from 400-2450 nm were smoothed by a Savitzky-Golay method and used for our analysis. Soil organic matter was determined colorimetrically after H2SO4-dichromate oxidation at 150◦C and used in this study. SOM of all

soil samples covers a wide range (1.66 - 94.55 g kg^{-1}.) with a mean of 21.73. A validation dataset of 50 samples were extracted systematic from all soil samples by the sort of SOM content, and the else 2732 samples were used as calibration dataset.

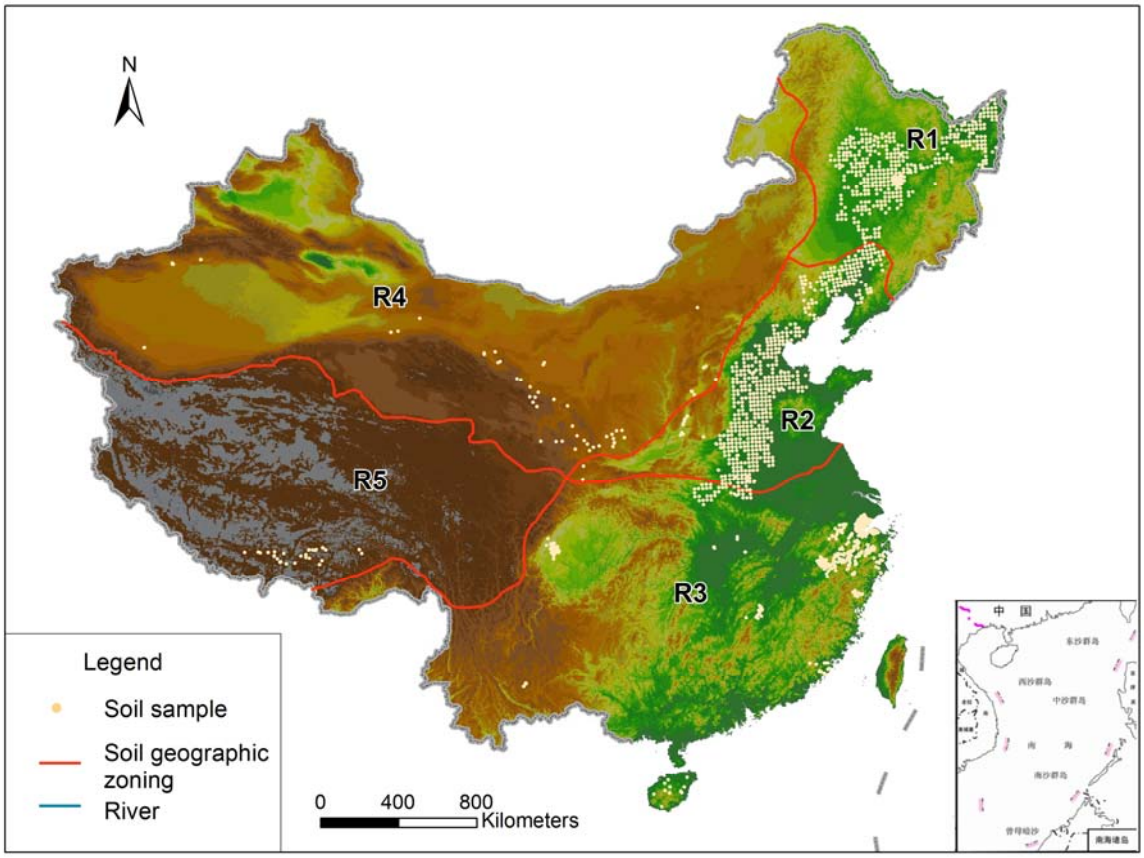

Figure 1. Spatial distribution of all soil samples and soil geographic zoning

2.2 Spectral pre-treatment

All spectra were transformed by the continuum removal method in order to emphasize absorption features in the spectra. To derive the continuum removed spectra, the continuum of each spectrum was derived by fitting a convex hull to each spectrum and then computing the deviations from the hull. Since of the highly collinear in VisNIR spectrum, the continuum-removed (CR) spectra were compressed by principal components analysis (PCA).

2.3 Calibration procedures

The cluster-local regression method consisted of two key steps (see Figure 2): (i) After pro-treatment, all the calibration spectra were classified into several clusters using K-mean classifier, and continually divided into several sub-clusters according to soil geographic zoning; (ii) A set of samples spectrally similar to new test sample were selected build a calibration model using local weighted regression and use the model to predict

soil organic matter of new test sample. All VisNIR data processing and statistical analyses were carried out with Unscrambler 10.1, JMP and R+ software.

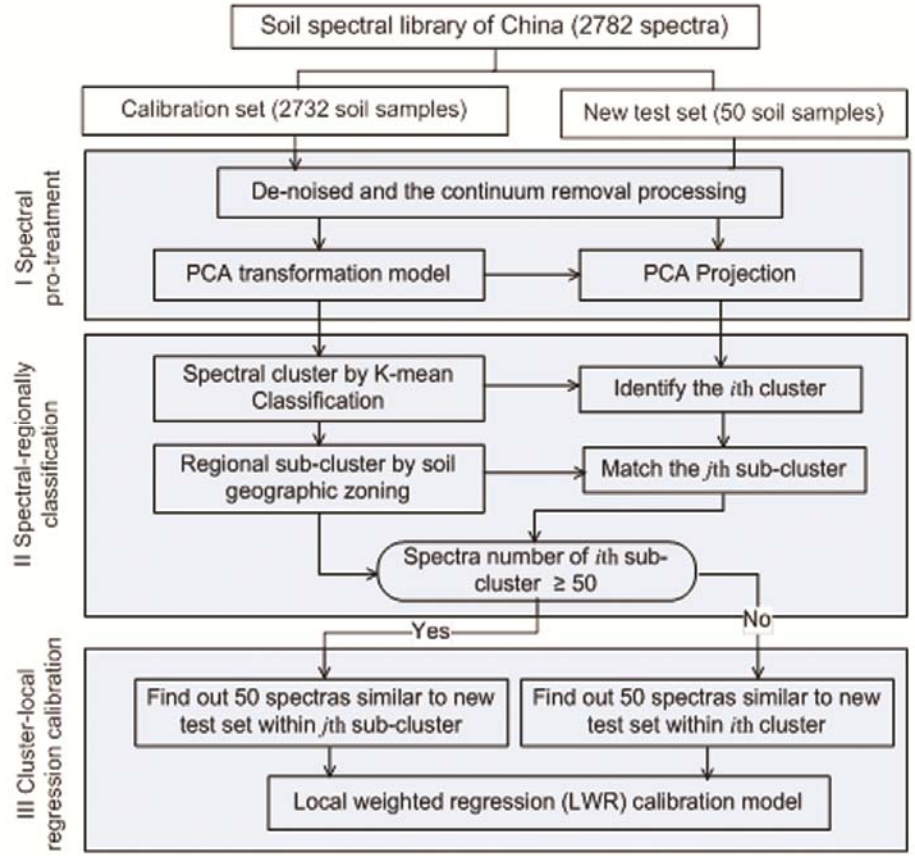

Figure 2. Flow chart of cluster-local regression for predicting soil organic matter

2.4 Locally weighted regression (LWR) for calibration

Locally weighted regression (LWR) utilizes this idea for each new prediction sample by first seeking samples which are close to it in spectral space and then using these local samples to fit a local linear regression equation. A subset of samples similar to the unknown sample, expressed in the same PC scores, is selected on the basis of the smallest metrics distance. In calculating these distances, a larger or smaller weigh can be assigned to each component, depending on its correlation with analytical values from the calibration database. The detailed algorithm was showed the relative literatures (Næs et al, 2004).

2.5 Validation

The validations were evaluated by the R^2 value of the relationship between the VisNIR estimate of the soil property and the reference measurement, the root mean squared error of prediction (RMSE). The ratio of performance to deviation (RPD) was calculated as the standard deviation (SD) of the validation set divided by the RMSE, mainly for comparison of calibration performance between parameters.

3 Results

3.1 Soil spectral characterization

To some extent, the characteristic variations in the soil reflectance can be interpreted in term of soil properties diagnostic for the higher categories of soil taxonomy (Stone & Baumgardner, 1981). Figure 3 showed the average reflectance spectra and soil organic matter of five soil groups in the Primosols order. The spectra of these five groups exhibited two distinct types with respect to their curve shape. The spectra of aeolian soils and alluvial soil from north-east China are similar to organic-affected type which exhibiting a low overall reflectance with a slowly flat increasing shape from 400 to 1300 nm. Other three groups (i.e. limtstone, skeletol and purplish soils) from south China, their spectra are belong to iron-affected type which is characterized by overall high reflectance and a stronger 900 nm iron absorption band. Although there exist the similar spectra for aeolian soils and alluvial soils, their soil organic matter content are significantly different (see Figure 3 right). Therefore, we selected soil geographical-zoning which is related to soil origin for soil clustering together with spectral information.

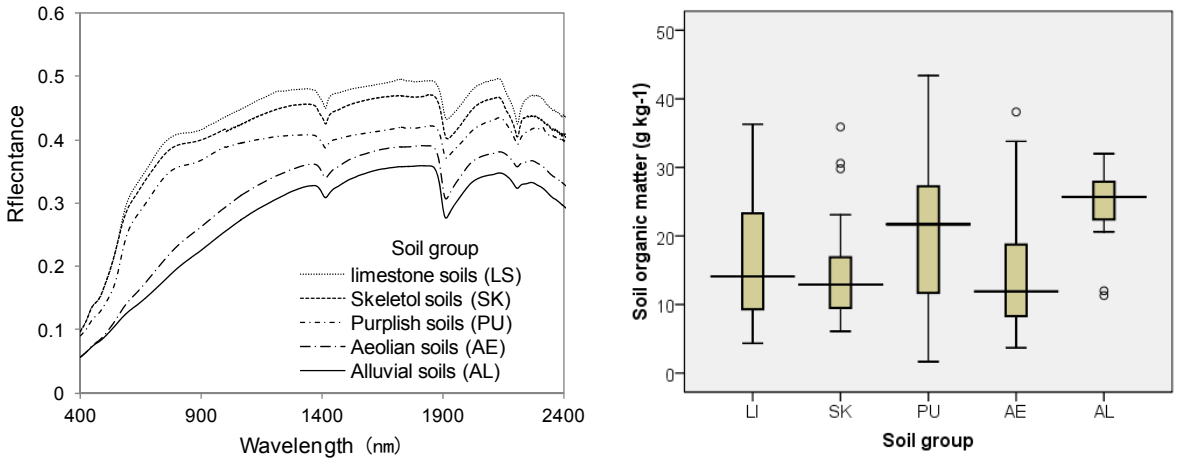

Figure 3. Average soil spectra and organic matter of five soil groups in the Primosols order

3.2 Soil spectral classification

Figure 4 showed the cumulative eigenvalue with the number of principal components (PCs). The first five PCs account for 93.87% were used for spectral classification using fuzzy k-mean clustering. Comparing with FPI, MPE and S value to different number of clusters, it indicates that the solution for 4 clusters is optimal in terms of the organization of the clusters. Figure 5 is a score plot of the first two PCs, colored by cluster. The second PCs axis is related to soil organic matter. C3 and C4 cluster with high SOM content (38.91 and 24.02 g kg^{-1}) is projected on the lower, C1 and C2 with low SOM content (16.11 and 21.4 g kg^{-1}) on the upper. The first PCs axis means the soil development and different mineralogy.

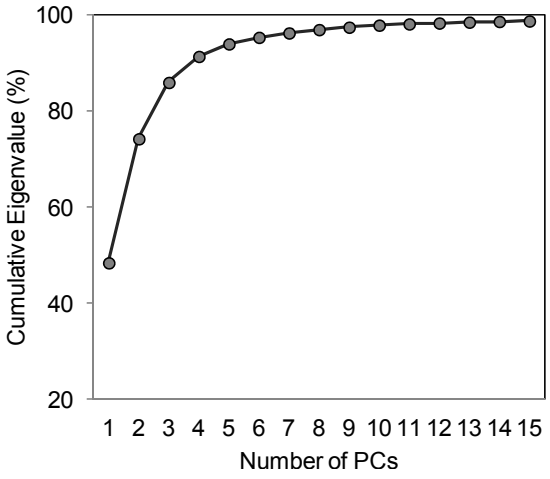

Figure 4. The cumulative eigenvalue with different number of principal components

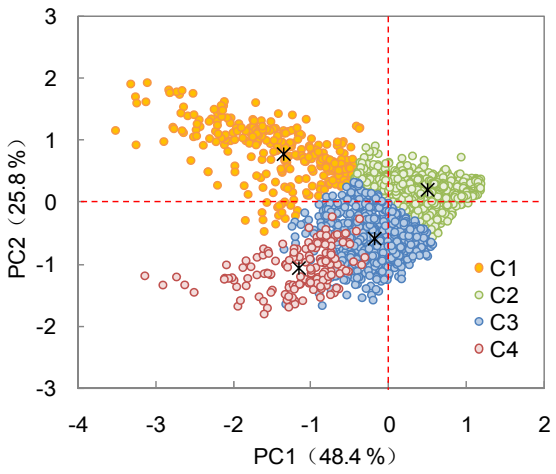

Figure 5. The score of the first two principal components and centre for four soil clusters

The soil geographical zoning is division of a territory into regions, which are one-type according to structure of soil cover, combination of soil-forming factors, and possibilities of agriculture use of soils. With referenced with the Chinese soil geographical zoning (Xi & Zhang, 1982), five regions (R1, R2, R3, R4 and R5, see Figure 1) were divided by similarity of temperature and humidification condition and a continentality of climate. Figure 6 showed the structure of two-level soil classification for Vis-NIR soil predicting with the corresponding the soil sampling numbers. It is worthy noted, there exists cross-relationship between the spectral classification and soil geographical zoning. For instance, the soil sampling within the spectral cluster of C3 are relatively homogenous and only from R1 region, and C1 cluster is almost similar. But the soil sample of C2 cluster were diversified, and subdivided into five regions in order to reducing its complexity.

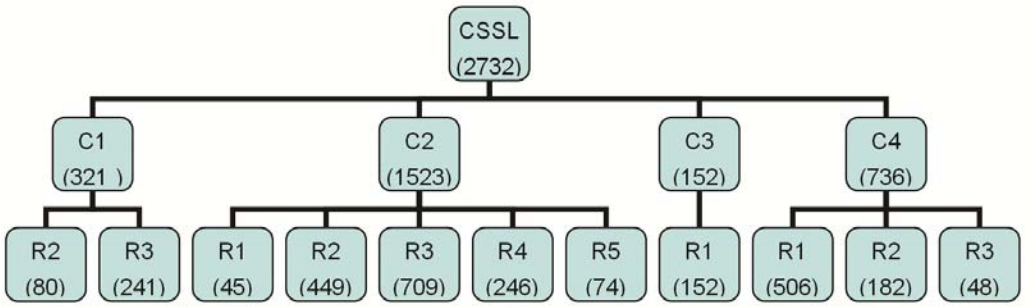

Figure 6. Structure and sampling number of two-levels soil classification

3.3 Calibration

Results of the predictive performance of the cluster-local regression (CLR), PLSR without classification (PLSR-All), and PLSR with spectral cluster (PLSR-SC) are presented in Figure 7. For CLR method, two parameters have to be optimized: the number of principal components (PCs) in the local regression and the number of samples to include in the training set for local calibration. In this study, the first ten PCs account for 97.77% were selected for local calibration, and the number of the nearest neighbors is selected 50 samples. Figure 7 shows that the accuracy of prediction is increasing as the number of calibration data set is decreased due to the reducing of data complexity. CLR method presents the satisfied accuracy in comparison to other two PLSR methods: R^2 increased from 0.498 to 0.879 and RPD from1.41 to 2.88, respectively.

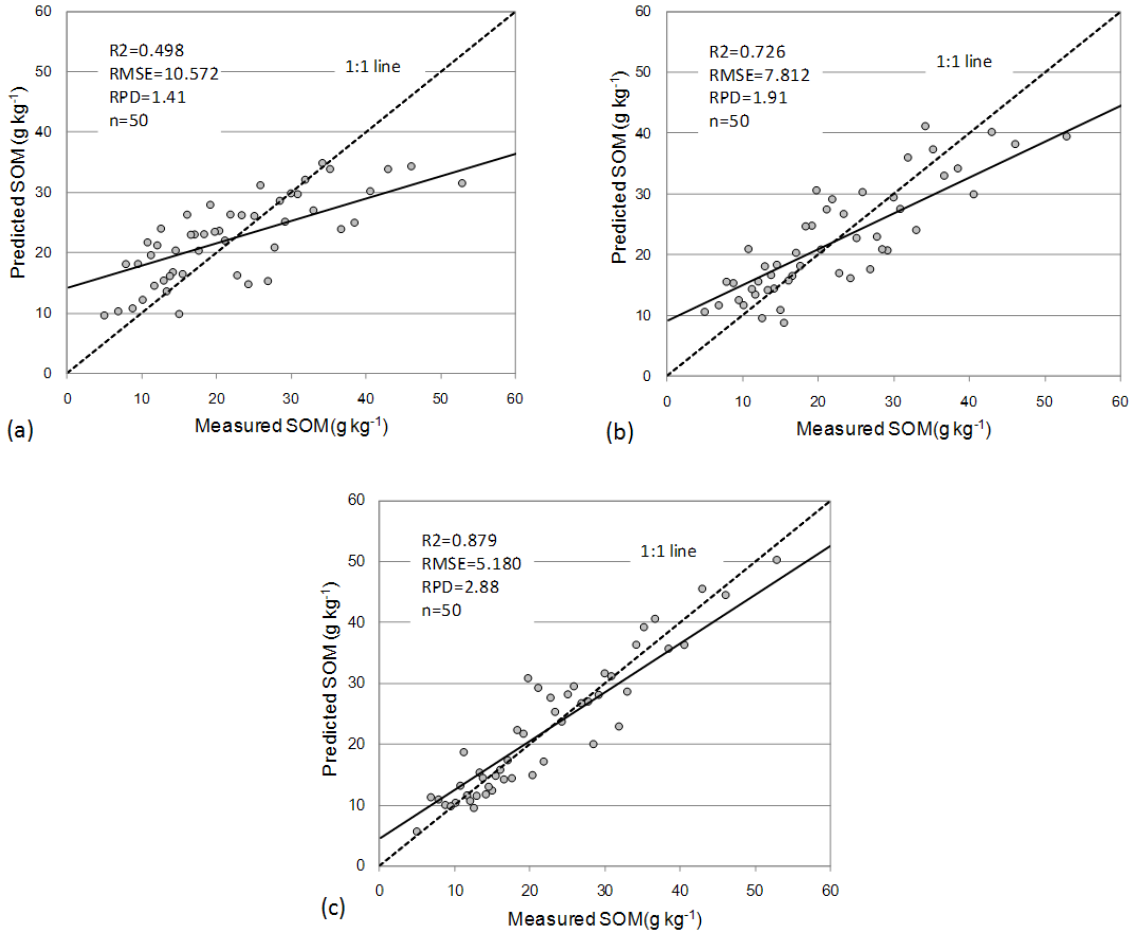

Figure 7. Predicted versus measured values of the validation set for organic matter using: (a) PLSR-All, (b)PLSR-SC, and (c)CLR method.

4 Discussion

Many countries are characterized by a remarkable diverse physiogeography. Thus pedo-diversity is a big challenge to use the national soil spectral library for local prediction. One feasible solution like our study is to build a rational classification rule to partitioning

all soil spectra into several relatively homogeneous clusters. In this study, we selected soil spectral and geographical zoning as two classified rules excluded soil class which some researchers' recommended, the reason is because two former information are easy to collect. We just need the geographical position by GPS device of new test soil sample for Vis-NIR prediction, so this strategy will be accepted by farmer or local agricultural consultant in China. On the other hand, the CSSL needs more representative soil samples from the whole country in order to avoiding the lack of sufficient samples within every cluster. For instance, two region of R4 and R5 covered 54% area of the whole China have only 320 samples with equivalent to 1/9 of the whole samples of CSSL.

5 Conclusion

In this study, taking account of the spectral and soil geographical information, the total soil samples from CSSL were divided into four spectral clusters and continually re-divided into five geographical zones using a two-levels classification, which reduced the complexity of a given larger soil spectral library at national scale for the predicting of soil property.

The comparison between the cluster-local regression used in this study and the conventional PLSR without classification, the former method is more effective and stable with the significantly increasing of predictive accuracy (R^2 increased from 0.498 to 0.879 and RPD from1.41 to 2.88, respectively), especially it solves the under estimation issue for the rich organic soils using Vis-NIR technology. Thus, the CLR strategy might enable better prediction for local soil predicting with a low number of samples are available. It can be important for the implement of Vis-NIR technique in the extensive area with embedded of a larger soil spectral library and CLR calibration model.

Acknowledgements

This project was funded in part by National Natural Science Foundation of China (No. 41271234), the program for New Century Talents in University (NCET-10-0694), Zhejiang Provincial Natural Science Foundation of China (R5100140); National Key Technologies R&D Program of China (2011BAD21B04) and National High Technology Research and Development Program 863 (2013AA102301). We would like to thank all participants from 13 universes and two academic institutes for their contribution to China Soil Spectral Library (CSSL).

References

BROWN, D. J., SHEPHERD, K. D., WALSH, M. G., MAYS, M. D., REINSCH, T. G. 2006. Global soil characterization with VNIR diffuse reflectance spectroscopy. Geoderma, **132** 273-290.

BROWN, D. J. 2007. Using a global VNIR soil-spectral library for local soil characterization and landscape modeling in a 2nd-order Uganda watershed. Geoderma, **140** 444-453.

GOGÉ, F., JOFFRE, R., JOLIVET, C., ROSS, I., RANJARD, L. 2012. Optimization criteria in sample selection step of local regression for quantitative analysis of large soil NIRS database Chemometrics and Intelligent laboratory systems, **110** 168-176.

GUERRERO, C., ZORNOZA, R., GÓMEZ, I., MATAIX–BENEYTO, J. 2010. Spiking of NIR regional models using samples from target sites: Effect of model size on prediction accuracy. Geoderma, **158** 66–77.

IGNE, B., REEVES III, J.B., MCCARTY, G., HIVELY, W.D., LUND, E., HURBURGH, C.R. 2010. Evaluation of spectral pretreatments, partial least squares, least squares support vector machines and locally weighted regression for quantitative spectroscopic analysis of soils. Journal of Near Infrared Spectroscopy, **18** 167–176.

JI, W. J., SHI, Z., ZHOU, Q., ZHOU, L. Q. 2012. Investigation on organic matter of different soil types by Visible and Near-Infrared reflectance spectroscopy. Journal of Infrared and Millimeter Waves, **31** 277-282.

KNADEL, M., DENG, F., THOMSEN, A., GREVE, M. H. 2012. Development of a Danish national Vis-NIR soil spectral library for soil organic carbon determination. In: Digital soil assessment and beyond, edited by B. Minasny, B. P. Malone and A. B. McBratney, Taylor & Francis Group, London, pp.403-408.

NÆS, T., ISAKSSON, T., FEARN, T., DAVIES, T. 2004. A user-friendly guide to multivariate calibration and classification. NIR Publications, Chichester UK, 344 pp.

RAMIREZ-LOPEZ, L, BEHRENS, T., SCHMIDT, K., STEVENS, A., DEMATTÊ, J.A.M., SCHOLTEN, T. 2013. The spectrum-based learner: A new local approach for modeling soil vis-NIR spectra of complex datasets. Geoderma, **195-196** 268-279.

SANKEY, J. B., BROWN, D. J., BERNARD, M .L., LAWRENCE, R.L. 2008. Comparing local vs. global visible and near-infrared (VisNIR) diffuse reflectance spectroscopy (DRS) calibrations for the prediction of soil clay, organic C and inorganic C. Geoderma, **148** 149-158.

SHEPHERD, K. D., WALSH, M.G. 2002. Development of reflectance spectral libraries for characterization of soil properties. Soil Science Society of America Journal, **66** 988–998.

STEVENS, A., UDELHOVEN, T., DENIS, A., TYCHON, B., LIOY, R., HOFFMANN, L., VAN WESEMAEL, B. 2010. Measuring soil organic carbon in croplands at regional scale using airborne imaging spectroscopy. Geoderma, **158** 32–45.

STONE, E. R., BAUMGARDNER. 1981. Characteristic Variations in Reflectance of Surface Soils. Soil Science Society American Journal, **45** 1161-1165.

VISCARRA ROSSEL, R. A., JEON, Y. S., ODEH I.O.A., MCBRATNEY, A.B. 2008. Using a legacy soil samples to develop a mid-IR spectral library. Australian Journal of Soil Research, **46** 1-16.

VISCARRA ROSSEL, R. A., WEBSTER, R. 2012. Predicting soil properties from the Australian soil visible-near infrared spectroscopic database. European Journal of Soil Science, **63** 848-860.

WETTERLIND, J., STENBERG, B. 2010. Near infrared spectroscopy for within field soil characterization small local calibrations compared with national libraries spiked with local samples. European Journal of Soil Science, **61** 823-843.

XI, C. F., ZHANG, J. M. 1982. The basis and regionalization of China's soil. Acta Pedological Sinica, **19** 97-109.

A robust FTIR database for Scotland

A.H. J. Robertson*, S. J. Hillier, C. Donald, H. R. Hill

The NSIS Team The James Hutton Institute, Craigiebuckler, Aberdeen, Scotland, AB15 8QH
**E-mail: jean.robertson@hutton.ac.uk*

Abstract

Using Fourier Transform Infrared Spectroscopy (FTIR) a spectral database of Scotland's soils has been produced using an Attenuated Total Reflectance (ATR) sampling method. Vital to the generation of high quality IR spectra of soil is sample preparation, in particular milling. Here we evaluated a number of milling procedures not only applicable to FTIR analysis, but which also enabled mineral analysis using X-ray power diffraction spectroscopy (XRPD). The robust spectral database produced allowed comparison between recently sampled and legacy samples, the development of calibrations with soil properties and provides a sound basis for the development of field based FTIR methodologies.

Keywords: FTIR, soil, MIR, ATR, XRPD.

1 Introduction

FTIR (Fourier Transform Infrared) spectra in the mid infrared (MIR) region (4000 to 400 cm^{-1}) of mineral and soil samples give an overall chemical profile of the sample. The spectra can be recorded using a range of different sampling methods: Transmission; Diffuse Reflectance (DRIFTS) and Attenuated Total Reflectance (ATR). ATR is a straightforward method which avoids the need for the sample preparation of transmission methods and produces spectra that have a number of advantages over those recorded by DRIFTS. These include ease of interpreting the bands arising from the fundamental vibrations in this spectral region, and the quality of correlations between spectra and soil properties. Both DRIFTS and ATR spectra can also be recorded in the field.

In order to produce an FTIR spectral database for Scotland's soils an ATR sampling method was selected. To ensure the ATR spectra were as representative and reproducible as possible, it was critical that a sample preparation protocol was developed which produced samples with the optimal particle size, whilst avoiding problems of contamination or degradation of the samples. The first aim of this study was to achieve this. The samples in the Scottish dataset were also being analysed by X-ray powder diffraction (XRPD) for mineralogy and, in order to ensure accurate correlations between the IR spectra and the quantitative mineralogy, the second aim was to produce a shared sample preparation method for the two techniques. This preparation procedure was primarily focussed on the milling and drying of the soil sample prior to analysis.

A high quality and diverse FTIR database for soils, such as this, provides not just an excellent basis for the development of calibrations between FTIR spectra and soil properties, but also a sound platform for the development of future field-based FTIR methodologies. The final aim of this work was to produce a robust spectral database suitable for this, and also for assessment of changes in soils over time.

2 Materials and Methods

2.1 Sample Preparation trials

For the milling protocol a small set of 12 samples representing a range of soil types, from organo-mineral soils, with limited soil organic matter to highly organic soils, with limited mineral content were selected. For each milling procedure tested, 2 replicates were run. All methods tested involved wet milling (in water or alcohol) due to the known danger of degrading the samples by the heat generated by dry milling [Russell, 1974]. The methods compared were hand milling, ball milling using a Retsch mill with tungsten carbide or agate balls and milling with a McCrone mill with corundum or agate barrels. Drying methods were also compared, with the samples either being spray dried or air dried. Milling time was also varied.

For the milling trials FTIR spectra of the milled soils were recorded on a Bruker Vertex 70 FTIR spectrometer using a DATR accessory in the range from 4000cm^{-1} to 400 cm^{-1} (ATR and baseline corrected) and compared with each other and with spectra of the unground soils.

2.2 FTIR spectral database

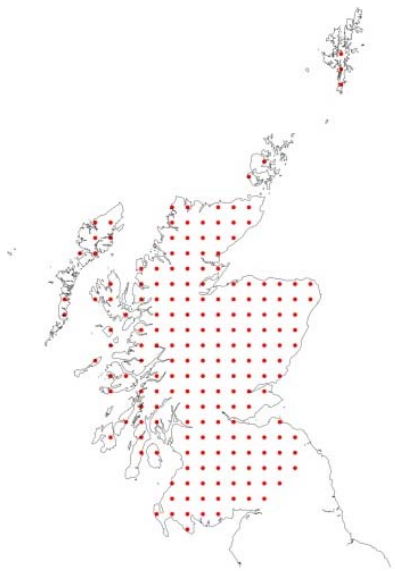

Figure 1. Location of NSIS grid points, each 20 km apart

FTIR analysis was carried out, as described above, on a spatial dataset of soils sampled on a 20km grid throughout Scotland (see Fig 1), as part of the National Soil Inventory of Scotland (NSIS) [Lilly et al, 2010]. Samples were from 183 different sites, top horizons of a pit profile. Where <10 cm deep, a second horizon was also included giving a total of 224 samples in the dataset. Both recently sampled (NSIS2, 2007-2009) and legacy samples (NSIS1, 1978-1988) were analysed. Scottish soils have a great diversity and the dataset had % C values ranging from 1- 50% [Aalders et al, 2009].

3 Results

3.1 Sample Preparation trials

Some methods showed contamination in the IR spectra and XRPD patterns. This was the case for the Retsch milling with agate balls and McCrone milling with corundum barrels, where the IR spectra were contaminated with visible silica and corundum bands. These methods were eliminated as unsuitable on this basis.

Retsch milling with tungsten carbide balls appeared to alter the Soil Organic Matter (SOM) profile in the IR spectra, particularly where there was low clay mineral content in the soil. There was an alteration in the 1800 – 1300 cm^{-1} region which may be consistent with free carboxylic acid being converted to the carboxylate. There also appeared to be a loss of intensity due to kaolinite bands. In addition, this method gave spectra with a sloping baseline and some poorly resolved mineral peaks, indicative of particle size not being sufficiently reduced. As expected, this was also found for hand milled samples.

Spray drying of the samples also seemed to alter the SOM profile in the IR spectrum, but was the preferred option for XRPD analysis. Spray drying also provides samples with randomised orientation, ideal for XRPD (Hillier, 1999), but which show different relative intensities for kaolinite bands in IR spectra compared with “normal” oriented samples.

McCrone milling with the agate barrels (12 minutes milling in water) followed by air drying and lightly grinding (in isopropyl alcohol) with the mortar and pestle gave the best results for the FTIR spectra. The organic matter pattern most closely resembled that of the un-milled soil, the particle size was appropriate and there was no evidence for contamination with silica. This was the protocol adopted for the FTIR spectra for the Scottish Soil Spectral Database. The samples for XRPD shared this preparation method up to the drying stage, when they were spray dried

3.2 FTIR spectral database

High quality FTIR spectra were achieved for the Scottish Soil Spectral Database and they were shown to be highly reproducible and representative by comparisons between

spectra of recently sample and legacy soils from the same sites. (See Fig 2) It is therefore possible to look at change over time.

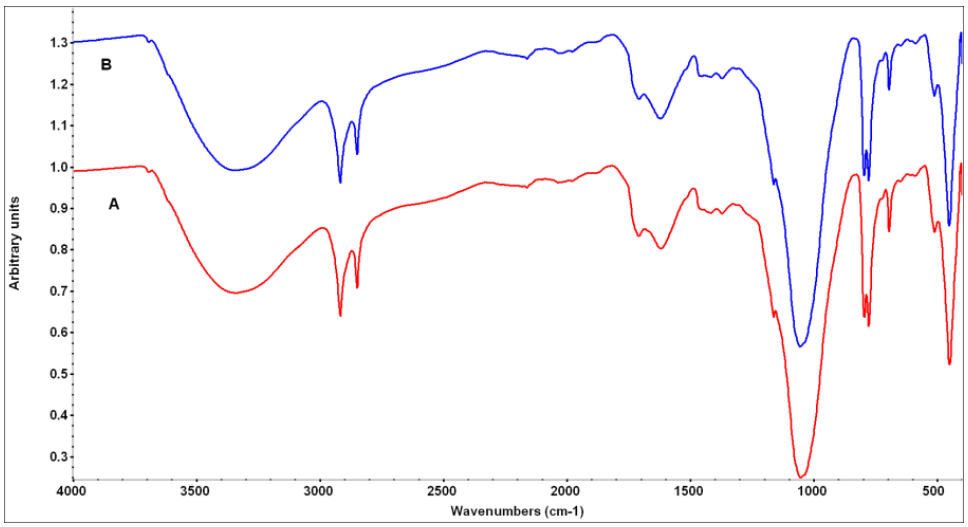

Figure 2. IR spectra of A) a legacy sample and B) a recent sample from the Windyhills site (NJ 800 400)

Successful calibrations have also been achieved for a number of soil parameters, including Soil Bulk Density, and comparisons can now be made between the IR spectra and the mineralogy from the XRPD data.

4 Discussion

A huge amount of information is contained in the FTIR “chemical profile” of soil, encompassing fundamental vibrations of both the organic and mineral aspects. The spectrum of each individual soil sample can therefore be interpreted and the nature of the soil determined. However an IR spectral database of well characterised soils also presents considerable opportunities for relating the spectra to soil properties and producing calibrations for different soil attributes. This gives the potential for extensive non-destructive analysis to be carried out in a single measurement. It also allows, for example, the comparison of soils sampled 30 years apart from the same location, a high priority in this laboratory following the re-sampling of the National Soil Inventory for Scotland. It is essential that the spectra recorded are representative and reproducible if reliable information is to be acquired. It can be argued as to whether using lab based FTIR to examine soil is proximal sensing (McBratney et al, 2011), however, establishing the best practice in the lab must also be considered key to moving it out into the field and developing robust methodologies for *in situ* FTIR analysis. Therefore this work not only has the intrinsic value associated with the lab based analysis but in addition can inform the development of field based analysis.

Sample preparation has many potential pitfalls which can alter IR spectra and their subsequent interpretation. Particle size should ideally be <2µm to avoid problems with sloping baselines, noisy spectra and poorly resolved mineral peaks [Russell, 1974]. Orientation of samples can affect the spectra too, particularly the relative intensity of absorption bands. Milling is required for soil samples to bring them into the ideal particle size range but any milling process will introduce some contamination, and may introduce other unexpected physical and chemical changes. Ball milling with the Retsch mill, dissipates a lot more energy than the roller milling of the McCrone mill and hence contamination is visible from the agate with Retsch but not McCrone (although the corundum barrels are not as durable and therefore lose material even with the McCrone). The combination of the energy dissipated by the Retsch mill and the presence of both clay minerals and tungsten carbide (possible catalyst) may be responsible for the alteration of the SOM pattern. Spray drying involves flash heating to over 100^{o}C and alteration in the SOM profile of soil samples has been noted previously for heating of SOM in presence of clay minerals (Russell et al, 1974) and may be the cause of changes seen in the spray dried samples.

A protocol was devised, here, to avoid the problems discussed above and give spectra of the desired quality. The protocol was shared between samples for FTIR analysis and for XRPD analysis, up to the final drying stage, ensuring direct links between the IR spectra and mineralogy data. The protocol was then applied to the NSIS samples, both legacy and resampled. For many of the samples there has been essentially no change between the FTIR spectra from legacy and resampled soils and the spectra can be almost exactly overlaid. Although not the initial intention, this can be regarded as a very effective validation of the whole chain of processes for NSIS sampling and analysis.

The NSIS soils are available, in their original state, from the Scottish soils archive for use in the next step for developing field based analysis, where the effects of particle size and moisture are likely to be the biggest challenges. Although the “best practice” milling protocol cannot be applied in the field the detailed interpretation of what is present in a given soil, from the lab based spectra, will be invaluable in development of reliable methodologies in the field. A sample which has been previously studied under ideal conditions can then be looked at under non-ideal conditions with a much greater understanding.

5 Conclusions

A shared protocol for soil preparation for FTIR analysis and XRPD analysis was developed which allowed high quality data to be recorded for both, and hence the IR spectra and quantitative mineralogy to be directly linked. Using the protocol a robust FTIR spectral database for Scotland’s soils was produced, for both legacy and recent samples, which allows change over time to be investigated. It also provides an excellent basis for developing field based methodology.

Acknowledgements

Particular thanks must go to Caroline Thomson and Gillian Green for their work processing the NSIS samples. Funding for this work was provided by the Scottish Government.

References

AALDERS, I.H., BALL, B., BLACK, H.I.J., CAMPBELL, C.D., GRIFFITHS, B., HOPKINS, D., HOUGH, R.L., LILLY, A., MCKENZIE, B.M., REES, R.M., SINCLAIR, A., TOWERS, W., WATSON, C. 2009. Considerations for Scottish soil monitoring in the European context. European Journal of Soil Science **60,** 833-843.

HILLIER, S. J. 1999. Use of an air-brush to spray dry samples for X-ray powder diffraction. Clay Mineralogy **34,** 127-135.

LILLY, A., BELL, J., HUDSON, G., NOLAN, A.J., & TOWERS, W. 2010. National Soil Inventory of Scotland 1 (NSIS_1): site location, sampling and profile description protocols. (1978-1988). Technical Bulletin, Macaulay Institute, Aberdeen, UK.

MCBRATNEY A., MINASNY B. AND WHELAN B. 2011. Defining proximal soil sensing. Invited talk, The Second Global Workshop on Proximal Soil Sensing, Montreal.

RUSSELL J. D. 1974. Instrumentation and Techniques, in The Infrared Spectra of Minerals, edited by V C Farmer, The Mineralogical Society, London, UK, pp. 11-25.

RUSSELL J D, FRASER A R, WATSON JR, PARSONS J W. 1974. Thermal decomposition of protein in soil organic matter. Geoderma **11,** 63-66.

Measurement of soil bulk density with fusion of visible and near infrared spectroscopy and frequency domain reflectometry

R. A. Al-Asadi, A. M. Mouazen*

Department of Environmental Science and Technology, Cranfield University, Cranfield, MK43 0AL, UK.

**E-mail: a.mouazen@cranfield.ac.uk*

Abstract

No reliable, speedy and objective measurement technique of soil bulk density (BD) is available today. This study introduces a new approach for *in situ* measurement of soil BD, which relays on combining visible and near infrared spectroscopy (vis-NIRS) (LabSpec®Pro Near Infrared Analyzer, Analytical Spectral Devices, Inc, USA) (ASDi) for the measurement soil gravimetric moisture content (ω) with frequency domain reflectometry (FDR) for the measurement of soil volumetric moisture content (θv) (ML2 ThetaProbe Delta-T Devices Ltd., 1996). By combining of ω and θv for the same soil sample, BD can be derived. A total of 1012 undisturbed soil samples were collected from England and Wales, from arable fields and grassland fields with different soil textures. Two calibration-validation procedures (CVP) were employed. The first CVP (CPV1) was based on partial least squares (PLS) regression (PLSR) with one-leave-out cross validation to calibrate the vis-NIRS for the measurement of ω using Unscrambler 7.8 software (CAMO Software, Woodbridge, Norway). The entire data was divided into calibration (70%) and validation (30%) sets. Gaskin and Miller's calibration method of ThetaProbe was conducted for the measurement of θv. The second CVP (CPV2) was based on artificial neural networks (ANN) analysis, run with Statistica toolbox, using ThetaProbe output voltage and ASDi spectra as input variables, and θv and ω are considered as output. The results showed high accuracy was obtained with CVP1 for the prediction of ω and θv, with R^2 and root mean square error of prediction (RMSEp) values of 0.91 and 0.027 g g^{-1}, and 0.95 and 0.026 cm^3 cm^{-3}, respectively. However, more accurate results was obtained by CVP2, with R^2 and RMSEp values of 0.98 and 0.014 g g^{-1} and 0.98 and 0.015 cm^3 cm^{-3}, respectively. The prediction of soil BD with the fusion of ω and θv data provided encouraging accuracy with both CVP method. However, more accurate results were achieved with CVP2 as compared to CVP1, with R^2 and RMSEp values of 0.81 and 0.095 g cm^{-3} and 0.53 and 0.19 g cm^{-3}, respectively. It can be concluded that it is possible to measure soil BD by the fusion of data from vis-NIRS and FDR.

Keywords: Compaction, Sensing, vis-NIRS, FDR, bulk density, data fusion.

1 Introduction

Heavy agriculture machinery, intensive use of the arable land and livestock heavy impact on grasslands during the wet soil conditions, are among the major factors that might lead to soil compaction. The compaction of soil can be defined as bulk density (BD) increase, or the closer backing of solid particles, resulting in less pore volume and less available air and water for plant growth and root development. Traditional measurement method of field BD is based on core sampling (e.g. Kopecki ring), which is time consuming, laborious and difficult procedure (Mouazen et al., 2005). They are subjected to error under dry soil conditions. Alternative methods to measure BD are required.

Recently, multiple sensors and data fusion approaches start to emerge in proximal soil sensing. Mouazen et al., (2005) developed an on-line multi-sensor platform for the measurement of BD, as a function of subsoiler draught, depth and gravimetric moisture content (ω), which was further calibrated for the majority of soil texture (Quraishi and Mouazen, 2013). Another on-line measurement system, reported by Naderi-Boldaji et al., (2012) fused a dielectric sensor together with a load cell to measure soil volumetric moisture content (θv), and horizontal penetration resistance, respectively. However, the prediction of BD based on empirical function provided rather poor accuracy (R2=0.21). Quraishi (2013) reported the development of a portable penetrometer system to asses BD, by fusion of data on ω, organic matter and clay content. The best result of soil BD prediction was with R^2 and root mean square error of prediction (RMSEp) values of 0.95 and 0.02 Mg m^{-3}, respectively. Author stated that artificial neural network (ANN) was the best tool to use for data fusion.

Visible and near infrared spectroscopy (vis-NIRS) has provided a proven and versatile analytical tools for agricultural, ecological, and forestry applications. It successfully adopted to measure soil properties including ω (Mouazen et al., 2006), a success which was attributed to the fact that O-H bond has a strong influence on vis-NIR spectra of soils (Kuang, 2012). Mouazen and Ramon (2006) developed a model to predict BD implementing the same on-line multi-sensor platform of Mouazen et al., (2005), their results were 0.75 and 0.054 Mg m^{-3} of R^2 and RMSEp, respectively. The dielectric constant (K) is a proven technique for the measurement of soil θv, due to the fact that K of the water (~80) is significantly greater than the dry soil matrix materials (~4) and of the air (~1) (Gaskin and Miller, 1996). Frequency domain reflectometry (FDR) or time domain reflectometry (TDR) are classified under K methods used frequently to measure θv. To our knowledge no report on combining vis-NIRS and FDR for the measurement of BD is available. The aim of the paper is to investigate the potential of combining vis-NIRS and FDR for the measurement of soil BD.

2 Material and methods

The hypothesis tested here is that by combining the vis-NIRS to measure ω (g g^{-1}) and FDR to measure θv (cm^3 cm^{-3}), BD (Mg m^{-3}) can then be derived using the following equation (Wijaya et al., 2003):

$$\mathrm{BD} = \frac{\theta_\mathrm{v}}{\omega} \tag{1}$$

A total of 1012 undisturbed soil samples collected from seven locations in England and Wales were used. They have been collected from the upper layer (10-20 cm) from arable and grassland fields from May 2011 to December 2012. These samples cover a wide range of variability including soil texture, moisture content, BD and different agriculture practices. ThetaProbe (Delta-T Devices Ltd., 1996) based on FDR was used to estimate θv, based on output voltage measured *in situ* of these sample. The output voltage is transferred to θv based on the relationship between the square root of the dielectric constant ($\sqrt{\boldsymbol{K}}$) and the output voltage of ThetaProbe (V) (Gaskin and Miller, 1996). Soil ω was estimated by means of the LabSpec®Pro visible and near infrared spectrophotometer (Analytical Spectral Devices, Inc, USA) (ASDi), with 350-2500 nm wavelengths. Two calibration-validation procedures (CVP) were employed. The first CVP (CPV1) was based on partial least squares regression (PLSR) to calculate ω and Gaskin and Miller's method of ThetaProbe to calculate θv. The second CVP (CPV2) was based on ANN analysis, using ThetaProbe output voltage (V) and ASDi spectra as input variables, and θv and ω are considered as outputs. PLSR with one-leave-out cross validation was run on the calibration set using Unscrambler 7.8 software (CAMO Software, Woodbridge, Norway). Spectra pre-treatment consisted successively of noise cut, maximum normalisation, 1st derivative and smoothing with S-G algorithms (Mouazen et al., 2006). The ANN toolbox of Statistica software was used to run the analysis of CVP2. During ANN, all data points were divided into training (60 %), test (10 %) and independent validation (30 %) sets. The ANN consisted of two input layers, eight hidden layers and two output layers (e.g. ω and θv). After ω and θv were obtained with CVP1 and CVP2, Eqn. (1) was used to calculate BD. The developed models were evaluated by means of R^2 and RMSEp.

3 Results and discussion

The results of ThetaProbe calibration for the prediction of θv for CVP1, based on Gaskin and Miller (1996) provided good prediction accuracy (R^2 = 0.95 and RMSEp = 0.026 cm^3 cm^{-3}), as shown in Table 1.

Table 1. The validation results of θv, ω and BD models obtained with CVP1 and CVP2 using the independent validation set (30 % of total samples).

Calibration Technique	θv		ω		BD	
	R^2	RMSEp ($cm^3\ cm^{-3}$)	R^2	RMSEp ($g\ g^{-1}$)	R^2	RMSEp ($g\ cm^{-3}$)
CVP1	0.95	0.026	0.91	0.027	0.53	0.19
CVP2	0.98	0.015	0.98	0.014	0.81	0.095

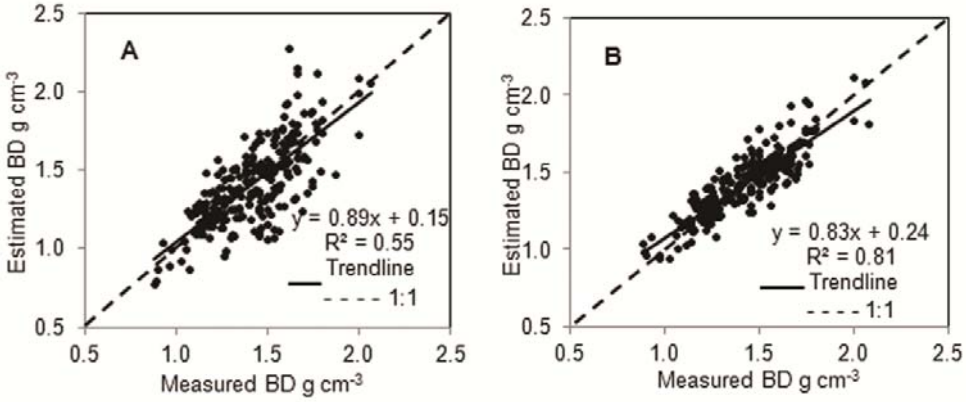

Figure 1. Scatter plot between estimated and measured BD by the tradition oven-drying method, for CVP1 (A) and CVP2 (B).

However, a slight better performance of ThetaProbe is recorded with CVP2, which reveals the capability of ANN, as compared to Gaskin and Miller (1996). On the other hand, considerable improvement for the measurement of ω is obtained with ANN analysis (CVP2), as compared to PLSR of CVP1 (Table 1). The ANN result for the prediction of ω is similar to that reported by Quraishi and Mouazen (2013) and by Kuang (2012). This led to a considerably higher accuracy for BD assessment with CVP2 (0.095 g cm^{-3}), as compared to CVP1 (0.19 g cm^{-3}), allowing the recommendation of ANN for the prediction of ω and θv, using fusion of data of a ThetaProbe *V* and spectra of a vis-NIRS.

4 Conclusions

High accuracy was achieved for the measurement of ω and θv with vis-NIRS and with ThetaProbe traditional calibration methods, respectively. Although, both CVP1 and CVP2 provided high accuracy for the measurement of ω and θv, the small RMSEp and high R^2 of CVP2 revealed a considerably higher accuracy can be obtained with CVP2, as compared to CVP1. This led to a considerably higher accuracy for the assessment of BD obtained with CVP2, as compared to CVP1, allowing the recommendation of ANN

for the prediction of ω and θv, using fusion of data of a ThetaProbe *V* and spectra of a vis-NIRS.

Acknowledgments

Authors acknowledge the financial support of the Engineering and Physical Science Research Council (EPSRC) and The Douglas Bomford trust.

References

GASKIN, G. J., J. D. MILLER. 1996. Measurement of soil water content using a simplified impedance measuring technique. J. Agric. Eng. Res. 63(2): 153-160.

KUANG, B. 2012. On-line Measurement of some selected soil properties for controlled input crop management systems. PhD thesis, School of Applied Sciences, Cranfield University, Bedfordshire, UK.

MOUAZEN, A.M., DE BAERDEMAEKER, J., RAMON, H. 2005. Towards development of on-line soil moisture content sensor using a fibre-type NI R spectrophotometer. Soil &Tillage Research 80 (1–2), 171– 183.

MOUAZEN A. M, RAMON, H. 2006. Development of on-line measurement system of bulk density based on on-line measured draught, depth and soil moisture content. Soil & Tillage Research 86 (2006) 218–229.

NADERI-BOLDAJI, M., ALIMARDANI, R., HEMMAT, A., SHARIfi, A., KEYHANI, A., DOLATSHA, N., KELLER, T. 2012. Improvement and field testing of a combined horizontal penetrometer for on-the-go measurement of soil water content and mechanical resistance. Soil and Tillage Research, 123, 1–10.

QURAISHI, M.Z., MOUAZEN, A.M. 2013. Calibration of an on-line sensor for measurement of topsoil bulk density in all soil textures. Soil &Tillage Research 126 (2013) 219–228.

QURAISHI, Z. 2013. Evaluation of field soil compaction for optimal mechanisation systems in controlled and non-controlled traffic systems. EngD thesis, Cranfield University, Bedfordshire, UK.

WIJAYA, K., NISHIMURA, Y., KATO, M. 2003. Estimation of dry bulk density of soils using amplitude domain reflectometry probe. J. Jpn. Soc. Soil Phys.

Combining electromagnetic induction and ground penetrating radar for industrial site characterization

E. Van de Vijver*, T. Saey, P. De Smedt, E. Meerschman, S. Delefortrie, P. Seuntjens, M. Van Meirvenne

Universiteit Gent, Department of Soil Management, Coupure links 653, Gent, Belgium
**E-mail: ervdevij.vandevijver@ugent.be*

1 Introduction

Industrial sites pose specific challenges to the conventional way of characterizing soil and groundwater properties through borehole drilling and well monitoring. The subsurface of old industrial sites typically exhibits a large heterogeneity resulting from various anthropogenic interventions. The natural soil may have been remolded or strongly disturbed by landfilling of foreign material such as construction and demolition debris and industrial waste. Also larger buried structures such as foundations, utility infrastructure and underground storage tanks are frequently present. Spills and leaks from industrial activities and leaching of buried waste may have caused additional soil and groundwater contamination. Trying to characterize the resulting complex and spatially heterogeneous soil matrix based on a limited number of conventional localized observations can lead to problematic results. Proximal soil sensors are useful tools to fill the spatial information gaps between the conventional observations, as these enable measuring soil properties in a non-invasive way. However, because the output of most soil sensors is affected by more than one soil property, the application of only one sensor is generally insufficient to discriminate between all contributing factors (Adamchuk et al., 2004). In particular, the complex and spatially heterogeneous environment of industrial sites requires approaching the site characterization problem with multiple sensors, in order to aid in discriminating between different soil properties. Therefore, industrial sites provide an interesting context to test a multi-sensor approach.

2 Objectives

In this case study we used a multi-sensor approach to (1) evaluate the detection potential for different types of anomalies and (2) appraise the added value of this approach in comparison with the conventional site characterization.

3 Materials and methods

The study area is part of a former manufactured gas plant site located in one of the seaport areas of Belgium. It has a surface area of 3400 m² and was the location of a phosphate production unit that was demolished at the end of the 1980s. Considering the long and complex history of the site we expected to find a typical "industrial" soil. Fur-

thermore, the studied area was located between buildings of the present industry, entailing additional practical challenges such as the presence of active utilities and aboveground obstacles. The area was surveyed using two proximal soil sensors based on two different geophysical methods: electromagnetic induction (EMI), to measure the apparent soil electrical conductivity (ECa) and magnetic susceptibility (MSa), and ground penetrating radar (GPR), to image contrasts in dielectric permittivity. For both methods one of the latest-generation instruments was used. For EMI, this was the multi-receiver DUALEM-21S sensor. This sensor contains four different transmitter-receiver coil pair configurations, which allows to record the ECa and MSa for four different soil volumes at the same time, thereby providing information about the vertical variation of these soil properties (e.g. Saey et al., 2012; De Smedt et al., 2013). GPR data were collected using a 3d-Radar stepped-frequency system with multi-channel antenna design (Eide and Hjelmstad, 2002). Both the EMI and GPR survey were performed in a mobile set-up with real-time georeferencing to obtain a high-resolution coverage of the area. The results of both surveys were validated with conventional site characterization that was conducted for a soil contamination investigation, and ancillary information such as aerial photographs and utility maps. Both methods were compared on their performance in detecting different types of anomalies.

4 Results

This presentation will show the first results of the combined application of EMI and GPR on the given study site. The results include the identification of several subsurface features that were not described by the conventional site characterization based on localized observations.

5 Conclusions

Based on these first results, we conclude that a multi-sensor approach can provide valuable extra information about soil properties variation compared to the conventional characterization. Therefore, it is a promising practice to expedite industrial site characterization.

References

ADAMCHUK V.I., HUMMEL J.W., MORGAN M.T., UPADHYAYA S.K. 2004. On-the-go soil sensors for precision agriculture. Computers and Electronics in Agriculture, 44:71-91.

DE SMEDT P., SAEY T., LEHOUCK A., STICHELBAUT B., VAN DE VIJVER E., ISLAM M.M., MEERSCHMAN E., VAN MEIRVENNE M. 2013. Exploring the potential of multi-receiver EMI survey for archaeological prospection: a 90 ha dataset. Geoderma, DOI: 10.1016/j.geoderma.2012.07.019

EIDE E.S., HJELMSTAD J.F. 2002. 3D utility mapping using electronically scanned antenna array. GPR 2002. Ninth International Conference on Ground Penetrating Radar, Santa Barbara, CA; 192-196.

SAEY T., DE SMEDT P., ISLAM M.M., MEERSCHMAN E., VAN DE VIJVER E., LEHOUCK A., VAN MEIRVENNE M. 2012. Depth slicing of multi-receiver EMI measurements to enhance the delineation of contrasting subsoil features. Geoderma, 189-190:514-521.

Improved predictions of soil texture and soil organic matter content by combining simultaneous *in-situ* measurements of visible and near infrared reflectance, electrical conductivity and insertion force

J. Wetterlind*, K. Piikki, B. Stenberg, M. Söderström

Swedish University of Agricultural Sciences, Department of Soil and Environment, Division of Precision Agriculture and Pedometrics, PO Box 234, SE-532 23 Skara, Sweden
**E-mail: johanna.wetterlind@slu.se*

Abstract

Data from three soil sensors, apparent electrical conductivity, visible and near infrared reflectance spectra and insertion force, were combined to enhance predictions of soil texture and soil organic matter content. The sensors were a part of a multi-sensor probe system that was used for measurements *in-situ* at two Swedish farms. The visible and near infrared spectrophotometer was the best single sensor for all tested soil properties. In general, the visible and near infrared wavelength range + insertion force rendered the best calibration results for SOM content, while the near infrared wavelength range + apparent electrical conductivity gave the best calibration results for clay, silt and sand.

Keywords: diffuse reflectance spectroscopy, apparent electrical conductivity, farm-soil mapping, penetration resistance.

1 Introduction

Combining data from conceptually different soil sensors have the potential to increase prediction accuracy and model robustness compared with the use of single sensors when trying to map different soil properties (e.g. Knadel et al., 2011; Kweon, 2012; Mahmood et al., 2012; Piikki et al., 2013 in press). The approach has gained interest with the development of integrated multi-sensor systems allowing for simultaneous collection of data from several sensors, thus overcoming some of the obstacles related to combining data from different sources. However, the number of studies is still fairly limited.

Objectives

The aim of this study was to explore the possibilities to enhance predictions of soil texture (clay, silt and sand) and soil organic matter content (SOM) by combining simultaneously collected data from three different soil sensors in a multi-sensor probe system, apparent electrical conductivity (ECa), visible and near infrared (vis-NIR) spectra and insertion force (IF).

2 Materials and methods

The study was conducted at two farms (adjacent fields with a total area of 55 and 37 ha, respectively) in southwest Sweden. Data from all three sensor measurements were collected using the Veris P4000 VIS-NIR-EC-Force Probe (Veris technologies Inc., Kansas, USA) at 20 sampling sites per farm. The sampling locations were selected to cover the spatial variation in an initial scanning by two non-invasive proximal sensors measuring ECa (EM38 Mk2 2; Geonics Ltd, Canada) and natural gamma radiation (The Mole, The Soil Company, the Netherlands). Two probings (0.1 – 0.8 m apart) were made at each location and data from the three sensors were logged simultaneously at about 0.75 measurements per centimetre down to 0.8 m.

In connection with the sensor measurements, composite soil samples (three soil cores/sampling location) down to 0.8 m were taken close to where the sensor probe was inserted. The soil cores were split into three depths (0-0.2 m, 0.4-0.6 m and 0.6-0.8 m) and were used for a reference analysis of SOM content and soil texture. SOM content was analysed as loss on ignition corrected for loss of structural water from clay minerals (Ekström, 1927). Soil texture was analysed using a sedimentation method (Gee and Bauder, 1986). The logged data from the three sensors were recalculated to correspond with the three depth intervals in the reference soil samples by depth-weighted averages.

The output vis-NIR spectra (absorbance) was transformed by first order Savitzky-Golay derivative (Savitzky and Golay, 1964). Calibrations were made, which included both the visible and near infrared wavelength range (vis-NIR) and which included the near infrared range only (NIR). For each farm, the three sensors were calibrated to each of the soil properties, one by one as well as in combinations using simple linear or partial least squares regression (PLSR). The calibration models were validated using cross validation in twenty segments, in which all three depth intervals from the same soil sampling site constituted one segment.

The calibrations were evaluated based on the root mean squared error of cross validation (RMSECV) and the R^2 value of the relationship between cross validated estimates and the reference measurements.

3 Results and discussion

For the calibrations using single sensors, the highest R^2 values and the lowest RMSECV values were obtained using the vis-NIR sensor for all soil properties (Table 1). The use of the vis-NIR wavelength range resulted in the best calibration results for SOM content, whereas when using only the NIR range, it gave the best results for clay, silt and sand (figures not shown). For soil texture, and especially for clay content, calibrations using only the ECa measurements were almost as good as the ones using NIR. Insertion force, on the other hand, could not by itself explain the variation in the soil tex-

tural classes. For SOM content, using only ECa or IF gave comparable results but with about twice as high RMSECV as when using vis-NIR.

Combining sensors slightly improved the calibration results for all soil properties except for clay at farm 1. The NIR-range in combination with ECa resulted in the highest R^2-values and lowest RMSECV for clay, silt and sand. Although IF, by itself, couldn't predict clay, silt and sand content, when it was combined with ECa, it resulted in higher R^2 and lower RMSECV compared with both ECa by itself and NIR by itself at farm 1. For SOM content, IF seemed to bring additional information to vis-NIR compared with ECa. This resulted in higher R^2 and lower RMSECV values when vis-NIR in combination with IF was used compared to vis-NIR combined with ECa, as well as when using vis-NIR by itself.

Since all three sensor measurements are affected by several soil properties, the possibility to separate the effects of these properties on the vis-NIR spectra compared with the incorporated information in the ECa and IF measurements (Adamchuk et al., 2004; Mahmood et al., 2012) could possibly explain why vis-NIR proved to be the best single sensor. With the rather moderate SOM content present at the two farms (on average 2.1 % and 3.6 % in the topsoil at the two farms, respectively), soil texture in combination with soil moisture will most likely be the prominent properties impinging on the sensor measurements. This is probably the reason why ECa managed to predict clay, as well as silt and sand at farm 1, with almost as good results as the vis-NIR sensor. The low prediction accuracy for clay, silt and sand using IF may be due to the influence of soil moisture on the measurements, with soil moisture influencing penetration resistance differently depending on soil texture (Dexter et al., 2007).

The results at the two farms were similar in terms of rank between the individual sensors and the sensor combinations. For SOM content, the best predictions using single sensors and a combination of sensors gave equally high R^2 values at the two farms. However, the RMSECV values were lower at farm 1, corresponding to the lower standard deviation in SOM content at that farm. The high R^2 values and low RMSECV values for sand and silt at farm 1 are possibly related to the very high correlation with clay content for both sand and silt (r^2 value of 0.98 and 0.94 respectively). Especially for silt, the correlations with clay content was not that pronounced at farm 2 (r^2 values of 0.81 and 0.13 for sand and silt, respectively).

Table 1. Calibration results for clay, silt, sand and SOM content using single sensors and/or a combination of sensors at the two farms.

	Clay		Silt		Sand		SOM	
	R^2	RMSECV (%)	R^2	RMSECV (%)	R^2	RMSECV (%)	R^2	RMSECV (%)
Farm 1		sd*=22.5		sd=15.8		sd=37.8		sd=0.98
ECa	0.92	6.5	0.81	7.1	0.89	13.0	0.29	0.82
IF	-	-	0.04	16.0	0.01	38.8	0.54	0.66
ECa + IF	0.94	5.6	0.87	5.8	0.92	10.7	0.83	0.40
(vis-)NIR**	0.94	5.5	0.84	6.6	0.91	11.6	0.90	0.31
(vis-)NIR + ECa	0.94	5.8	0.88	5.7	0.92	10.8	0.90	0.31
(vis-)NIR + IF	0.93	6.1	0.82	6.9	0.90	12.6	0.92	0.28
(vis-)NIR + ECa + IF	0.94	5.8	0.88	5.8	0.93	10.3	0.93	0.26
Farm 2		sd=12.6		sd=7.5		sd=16.7		sd=2.2
ECa	0.75	6.4	0.01	7.7	0.53	11.9	0.23	1.94
IF	-	-	-	-	-	-	0.20	1.97
ECa + IF	0.75	6.5	-	-	0.49	12.4	0.40	1.71
(vis-)NIR	0.76	6.4	0.37	6.2	0.64	10.4	0.89	0.74
(vis-)NIR + ECa	0.81	5.6	0.40	6.0	0.73	8.9	0.88	0.76
(vis-)NIR + IF	0.74	6.6	0.30	6.5	0.62	10.7	0.93	0.60
(vis-)NIR + ECa + IF	0.81	5.6	0.37	6.1	0.72	9.1	0.93	0.60

* standard deviation for comparison with RMSECV
** NIR range for clay, silt and sand and vis-NIR range for SOM

4 Conclusions

In most cases, a combination of more than one sensor rendered the best calibration results. However, the improvements compared with the best single sensor were not extensive.

Vis-NIR was the best single sensor for all tested soil properties (NIR-range for clay, silt and sand and vis-NIR-range for SOM content). In general, the vis-NIR-range in combination with IF rendered the best calibration results for SOM content, while the NIR-range combined with ECa gave the best calibration results for clay, silt and sand.

Acknowledgements

This project was funded by the Swedish Farmers' Foundation for Agricultural Research and the Swedish Research Council Formas.

References

ADAMCHUK, V.I., HUMMEL, J.W., MORGAN, M.T., UPADHYAYA, S.K. 2004. On-the-go soil sensors for precision agriculture. Computers and Electronics in Agriculture **44**(1) 71-91.

DEXTER, A.R., CZYZ, E.A., GATE, O.P. 2007. A method for prediction of soil penetration resistance. Soil & Tillage Research **93**(2) 412-419.

EKSTRÖM, G. 1927. Klassifikation av Svenska Åkerjordar (Classification of Swedish arable soils). 345 (Årsbok 20), Sveriges Geologiska Undersökning, Ser C. No. 345 (Årsbok 20), 161 pp.

GEE, G.W., BAUDER, J.W., 1986. Particle-size analysis. In: A. Klute (Ed.), Physical and mineralogical methods. Agronomy series. Soil Science Society of America, Madison, pp. 383-411.

KNADEL, M., THOMSEN, A., GREVE, M.H. 2011. Multisensor On-The-Go Mapping of Soil Organic Carbon Content. Soil Sci. Soc. Am. J. **75**(5) 1799-1806.

KWEON, G. 2012. Toward the Ultimate Soil Survey: Sensing Multiple Soil and Landscape Properties in One Pass. Agron. J. **104**(6) 1547-1557.

MAHMOOD, H.S., HOOGMOED, W.B., VAN HENTEN, E.J. 2012. Sensor data fusion to predict multiple soil properties. Precis. Agric. **13**(6) 628-645.

PIIKKI, K., SÖDERSTRÖM, M., STENBERG, B. 2013. Sensor data fusion for topsoil clay mapping. Geoderma **199** 106-116.

SAVITZKY, A., GOLAY, M. 1964. Smoothing and differentiation of data by simplified least squares procedures. Analytical chemistry **36** 1627-1639.

Mobile system for on-the-go measuring and mapping soil permittivity, electrical conductivity, moisture content, temperature and mechanical resistance

I. Ananyev*, V. Zubets, A. Belov, Y. Blokhin

Agrophysical Research Institute of Russian Academy of Agricultural Sciences 14, Grazhdansky prospect, Saint-Petersburg, 195220, Russia
**E-mail: ananyev_igor@ inbox.ru*

Abstract

A mobile system intended for contact on-the-go measuring and mapping dielectric permittivity, electrical conductivity, temperature and horizontal penetration resistance of topsoil is considered in this paper. The design of the system and measuring sensors is described, resulted from calibration characteristics and areas of expedient application of the system in precision agriculture technologies are specified.

Keywords: mobile system, on-the-go measuring, topsoil characteristics, sensors.

1 Introduction

An important task of precision agriculture is to obtain the spatial variability information of topsoil characteristics that is necessary for site-specific crop management. Collecting data by point measurements or field sampling and laboratory analysis is expensive and does not meet requirements of the operational management in agricultural technologies. This paper aims at reporting on the mobile system for on-the-go measuring and mapping permittivity, electrical conductivity, moisture content, temperature and mechanical resistance of soil plow layer.

2 Instrumentation, materials and methods

The main assembly of the mobile system is a flat vertical measuring unit with three sensors placed at the same horizontal level: capacitive sensor of soil dielectric constant, conductivity and volumetric moisture content, soil temperature sensor and a sensor of soil horizontal penetration resistance (figure 1). The measuring unit is installed on the frame, which is used to suspend the system on a tractor with coupling hitch. The depth of measuring unit with sensors in the soil is regulated by supporting ski installed above the measuring unit and attached to the frame by foot with the ability to set the position of the sensors in the soil at a depth of 15, 20, 25 or 30 cm. The measuring unit embeds into the soil under the system own weight and additional load, for which a box is installed on the frame. To select the mode of embedding, as well as to protect the measuring unit from damage when hit by a stone, measuring unit is provided with a beveled

down-back frontal edge and in front of the unit a slotting knife is set, mounted on a frame with adjustable cutting angle from +30 (bevel down and forward) to -30 degrees (bevel down-back) through 10 degrees. If a collision with a stone occurs safety bolt holding the upper part of the slotting knife on the frame cuts away. The slotting knife takes a position parallel to the frontal edge of the measuring unit and the tractor drags the entire structure on top of the stone, then one must install a new safety bolt and install slotting knife in previous angular position. Initial embedding measuring unit into the soil, extracting it from the soil and retention in the transport position is executed by a tractor hydraulic drive.

The measuring unit is made of stainless steel with a thickness of 30 mm, and the sensors are embedded in its body. Sensors are equipped with double-sided sensing elements, mounted symmetrically on both sides of the measuring unit.

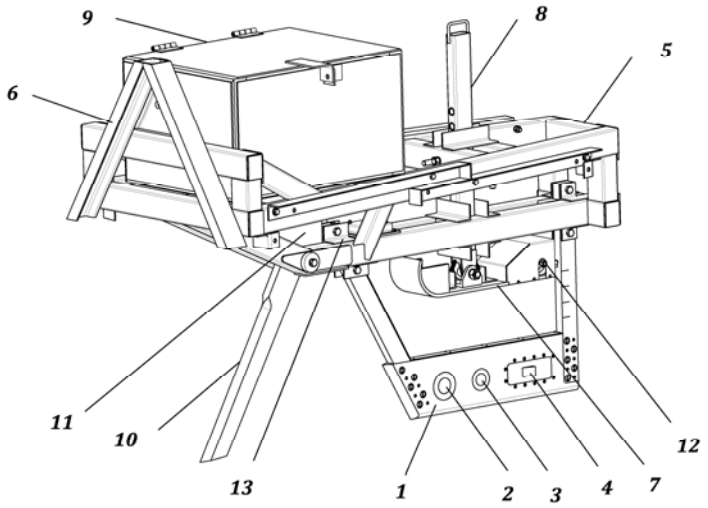

Figure 1. Mobile system design: 1 – measuring unit, 2 - capacitive sensor of soil dielectric constant, electrical conductivity and volumetric moisture content, 3 – soil temperature sensor, 4 – sensor of soil horizontal penetration resistance, 5 – frame, 6 – coupling hitch, 7 – supporting ski, 8 – foot with holes and workholder for setting position of the sensors in soil, 9 – box for additional embedding load, 10 – slotting knife, 11 – arrangement for catting angle setting and knife protection in case of collision with a stone, 12 – travel speed and distance sensor, 13 – electronic unit for collecting and recording the measurement data.

Capacitive sensor contains electrodes in the form of disks installed through insulators in the measuring unit. Sensor is connected into oscillating circuit of a two-component complex permittivity transducer with inertial stabilization of oscillation amplitude which measures the real component of complex permittivity and soil volumetric moisture through the frequency of oscillations and soil electrical conductivity through the gain control voltage of oscillator amplifier (Russian Patent No 2361226, 2009). The range of transducer operating frequencies is (11 – 22) MHz, the range of measured values of complex permittivity real component is 1 - 80, the range of electrical conductivities is (0 - 0.1) S/m, the range of measured volumetric moisture is (0 – 100) %.The temperature

sensor is in the form of two insulated disk heat sink with located inside temperature transducers TD-5 of HONEYWELL Company (USA). Temperature measurement range is (0 – 70) ºC, accuracy of measurements is 0.2 ºC.

Horizontal penetration resistance sensor (figure 2) is used to measure on-the-go strength of soil mechanical resistance, acting on two sensitive prismatic elements symmetrically protruding from the side surfaces of the measuring unit, which are connected as a load to the Z-shaped tensometric transducer YZ-101BN of Youngzon Transducer Co. Ltd (Taiwan). The range of measured pressures of horizontal penetration is (0 – 250) N/cm^2.

Figure 2. Horizontal penetration resistance sensor.

The sensors are connected to the electronic unit for collecting and recording the measurement data. The electronic unit transforms the analog data received from sensors into digital form and transmits this information to the tractor's on-board computer combined with the DGPS-receiver.

3 Results

The figure 3 shows the calibration characteristics of an oscillating two-component complex permittivity transducer with a capacitive sensor measuring the real component ε' of the complex dielectric permittivity and electrical conductivity σ of the soil, as well as measuring volumetric soil water content θ for samples of sod-podzolic soils, moistened with distilled water (lower curve with values θ) and moistened with KCl- solution of conductivity σ = 0.2 S/m (upper curve with the values of θ). These characteristics are presented in the coordinates of the measured output parameters of the oscillating transducer: oscillation frequency f_{OSC} and gain control voltage U_{CTR} of the transducer amplifier.

From figure 3 it is clear that with the help of the pair of on-the-go measured output parameters of oscillating transducer - f_{OSC} and U_{CTR} and a calibration grid ε' , σ one can determine the real component ε' of complex permittivity and electrical conductivity σ of the soil. Also, if calibration characteristics of oscillating transducer as measuring volumetric water content θ are investigated for the types of soil, which is examined by the

mobile system, then we can define the soil moisture content through the output parameters of the oscillating transducer.

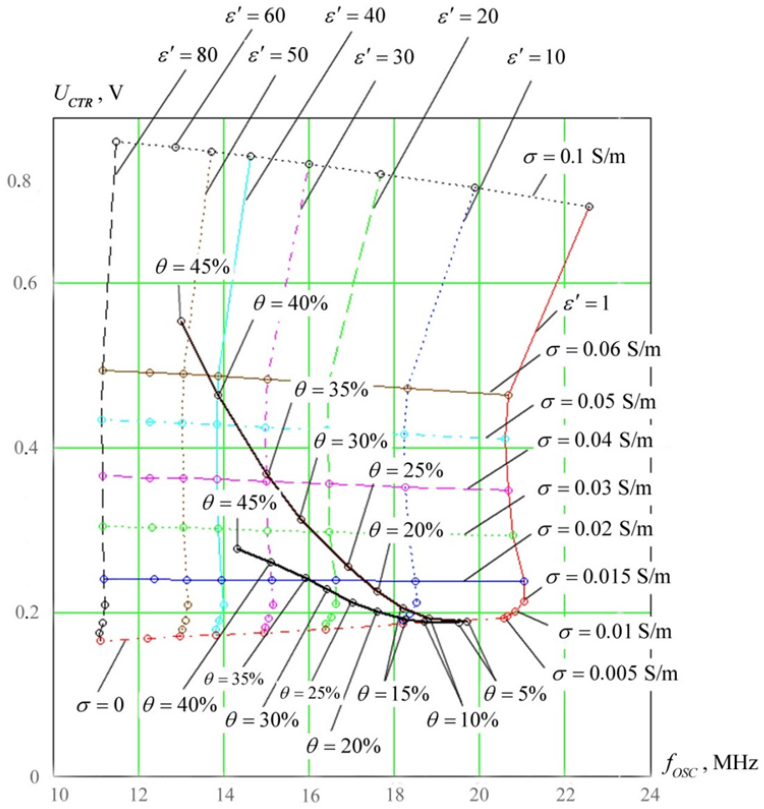

Figure 3. Calibration grid lines of soil equal real component ε' of complex permittivity and equal electrical conductivity σ in coordinates f_{OSC}, U_{CTR}. Moistening curves of sod-podzolic soil samples: a sample of constant salt composition, moistened with distilled water (lower moistening curve); sample, moistened with KCl-solution of conductivity σ = 0.2 S/m (upper moistening curve); θ - volumetric soil moisture content.

There is the possibility to construct calibration curves of oscillating transducer with a capacitive sensor as measuring volumetric water content θ and soil electrical conductivity σ, and at the same time determining the electrical conductivity of the soil solution σ_{SS}. Electrical conductivity σ_{SS} of the soil solution characterizes total dissolved mineral nutrients in the soil solution, used by roots for plant nutrition and growth. To perform such a calibration the soil samples should be pre-washed several times in distilled water to remove most of the soluble salts. Then we construct moistening curves similar to the curves in figure 3, by moistening the soil samples with KCl-solutions having given for each curve constant value of electrical conductivity. Gradually increasing solution conductivity for each curve, we get a family of moistening curves for solutions of different conductivity. During field measurements with the help of obtained family of moistening curves and measured output parameters of oscillating transducer f_{OSC}, U_{CTR} we determine the volumetric content of the soil solution and its conductivity σ_{SS}, which is equivalent to conductivity of the KCl-solution. The σ_{SS} values are found on

known electrical conductivities of KCl-solutions for moistening curves. The error in determining the electrical conductivity σ_{SS} of the soil solution will depend on residual conductivity of soil water due to incomplete removal of soluble salts under washing the soil samples used to construct the calibration curves. To obtain a small error on the residual conductivity of soil water during calibration, electrical conductivity of distilled water used for washing the samples, after a number of washing and for water-saturated state of samples shall not exceed 10 to 20% of the minimum conductivity of the KCl-solutions with constant electrical conductivity used to construct the moistening curves.

A method of determination developed, and experimental studies executed of the dynamic components of temperature sensors error, one of which is caused by heating of the sensor on movement due to friction with the ground, and the second is due to the inertia of the sensor, resulting in smoothing of the readings in case of rapid temporal changes in soil temperature at the contact with the sensor on the route of moving.

The first component of the dynamic error increases with increasing speed, and it depends on the volumetric moisture content, bulk density and particle size distribution of soil. The proposed methodology of experimental determination of this error is the following. Mobile system is moved across the field at a given depth of the sensors and at a predetermined velocity for which we want to define this component of the error, during the time required to reach steady-state values of the change of sensor temperature due to the friction of the soil $\Delta_H T$ (this time is easily found experimentally). Simultaneously, continuous record of sensors temperature readings is carried out (frequency of recording should be (0.5 - 2) s). After this the system is stopped but recording and observing changes in the temperature are continued. Due to the system stop, heating of the sensors by friction is terminated, the aperiodic process of sensor cooling with a gradual decrease in temperature from the fixed temperature of the heated by friction sensor T_H to the temperature of ambient soil T_S is going on (figure 4, a).

The difference of temperature readings between the sensor heated by friction T_H and the sensor cooled to the temperature of ambient soil T_S is the first component of the dynamic error: $\Delta_H T = T_H - T_S$. Due to the fact that the temperature sensor has a thermal inertia and in contact with the soil can be considered as an aperiodic link of the first order with a time constant τ, the process of change in the sensor temperature T at cooling is described by the formula:

$$T = \left(\Delta_H T\right) e^{-\frac{t}{\tau}} + T_S = \left(T_H - T_S\right) e^{-\frac{t}{\tau}} + T_S = T_S \left[\left(\frac{T_H}{T_S} - 1 \right) e^{-\frac{t}{\tau}} + 1 \right]. \quad (1)$$

Aperiodic nature of the cooling process allows to find the time constant τ of the sensor in contact with the ground on the sensor cooling curve using known methods: the tangential approach to the exponential curve, or falling the curve down to a level equal 0.368 from the difference of T_H - T_S (see figure 4, a).

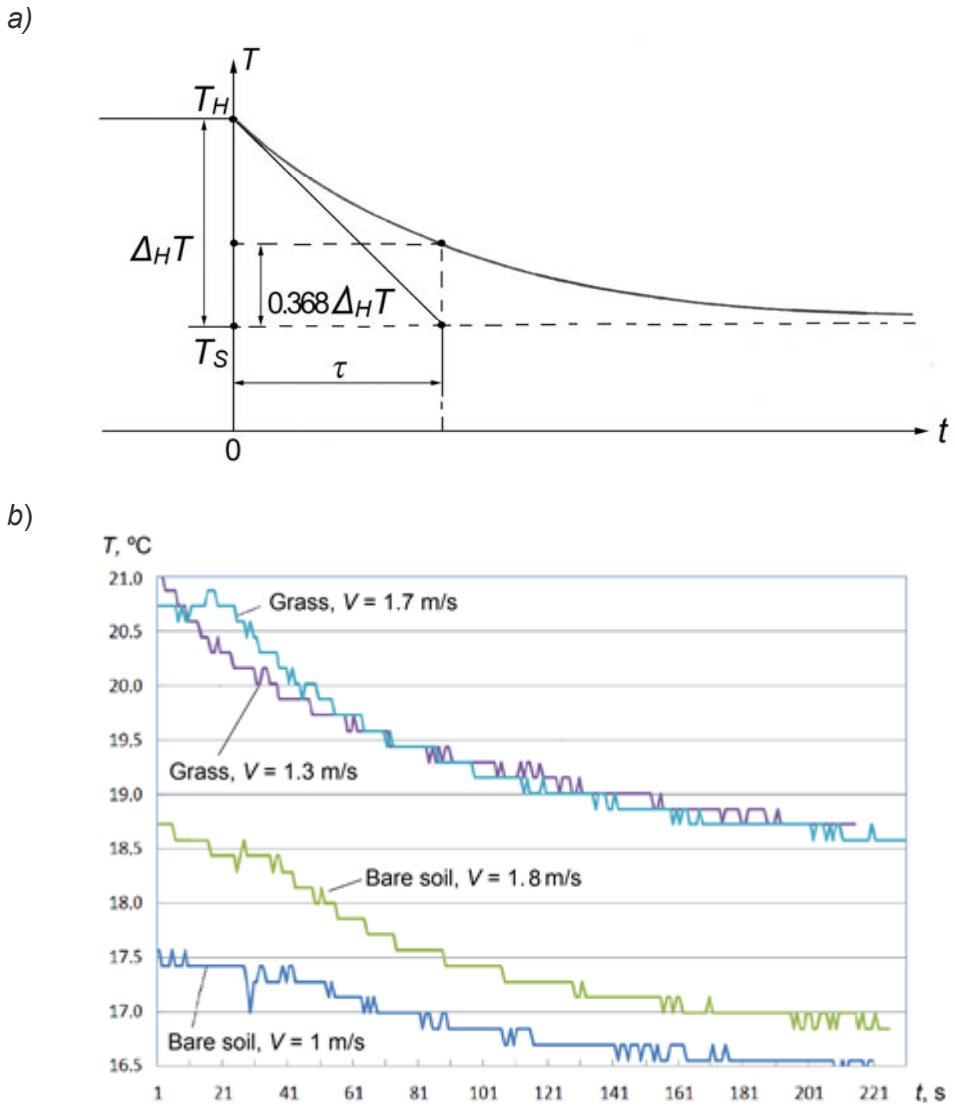

Figure 4. a) Graph illustrating the method for determining the dynamic error component $\Delta_H T$ of temperature measurement caused by heating of the sensor on movement due to friction with the ground. b) Charts of aperiodic process of the temperature sensor cooling after stopping the mobile system which was moving with speeds indicated on the graph in the field of perennial grass and in the field of bare soil for 180 s.

The figure 4, b shows the experimentally obtained curves of aperiodic cooling process of one of the temperature sensors (right in the direction of motion) when stopped after driving the sensor at a depth of 200 mm in the field of perennial grasses and the field of bare soil moving with speeds indicated on the graph for 180 s. From the graphs it is followed that the dynamic error due to friction on the field of bare soil was 1.9 ºC at a speed of 1.8 m/s. For a field of perennial grass at a speed of 1.7 m/s, this error was 2.2 ºC. The inertia of the sensor in contact with the soil which is characterized by a time constant τ of the temperature aperiodic process decay during cooling after stopping is determined graphically and is equal to (30 - 60) s. Therefore, to establish a steady-state value of the sensor temperature increment $\Delta_H T$ due to friction of the soil at a given

speed it is enough to move on the field during 180 s before stopping to measure the aperiodic cooling process, that is at least three times more than τ .

The component of dynamic error of friction can be considered as a correction in the processing of measurement results. In the process of field measurements and mapping the stopping to determine this error can be made at regular intervals to improve the accuracy of measurements. Furthermore, such parameters as the dependence of this error on the speed, volume water content and soil horizontal penetration resistance using sensor-mobile system may be specifically investigated. The information obtained can be used to automatically introduce corrections due to the friction of the ground to on-the-go measured temperature without stopping the mobile device. As a result, one can get the soil temperature measurement error on-the-go, not exceeding (0.5 - 1) ºC, which is significantly higher than the accuracy of soil temperature infrared radiation thermometers, which readings are substantially dependent on the reflectivity of the soil. The second component of the dynamic error, determined by the thermal inertia of the sensor, produces the smoothing of reading under rapid temporal variation of soil temperature on the route of moving and will be revealed when the period of the soil temperature change in the area of contact with the temperature sensor on the route of moving is less than (2 - 3)τ . In this case, to reduce or eliminate the second component of the error, the velocity of the field measurements must be reduced.

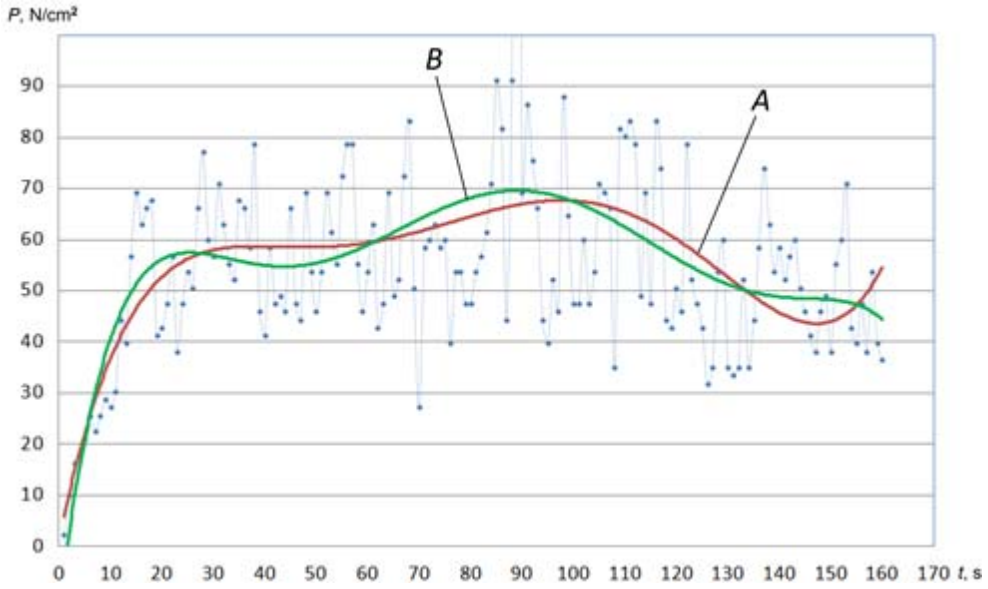

Figure 5. Data smoothing of horizontal penetration resistance obtained with 1 s record intervals under the mobile system motion at a speed of 1 m/s in the field of bare soil, using polynomial regression of the 5th (A) and 6th (B) degree. The initial part (0 - 10) s in the graph corresponds to the gradual embedding of the penetration sensor into the soil after the beginning of the movement.

Horizontal penetration resistance measurements showed that when moving on the field of bare soil with speeds of 1.0, 1.5 and 1.8 m/s, the resistance values are in the range

of (30 - 80) N/sm^2 (figure 5). When the mobile system moves in the field of perennial grasses with speeds of 1.3 and 1.7 m/s, the horizontal penetration resistance is in the range of (50 - 80) N/sm^2. The soil pressure force on the tensometric transducer in the measurements is in the range of (200 - 500) N with single amplitudes up to 900 N, that with the nominal range of the transducer (0 - 200) N doesn't create the risk of overloading the transducer.

For the chosen design of a mobile system containing slotting knife producing preliminary soil compaction in the channel on which the prismatic sensitive elements of the sensor of soil horizontal penetration resistance move, this sensor readings should be compared with the readings of the conventional vertical cone penetrometer which is used to measure the mechanical resistance and degree of surveyed soils compaction. The critical values of soil penetration resistance for cone penetrometer are (200 - 300) N/sm^2.

4 Discussion

The complex of topsoil characteristics measurement by the mobile system makes it possible to obtain additional information using data fusion.

Measuring two output parameters of the oscillating two-component complex permittivity transducer with a capacitive sensor - oscillation frequency f_{OSC} and gain control voltage U_{CTR} of the transducer amplifier allows to determine soil real component of complex permittivity ε' and electrical conductivity σ. Calibration curves of moistening with distilled water and salt solutions for selected soil types enable to define soil volumetric moisture content θ and electrical conductivity of soil solution σ_{SS}.

Measurement of the temperature sensor reading and the mobile system speed makes it possible to limit the sensor dynamic error due to friction of the soil.

Measurement of horizontal penetration resistance and speed of movement makes it possible to explore the dependence of the resistance on the rate of penetration.

Horizontal penetration resistance measurement and determination of the soil moisture content enables using the statistical model (Mouazen, 2003) to calculate the density of the dry soil.

5 Conclusions

Developed mobile system can be used for on-the-go measuring and mapping spatial and temporal variability of topsoil characteristics that is necessary for site-specific crop management in technologies of precision agriculture. It can be used to measure and map the temperature and water content regime of soils in agricultural fields to make decisions about the optimal timing of the field work, to determine the electrical conductivity of the soil solution in assessing the total dissolved mineral nutrients and making deci-

sions on fertilizing, to measure and map the soil hardness, to determine the density of the soil, as one of the main indicators of physical condition and applicability of the soil for crops, as well as for other tasks.

References

MOUAZEN, A. M., HERMAN RAMON, DE BAERDEMAEKER, J. 2003. Modelling compaction from on-line measurement of soil properties and sensor draught. Pecision Agriculture, 4(2): 203-212.

Integrated modeling of near-field ground-penetrating radar and electromagnetic induction data for digital soil mapping

F. André*, A.P. Tran, N. Mourmeaux, M.R. Ardekani, P. Bogaert, S. Lambot

Earth and Life Institute, Environmental Sciences, Université catholique de Louvain, Croix du Sud 2, box L7.05.02, B-1348 Louvain-la-Neuve, Belgium
**E-mail: frederic.andre@uclouvain.be*

Abstract

We present an integrated modeling procedure for near-field ground-penetrating radar (GPR) and electromagnetic induction (EMI) for the non-invasive determination of the constitutive properties of planar layered media in a high-resolution digital soil mapping framework. We validated the approach using GPR and EMI instruments set up using vector network analyzer technology, though the proposed methods also apply to conventional instruments. The antennas are modeled using a set of infinitesimal dipoles and characteristic, frequency-dependent, global reflection and transmission coefficients. The GPR and EMI antennas were calibrated using measurements at different heights over water. The electromagnetic models were then successfully validated using measurements acquired over water subject to different salinity levels. Finally, GPR and EMI data fusion strategies were investigated for resolving non-uniqueness issues that are inherent to multilayered media reconstruction.

Keywords: ground-penetrating radar, electromagnetic induction, near-field modeling, digital soil mapping, data fusion.

1 Introduction

Sustainable and optimal agricultural and environmental management of soil and water resources notably relies on accurate characterization and monitoring of the soil hydrogeophysical properties. Recent advances in environmental modeling, engineering and decision support systems have progressively enabled technological improvements of management practices. However, given the inaccessibility of the subsurface and its inherent spatiotemporal variability, quantitative information regarding the distribution of the soil properties and their dynamics at scales that are relevant for management practices is still limited. In that context, the development and integration of non-invasive monitoring techniques of both surface and subsurface processes is essential.

Ground-penetrating radar (GPR) and electromagnetic induction (EMI) present particular interests for digital soil mapping as they are non-invasive and real-time data acquisition permits field scale mapping with a high spatiotemporal resolution. Yet, despite the significant advancements particularly made during the last decade, accurate quantitative reconstruction of soil electrical properties through inverse modeling of GPR and EMI

data has remained a challenge in the geophysics community. Indeed, existing modeling approaches used to process the data usually neglect the antenna effects and consider strongly simplifying assumptions with respect to field propagation phenomena. The most advanced modeling approaches commonly used for GPR and EMI data processing resort to the finite-difference method (Warren & Giannopoulos, 2011), the finite-element method (Ilic et al, 2009), or the method of moment (Craeye et al, 2009). These methods present however the limitation of requiring large computing resources. In addition, these methods still present shortcomings for accurately representing real data due to the inherent discrepancies between the conceptualized models and the reality. . Alternatively, the integral equation methods (Alvarez et al., 2007) emulate the antenna radiative properties using a set of equivalent infinitesimal dipoles, which is much more efficient compared to numerical approaches. However, these methods do not directly account for the interactions occurring between the antenna and the medium as well as field propagation phenomena between the source and field points and instrument measurement plane. In addition, the parameterization of sources for proper representation of the antenna radiative properties is not straightforward. Finally, the reconstruction of the medium properties from either GPR or EMI may suffer from uniqueness and instability issues in the inverse problem. In that respect, more robust characterization of soils and materials may be obtained from the combination of both techniques as they present complementary information through their different sensitivities to the medium electrical properties.

In order to overcome forward modeling limitations, Lambot et al (2004) proposed a new approach for accurate and fast processing of GPR data when the antenna is located in far-field conditions above a planar layered medium. This approach accounts for all antenna effects, including antenna-medium coupling, and considers an exact solution of the 3-D Maxwell's equations for wave propagation in the planar layered media. This modeling approach being independent of frequency, it was also successfully applied to EMI (Moghadas et al, 2010). More recently, Lambot and André (2013) generalized the far-field model to near-field conditions.

The objective of this paper is to present the integrated GPR and EMI near-field models and to show validation results. Furthermore, GPR and EMI data fusion strategies are analyzed in order to investigate the benefits of combining both sources of information and provide insights into the way to perform such integration.

2 Materials and methods

2.1 GPR and EMI forward models

The near-field modeling procedure is identical for both GPR and EMI and, as aforementioned, constitutes a generalization of the far-field GPR modeling approach introduced by Lambot et al (2004) and applied to EMI by Moghadas et al (2010). In this approach,

a local planar field distribution is assumed for the backscattered field over the antenna aperture. This assumption holds if the antenna is located far enough above the medium (in practice, at a height larger than the antenna aperture). In this case, the antenna can be considered as a single point source and receiver. In near-field conditions, i.e., when the antenna is located closer or in contact with the medium, the planar field assumption does not hold anymore and the transmitting and receiving antennas should be described using an equivalent set of infinitesimal point sources and field points placed over the antenna apertures, thereby resulting in a planar field decomposition (Lambot & André, 2013). For both the far-field and near-field models, the field propagation between the point sources and field points and the transmission line reference plane is accounted for using complex frequency-dependent global reflection and transmission coefficients, which result in a closed-form expression in the frequency domain. We refer to the aforementioned references for a more detailed description of the modeling procedures.

2.2 Model inversion

The retrieval of the multilayered medium constitutive properties is carried out by minimizing an objective function defined as follows:

$$\emptyset(\boldsymbol{b}) = \sum_{\omega} \left| S_{**}^{meas}(\omega) - S_{**}^{mod}(\omega, \boldsymbol{b}) \right|^2 \quad (1)$$

where $S_{**}^{meas}(\omega)$ and $S_{**}^{mod}(\omega, b)$ are, respectively, the measured and modeled GPR and EMI data, $\mathbf{b}$ is the parameter vector to be optimized, including the layer electromagnetic properties and thicknesses, and ω and is the angular frequency. In this study, we used the Levenberg-Marquardt local optimization algorithm to minimize (1) and determine optimal parameter values.

2.3 GPR and EMI laboratory setups

Laboratory experiments were performed to validate the near-field GPR and EMI models. Both GPR and EMI sensors were set up using a vector network analyzer (VNA, ZVL from Rohde & Schwarz, Munich, Germany) as a stepped-frequency continuous-wave (SFCW) system.For GPR, a linear polarized double-ridged broadband horn antenna was used (BBHA 9120 A, Schwarzbeck Mess-Elektronik, Schönau, Germany). The antenna dimensions are 15 cm in length and 24×14 cm^2 in aperture area and the nominal frequency range is 0.8-5.2 GHz. The antenna was connected to the reflection port of the VNA with a high quality 50-Ω coaxial cable with N-type connectors. The VNA was calibrated at the cable-antenna connection using a standard Open-Short-Match (OSM) calibration kit. The frequency-dependent complex ratio S_{11} between the returned and the

emitted signals was measured sequentially at 1101 stepped frequencies from 0.8 to 3.0 GHz, with a frequency step of 2 MHz.

For EMI, we designed a specific prototype bistatic antenna operating in zero-offset mode. The transmitting antenna consists of two concentric and coplanar coils. The outer and the inner coils have both 3 cm height with 33 cm and 25 cm diameter, respectively, and are made of 109 and 75 turns of enameled copper wire (section of 0.52 mm^2). The current in the inner coil is traveling in opposite direction compared to the outer coil, leading to two magnetic fields with opposite polarities. This tends to cancel the magnetic field in the center of the coils where a 120 turns, 18 cm diameter and 1.5 cm height regular receiving coil is placed. This design permits to reduce the direct coupling between the transmitter and the receiver, thereby increasing significantly the sensitivity of the EMI system compared to setups based on regular loops. The transmitting and receiving coils were connected with variable capacitors allowing tuning of the resonant frequencies of both antennas and make them match. In addition, a 200 W wideband amplifier was used to amplify the emitted signal. The transmitting and the emitting antennas were, respectively, connected to the first port and the second port of the VNA using coaxial cables. In this case, we performed a full two-port calibration of the VNA using a Through-Open-Short-Match (TOSM) calibration kit. The antenna resonant frequencies were fixed at 38.1 kHz and the measurements consisted in the S_{21} ratio between the received and emitted signals.

For the laboratory validations, antenna calibration data were first collected by performing measurements at 100 heights ranging from near-field to far-field conditions over well-known configurations, namely, a 3×3 m² copper plane overlaid by a water layer of 0.045 m thickness and 0.090 m S/m electrical conductivity for GPR and of 0.98 m thickness and 1.980 S/m electrical conductivity for EMI. The responses corresponding to these known configurations were calculated through Green's functions for each height level and the antenna characteristic global transmission and reflection coefficients were determined using a specific optimization strategy (Lambot & André, 2013). The GPR horn antenna was modeled considering 8 point sources and field points evenly distributed along a profile at a few centimeters inward from the antenna aperture, while the EMI antenna was represented by a set of 6 point sources and field points equally spaced along the antenna diameter.

Then, validation data were collected considering measurements over water subject to different salinity levels. For comparison with values retrieved from full-wave inversion, water electrical conductivity was measured using a conductivity meter (WTW LF 318, probe WTW TetraCon 325) for a reference temperature of 25°C, and was translated to the measurement temperature using the equation proposed by Sorensen and Glass (1987). Water electrical conductivity ranged from 0.090 to 0.583 S/m for GPR and from 0.061 to 1.980 S/m for EMI. For both GPR and EMI, the copper plane was used as bottom boundary condition in the electromagnetic model. Furthermore, for GPR, we used

the Debye model to account for the frequency dependence of the free water apparent electrical conductivity with the parameterizations from Klein and Swift (1977) and Stogryn (1970) for the relaxation time and complex permittivity values as a function of temperature and salinity.

2.4 Data fusion

Potentialities of near-field GPR and EMI data fusion were investigated through numerical experiments. For this, antenna calibrations determined from the laboratory experiments (see above) were used to generate synthetic GPR and EMI data considering a two-layered medium with the following constitutive properties: first and second layer permittivities $\varepsilon_{r,1} = 9$ and $\varepsilon_{r,1} = 15$, first and second layer electrical conductivities $\sigma_1 = 10^{-2}$ S/m and $\sigma_1 = 10^{-1}$ S/m, first layer thickness h_1 = 0.15 m, and the second layer constituting the lower half-space. This medium configuration corresponds to that considered by Moghadas et al (2010) who investigated GPR and EMI data fusion for the far-field case, i.e., considering an antenna height h_0 = 0.20 m above the medium surface, while it was set to h_0 = 0.02 m for near-field data fusion in the present study. This common configuration allows for direct comparison between far-field and near-field data fusion results. The frequencies ranged from 800 to 2000 MHz for GPR and from 37 to 39 kHz for EMI with frequency steps of 6 MHz and 50 Hz, respectively.

In this study, data fusion potentialities were investigated through two different strategies for combining the respective GPR and EMI objective functions (see Equation (1)) into a single integrated objective function. For the first strategy, the global objective function is defined as (Kozlovskaya et al, 2007):

$$\emptyset_1 = \frac{\emptyset_{xx} - \min(\emptyset_{xx})}{\max(\emptyset_{xx}) - \min(\emptyset_{xx})} + \frac{\emptyset_{zz} - \min(\emptyset_{zz})}{\max(\emptyset_{zz}) - \min(\emptyset_{zz})} \quad (2)$$

where subscripts *xx* and *zz* denote GPR and EMI, respectively. It corresponds to one of the strategies adopted by Moghadas et al (2010).

The second strategy considered here is based on the following formulation (Ardakani et al, 2013):

$$\emptyset_2 = {\emptyset_{xx}}^{0.5} \times {\emptyset_{zz}}^{0.5} \quad (3)$$

3 Results

3.1 Antenna calibrations and data inversions

The GPR and EMI antennas were successfully calibrated, showing very good correspondence between measured and modeled data with correlation coefficients of r = 0.99807 and r = 0.99998, respectively.The values of the antenna characteristic coefficients obtained from these calibrations were then used for inversion of the validation

data so as to retrieve the medium properties. GPR inversions were performed considering the antenna height above water (h_0), water thickness (h_1), and water electrical conductivity (σ_1) as unknowns, while EMI data were inverted for water electrical conductivity only. The other parameters were fixed to their theoretical or measured values.

As illustrated in Fig. 1(a) for GPR data collected with h_0 = 0.01 m for a 0.208 S/m electrical conductivity, the model describes the measurements with a high accuracy in both the frequency and the time domains, even for such a small antenna height above the water surface (antenna-medium coupling is relatively important). Values of the antenna height (h_0) retrieved from GPR data inversion for each water salinity level show close agreement with corresponding measured values (Fig. 2(a)). Similarly, water thickness (h_1) was properly estimated by signal inversion, while, in contrast, poor agreement was observed between estimated and measured σ_1 (data not shown) because of limited sensitivity of the GPR data to this parameter for the considered frequencies and medium configuration.

Regarding EMI, close agreement is generally found between measured and modeled data, as illustrated in Fig. 1(b) for water electrical conductivity $\sigma_1 = 1.590$ S/m with the antenna located just above the water surface (i.e., h_0 = 0.00 m). For the lowest salinity levels (i.e., $\sigma_1 \leq 0.167$ S/m), the quality of the fit decreases (data not shown) as a result of a lack of sensitivity of the EMI system for these configurations, as also observable from the poorer agreement between corresponding estimated and measured water electrical conductivity values compared to the higher salinity levels (Fig. 2(b)).

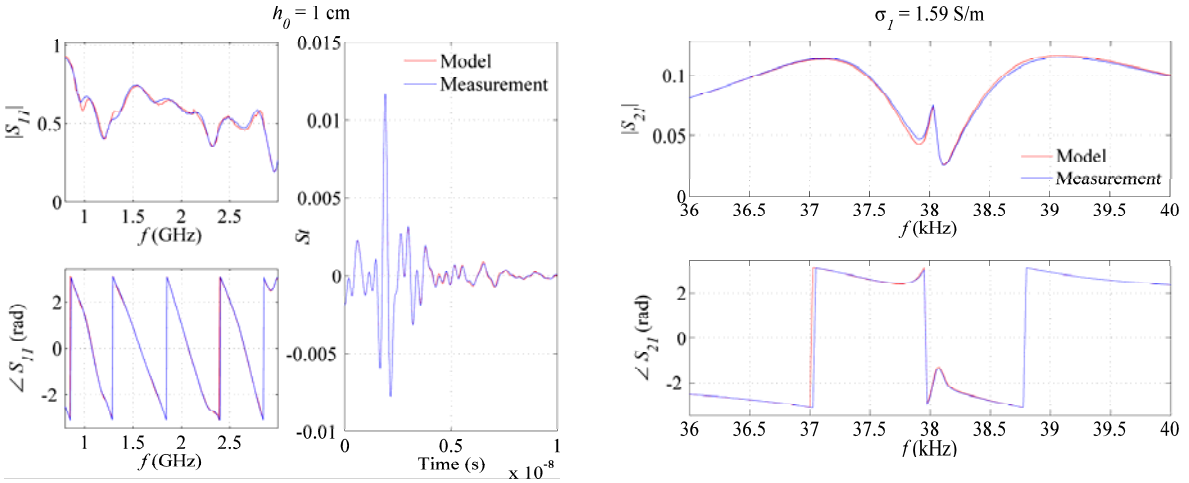

Figure 1. Modeled and measured data (a) in the frequency and time domains for GPR with a 0.01 m antenna height above the water surface (h_0) and with 0.208 S/m water electrical conductivity (σ_1) and (b) in the frequency domain for EMI with $\sigma_1 = 1.59$ S/m and for h_0 = 0.00 m

It is worth noting that, besides these laboratory experiments, the presented GPR setup and modeling procedure is already applied in field conditions, in particular for real-time mapping of soil water content as illustrated in Fig. 3. The lack of sensitivity of the

prototype EMI system to electrical conductivity levels comparable to those of soils (see Fig. 2(b)) impede its practical utilization, but future research will focus on the application of the same modeling procedure to commercial EMI sensors.

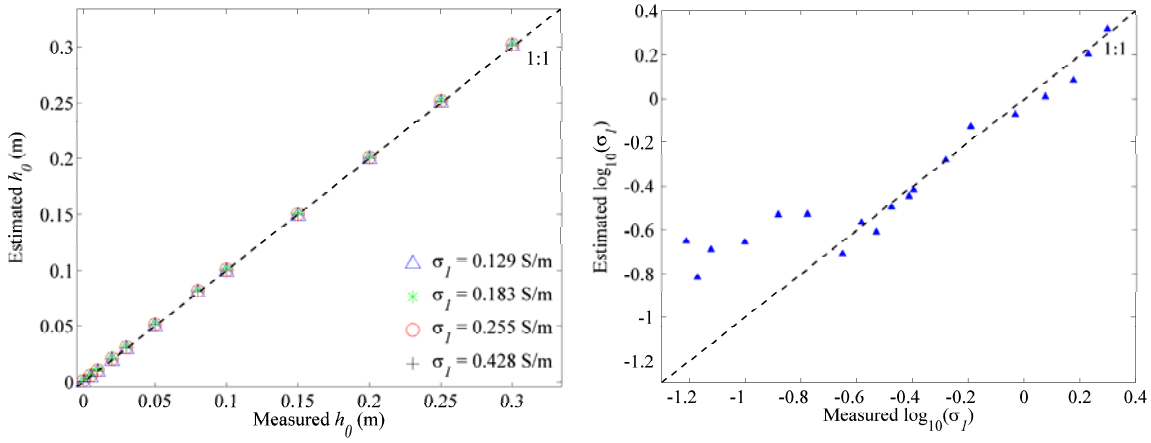

(a) (b)

Figure 2. Comparison between measured and inversely estimated (a) antenna height above the water surface (h_0) for GPR and (b) water electrical conductivity (σ_1) for EMI. The dashed lines are 1:1 lines.

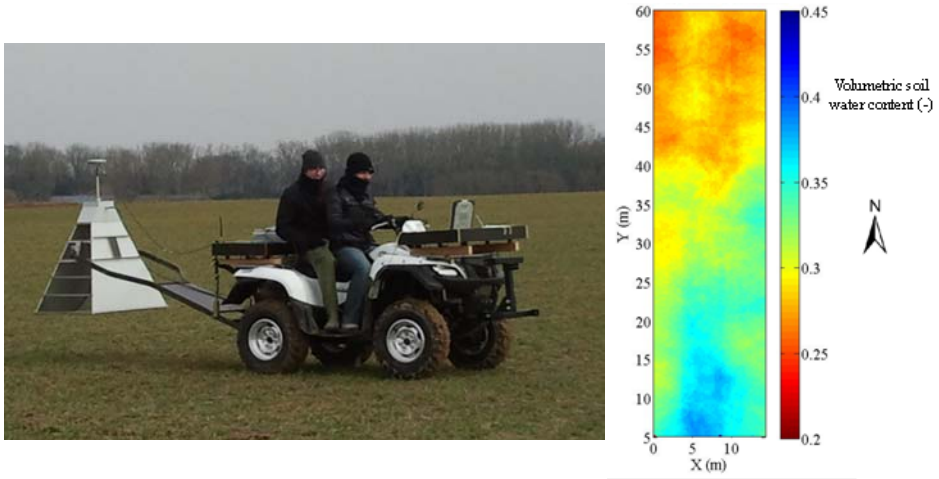

(a) (b)

Figure 3. (a) Mobile GPR platform for digital soil mapping and (b) map of volumetric soil water content determined from on-ground GPR measurements on an agricultural field (Bologna, Italy).

3.2 Data fusion

Fig. 4 shows the response surfaces of the considered objective functions for different parameter planes of the full objective function. The two first columns of the figure correspond to the individual EMI and GPR objective functions, while the third and the fourth columns present the combined objective functions according to the first (Equation (2)) and the second (Equation (3)) formulations, respectively.

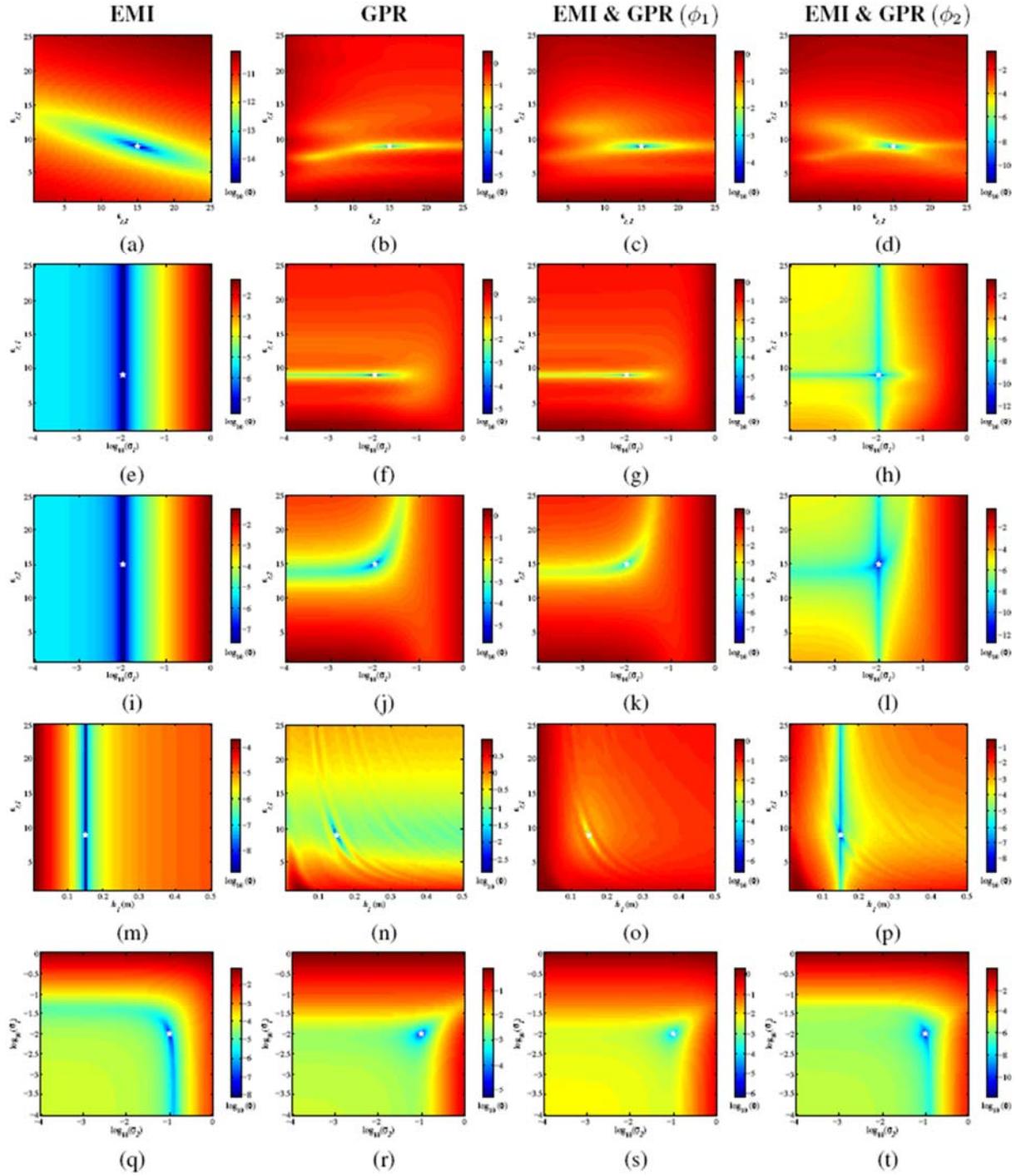

Figure 4. Response surfaces of the objective functions for the different investigated formulations, considering GPR and EMI separately and jointly, and for different parameter planes. The white star represents the true values of the parameters.

These figures clearly illustrate the complementary information content of the GPR and EMI data, with negligible sensitivities of EMI to layer dielectric permitivities ($\varepsilon_{r,1}, \varepsilon_{r,2}$) and high sensitivity to electrical conductivities (σ_1, σ_2) and first layer thickness (h_1), while GPR is mainly sensitive to dielectric permitivitties and to a lower extent to electrical conductivities. In addition, correlations appearing amongst parameters (e.g., σ_1 vs σ_2 for

EMI, $\varepsilon_{r,2}\ vs\ \sigma_1$ and $\varepsilon_{r,1}\ vs\ \mathrm{h}_1$ for GPR) further jeopardize accurate reconstruction of medium properties from individual EMI or GPR data. As observable in Fig. 4, EMI and GPR data fusion through the combination of the individual objective functions allows for a better definition of the global minimum and at least partially reduce the limitations arising from poor sensitivities and parameter correlations on the retrieval of the constitutive medium properties. Amongst the two considered strategies, the second formulation ($\emptyset_2$) appears to provide a better defined global minimum compared to the first formulation ($\emptyset_1$) for the $\varepsilon_{r,1} - \varepsilon_{r,2}$, $\varepsilon_{r,1} - \sigma_1$ and $\varepsilon_{r,2} - \sigma_1$ planes, while the opposite is observed for the $\varepsilon_{r,1} - \mathrm{h}_1$ and $\sigma_1 - \sigma_2$ planes. Further research is needed to deepen the analysis of these preliminary results in order to define an optimal formulation of the combined objective function. Also, methods resorting to naïve Bayesian data fusion should be considered (Bobaert & Fasbender, 2007).

Finally, comparing the near-field objectives functions of the present paper with those found by Moghadas et al (2010) for the far-field model with the same subsurface properties clearly shows the advantage of the near-field configuration compared to the far-field, the former allowing for improved parameter sensitivity especially for GPR but also, to a lesser extent, for EMI.

4 Conclusions

This study validated a new integrated modeling approach of near-field GPR and EMI data for reconstructing planar layered media, resorting to a planar field decomposition for accounting for all antenna effects and antenna-subsurface interactions using antenna characteristic functions. After calibration of the GPR and EMI antennas from measurements over known medium configurations, measurements above water subject to different salinity levels were used to successfully validate the approach. The model described GPR and EMI data with a very high accuracy and close correspondence was found between the medium constitutive properties retrieved from signal inversion and their measured values. Yet, discrepancies between inversely estimated and measured water electrical conductivity were observed for GPR as well as for the lowest salinity levels for EMI, as a result of a lack of sensitivity to this parameter in these particular cases.

Finally, the modeling approach being similar for both GPR and EMI, it is particularly convenient for fusion of data from both techniques. The combination of the individual GPR and EMI objective functions into a joint objective function was shown to generally improve the well-posedness of the inverse problem. However, as a result of the very different sensitivities of both techniques to the medium parameters, the way of combining their information is not straightforward and further research is needed for the definition of an optimal data fusion procedure.

Acknowledgments

This research was supported by the Fonds de la Recherche Scientifique (FNRS, Belgium) and the DIGISOIL project financed by the European Commission under the 7th Framework Programme for Research and Technological Development, Area "Environment", Activity 6.3 "Environmental Technologies".

References

ARDAKANI, M.K., WULFF, S.S. 2013. An Overview of Optimization Formulations for Multiresponse Surface Problems. Quality and Reliability Engineering International, **29**(1) 3-16.

ALVAREZ, Y., LAS-HERAS, F., PINO, M.R. 2007. Reconstruction of equivalent currents distribution over arbitrary three-dimensional surfaces based on integral equation algorithms. IEEE Transactions on Antennas and Propagation, **55**(12) 3460-3468.

BOGAERT, P., FASBENDER, D. 2007. Bayesian data fusion in a spatial prediction context: a general formulation. Stochastic Environmental Research and Risk Assessment, **21**(6) 695-709.

CRAEYE, C., GONZALEZ-OVEJERO, D., DARDENNE, X. 2009. Efficient numerical analysis of arrays of identical elements with complex shapes. Applied Computational Electromagnetics Society Journal, **24**(2) 224-232.

ILIC, M.M., DJORDJEVIC, M., ILIC, A.Z., NOTAROS, B.M. 2009. Higher order hybrid FEM-MoM technique for analysis of antennas and scatterers. IEEE Transactions on Antennas and Propagation, **57**(5) 1452-1460.

KLEIN, L., SWIFT, C. 1977. Improved model for dielectric-constant of sea-water at microwave-frequencies. IEEE Transactions on Antennas and Propagation, **25**(1) 104-111.

KOZLOVSKAYA, E., VECSEY, L., PLOMEROVÁ, J., RAITA, T. 2007. Joint inversion of multiple data types with the use of multiobjective optimization: problem formulation and application to the seismic anisotropy investigations. Geophysical Journal International, **171**(2) 761-779.

LAMBOT, S., SLOB, E.C., VAN DEN BOSCH, I., STOCKBROECKX, B., VANCLOOSTER, M. 2004. Modeling of ground-penetrating radar for accurate characterization of subsurface electric properties. IEEE Transactions on Geoscience and Remote Sensing, **42** 2555-2568.

LAMBOT, S., ANDRÉ, F. 2013. Full-wave modeling of near-field radar data to reconstruct planar layered media. IEEE Transactions on Geoscience and Remote Sensing *In press*.

MOGHADAS, D., ANDRÉ, F., SLOB, E.C., VEREECKEN, H., LAMBOT, S. 2010. Joint full-waveform analysis of off-ground zero-offset ground penetrating radar and electromagnetic induction synthetic data for estimating soil electrical properties. Geophysical Journal International, **182**(3) 1267-1278.

SORENSEN, J.A., GLASS, G.E. 1987. Ion and temperature dependence of electrical conductance for natural waters. Analytical Chemistry, **59**(13) 1594-1597.

STOGRYN, A. 1970. Brightness temperature of a vertically structured medium. Radio Science, **5**(12) 1397-1406.

WARREN, C., GIANNOPOULOS, A. 2011. Creating FDTD models of commercial GPR antennas using Taguchi's optimisation method. Geophysics, **76** G37.

Gamma-ray spectrometry and electromagnetic induction as complementary tools to map soil properties with a high spatial resolution

A. Rodionov, G. Angst, W. Amelung, S. Pätzold, G. Welp*

University of Bonn, Institute of Crop Science and Resource Conservation (INRES), Soil Science, Nussallee 13, 53115 Bonn, Germany
**E-mail: g.welp@uni-bonn.de*

Abstract

Electromagnetic induction (EMI) is widely used to describe the spatial variability of soil texture. Yet, the sensor signal can be strongly influenced by other parameters, especially soil moisture. We tried to elucidate, (i) whether an additional γ ray sensing might be useful to better classify or interpret EMI data, and (ii), whether both sensor signals may be used complementarily. Parallel measurements of EMI and γ radiation at 5 test sites revealed: (i) Spatial patterns of the sensor signals are similar, if soil moisture does not vary distinctly across the field; or: similar sensor patterns indicate textural variability. (ii) The degree of textural variability can be estimated for several depth intervals. Thus, given certain boundary conditions, EMI and γ spectrometry (γ-S) may be used as complementary tools to map soil properties with a high spatial resolution.

Keywords: Gamma-ray spectrometry, electromagnetic induction, on-the-go soil mapping.

1 Introduction and objectives

Gamma-ray spectrometry has been widely used for geological purposes (e.g., ore prospection) and environmental monitoring of radioactivity (IAEA, 2003). Meanwhile, technical progress allows us to quantify γ-radiation of soils on-the-go (Erbe et al., 2011). Main γ-emitters are ^{40}K and daughter nuclides of ^{238}U and ^{232}Th. Since these nuclides are associated with different soil forming materials, the varying concentration of the nuclides may be used as proxy for soil properties like contents of clay, potassium, and pedogenic Fe oxides (Wong & Harper, 1999). Electromagnetic induction (EMI, e.g. measured by on-the-go EM38 sensing) has been extensively used as proxy for soil texture, but also for salinity and soil moisture (Mertens et al., 2008).

Our intensive use of EM38 revealed that apparent electrical conductivity (ECa) is a suitable proxy for soil texture, layering, water holding capacity, and even for the patchy appearance of beet cyst nematodes, always provided that an adequate local calibration is included (Mertens et al., 2008; Pätzold et al., 2008; Hbirkou et al., 2011). Yet, ECa is also influenced by soil moisture and the EM38 signal integrates over a depth (about 7.5 or 15 dm) that goes beyond the main root zone. In contrast, γ signals represent the up-

permost 3–4 dm and are less influenced by soil moisture. So, both techniques reveal *different* pros and cons. Our hypothesis is that the combined use of γ-S and EMI may deliver additional information about the spatial heterogeneity of soil characteristics.

2 Materials and methods

The five field sites used in our study are arable soils from different regions in Germany. They reveal a high variability in bedrock (loess, trachyte tuff, terrace sediments, bunter sandstone, muschelkalk, molasse) and soil constituents. Moreover, the sites (2-10 ha) are characterized by a considerable within-field heterogeneity. The γ ray survey was carried out with a RSI-700 system (Radiation Solutions Inc., Canada), consisting of two thallium-doped NaI crystals (each 4.2 L). The activity of ^{40}K, ^{238}U and ^{232}Th was calculated via regions of interest (ROI). ECa was measured with the EM38 sensor (Geonics, Canada). Both the γ spectra and the ECa values were collected on transects spaced 8–10 m apart. The georeferenced data points were processed in ArcGIS 9.2 (ESRI, USA).

Parallel to the non-invasive sensing, soil samples were taken and analysed in the lab for ground truth data (soil moisture (gravimetric), texture (combines sieving and pipette method), pedogenic Fe oxides (DCB method)). Potential cation exchange capacity (CECpot) was calculated using an empirical equation (Ad-hoc-AG Boden, 2005): CECpot (cmolc kg^{-1}) = 0.5 clay content (%) + 0.05 silt content (%).

3 Results and discussion

3.1 Gamma radiation and soil characteristics

Unlike published data from Australia (e.g., Viscarra Rossel et al., 2007), we did not find significant correlations between the activity of ^{232}Th and the concentration of Fe oxides. This could be due to the rather low content and the low variability of Fe oxides in our soils.

Yet, partly very strong correlations were found for γ data and texture. Total γ counts as well as counts for ^{40}K, ^{238}U and ^{232}Th increased with increasing clay contents. These relations got closer in case of local calibrations, i.e., if the data were calculated separately for the different fields. In Table 1 the correlation coefficients for the test site “Scheyern” are listed.

With regard to ^{40}K as proxy for clay contents, our data approve earlier findings (e.g. Wong & Harper, 1999). Beyond that, this compilation reveals that ^{238}U and especially ^{232}Th even correlate closer with the contents of sand, silt, and clay and (texture based) CECpot. Thus, in our soils both ^{238}U and ^{232}Th exhibit a high affinity to minerals within the clay fraction (dominantly clay minerals, but also Fe and Mn oxides). The absence of γ radiation in the quartz dominated sand fraction leads to negative relations, which are

even stronger than those for clay. This is due to the higher variability of sand contents compared to clay.

Table 1. Correlation coefficients for the relations between γ radiation and texture data and CECpot at the test site “Scheyern” (only significant r values are listed)

	Total	^{40}K	^{238}U	^{232}Th
Sand	-0.91	-0.66	-0.90	-0.93
Silt	0.81	0.59	0.85	0.84
Clay	0.84	0.61	0.76	0.85
CECpot	0.88	0.64	0.80	0.89

3.2 Gamma radiation and EMI as complementary tools

At our study sites, γ radiation and EMI mostly exhibit similar spatial patterns. An example is given in Figure 1. Both sensor parameters, in turn, run parallel with patterns of texture and also with yield patterns of wheat, barley and maize (data not shown). This indicates that ECa and γ radiation at this field are governed by texture and suggests that ECa in this case is not disturbed by variations in soil moisture. Contrariwise, a neighboring field revealed distinct ECa patterns, but almost no variability in γ radiation (data not shown). Ground truth data corroborated our hypothesis that soil moisture was highly variable and texture (3 m loess) was very constant.

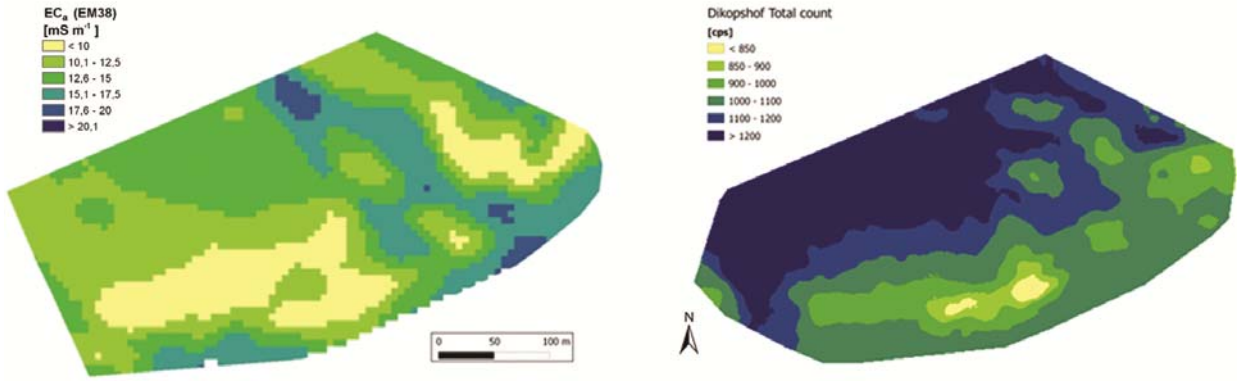

Figure 1. Spatial distribution of ECa (15 dm; above) and total γ counts (below) at the test site “Dikopshof”

The complementarity of EMI and γ radiation also arises from the different penetration depths of the signals (see above). Referring to the situation at our test site “Dikopshof” (Figure 1) we may conclude two aspects: (i) The textural spatial heterogeneity in the topsoil continues in the subsoil. (ii) The within-field variability of γ radiation is much lower than the variation of ECa. Thus, the non-invasive signals prove our finding from many classical soil surveys that the extent of spatial heterogeneity is less pronounced in the plough layer (γ-S) compared to 7.5 or 15 dm (EMI).

4 Conclusions

EMI and γ radiation sensors base on totally different physical and chemical mechanisms. Yet, given certain boundary conditions (esp. limited soil moisture variability), both sensor signals are proxies for soil texture and can be used complementarily. The combined use of both sensors allows to cover simultaneously the wide range from topsoil (γ-S, 3-4 dm) to subsoil (EMI; 7.5 and 15 dm in case of EM38). EMI, especially EM38, is much more used for soil survey than γ-S. The use of both techniques would reduce the uncertainties of EMI measurements and would add valuable information for the main root zone of crops.

Acknowledgements

The project was funded by the German Federal Ministry of Education and Research (BMBF) and the State Ministry of Innovation, Science, Research and Technology of North Rhine-Westphalia (Germany) as part of the CROP.SENSe.net network.

References

AD-HOC-AG BODEN, 2005. Bodenkundliche Kartieranleitung (Soil Survey Manual). Schweizerbart'sche Verlagsbuchhandlung, Hannover. 438 pp.

ERBE, P., SCHULER, U., STAHR, K., HERRMANN, L. 2011. Gammaspektrometrie – eine vielversprechende Methode zur Feldbestimmung und luftgestützten Erkundung von Böden (Gamma spectrometry – a promising method for proximal and remote sensing of soils). Tagungsbeitrag zur Jahrestagung der DGB, Berlin 2011. http://eprints.dbges.de/599/.

HBIRKOU, C., WELP, G., REHBEIN, K., HILLNHÜTTER, C., DAUB, M., OLIVER, M.A., PÄTZOLD, S. 2011. The effect of soil heterogeneity on the spatial distribution of *Heterodera schachtii* within sugar beet fields. Applied Soil Ecology 51, 25-34.

IAEA (INTERNATIONAL ATOMIC ENERGY AGENCY), 2003. Guidelines for radioelement mapping using gamma ray spectrometry data. IAEA, Vienna. 173 pp.

MERTENS, F.M., PÄTZOLD, S., WELP, G. 2008. Spatial heterogeneity of soil properties and its mapping with apparent electrical conductivity. J. Plant Nutr. Soil Sci. . 171, 2, 146-154.

PÄTZOLD, S., MERTENS, F.M., BORNEMANN, L., KOLECZEK, B., FRANKE, J., FEILHAUER, H., WELP, G. 2008. Soil heterogeneity at the field scale: a challenge for precision crop protection. Precis. Agric. 9, 367-390.

VISCARRA ROSSEL, R.A., TAYLOR, H.J., MCBRATNEY, A.B. 2007. Multivariate calibration of hyperspectral γ-ray energy spectra for proximal soil sensing. Eur. J. Soil Sci. 58, 343-353.

WONG, M.T.F., HARPER, R.J. 1999. Use of on-ground gamma-ray spectrometry to measure plant-available potassium and other topsoil attributes. Australian Journal of Soil Research 37, 267–277.

Soil sensing and yield improvement on marginal soils in Spain

F.M. van Egmond*, R.L. Koomans

Medusa Explorations BV, Verlengde Bremenweg 4, 9723 JV, Groningen, The Netherlands
**E-mail: fenny@medusa-online.com*

Abstract

Soil mapping provides information on the variation in physical characteristics of agricultural fields. For the EU Life+ project 'Crops for better soil' we developed a soil mapping tool consisting of a gamma spectrometer and GPR on a 4x4 car, which was able to map large and widespread areas fast and effectively. Without a direct translation to soil properties, the geophysical data serves as a first indication of the quality of the fields and proved to be an important base for communication between farmers and agronomists. The spatial information on local variation of soil properties provides a base for sound crop advise and selection of lands suitable for farming.

Keywords: Gamma spectrometry, GPR, Spain, soil properties, measurement campaign, communication.

1 Introduction

The vast threat of soil erosion and the urgency to increase soil productivity to create sustainable incomes is a major issue in the Mediterranean region. As an answer to this, several Spanish, German and Dutch companies started the EU Life+ project 'Crops for Better Soil' (www.traditional-crops.com). The project aims to demonstrate that using organic farming techniques, crop rotation and the re-introduction of traditional crops improves the soil and increases yields of 400 hectares of marginal Spanish soils in a 5 year time span. Soil sensing techniques are used to provide detailed information on soil properties and to monitor improvement of the soils.

These 400 hectares are selected within 4 regions in Spain: Castilla la Mancha, Castilla y León, Aragón and Navarra. The first three are referred to as Guadalajara, Zamora and Zaragoza (figure 1). The regions and fields contain a range of different parent materials and geology thus presenting a representative subset of rainfed Spanish soils. Soils or fields are defined as marginal when they are rainfed, managed extensively and are often not or hardly profitable without subsidies. The size of the fields varies from over 25 hectares to less than 1 hectare. There are on average 6 farmers per region and farmers may have one or more fields in the project. One agronomist advises the farmers on the possibilities of traditional crops and organic management of the fields for each region.

The change to organic farming, the crop rotation and the use of crops that do not yet have a large market share, causes a lower income for the farmer during the first few years before the benefits of such an approach start to show in the yields. Therefore, a seed trading company buys the yields of the farmers each year to guarantee their income.

2 Objectives

The objective of the soil sensing techniques is to gather soil data that provides detailed and targeted information on the textural composition, structure and density of the soil. Because of the large variation in parent materials and soils, the differences between fields and the differences within fields are highly relevant. At present the mechanisation (eg. GPS aided variable rate application) is not available to the farmers for automated precision agriculture. However, the information will assist the agronomists and farmers in determining the suitability of the soil for certain selected (traditional) crops and in designing the crop rotation scheme. This will be primarily per field but may in some circumstances result in a within-field differentiation.

Figure 1. Project fields in four regions in the central part of Spain. (source: Bing Aerial)

Moreover, the measurements aim to provide information on the improvement of soil fertility and structure and decrease of erosion in 5 years time.

The systems used have regularly been applied on large flat fields in the Netherlands (van de Klooster et al. (2011), van Egmond et al. (2010)). However, the stony Spanish soils provide completely different circumstances and most of the fields are small and are distributed over a wide area. To that end, the tools have been re-engineered for this project.

3 Materials and methods

The sensors employed were a MS-4000, 4 L CsI gamma spectrometer with full spectrum data analysis (FSA) (Hendriks et al., 2001), a 750 MHz air-coupled GPR and GPS on a 4x4 vehicle. The gamma spectrometer was mounted in a rugged steel casing in front of the car. The GPS was positioned on the roof and the GPR was towed on a custom-made cart behind the car. The system was powered by the car-engine and data was logged on a rugged field computer. Fields were scanned at 10 km/h in 5-15 m interval lines depending on apparent variation in geomorphology and gamma radiation. Soil samples of 0-20 cm depth were taken per 5 hectares. These were analysed on the concentration of radionuclides and on physical and chemical soil properties in the lab.

Figure 2. Measurement setup with a gamma spectrometer in front of the vehicle and GPR behind in a carriage the vehicle

4 Results

The designed hardware system operated well under the stony Spanish circumstances. Built-up time was small (5 minutes) which increased the number of hectares and fields that could be scanned per day. The topsoil stoniness caused a decreased GPR reflection of the soil below, which proved visual interpretation of the GPR data difficult. Depth slices of GPR reflection, however, show clear patterns that are now verified in discussions with the farmers involved.

The results of the gamma spectrometer aim to deliver quantified properties of the soil such as clay content, stoniness and potentially soil quality. Correlations between soil lab data and lab data on radionuclide concentrations still have to be performed.

During the measurement campaign and in discussions with farmers the sensor data proved to be a good communication tool between farmers, agronomists and geophysicists. The data, in combination with regional knowledge, provided a good aid for differentiation in soil quality and suitability for various crops. In these discussions it was very helpful that the gamma-ray count rate data could be viewed real time during measurements. Many farmers recognised zones of good and poor production on-the-go. This increased their awareness that sensor data provide useful information for farming. The knowledge of the farmers on organic farming and different crops is quite variable. Part of the aim of the project is to educate and aid farmers in applying organic farming and using different crops. Apart from maps of physical soil properties, additional maps will be made that assess the overall quality of the soil. These maps can be a useful tool for designing crop rotation schemes and for determining soil suitability for certain crops as well as for discussing ecological farming possibilities with the farmers. The data will therefore be used for educational as well as advisory purposes.

5 Example

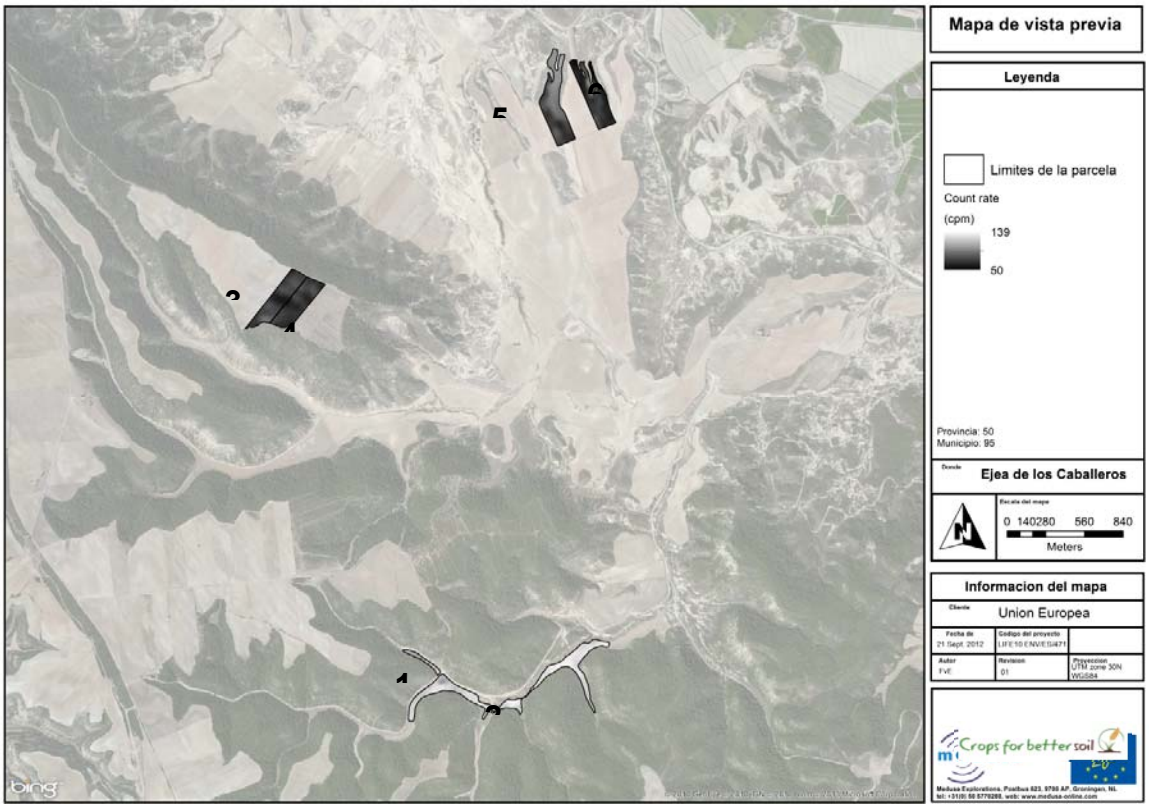

Figure 3. Count rate (cpm) of 6 fields near Ejea de los Caballeros, Aragón, Spain.

Figure 3 shows the count rate maps of 6 fields of one farmer near Ejea de los Caballeros in Aragón. The differences between the fields are apparent. The southern fields (1, 2) are situated in a valley and have a much higher clay percentage, contain

less stones, have a large rooting depth, and give a higher yield in moderate years. The 4 northern fields (3-6) are situated on flat hilltops (small mesetas). and have a lower clay percentage, a slightly higher sand percentage and a much higher stoniness than the southern fields. The top soil layer of the northern fields consists mostly of stones with some soil. In wet years these soils have better yields because of their good drainage properties. In dry years yields may be non-existent.

Within most fields differences in count rate can be observed. This is most apparent in field 5. The northern part lies in a valley that consists of a different geological clay-rich layer. In discussions with the agronomist it was apparent that the choice of crops for fields 3-6 can be grouped and differs from what would be suitable for fields 1 and 2. Because of the large difference in properties within field 5, it is qualified as less suitable for every year farming.

The local knowledge on differences in soil properties is partly known by the farmers, but visualisation of this data helps the farmers and agronomists to make decisions on semi-quantitative grounds.

6 Conclusions

Within the EU Life+ project `Crops for better soil´ Medusa Explorations has used a flexible, fast and robust sensor platform containing a GPR and a gamma spectrometer to measure the physical soil properties of 400 hectares of marginal Spanish soils. The designed sensor platform and sensors performed well. Gamma-ray data provided a fast and effective insight in the quality of the soil and proved to be a good quantitative communication tool for discussion with the farmers. An important aim of the project is to educate and aid farmers in applying organic farming and using different crops. The maps of geophysical data proved to be a useful semi-quantitative result to assist in the process of communication.

Acknowledgements

This project is co-financed by the European Union Life+ program and is part of LIFE10 ENV/ES/471 Crops for Better Soil.

References

HENDRIKS, P.H.G.M., J. LIMBURG, R.J. DE MEIJER. 2001. Full-spectrum analysis of natural ɣ-ray spectra. Journal of Environmental Radioactivity, 53, pp 365-380.

VAN DER KLOOSTER, E., F.M. VAN EGMOND, M.P.W. SONNEVELD. 2011. Mapping soil clay contents in Dutch marine districts using gamma-ray spectrometry. European Journal of Soil Science, 62-5 (pp 657-764).

VAN EGMOND, F.M., E.H. LOONSTRA, J. LIMBURG. 2010. Gamma-ray sensor for topsoil mapping; the mole. In: Proximal Soil Sensing (eds. R.A. Viscarra Rossel, A. McBratney & B. Minasny), pp. 323-332. Springer, Dordrecht.

Simultaneous measurement of soil electrical resistivity and gamma activity of different sites in Germany

J. Rühlmann[1*], E. Lück[2]

[1]*Leibniz-Institute of Vegetable and Ornamental Crops, D-14979 Großbeeren, Germany*
[2]*University of Potsdam, Germany, Karl-Liebknecht-Str. 24, D-14476 Golm/Potsdam, Germany*
[*]*E-Mail: ruehlmann@igzev.de*

Abstract

Mobile measuring soil electrical resistivity represents a very powerful tool to get detailed information about the spatial heterogeneity of physical soil properties. However, soil electrical resistivity is affected by diverse factors and it is impossible to quantify their specific contribution to the resistivity value measured at a time. Therefore, multi-sensor approaches are required to solve this problem.

During a ten years period, the GEOPHILUS soil mapping system was developed within a collaboration of the IGZ and the UP. The GEOPHILUS system measures the soil's electrical resistivity using i) a modular system of five equatorial dipole-dipole arrays (six pairs of galvanic coupling electrodes, 1 transmitter dipole and 5 receiver dipoles) and ii) a resistivity measurement instrument. The electrodes design allow to measure at five depth levels up to 1.5 meters soil depth. The system records about once per second complex resistivity (amplitude and phase) simultaneously for four frequencies within a frequency range between 1 mHz and 1 kHz. Detailed information to the GEOPHILUS system are given by Lueck & Ruehlmann (2012). Recently, the GEOPHILUS system was extended by a gamma ray detector which consists of polysterene. Contrasting to most gamma ray detectors applied for geophysical purposes, it measures only the total count and is not able to provide spectral information. However, this sensor is very useful to measure "on the go" with velocities up to 15 kmh-1 according to its large volume of about 10 liters.

The combination of the GEOPHILUS system and the gamma detector was applied qualitatively to test their relative sensitivity towards differences in

- the soil type and mineral composition
- soil physical properties as moisture and bulk density
- soil P and K contents according to different long-term fertilization strategies.

The tests were performed i) on a site characterized by a transitional area between lowland fen - half bog - sandy soil and ii) on two loess sites; on one of them, the loess cover is associated with weathered bedrock material consisting of calcareous sandstone.

Generally, the resistivity measurement was more sensitive towards differences in soil moisture and density whereas the gamma sensor reflected especially geological effects.

Regarding soil moisture differences, the sensitivity of electrical resistivity measurement seems to have another order of magnitude compared to the gamma measurement.

References

E. LUECK, J. RUEHLMANN. 2012. Resistivity mapping with GEOPHILUS ELECTRICUS - Information about lateral and vertical soil heterogeneity. Geoderma, http://dx.doi.org/10.1016/j.geoderma.2012.11.009

Posters

Local scale application of soil proximal sensing to study degraded soils: portable spectroscopy analyses for soil quality assessment and monitoring in a contaminated site of Apulia

V. Ancona[1*], R. Salvatori[2], R. Salzano[2], A. Calabrese[1], V. F. Uricchio[1]

[1]*IRSA-CNR, Viale F. De Blasio 5, 70132 Bari, Italy*
[2]*IIA-CNR, via Salaria km 29,300 Monterotondo, Italy*
[*]*E-mail: valeria.ancona@ba.irsa.cnr.it*

Abstract

In recent years land degradation processes have drastically increased in their extent and intensity. Consequently, opportune mitigation strategies have been taken in order to evaluate and reduce the major threats that have already damaged the soil resource. A detailed and deep knowledge of the degraded soils properties can play a key role in understanding land degradation processes and also in assessing as much as soil quality has been compromised. A non-destructive and reproducible method for soil surveys is portable spectroscopy, which is able to collect spectral data in situ to monitor soil structure and composition.

In this work we used a portable spectroradiometer (ASD-FieldSpec) to investigate soil properties in a contaminated site of Apulia Region with the aim to collect spectral information useful to study soil quality attributes. Among these, we have chosen soil organic carbon content as one of the indicators of soil quality.

Statistical analysis have been conducted to test a prediction model of soil organic matter based on reflectance by simply using an inexpensive portable spectrometer operating between 400-2500 nm.

Keywords: land degradation processes, portable spectroscopy, soil organic matter.

1 Introduction

The European strategy for soil protection (COM, 2006) has indicated that one of the most relevant land degradation processes is soil contamination. In recent years this phenomenon has been widely spread on European territory cause of the industrial activities raise which threats quality of the soil and water resources. In Apulia, one of the regions located in South Italy, several pollution phenomena have been discovered in Taranto province where an important industrial district (ILVA) was active for thirty years. In

order to understand soil contamination processes and to prevent environmental damages is necessary developing efficient systems for soil assessment and monitoring. Visible-Near infrared reflectance spectroscopy is a rapid, non-destructive, reproducible and cost-effective analytical method able to measure intrinsic optical properties of the soil in the range of electromagnetic spectrum between 400-2500 nm (Ben-Dor et al, 1999; Viscarra Rossel et al., 2006). Field and laboratory experiments have shown that wavelength absorption of electromagnetic radiation in the Vis-NIR provides diagnostic reflectance spectra for the chemical, physical and mineralogical composition of the soil (Obukhov & Orlov, 1964; Bowers & Hanks, 1965; Baumgardner et al., 1985; Ben Dor & Banin, 1995; Viscarra rossel & McBratney, 1998b). Vis-NIR spectral reflectance can be used to characterize spatial and temporal variations in the soil constituents (Brown et al., 2006; Viscarra Rossel et al., 2006) and potentially its surface structure (Chappell et al., 2006, 2007; Sellitto et al., 2008), therefore it can be a useful method to study soils affected by land degradation process. In this work we realized ground-based (in situ) and laboratory measurements with a portable rapid-acquisition spectroradiometer (ASD-FieldSpec) to investigate soil properties in a contaminated site localized in Taranto with the aim to collect spectral information useful to study soil quality attributes. The spectral analysis has been focused on investigating the soil organic carbon content, thus soil organic matter (SOM) is one of the main indicators of soil quality. Udelhoven et al. (2003) have been used ASD FieldSpec to assess the potential of determining SOM and other soil properties at pilot and landscape scales.

SOM and $CaCO_3$ predictions, from field and laboratory spectral measurements have been tested in order to calibrate these two parameters based on reflectance by simply using a portable spectrometer operating between 400-2500 nm.

2 Materials and methods

Topsoil (0-20cm) samples have been collected from an Apulia site, located near Taranto, contaminated by organic compounds (PCBs) and inorganic elements. The study site (fig 1) has been divided in two sectors considering the land-use: sector A is characterized by a more developed soil profile where spills occurred; sector B shows poor soils covered by hazardous wastes. Soils have been sampled, creating two separate data sets, in order to show possible spatial variability in contamination and soil organic matter evaluation.

Soil samples have been characterized determining: texture, pH, organic carbon, total nitrogen, available phosphorous, organic and inorganic contaminants.

Soil reflectance have been acquired by using a portable FieldSpec 3 spectroradiometer (ASD) on field and in a darkroom under controlled conditions (sieved and dried samples). Reflectance measurements have been referred to a lambertian reflector (Spectralon) and spectra were pre-treated using Savitzky-Golay smoothing filter. Vis-NIR data

have been analysed with chemometric tools such as the ChemometricsWithR package (Wehrens, 2011) available in R programming language. The partial least-square regression method has been used in order to find a relation between the two considered variables (SOM and $CaCO_3$ contents) and the Vis-NIR spectra. The performance of the obtained predicting model has been determined using the Leave-One-Out cross validation and the selection of the best number of components has been performed finding the lowest root mean-squared error (RMSE).

3 Results

The available chemical and physical information on the sampled soils have confirmed the discrimination between the two sectors (A and B) individuated in the study site, from a land-use point of view. Soil organic matter in the first data set (A) has showed a low variability (SOM ranges between 24-30%), while in the second one (B), soil samples show a larger range of content (12-37%). Also the values of nitrogen and available phosphorous concentrations of the soils of data set “B” are lower than those of data set “A”. The carbonate content ($CaCO_3$) is a marker of the bedrock where these soil are imposed and the resulting measurements present a different behaviour compared to SOM. The two data set are completely overlapped and they can be described as a unique population of data.

The determination of organic pollutants have evidenced the presence of polychlorinated biphenyl (PCBs) compounds dominantly in the sector A, while trace elements have outlined anomalous Zn and V values in sector B.

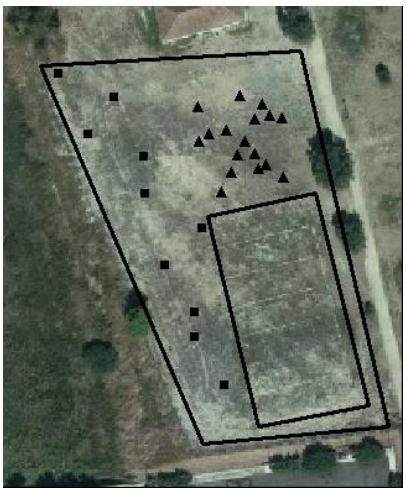

Figure 1. Site of investigation (1:600): in the polygon largest are shown soil samples of data set “A” (triangle) and soil samples of data set “B” (square symbols).

Two models one for SOM% and one for $CaCO_3$ were calibrated by means of PLS regression and their predictions were compared considering the coefficient of determination (R^2) and the RMSE. Plot on the left of figure 2 relates the measured vs.

predicted SOM content (%) in the case of the 5-components model for the two data sets investigated. As may be observed, the points referred to sampling zone “A” are concentrated in a restricted cloud of values, while for the points of sampling zone “B” are more heavily dispersed on both sides of the first bisector. Plot shown on the right of figure 2 relates the measured vs. predicted $CaCO_3$ content (%) in the case of the 3-components model for both data sets (A and B). For the sampling zone “A” the model validation led to predictions with R^2=0,75 and RPD=1.9.

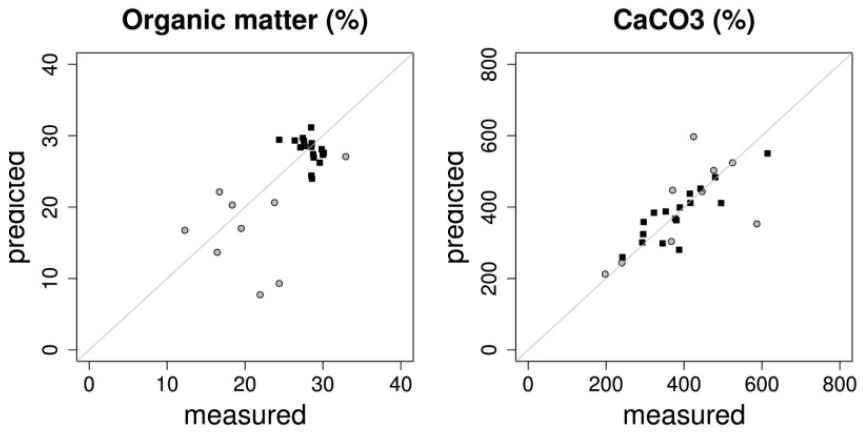

Figure 2. Measured vs. predicted SOM % (left plot) and measured vs. predicted $CaCO_3$ % (right plot). Dark symbols referred to data set “A” while grey symbols referred to data set “B”.

4 Conclusion

The prediction of soil organic matter by means of PLSR for the two sampling zones of the investigated site are not satisfactory, probably due to the different chemical pollution of these sub sites. The organic pollutants are widely present in sampling zone “A” while high concentrations of metals were major observed in the sampling zone “B”. These preliminary results have evidenced a separation in terms of SOM between observations detected on sector A and B, but a different behaviour has been identified for the carbonate content. The two predictions of carbonate content are, in fact, overlapped and PLSR gave interesting results especially for the sampling zone “A”. These results, coherently to chemical analyses, indicate that the two sub sites are characterized by different spectral behaviour and that Vis-NIR spectroscopy can support the estimation of soil quality where contamination is associated to human activities (sector A) or to waste disposal areas (sector B).

The portable spectroscopy application tested in this work proved to be an efficient and rapid method to acquire useful information for soil properties characterization and also to collect data for assessing and monitoring soil quality when contamination processes occur. Further studies are necessary to understand how to discriminate the information related to toxic organic compounds and to develop models able to predict soil properties in contaminated sites.

Acknowledgments

Authors want to thank Padre Nicola Preziuso, Pasquale Carmignano, Michele Arcangelo D'alessandro and Vito Nicola Palmisano for the useful technical support provided during field acquisition.

References

BAUMGARDNER, M.F., SILVA, L.F., BIEHL, L.L., STONER, E.R. 1985. Reflectance properties of soils. Advances in Agronomy 38, 1-44.

BEN DOR, E., BANIN, A. 1995. Near-infrared analysis as a rapid method to simultaneously evaluate several soil properties. Soil Science Society of America Journal 59, 364-372.

BEN-DOR, E., IRONS, J.R., EPEMA G. 1999. Soil reflectance. In: Remote sensing for the Earth Science, Volume 3 (ed A.N. Rencz), pp. 111-1888. John Wiley & Sons, New York.

BOWERS, S.A., HANKS, R.J. 1965. Reflection of radiant energy from soils. Soil Science 100, 130-138.

BROWN, D.J., SHEPERD, K.D., WALSH, M.G., DEWAYNE MAYS, M., REINSCH, T.G. 2006. Global soil characterization with VNIR diffuse reflectance spectroscopy. Geoderma 132, 273-290.

CHAPPELL, A., ZOBECK, T.M., BRUNNER, G. 2006. Using bi-directional soil spectral reflectance to model soil surface changes induced by rainfall and wind-tunnel abrasion. Remote Sensing of Environment, 102, 328-343.

CHAPPELL, A., STRONG, C., MCTANISH, G., LEYS, J. 2007. Detecting induced in situ erodibility of a dust-producing playa in Australia using a bi-directional soil spectral reflectance model. Remote Sensing of Environment 106, 508-524.

COM. 2006. Communication from the Commission to the Council, The European Parliament, the European economic and Social Committee and the Committee of the regions. Thematic Strategy of Soil Protection.

OBUKHOV, A.I., ORLOV, D.C. 1964. Spectral reflectance of the major soil groups and the possibility of using diffuse reflectance in soil investigations. Soviet Soil Science 2, 174-184.

SELLITTO, V.M., BARRÓN, V., PALUMBO, G., SALZANO R., COLOMBO, C. 2008. Uso della spettrometria di riflettanza diffusa (DRS) e bi-direzionale (BRF) per lo studio dei suoli vulcanici europei. Rivista italiana di Telerilevamento 40 (1): 21 – 34.

UDELHOVEN, T, EMMERLING, C., JARMER, T. 2003. Quantitative analysis of soil chemical properties with diffuse reflectance spectrometry and partial least-square regression: a feasibility study. Plant and Soil 251 (2), 319-329.

VISCARRA ROSSEL, R.A., MCBRATNEY, A.B. 1998B. Laboratory evaluation of a proximal sensing technique for simultaneous measurement of clay and water content. Geoderma 85, 19-39.

VISCARRA ROSSEL, R.A., WALVOORT, D.J.J., MCBRATNEY, A.B., JANIK, L.J., SKJEMSTAD, J.O. 2006. Visible, near-infrared, mid-infrared or combined diffuse reflectance spectroscopy for simultaneous assessment of various soil properties. Geoderma 131, 59-75.

WEHRENS, R. 2011. Chemometrics with R - Multivariate Data Analysis in the Natural Sciences and Life Sciences. Springer.

Using Reflectance Spectroscopy for the assessment of soil potentially toxic elements (PTEs) in agricultural soils: an application in southern Italy

G. Buttafuoco*, I. Guagliardi, L. Bastone, N. Ricca, M. Conforti

Institute for Agricultural and Forest Systems in the Mediterranean, National Research Council of Italy, Via Cavour 4-6, 87036, Rende CS, Italy

**E-mail: gabriele.buttafuoco@cnr.it*

Abstract

Assessing soil potentially toxic elements (PTEs) contamination is an important objective, as high levels of some trace elements may be ecotoxicologically relevant and harmful when passing the food chain. This study focused on agricultural soil in southern Italy. The study examined the feasibility of predicting some PTEs concentration in soil samples using reflectance spectroscopy. Partial least squares regression was used to establish the relationship between reflectance spectra in the visible-near-infrared (Vis-NIR) region and PTEs. Among the PTEs analysed, only for Pb and V have been obtained successful results.

Keywords: potentially toxic elements (PTEs), visible-near infrared spectroscopy, PLSR.

1 Introduction

Soil monitoring for food safety and for general environmental control requires soil sampling and chemical analyses for determining the concentration of potentially toxic elements (PTEs). High concentrations of PTEs in soil pose a threat for human health because they can be taken up into the trophic chain via assimilation by plants. Reflectance spectroscopy within the visible-near infrared (Vis-NIR) region has been widely used to predict spectrally soil properties quantitatively (Ben-Dor et al., 1999; Brown et al., 2006; Viscarra Rossel et al., 2006). Compared to conventional laboratory analysis, Vis-NIR spectroscopy techniques are rapid, relatively inexpensive, require minimal sample preparation, are non-destructive, require no hazardous chemicals and several soil properties can be measured from a single scan. Quantification and relationships between spectral reflectance and soil properties, such as soil organic matter content, iron oxides, calcium carbonate content, soil heavy-metal (Cu, Pb, and Zn), etc. have been established in many studies by means of statistical models (Kemper and Sommer, 2002; Viscarra Rossel et al., 2006). The main aim of this study was to examine the feasibility of predicting some PTEs concentration in soil samples using reflectance spectroscopy.

2 Materials and methods

The experimental area (100 m x 100 m) was an olive orchard located in southern Italy (Calabria) where, at 100 locations, topsoil (0-0.20 m) samples were collected (Figure 1). Soil samples were ground, dried, weighed, sieved (<2 mm), and then split into two subsamples: one was used for spectroscopic measurements, while the other for conventional laboratory analysis. The samples for conventional laboratory analysis were digested in aqua regia and analyzed for cadmium (Cd), chromium (Cr), copper (Cu), lead (Pb), thallium (Tl), vanadium (V), and zinc (Zn) content using Inductively Coupled Plasma Mass Spectrometry (ICP-MS).

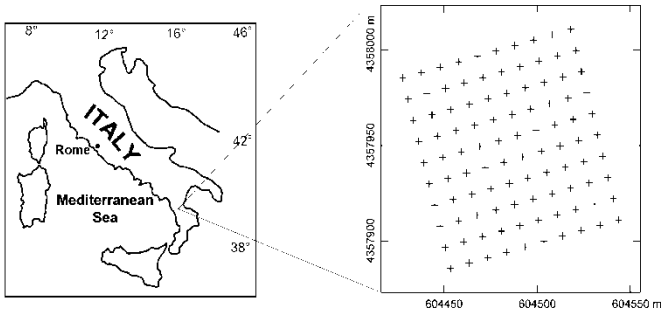

Figure 1. Study area and sampling point (black cross) locations.

To minimize the noise level, every measurement was recorded as the average of four consecutively acquired spectra. Finally, conversion to spectral reflectance was performed by means of dividing the radiance of spectra of the samples by the radiance spectrum of the standard white reference. Prior to statistical analysis, the spectral reflectance curves were re-sampled at 10 nm interval, reducing the number of wavelength from 2151 to 216, which smoothed the spectra and reduced the problem of over-fitting (Kemper and Sommer, 2002). Partial Least Squares Regression (PLSR) analysis (Geladi and Kowalski, 1986) was applied to establish the relationships between spectral reflectance and measured soil PTEs. In this study, leave-one-out cross-validation (Efron and Tibshirani 1994) was used to determine the number of factors to be retained in the calibration models. 30 bilinear factors (latent variables) were tested. The prediction performance was evaluated on predicted and measured tracer values, using the adjusted coefficient of determination (R^2_{adj}) and the root mean square error (RMSE) of cross-validation. RMSE of predictions was used to select the optimal cross-validated calibration model. In addition, to evaluate the performance of prediction models, the residual predictive deviation (RPD) was used. RPD is defined as the ratio of standard deviation of measured values of the soil properties to the RMSE (Williams, 2001).

PLSR analysis was performed using the PArLeS vs3.1 software developed by Viscarra Rossel (2008). Finally, using Ordinary Kriging (Webster and Oliver, 2007), the values of the spectrally predicted PTEs were interpolated and mapped.

3 Results and discussion

Descriptive statistics of the PTEs data are summarised in Table 1, which shows that zinc is the most abundant PTE (mean content 83.30 mg kg^{-1}), while cadmium is the less abundant (mean content 0.40 mg kg^{-1}). The PTEs concentrations are less than the ones for urban and peri-urban soils, but there are no PTEs data for agricultural soils in the in the neighbourhood of the study area. Table 2 reports the results of the PLSR: the latent factors in the PLSR models used for prediction ranged from 4 to 17. Results of the level of agreement between measured and predicted values show that better results have been obtained for Pb ($R^2_{adj} = 0.74$; RMSE=1.86; RPD=2.0) and V ($R^2_{adj} = 0.69$; RMSE=5.27; RPD=2.0). Estimates of moderate quality of the prediction models have been obtained for Cr and Tl with R^2_{adj} of 0.64 and 0.62, respectively. The remaining elements (Cu, Cd and Zn) have been poorly predicted (Table 2); therefore, these results can be considered to be generally used for an approximate screening.

Table 1. Basic statistics of PTEs concentrations (mg kg^{-1} dry weight).

PTE	Min	Max	Mean	Median	S. D.	CV	Skewness	Kurtosis
Cd	0.08	0.40	0.18	0.17	0.07	0.38	0.83	3.33
Cr	20.79	103.90	39.68	37.88	10.22	0.26	2.60	16.60
Cu	9.60	33.37	19.31	18.98	3.88	0.20	0.87	4.56
Pb	0.22	21.19	13.06	12.51	3.83	0.29	0.11	3.01
Tl	0.18	16.85	0.62	0.33	1.69	2.74	8.93	84.84
V	27.44	91.81	51.34	49.46	10.21	0.20	0.86	4.64
Zn	33.46	172.36	83.30	77.52	25.58	0.31	1.42	5.48

S.D. Standard deviation; CV Coefficient of variation

Table 2. Results of PLSR spectral analysis. NF: number of factors; R^2_{adj} : coefficient of determination; RMSE: root mean square error; RPD: residual predictive deviation.

PTE	NF	R^2_{adj}	RMSE	RPD
Pb	8	0.74	1.86	2.0
V	7	0.69	5.27	2.0
Cr	4	0.64	4.81	1.7
Ti	6	0.62	92.21	1.8
Cu	10	0.57	2.57	1.5
Cd	5	0.45	0.05	1.4
Zn	17	0.44	19.97	1.3

Among the PTEs only the predicted values of Pb and V, which have obtained the better results, have been interpolated and mapped. In the variographic analysis, in order to check the behaviour of Pb and V data in terms of anisotropy, two variogram maps (not shown) were calculated revealing no significant difference as a function of direction for V and an anisotropic behaviour for Pb. Then, a bounded isotropic variogram model was assumed for V and the variogram fitted to the experimental values of semivariance, included a nugget effect [sill=12 (mg kg^{-1})^2] and an spherical model (Webster and Oliver, 2007) with a range of about 74 m and a sill equal to 81 (mg kg^{-1})^2. For Pb, the fitted variogram in the direction N75E included a nugget effect [sill=1 (mg kg^{-1})^2]) and a K-Bessel model (Webster and Oliver, 2007) with a range of about 25 m and a sill of 16 (mg kg^{-1})^2, while in the direction N165E the fitted variogram included a cubic model with a range of about 80 m and a sill equal to 4.34 (mg kg^{-1})^2. The above variogram models were used with ordinary kriging to produce the maps of spectrally predicted Pb and V.

4 Conclusions

The study allowed to examine the feasibility of predicting some PTEs concentration in soil samples using reflectance spectroscopy. Only for Pb and V have been obtained successful results. The difficulty in predicting spectrally PTEs could be due to the fact that pure PTEs do not exhibit characteristic absorption in the Vis-NIR region and that they are detected indirectly taking into account the binding reaction of the PTEs onto the mineral surface. The study was the first step to in-field spectroscopy for PTEs.

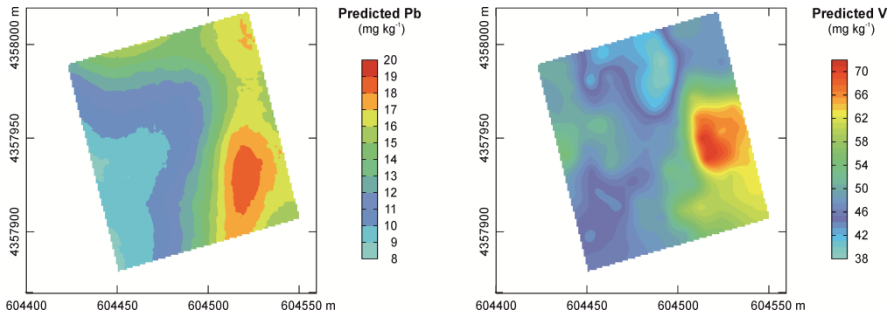

Figure 2. Maps of spectrally predicted Pb and V obtained using ordinary kriging.

Acknowledgements

This project was funded by the ACTION 2 - Public research laboratory mission oriented, APQ – Scientific Research and Technological Innovation in Calabria Region. Laboratory for Food Quality, Safety and Origin (QUASIORA).

References

BEN-DOR, E., IRONS, J.R., EPEMA, G.F. 1999. Soil reflectance. In: Rencz, A.N. (Ed.), Remote Sensing for the Earth Sciences. Manual of Remote sensing, vol. 3. Wiley & Sons, New York, pp. 111–188.

BROWN, D.J., SHEPHERD, K.D., WALSH, M.G., DEWAYNE MAYS, M., REINSCH, T.G. 2006. Global soil characterization with VNIR diffuse reflectance spectroscopy. Geoderma 132, 273–290.

EFRON, B., TIBSHIRANI, R. 1994. An introduction to the bootstrap. Monographs on statistics and applied probability. Vol. 57, Chapman and Hall, London, UK, 436pp.

GELADI, P., KOWALSKI, B.R. 1986. Partial Least-Squares regression: a tutorial. Analytica Chimica Acta 185, 1-17.

KEMPER, T., SOMMER, S. 2002. Estimate of heavy metal contamination in soils after a mining accident using reflectance spectroscopy. Environmental Science & Technology 36, 2742–2747.

VISCARRA ROSSEL, R.A., WALVOORT, D.J.J., MCBRATNEY, A.B., JANIK, L.J., SKJEMSTAD, J.O. 2006. Visible, near infrared, mid infrared or combined diffuse reflectance spectroscopy for simultaneous assessment of various soil properties. Geoderma 131, 59–75.

VISCARRA ROSSEL, R.A. 2008. ParLeS: Software for chemometric analysis of spectroscopic data. Chemometrics and Intelligent Laboratory Systems 90, 72-83.

WEBSTER, R., OLIVER, M. A. 2007. Geostatistics for environmental scientists. Wiley, Chichester, UK.

WILLIAMS, P.C. 2001. Implementation of near-infrared technology. In: Williams, P.C., Norris, K. (Eds.). Near-Infrared Technology in the Agricultural and Food Industries, second ed. American Association of Cereal Chemists Inc., St. Paul, Minnesota, USA, pp. 145-169.

Multiscale analysis of soil reflectance data for assessment of erosion state in agricult ural semi-arid Spain (Camarena)

S. Chabrillat[1*], T. Schmid[2], A. Palacios-Orueta[3], A. Bracken[3], E. Rodriguez[2], M. Rodríguez[2], R. Milewski[1]

[1]Helmholtz Centre Potsdam, GFZ German Research Centre for Geosciences, Section 1.4, Remote Sensing, Telegrafenberg, A17 20.25, 14473 Potsdam, Germany
[2]Research Centre for Energy, Environment and Technology, Avda. Complutense,22, 28040 Madrid, Spain
[3]Dpto. Silvopascicultura. U.D. Edafología, ETSI Montes. Universidad Politécnica de Madrid, Ciudad Universitaria s/n, Madrid 28040, Spain
[*]E-mail: chabri@gfz-potsdam.de

Abstract

Identification and quantification of soil surface properties based on the analyses of spectral reflectance data in the visible-near infrared region of the electromagnetic spectrum allow characterisation of the present status of soil surfaces linked with past surface processes. In particular, in arid and semi-arid agricultural regions sensitive to (wind and water) soil erosion processes, the analyses of the spatial distribution of varying surface soil properties can be used to infer erosion and deposition stages in selected areas. In this frame, the objective of this work is to determine the potential of soil spectroscopy techniques for the mapping and identification of soil erosion and deposition stages. A further objective, in regard to the future upcoming availability of high signal-to-noise ratio imaging spectrometers from space, is to test this potential at different spatial scales, ranging from the field to future Earth observation sensors spatial scale.

For this, the Camarena area in central Spain (Toledo, Madrid) has been chosen as a representative area of Mediterranean agricultural environments that present contrasted soil horizons at the surface, and is very sensitive to erosion processes. There, soils and rock outcrops as well as stony, clayey or sandy soils are exposed at the surface as a consequence of soil erosion which have potentially adverse effects on crop production and soil management. Soil reflectance data were acquired over the Camarena area multitemporally in the field since 2011. Two airborne campaigns were performed during the dry season in August 2011 acquiring data at different altitudes with the hyperspectral airborne AISA Eagle and Hawk sensors. During the airborne campaign, data was simultaneously acquired with a ALS50 (II) laser scanner sensor for the derivation of accurate topographical data. Analyses of soil morphological, physical, chemical and mineralogical properties were performed from field sampling concordant with the airborne survey. Then, pre-processing of the hyperspectral images was performed to correct for geometric distorsions and Eagle/Hawk data fusion. Atmospheric correction (ATCOR4) and field calibration allowed the delivery of geocoded surface reflectance images from

0.4 to 2.5 microns at 3 m, 6 m, and simulated EnMAp 30m resolution using the EnMAp simulator available at the GFZ (Eetes). Based on the laser scanner data, a digital surface model was generated to derive terrain properties related to soil degradation stages.

Preliminary analyses of spectral variability along the surface were performed using several algorithms. Mapping of variable occurrences of clay, carbonate and iron content allowed identification of the different soil horizons exposed at the surface. This presentation will show preliminary results towards accurate mapping of surface geo-chemical and physical characteristics based on spectral data at different spatial scales. Furthermore, we will explore the implementation of adequate methodologies for the identification of erosion and accumulation stages in selected locations using soil erosion models from the Camarena area.

Prediction of soil pH, soil organic carbon and calcium carbonate content based on reflectance measurements

Á. Csorba[1*], V. Láng[1], K. Szalay[2], L. Fenyvesi[2], E. Michéli[1]

[1]*Department of Soil Science and Agrochemistry, Institute of Environmental Sciences, Faculty of Agricultural and Environmental Sciences, Szent István University, H-2103, Gödöllő, Páter K. u. 1. Hungary*

[2]*Hungarian Institute of Agricultural Engineering, H-2100, Gödöllő, Tessedik S. u. 4.*

[*]*E-mail: csorba.adam@mkk.szie.hu*

Abstract

This study aims the prediction of key soil parameters based on VIS-NIR-SWIR reflectance spectroscopy coupled with multivariate mathematical statistical (also called chemometric) methods. Partial Least Squares Regression (PLSR) was implemented to construct calibration models, which were independently tested for the predictions of soil pH, soil organic carbon (SOC) and $CaCO_3$ content from the soil spectra.

Keywords: reflectance, spectroscopy, multivariate analysis, chemometrics.

1 Introduction and objectives

The environmental changes, the implication of the energy management, the requirements of the sustainable development and the understanding of the related global problems highlighted the significance of the agricultural and other environmental functions of soils. This growing interest towards the soils revealed the spatial, temporal and financial limits of the conventional soil observation and analytical methods. Recently, a global trend is forming which supports the development and use of technologies which enable data collection and analysis in a rapid, cheap and environment friendly way (Minasny & McBratney, 2010). Based on reflectance measurements in the visible (VIS), near-infrared (NIR) and short-wave infrared (SWIR) region of the electromagnetic spectrum (350 - 2500 nm), reflectance spectroscopy is suitable to satisfy the mentioned requirements. Considering the rich information content of the reflectance spectra and the presence of characteristic spectral fingerprints of a wide range of important soil constituents it is possible to simultaneously derive a lot of information from a single spectrum (Viscarra Rossel et al, 2006).

Most absorption features in the VIS-NIR-SWIR region are overtone or combination bands in the infrared region of the electromagnetic spectrum which are due to vibrational and rotational transition processes (Clark, 1999). Specifically, the VIS range provides a measure of soil color; broad and shallow absorption bands near 500-700 nm are due to iron oxides, oxihydroxides, hydroxides (Ben-Dor et al, 2006); narrow, well defined absorptions near 1400 and 1900 nm can be related to hydroxyl and water molecules

(Haubrock et al, 2008); absorption features beyond 2000 nm are due to clay minerals (Chabrillat et al, 2002), organic constituents (Stevens et al, 2008), carbonates (Lagacherie et al, 2008) and a wide range of salt minerals (Metternicht & Zinck, 2003). Various other absorptions due to soil constituents also occur throughout the 350-2500 nm range, however these are often difficult to identify because they may represent much weaker large-order overtones of the soil constituents, which can also overlap.

Because the VIS-NIR-SWIR reflectance spectra are essentially composed of a large set of overtone and combination bands coupled with other phenomena (ec. electronic processes) in combination with the complex composition of soils causes the VIS-NIR-SWIR spectra to be highly convoluted. As a consequence, it is difficult to relate specific absorption bands, or spectral phenomena to specific constituent or property. Considering the mentioned facts, sophisticated multivariate statistical techniques (also called chemometrics) are therefore required to extract the information about quality attributes which are hidden in the VIS-NIR-SWIR spectra (Duckworth, 1998).

In this study relationships between soil pH, SOC and $CaCO_3$ content and reflectance spectra measured in the visible (VIS), near-infrared (NIR) and short-wave infrared (SWIR) region of the electromagnetic spectrum have been analyzed. Partial Least Squares Regression (PLSR), one of the most widely used modeling methods in chemometrics was applied to build predictive models using reflectance spectra acquired under laboratory conditions.

2 Materials and methods

The study area included agricultural and forested areas in the Gödöllő hilly region (Northern Hungary) mostly covered by Cambisols, Chernozems, Phaeozems and Luvisols according to the WRB (IUSS Working Group WRB, 2006). The samples were taken to 1 m depth in 20 cm depth increments. The samples were oven dried, ground and sieved to a size fraction smaller than 2 mm. The number of samples analyzed and laboratory soil analyses performed are summarized in Table1.

Table 1. Laboratory methods of soil analyses

Soil parameter	n	Method	Reference
Soil organic carbon (%)	160	Walkley-Black	van Reeuwijk, 2002
$CaCO_3$ (%)	120	Calcimeter	van Reeuwijk, 2002
pH_{H2O}, pH_{KCl}	210	Electrochemical	van Reeuwijk, 2002

The instrument used for the laboratory spectroscopic measurements was the Analytical Spectral Devices (ASD) FieldSpec 3 MAX portable spectroradiometer with a Contact Probe attachment. The instrument has a spectral range between 350 and 2500 nm.

Before scanning, the instrument was calibrated with a Spectralon® white reference panel. For each soil measurement 25 spectra were averaged to improve signal-to-noise ratio. 5 reflectance spectra were acquired of every soil sample.

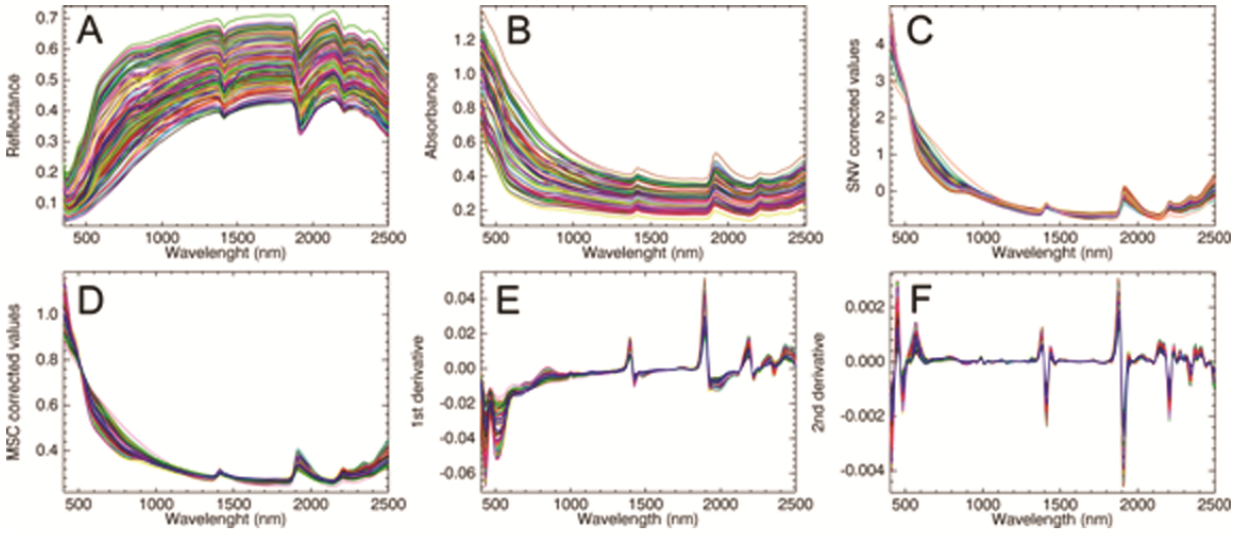

Figure 1. Reflectance spectra recorded (A) and the results of the spectroscopic transformations: B. Absorbance; C. Absorbance + MSC correction (Multiplicative Scatter Correction); D. Absorbance + SNV (Standard Normal Variate) correction; E. Absorbance + SNV correction + first derivatives; F. Absorbance + SNV correction + second derivatives.

Because the acquired spectrum of a sample is dependent on many different factors, spectroscopic preprocessing algorithms were applied on the reflectance data. To reduce non-linearities the spectra were transformed to absorbance (*log(1/reflectance)*) units. To remove the major effects of light scattering processes Standard Normal Variate (SNV) and Multiplicative Scatter Correction were applied. Furthermore the first and second derivatives of the SNV corrected spectra were calculated. The results of the preprocessing are shown in the Figure 1.

Partial Least Squares Regression (PLSR), one the most popular spectral decomposition technique with leave-one-out cross validation was used to calibrate the spectral data with the reference (laboratory) soil data. Unlike Principal Component Regression PLSR uses the laboratory information during the decomposition process, and collects as much information as possible into the first few loading vectors. The calibration models with the highest R^2 value were selected and were validated by using independent soil data.

The preprocessing and modeling were performed by using the PLS_Toolbox (Eigenvector Research Inc.)

3 Results and discussion

The influence of the different spectroscopic transformations and preprocessing methods on the R^2 values for the cross-validated predictions is shown on the Figure 2.

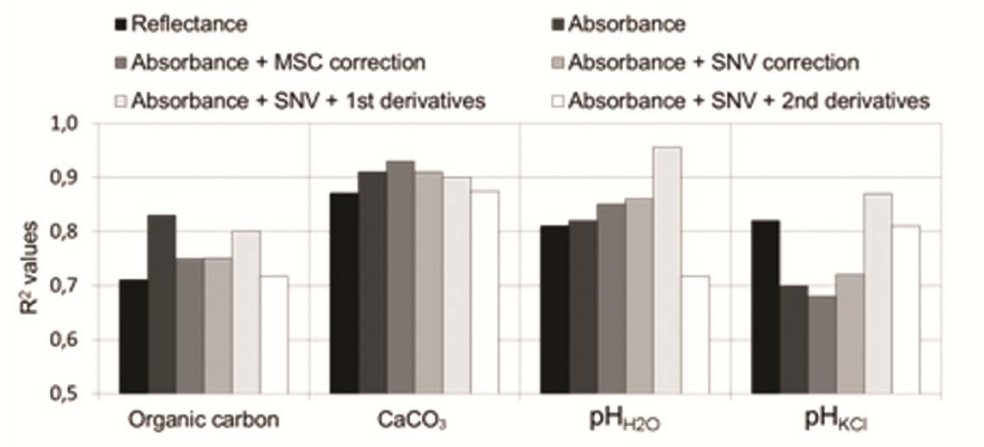

Figure 2. Comparison between the R^2 values of predictions of various soil parameters using different spectroscopic transformations

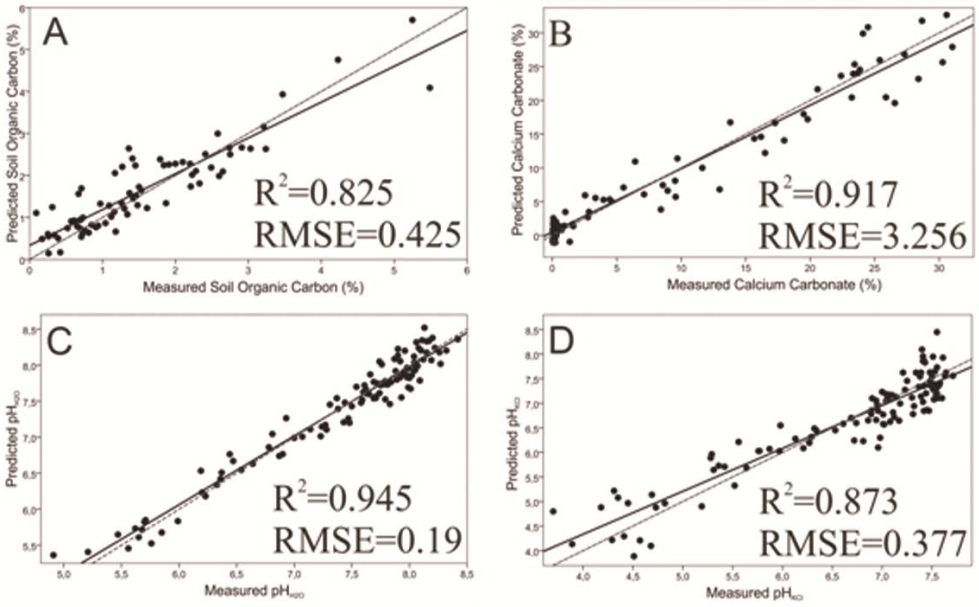

Figure 3. The measured versus the predicted values for (A) organic carbon content, (B) calcium carbonate content (C) soil pH measured in distilled water and (D) soil pH measured in KCl suspension. Solid lines: fit lines; dashed lines: 1:1 lines

The predictive capacity of reflectance spectroscopy and PLSR is high (R^2=0.825) for the SOC content. In case of the $CaCO_3$ content the prediction capacity of the method is very high (R^2=0.917). These results can be explained by the strong spectral activity of SOC and $CaCO_3$ in the VIS-NIR-SWIR region. The accuracy of the models ($RMSE_{(SOC)}$=0.425, $RMSE_{(CaCO3)}$=3.256) is moderate indicating the need of improving

the measurement protocol to achieve more reliable data, and to test other preprocessing and modeling methods as well. In case of soil pH predictions the method provided very accurate models ($R^2_{pH(H2O)}$=0.945; $R^2_{pH(KCl)}$=0.873, $RMSE_{pH(H2O)}$=0.19, $RMSE_{pH(KCl)}$=0.377). This result indicates that the method is capable to predict soil parameters which do not have well defined spectral signatures.

4 Conclusion

This work demonstrated the high potential of reflectance spectroscopy using VIS-NIR-SWIR spectra and multivariate analysis in prediction of soil pH, soil organic carbon and $CaCO_3$ content. The technique is rapid, cost- and time-effective making it possible to analyze a large number of samples. This properties and this study confirms the significance of spectroscopic analyses combined with multivariate methods in environmental studies and modeling.

References

BEN-DOR, E., LEVIN, N., SINGER, A., KARNIELI, A., BRAUN, O., KIDRON, G. J. 2006. Quantitaive mapping of the soil rubification process on sand dunes using an airborne hyperspectral sensor. Geoderma. 131: 1 - 21.

CHABRILLAT, S., GOETZ, A. F. H., KROSLEY, L., OLSEN, H. W. 2002. Use of hyperspectral images in identification and mapping of expansive clay soils and the role of spatial resolution. Remote Sensing of Environment. 82: 431 – 445.

CLARK, R. N. 1999. Spectroscopy of Rocks and Minerals, and Principles of Spectroscopy. In: Rencz, A. (ed.), Manual of Remote Sensing. Wiley. New York. 3 – 58.

DUCKWORTH, J. H. 1998. Spectroscopic quantitative analysis. In: Applied Spectroscopy (Eds.: WORKMAN, J. & SPRINGSTEEN, A.) 93–163. Academic Press. San Diego, California. 93 – 165.

HAUBROCK, S. N., CHABRILLAT, S., KUHNERT, M., HOSTERT, O., KAUFMANN, H. 2008. Surface soil moisture quantification and validation based on hyperspectral data and field measurements. Journal of Applied Remote Sensing, 2:1, 023552 (online publication)

IUSS WORKING GROUP WRB. 2006. World Reference Base for Soil Resources. 2nd ed. World Soil Resources Report No. 103. Fao. Rome

LAGACHERIE, P., BARET, F., FERET, J-B., NETTÓ, J. M., ROBBEZ-MASSON, J. M. 2008. Estimation of soil clay and calcium carbonate using laboratory, field and airborne hyperspectral measurements. Remote Sensing Environment 112: 825 – 835.

METTERNICHT, G. I., ZINCK, J. A. 2003. Remote sensing of salinity: potentials and constraints. Remote Sensing of Environment 85: 1. 1 – 20.

MINASNY, B., MCBRATNEY, A. B. 2010. Methodologies for Global Soil Mapping. Dordrecht, Springer Netherlands, pp. 429 – 436.

STEVENS, A., WASEMAEL, B., BARTHOLOMEUS, H., ROSILLON, D., TYCHON, B., BEN-DOR, E. 2008. Laboratory, field and airborne spectroscopy for monitoring organic carbon content in agricultural soils. Geoderma 144: 395 – 404.

VISCARRA ROSSEL, R. A., WALVOORT, D. J. J., MCBRATNEY, A. B., JANIK, L. J., SKJEMSTAD, J. O. 2006. Visible, near infrared, mid infrared or combined diffuse reflectance spectroscopy for simultaneous assesment of various soil properties. Geoderma 131: 59 – 75.

On-the-go mapping of soil organic carbon content in Western Poland

G. Debaene*, J. Niedźwiecki, A. Pecio

Institute of Soil Science and Plant Cultivation – State Research Institute, ul. Czartoryskich 8, Puławy, Poland

** E-mail: gdebaene@iung.pulawy.pl*

Abstract

The aim of the present paper was to report the first investigation of on-the-go mapping of soil organic carbon (SOC) with visible and near-infrared spectrometry (VIS-NIRS) in Poland. Measurements were carried out during Spring 2011 at a farm situated in Western Poland by means of the Veris spectrophotometer. The prediction of SOC was based on calibration obtained with samples (20) selected by the Veris software fuzzy logic algorithm. Results are promising but further investigation is needed. Results were compared with those obtained using conventional VIS-NIRS based on a grid-sampling strategy and proved to be very similar.

Keywords: visible and near-infrared spectroscopy, soil organic carbon, precision agriculture, partial least squares

1 Introduction

Accurate and numerous measurements of soil organic carbon are required for precision agriculture (PA) and because soil is acting as one of the major carbon pool. On-the-go soil sensing systems have been developed with that aim in mind (Adamchuk et al, 2004). In Eastern Europe, proximal soil sensing is not yet sufficiently developed, partly because of the farm size. Visible and near-infrared spectroscopy is a method to access high-resolution soil data, which are needed to achieve site-specific management. VIS-NIRS is a rapid and non-destructive analytical technique that correlates diffusely reflected near-infrared radiation with the chemical and physical properties of materials (Chang & Laird, 2002). The size, the possibility of analysing wet samples and of using fibre optic make VIS-NIRS suitable as an on-the-go-sensor (Christy, 2008).

The aim of our study was to investigate the potential of on-the-go VIS-NIRS for estimating the SOC distribution of a mineral soil – dominant type in Poland – in a farm in Western Poland and to compare to the results obtained from VIS-NIRS method based on the analysis of samples from a grid.

2 Materials and methods

2.1 Sample collection and spectral measurements for conventional mapping

One hundred and eighty samples were collected from a soil sampling grid in Baborówko, Western Poland. The soil grid was georeferenced by means of a global positioning system. The area of the field is 22 ha. The soil type is a podzoluvisol (World Reference Base for Soil Resources – WRB). The samples were scanned from 350 to 2220 nm with the Veris spectrophotometer (Veris technologies, Salina, KS, USA) in bench top mode. The sampling resolution was about 4-7 nm. A detailed description of (1) the system and of (2) the spectral acquisition procedures can be found in Kweon et al, (2009).

2.2 On-the-go measurements

The Veris on-the-go system is described at length in Christy, 2008. The shank mounted in a toolbar was lowered into the ground to approximately 7 cm and pulled through the field at 7 $km.h^{-1}$. The range of measurements was 350-2220 nm. After mapping completion, 20 representative samples – to be collected for chemical analysis – were located by the software (see Christy, 2008).

2.3 Chemical analysis

The SOC content was determined by the Tiurin method (K dichromate digestion) for all samples (grid + on-the-go).

2.4 Calibration model development

The spectra were reduced to 400-2200 nm due to the low signal-to-noise ratio. Multiplicative scatter correction (MSC), standard normal variate (SNV), first and second Savitzky-Golay have been applied to the raw spectra using Unscrambler X® (Camo Inc., Oslo, Norway) Partial least square (PLS) regression was applied to determine the best correlation between chemical and spectral data. Two third (120) of the samples from the grid were used as an independent validation set. Calibrations using the 20 samples from on-the-go mapping were validated with leave-one-out cross validation.

2.5 Map generation

A map of the difference between conventional and on-the-go mapping was generated using ArcGis 9.3 (ESRI, USA) using inverse distance weighted (IDW) for interpolation.

3 Results

The best PLS calibration models for conventional and on-the-go models are presented in Table 1. They were both obtained using the SNV pretreatment. Overall, all pretreatment gave similar results. The map of the difference (%) between conventional and on-the-go SOC values is presented in Figure 1. In the view of Figure 1, it seems that there is a good agreement between conventional and on-the-go mapping for SOC. More than 70% of the map show differences less than 0.2% in SOC content.

Table 1. Soil organic carbon calibration results.

	Cross-Validation		Validation			
n	r^2	RMSE	r^2	RMSE	RPD	NF
			Conventional			
60	0.71	0.14	0.72	0.13	1.9	7
			On-the-go			
20	0.70	0.19	-	-	-	6

RMSE – root mean square of error; RPD – ratio of performance to deviation; NF – number of factors

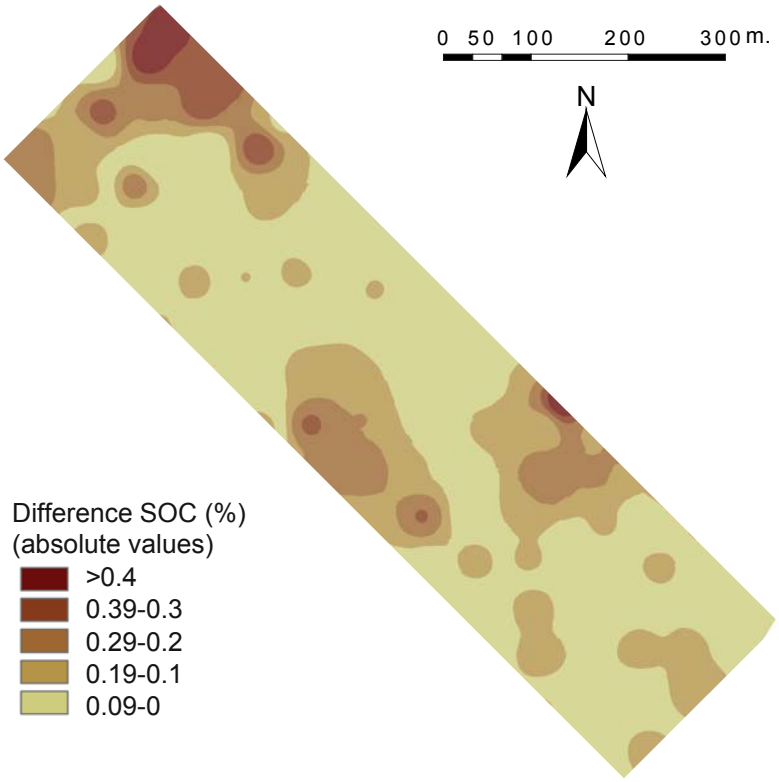

Figure 1. Map of the difference (%) between VIS-NIRS laboratory model and on-the-go SOC values.

4 Discussion

Soil organic carbon has been intensively investigated in the last few years. Our VIS-NIRS laboratory results are similar to those found in literature (see Viscarra Rossel & MCBratney, 2008). On-the-go results are similar to that of Knadel et al, 2009. VIS-NIRS on-the-go mapping of SOC seems to be promising for the mineral soils of western Poland with low SOC content. A relatively good precision of the results is probably due to the low level of SOC (0.65 – 2.0%). In the view of the results and of our knowledge of the field of Baborówko, more attention should be paid in areas with higher SOC content since these areas presented more discrepancies between the methods with over or under prediction

5 Conclusions

This paper report the use of VIS-NIRS for prediction and mapping SOC content. The on-the-go method is suitable to map mineral soils with a low SOC content. There is a good agreement of results between laboratory and on-the-go based VIS-NIRS models. The on-the-go method has the potential to contribute to the rapid development of precision agriculture in Eastern Europe.

Acknowledgements

Work/part of the work has been supported by European Community 7th Framework Program project Proficiency (FP7-REGPOT-2009-1-245751) and by the Polish Ministry of Science and Higher Education grant NN310 079836.

References

ADAMCHUCK, V.I., HUMMEL, J.W., MORGAN, M.T., UPADHYAYA. S.K. 2004. On-the-go soil sensors for precision agriculture. Computers and electronics in agriculture, **44** (1) 71-91.

CHANG, C.W., LAIRD, D.A. 2002. Near-infrared reflectance spectroscopy analysis of soil C and N. Soil Science, **167** (2) 110-116.

CHRISTY, C.D. 2008. Real-time measurement of soil attributes using on-the-go near infrared reflectance spectroscopy. Computers and electronics in agriculture, **61** (1) 10-19.

KNADEL, M., THOMSEN, A., GREVE, M.H. 2011. Multisensor on-the-go mapping of soil organic carbon content. Soil Science Society of America Journal, **75** (5) 1799-1806.

KWEON, G.Y., LUND, E., MAXTON C., DRUMMOND, P., JENSEN, K. 2009. Soil Profile Measurement of Carbon Contents using a Probe-type VIS-NIR Spectrophotometer. Journal of biosystems engineering, **34** (5) 382-389.

VISCARRA ROSSEL, R.A., MCBRATNEY, A.B. 2008. Diffuse Reflectance Spectroscopy as a Tool for Digital Soil Mapping. In: Digital soil mapping with limited data. Developments in Soil Science series, edited by Hartemink, A.E., McBratney, A.B., Mendonça-Santos, L., Elsevier Science, Amsterdam, NL, pp. 165-172.

Using iodine as a tracer in the field and the detection thereof to reflect on water and salt movement in these soils.

W.P. de Clercq*, A Rozanov

Soil Science, Stellenbosch University, P/Bag X1, Matieland, 7602, ZA
**E-mail: wpdc@sun.ac.za*

Abstract

The study was conducted on a farm, Goedertrou, close to the town Riebeeck West in the Western Cape Province of South Africa. The soils of the Goedertrou site are mainly Glenrosa soils (Cambisols), which tend to be dry and hard in summer. The soils are generally shallow with a very dense B-horizon and with a C-horizon in some places but mostly bedrock below the B-horizon. In 2005 it was decided to study the infiltration characteristics of these soils using a KI dye. The soils were also scanned with an EM38 proximal sensor. In 2012, it was decided to use the KI that was introduced in 2005 during the infiltration study, as a tracer to indicate the movement of Cl^- in this landscape. For this study a handheld Niton XRF scanner was used to detect iodine in the field. Measurements were made on the soil surface and at 10, 15, 30, 40, and 45 cm depths.

Experiments with ring infiltrometers on Glenrosa soil form (ClLm) were uneventful. The tests showed extremely low infiltration rates (under 2 mm/hour) due to high clay content and the dense B-horizon that ocurred at about 20cm depth. The experiment indicated preferential flow paths where old root canals existed through the dense horizon. Regarding the Iodine, the highest readings related to the upper part of the B-horizon and very low readings below the B-horizon. In fact we found that any sign of iodine in the soil profile would firstly be found on or close to the soil surface, in the first 10 cm. This is consistent with the finding that a high amount of capillarity rise exists in these soils, bringing salts to the surface during summer months. As a result of this study we could calculate the amount of iodine lost from these soils over the 6 year period. We could also establish a trail of iodine down the small catchment indicating the water flowpath down the catchment. The information presented in this study led to a better understanding of the movement and residence time of chlorine in the system.

Keywords: Tracer, soil salinity, proximal sensing, XRF.

1 Introduction

It is often necessary to find a measure of the salinity dynamics in a salt affected region. The dynamics is then studied using a tracer, mostly isotopes, and the study is then mostly quite expensive. In the dryland type systems, we also know that the salts (mainly NaCl) has a temporal dynamics linked to it as a result of water movement which causes a horizontal and vertical displacement of salt at any point. We also know that the region

in which the study was done, is influenced by a recharge effect in terms of salts, as a result of the closeness to the sea.

Under these circumstances, a tracer would therefore be quite helpful to establish the rate of movement of salt through the particular landscape as it could also indicate the possibility that salts are generally on the increase or decrease. Changes in climate could impact dramatically on salinity behaviour in any landscape and will have a dramatic impact on the water resources of such a region.

The KI used in this study could be used to indicate a salt depletion rate similar to studies done by Davis et al. (1997) and Phillips et al (2007). Phillips et al (1997) looked at the chloride and bromide ratios while Phillips et al. (2007) looked environmental tracers and also confirmed that the chloride/bromide ratios helped to characterize the environmental impact.

Soil proximal sensing through the use of an EM38 is usefull in establishing soil bulk salinity and to some extent being able to map the seasonal responses regarding salinity in any landscape. It is not possible though to see from these results what happened to the salts in the landscape and where it moved to. However by using the mapped EM38 salinity results, and knowing something about the potential change in salinity at any point in the landcape through a chloride/iodine ratio, we could contribute more value to the soil proximal sensing work (de Clercq et al., 2010).

2 Materials and methods

The study was conducted on a farm, Goedertrou, close to the town Riebeeck West in the Western Cape Province of South Africa. The soils of the Goedertrou site are mainly Glenrosa soils (Cambisols), which tend to be dry and hard in summer. The soils are generally shallow with a very dense B-horizon and with a C-horizon in some places but mostly bedrock below the B-horizon. Soils in the region are subjected to a salt influx from an extensive recharge zone at the top of the catchment or to exposure of saline saprolite through natural erosion. The poorly structured, low carbon topsoil (with a clay fraction consisting chiefly of kaolinite and mica), although lighter textured than the subsoil, exhibits strong crusting. Runoff during rain events is consequently intense (De Clercq et al., 2009). The more clayey subsoil, low hydraulic conductivity and high compaction (average bulk density in the B-horizon, where present, is 1.89 g cm^{-3}) represents a further barrier to recharge, and lateral migration of perched water through the surface horizon is therefore common.

In 2005 it was decided to study the infiltration characteristics of these soils. A similar infiltration experiment, but with a rainfall simulator was conducted to understand the impact of wheat on interception redistribution and channelling of rain water. Also in 2005, an EM38 study was done to map salinity in the small catchment. Regular measurement

was also conducted of two hill slope trajectories to establish the salinity patterns between winter (rain period) and summer (dry period).

In 2012, it was decided to use the KI that was introduced during the 2005 infiltration study, as a tracer. This decision was based on the fact that these soils do not contain any I- and the fact that I^- would react similarly to Cl^- in these soils. Therefore the iodine was accepted as a good element to resemble the movement of chloride in these fields. For this study a handheld Niton XRF scanner was used to detect iodine in the field. The main aim was to find out firstly how much iodine was left in the positions of application and secondly whether we could pick up hints of the flowpath towards the small dam on the premises. The spots where iodine was introduced in the field were identified again, carefully opened and scanned. Small access holes were dug 45 cm deep to the bedrock. Measurements were made on the soil surface and at 10, 15, 30, 40, and 45 cm depths.

Equipment used:

EM38 soil proximal sensor linked to a Trimble GeoXT GPS, a ThermoNiton XRF handheld analyser.

3 Results

Experiments with ring infiltrometers on Glenrosa soil form (ClLm) were uneventful. The tests showed extremely low infiltration rates (under 2 mm/hour) due to high clay content and the dense B-horizon that occurred at about 20cm depth. The experiment indicated preferential flow paths where old root canals existed through the dense B horizon and the KI had enough time to adequately infiltrate into the soil.

3.1 The XRF measurements

The measurements were made at positions p1 to p7 as indicated on the map, Figure 1. One of the measurements is given in Figure 2. The aim was to gather information related to the expected soil proximal sensor scanning depts. The summarized results can be seen in Table 1. Point p7 was measured as a position where no KI was introduced.

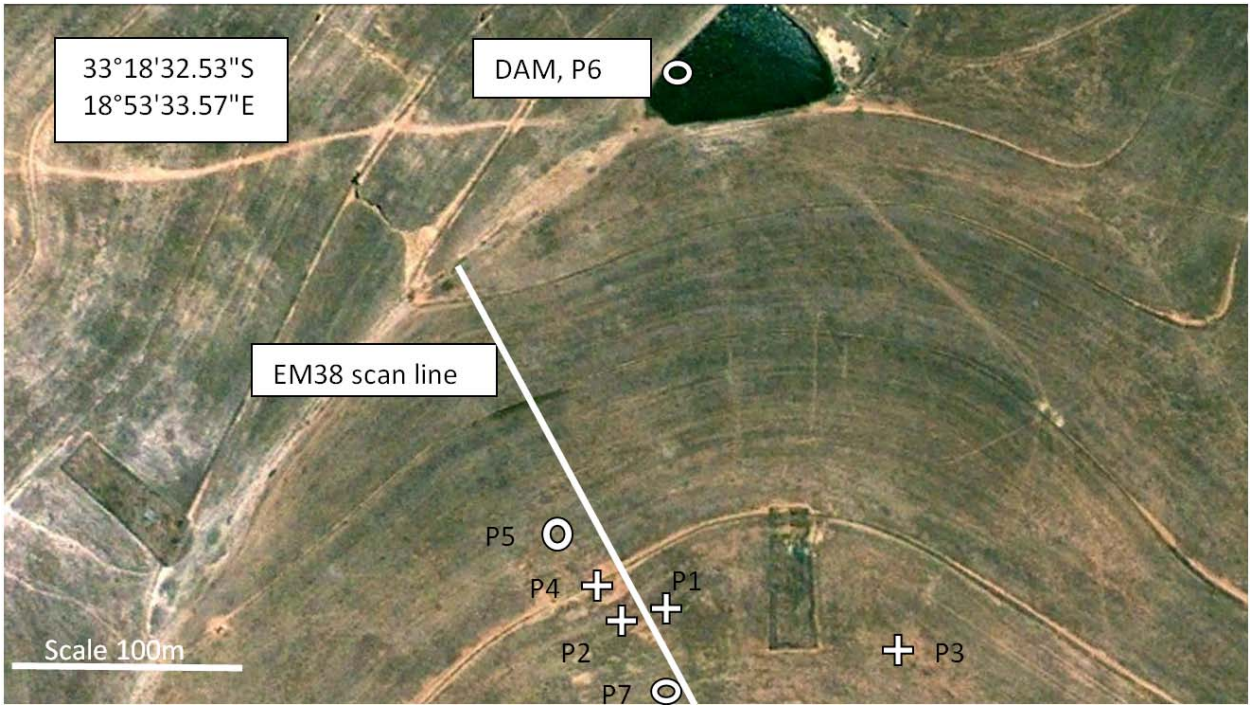

Figure 1. The Goedertrou farm where '+' indicates where Iodine was introduced and 'O' where iodine was monitored. P7 was used to test the normal Cl/I ratio for this landscape.

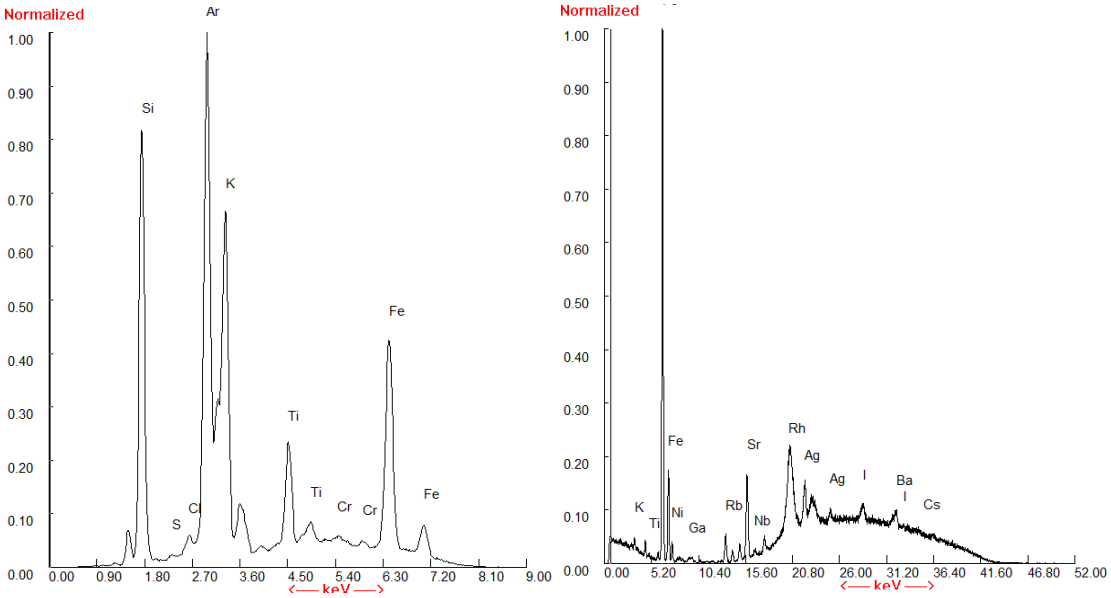

Figure 2. XRF scans, 30 cm depth from the soil surface below the b-horizon in spots where iodine was introduced at the Goedertrou catchment

Table 1. The XRF iodine counts and Cl/I ratios for seven positions in the Goedertrou Catchment

	Position in the landscape							
	1	1	2	2	3	3	4	4
Horizon	I	Ratio	I	Ratio	I	Ratio	I	Ratio
A	17.04	16.20	24.02	17.70	23.00	22.17	26.50	19.80
B			26.14	18.15	24.58	18.42		

	Position in the landscape					
	5	5	6	6	7	7
Horizon	I	Ratio	I	Ratio	I	Ratio
A	25.14	19.30	25.60	21.10	15.60	30.47
B	27.23	21.10				

I= iodine and Ratio = Cl/I

3.2 The EM38 trajectory scan

The vertical and horizontal scans obtained with the EM38 meter on the North-facing hillslope transect are shown in Figure 3. The measurements were taken at the end of summer (April 2007) when the soils were driest and a lot of salt occurred on and/or close to the soil surface. The EM-38 data represent the average bulk soil EC at each measuring point over the measuring depth. The squares in Figure 3 indicate the position of the contour banks in this landscape.

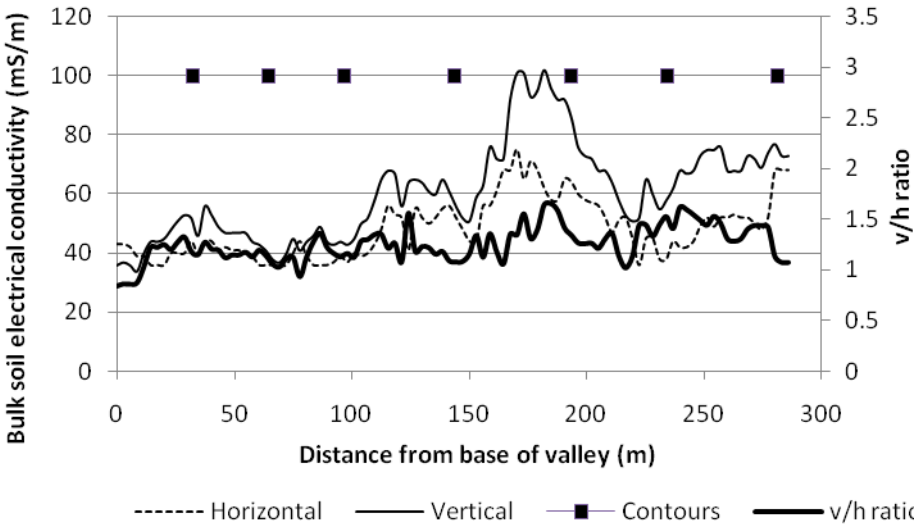

Figure 3. Bulk soil electrical conductivity vertical and horizontal readings taken with an EM-38 meter on a North-facing hillslope transect (April) and a smoothed ratio of vertical and horizontal readings (moving point average of nine readings). With contours, the position of the contour banks in the landscape are indicated.

It is clear that salinity in the landscape varies at different sections of the topo-sequence and that anti-erosion contours showed a marked effect on salinity distribution in the catchment. The vertical to horizontal ratio declined downslope and approached 1 towards the base of the valley meaning that, lower down in the catchment, a homogeneous profile of salt seems to be the norm. In the upper part of the catchment, the vertical reading is much higher than the horizontal reading, indicating much more salts lower down in the soil profile compared to the soil surface layer. This information compared well with the XRF readings and it was thus possible to indicate the potential difference in chloride and iodine responses along the slope with regard to the total chloride response in the catchment from 2006 to 2012.

3.3 The EM38 scan of the catchment

A soil salinity map for the Goedertrou catchment was developed using measurements taken with the EM38 in April 2005 (Figure 4). The data collected on a 1 m x 1 m grid represented the vertical scan (0.2-1.5 m depth), and they were interpolated using ordinary kriging. The map shows that bulk soil salinity varied between approximately 20 and 180 mS m^{-1} across the small catchment (Figure 1).

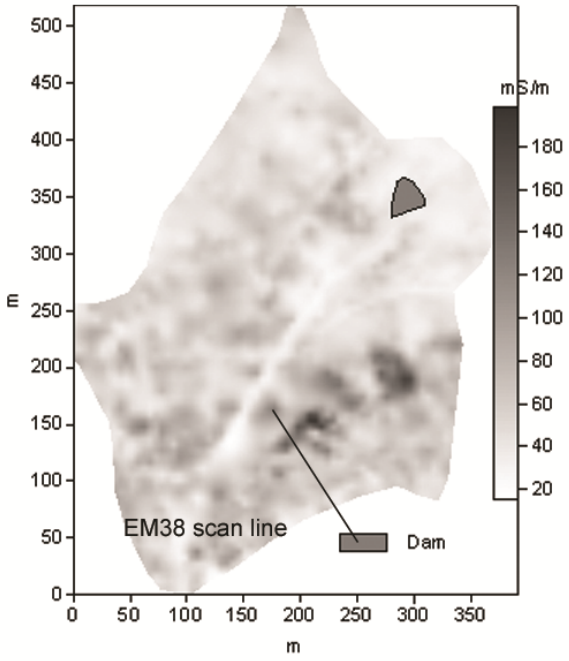

Figure 4. EM38 scan of the Goedertrou catchment indicating salinity (mS m-1) and the spatial distribution thereof in the catchment. The coordinates are in m.

Bulk soil salinity was generally higher on the North-facing slope, in particular at a convex position on the mid-slope, where salinity effects were visible in the form of a saline scald where wheat fails to germinate. In most of these very saline spots, the B horizon is absent leaving a very thin A horizon directly on shale. Down-slope leaching

from the crest and down-valley leaching from the foot-slope soils could possibly account for this mid-slope salinity maximum.

4 Discussion

The most meaningful results were found in the upper part of the soils. The highest readings related to the B-horizon and very low readings below the B-horizon. In fact we found that any sign of iodine in the soil profile would firstly be found on or close to the soil surface, in the first 10 cm. This is consistent with the finding that a high amount of capillarity rise exists in these soils, bringing salts to the surface during summer months. It was indicated that the amount of iodine lost from the profiles measured, was an average of 84% of what was applied. However, the amount of iodine redistributed is still difficult to indicate. From Figure 1 and Table 1 it is clear that the iodine was transported lower down in the catchment and traces were picked up in the dam. However, what is important, is the 84 % iodine removed from the points of application over the 6 years. This provides a new perspective to the dynamics imbedded in Figure 4.

5 Conclusion

As a result of this study we could calculate the amount of iodine lost from these soils over the 6 year period. We could also establish a trail of iodine down the small catchment indicating the water flowpath down the catchment. The information presented in this study led to a better understanding of the movement and residence time of chlorine in the system. The study will continue for another 2 years.

Acknowledgements

The Water Research Commission of South Africa for funding.

References

DE CLERCQ, W.P. 2009. Space-time variability of soil salinity in irrigated soils of South Africa. Gent, Belgium. (ISBN: 978-90-5989-276-7).

DE CLERCQ, W.P., JOVANOVIC, N., FEY, M. 2010. Land use impacts on salinity in Berg River water: Research on Berg River water management. WRC Report no: 1503/1/10 (ISBN: 978-1-77005-971-9) p 126

PHILLIPS, F.M., HOGAN J., MILLS, S., HENDRICKX, J.M.H. 2007. ENVIRONMENTAL Tracers Applied to Quantifying Causes of Salinity in Arid-Region Rivers: Preliminary Results from the Rio Grande, Southwestern USA . Hydrogeology Journal, Volume 16, Number **4** 737-747

DAVIS, S.N. WHITTEMORE, D.O. FABRYKA-MARTIN, J. 1997. Uses of Chloride/Bromide Ratios in Studies of Potable Water. Ground Water, **36**, 338 - 350

Construction of an electrochemical detector for determining the dispersion of fluoranthene in soil type Gleysol at laboratory level

R. Flores, E. Bustos*

Centro de Investigación y Desarrollo Tecnológico en Electroquímica, S. C., Parque Tecnológico, Querétaro, Sanfandila, Pedro Escobedo 76703,Querétaro, Mexico.
**E-mail: ebustos@cideteq.mx*

Abstract

The electrochemical techniques can develop electrochemical detectors which are characterized by selective, allow a direct or indirect pollutants, they are simple to develop not only comfortable to use and can be miniaturized. Based on the foregoing, this research shows the results of the construction of an electrochemical detector for determining a dispersion of fluoranthene in soil type Gleysol at laboratory level, these detections were developpe using modified graphite electrodes (G) with a coordination compound of $KFe_4^{II}[Fe^{III}(CN)_6]_3$, $KCo_4^{II}[Fe^{III}(CN)_6]_3$, $KNi_4^{II}[Fe^{III}(CN)_6]_3$ and $Fe_4^{III}[Fe^{III}(CN)_6]_4$, which the best electrochemical detection of the pollutant was obtained with G - $Co_4^{II}[Fe^{II}(CN)_6]_2$.

Keywords: prusiate, fluoranthene, Gleysol, cobalt.

1 Introduction

Currently soil pollution is a major environmental problem. It is very common to find soils exposed tool spills causing a health risk, being highly toxic and carcinogenic compounds. Given the different sources of these compounds and the fact that some population groups who live or working environments with hydrocarbons, it is necessary to monitor the exposition to these compounds by chromatographic analyses (Mastandrea et al, 2005), which are expensive, highly specialized and time-consuming. Therefore, there is a need to develop and implement efficient and effective analytical techniques.

The electrochemical techniques can develop electrochemical detectors which are characterized by selective, allow a direct or indirect pollutants, they are simple to develop not only comfortable to use and can be miniaturized (Roberts et al, 2009).

Based on the foregoing, the present work shows the results of the construction of an electrochemical detector for determining a dispersion of fluoranthene in soil type Gleysol at laboratory level. To achieve this, we worked with soil contaminated with hydrocarbon type Gleysol from the area of re-pumping of crude in Nuevo Teapa, Vera-

cruz, Mexico, which was generated by oil spilling 2007 following clandestine take crude in a pipeline 30 inches in diameter.

2 Material and methods

To detect the fluoranthene in soil type Gleysol was used a modified electrode with a Prusiate of cobalt, which was chemically synthesized using the next combination of reactive in 0.05 M HCl in base of the literature (Chen and Chia – Ming, 2003):

1. 0.05 M $FeCl_3 * 6H_2O$ + 0.05 M $K_3[Fe(CN)_6]$
2. 0.05 M $FeCl_2 * 6H_2O$ + 0.05 M $K_3[Fe(CN)_6]$
3. 0.05 M $CoCl_2 * 6H_2O$ + 0.05 M $K_3[Fe(CN)_6]$
4. 0.05 M $NiCl_2 * 6H_2O$ + 0.05 M $K_3[Fe(CN)_6]$

All the solutions were characterized by UV-Visible spectrophotometry on a Perkin Elmer Lambda XLS. To have the modified graphite (1.4 cm^2, G) with $KCo_4^{II}[Fe^{III}(CN)_6]_3$, $Fe_4^{III}[Fe^{III}(CN)_6]_4 \cdot H_2O$ and $KNi_4^{II}[Fe^{III}(CN)_6]_3$ in an electrochemical cell was applied 12 µA using cronoamperometry at different times: 15, 30, 45, 60, 75, 90, 105, 120, 135 and 150 s. The modified surfaces were characterized by cyclic voltammetry (CV), Raman spectroscopy, scanning electron microscopy (SEM) and emission diffraction spectroscopy (EDS).

3 Results

According to the values of the molar extinction coefficient obtained, $KFe_4^{II}[Fe^{III}(CN)_6]_3$ was the most soluble coordination complex of all Prusiates study, followed by the $KCo_4^{II}[Fe^{III}(CN)_6]_3$, $Fe_4^{III}[Fe^{III}(CN)_6]_4 \cdot H_2O$ and finally $KNi_4^{II}[Fe^{III}(CN)_6]_3$.

On other hand, during the chemical synthesis of the different Prusiates, it was observed that the best times for each synthesis coordination complexes according to the highest current density obtained in presence of each Prusiate using cyclic voltammetry were observed: 30, 15, 30 and 60 s for G - $KFe_4^{II}[Fe^{III}(CN)_6]_3$, G - $KCo_4^{II}[Fe^{III}(CN)_6]_3$, G - $KNi_4^{II}[Fe^{III}(CN)_6]_3$ and G - $Fe_4^{III}[Fe^{II}(CN)_6]_4$, respectively.

The electrode G - $Ni_4^{II}[Fe^{III}(CN)_6]_2$ had a major capacitive resistance than G - $Co_4^{II}[Fe^{III}(CN)_6]_2$, which had the highest faradaic current density of fluoranthene. This signal showed an anodic peak potential E_{pa} = 710 mV vs. $Fc^+ | Fc$, a half-cell potential $E_{½}$ = 380 mV vs. $Fc^+ | Fc$ and anodic peak current $I_{pa} = 9.06 \times 10^{-6}$ A by the transfer of one electron according the literature (Bard and Faulkner, 2001).

G - $Co_4^{II}[Fe^{III}(CN)_6]_2$ was probed in presence of different concentrations of fluoranthene in HFTA and DMF by square wave voltammetry (SWV) at 298 K using the electrochemical cell to construct the calibration curve. We obtained a detection limit of 0.052 M or 106.38 ppm with a quantification limit of 0.175 M or 354.76 ppm of fluoranthene using G - $Co_4^{II}[Fe^{III}(CN)_6]_2$. Finally, using the dispersion of fluoranthene in 30 g of soil type Gleysol was followed by the best modified electrode with cobalt by SWV.

4 Discussion

The electrochemical detection of the fluoranthene in organic medium using SWV with the modified electrodes with Prusiates indicates a better sensitivity than the results obtained by gas chromatography with mass spectrometry. In this sense, a plume of flouranthene was defined and following during three weeks in a soil sample type Gleysol from Nuevo Teapa, Veracruz in Mexico using G - $Co_4^{II}[Fe^{III}(CN)_6]_2$ (Figure 1).

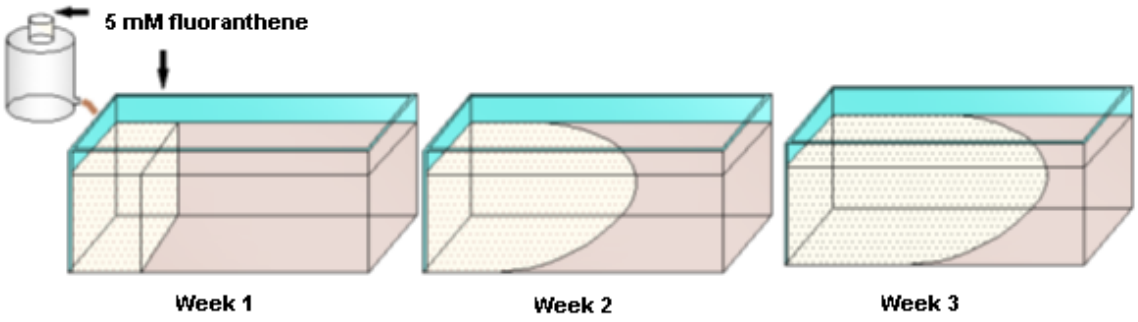

Figure 1. Representation of the plume of fluoranthene generated during three weeks in a soil sample type Gleysol from Nuevo Teapa, Veracruz in Mexico using a reactor of acrylic.

For week 2, the detection of fluoranthene indicated a higher concentration at 5 cm depth, recording a current density of 0.492 $\mu A\ cm^{-2}$, while for 3 weeks, it was observed that at a distance of 9 cm increased, showing a current density of 0.211 $\mu A\ cm^{-2}$.

All the variables were correlated for additional information using the statistical software MiniTab1.4. The correlation of the data obtained in the electrochemical determination, taking the following variants: concentration, depth, horizontal distance and time, getting the results of p (p = statistical correlation) obtaining a $p < 0.05$. The p value for concentration versus depth is 0.016, the distance is about 0.04, and is 0.04 times, which determines the feasibility of the sensor.

5 Conclusions

Once taking soil samples from the reactor of acrylic at different distances, depths and times during three weeks, these were assayed using the modified electrode G - $Co_4^{II}[Fe^{III}(CN)_6]_3$ with SWV and we constructed the plume of pollutant in a laboratory

level. Data validated with the simulation of these results with the Miniltab 1.4 program obtaining a correlation of the data around $p < 0.05$, and determining the viability of this modified electrode like an electrochemical detector of fluoranthene.

Acknowledgements

The authors would like to thank Consejo Nacional de Ciencia y Tecnología de los Estados Unidos Mexicanos (CONACyT), Academia Mexicana de Ciencias (AMC), Fundación México – Estados Unidos para la Ciencia (FUMEC) and International Cooperation Program across Bilateral Cooperation Mexico – Hungary for the funding of this research.

References

BARD, A. J., FAULKNER, L.R. 2001. Electrochemical Methods Fundamentals and Applications. John Wiley. New York, USA.

CHEN, S. M., CHIA – MING, CH. 2003. Preparation, characterization, and electrocatalytic properties of copper hexacyanoferrate film and bilayer film modified electrodes. Journal of Electroanalytical Chemistry, 543, 2, 161 - 173.

MASTANDREA, C., CHICHIZOLA, C., LUDUEÑA, B., SÁNCHEZ, H., ÁLVAREZ, H., GUTIÉRREZ, A. 2005. Hidrocarburos aromáticos policíclicos. Riesgos para la salud y marcadores biológicos (Polycyclic aromatic hydrocarbons. Health hazards and biological markers). Acta Bioquímica Clínica Latinoamericana, 39, 1, 27 - 36.

ROBERTS, M. E., MANNSFELD, S. C. B., STOLTENBERG, R. M., BAO, Z. 2009. Fexible, plastic transistor – based chemical sensor. Organic Electronics, 10, 377 - 383.

Soil properties and lime requirement assessment using on-the-go Vis-NIR-SWIR reflectance spectroscopy

M. H. D. Franceschini*, J. A. M. Demattè, J. P. Molin

Escola Superior de Agricultura Luiz de Queiroz (ESALQ), Universidade de São Paulo (USP), Brasil

**E-mail: marston_f@yahoo.com.br*

Abstract

The soil fertility assessment is essential to assure appropriate soil management, increasing economic profit of the agricultural production and avoiding environmental damages. Nowadays, the soil sampling and analysis is the most used method to determine soil physical and chemical properties. However, the conventional method becomes too expensive when the amount of information needed increases. This happens especially when Precision Agriculture techniques are adopted. Besides, high amounts of laboratory analysis are time consuming and produce potentially polluting waste. So, the relationship between the electromagnetic energy reflected by the soil and his composition can help in the soil variability assessment, reducing costs and the time spent. In the last years several authors have achieved promising results in the prediction of soil physical and chemical variability using the soil spectral behavior in the visible, proximal infrared and short wave infrared (Vis-NIR-SWIR, 350-2500 nm) coupled with mathematical methods like Partial Least Squares Regression (PLSR). In this study it's evaluated and compared the use of different spectral data to quantify soil properties. Spectral data were collected in the field (on-the-go) and laboratory conditions, using the Veris Vis-NIR Spectrophotometer (Veris Technologies Inc., Salinas, Kansas, USA). The on-the-go measurements were taken in field plots (10 x 15 m) in which different rates of lime were applied. These levels of lime were calculated based on V%, the base saturation (K, Ca, Mg, Na) of the soil CEC (Cation Exchange Capacity). The plots were allocated in two fields with different soil textures one with about 100 g kg^{-1} of clay (area 1) and another with about 320 g kg^{-1} of clay (area 2). In each field 25 plots were allocated and among these plots 15 received lime to achieve 90%, 75% or 65% of soil base saturation, and the other 10 plots were used as control, in which lime was not applied. Spectral data were collected in the field seven months after lime application in order to allow lime reaction in the soil solution. Laboratory measurements were conducted in 300 soil samples, 150 for each field, collected on the same lines where the sensor took the spectral measurements. Samples were not dried or sieved before spectral data acquisition at the laboratory and measurements were taken using a sample holder block were a portion of homogenized soil was placed. Soil homogenization was done manually sample by sample in order to eliminate soil aggregates. Better predictions were obtained with spectral data measured at the laboratory, especially for the area 1. Validation results for

the area 1 (validation set = 50 samples, laboratory/field): organic matter – R^2=0.59/-0.09, RMSE=2.0/3.2 g dm^{-3}; CEC – R^2=0.60/0.05, RMSE=4.7/7.3 mmolc dm^{-3}; V% – R^2=0.28/-0.02, RMSE=7.2/8.6 %; moisture – R^2=0.85/0.20, RMSE=0.003/0.008 g kg^{-1}. Validation results for the area 2 (validation set = 50 samples, laboratory/field): organic matter – R^2=0.12/0.43, RMSE=2.5/2.0 g dm^{-3}; CEC – R^2=0.41/0.33, RMSE=5.8/6.2 mmolc dm^{-3}; V% – R^2=0.65/0.38, RMSE=10.9/14.5 %; moisture – R^2=0.63/0.30, RMSE=0.008/0.011 g kg^{-1}. In addition, the predicted values of the soil properties were used to calculate lime requirement for each area. Comparison between measured and predicted values of lime requirement (for V=85%; validation set = 50 samples; laboratory/field): area 1 - R2=0.21/0.05, RMSE=0.507/0.555 Mg ha^{-1}; area 2 - R2=0.61/0.35, RMSE=1.050/1.360 Mg ha^{-1}. Soil samples under laboratory conditions were probably more homogenous than the soil was in the field. So, the results indicate that with standardized samples it is possible to achieve better predictions. Also, the lime requirement was better predicted in the area 2 (clayey soil) for both spectral data sets. It can be concluded that field measurements helped to depict the soil variability, however this kind of spectral data do not allowed accurate predictions of soil properties, like laboratory spectral data did in some cases.

Building a soil spectral library for Tajikistan comparing local and global modeling approaches

C. Hergarten[1*], F. Nazarmavloev[2], B. Wolfgramm[1,2]

[1]*Centre for Development and Environment, University of Bern, Switzerland*
[2]*Mountain Societies Research Center, University of Central Asia, Bishkek, Kyrgyzstan*
[*]*E-mail: christian.hergarten@cde.unibe.ch*

Abstract

Over the last ~20 years, soil spectral libraries storing near-infrared reflectance (NIR) spectra from diverse soil samples have been built for many places, since almost 10 years also for Tajikistan. Many calibration approaches have been reported and used for prediction from large and heterogeneous libraries, but most are hampered by the high diversity of the soils, where the mineral background is heavily influencing spectral features. In such cases, local learning strategies have the advantage of building locally adapted calibrations, which can deal better with nonlinearities. Therefore, it was our major aim to identify the most efficient approach to develop an accurate and stable locally weigthed calibration model using a spectral library compiled over the past years.

Keywords: Tajikistan, Near-Infrared spectroscopy (NIRS), soil organic carbon, locally weighted regression, regional and local spectral library.

1 Introduction

Since the collapse of the Soviet Union, soils are poorly managed in Central Asia. Therefore, monitoring of soil properties is an important issue. However, lack of laboratory capacities makes it very difficult to implement operational soil monitoring. Therefore, soil spectroscopy provides an efficient, promising and cost saving approach to tackle such challenges. The use of NIR spectroscopy has become cheaper, leading to its use in many new fields of technology and science. Classical calibration approaches encompass partial least Square regression (PLSR) and principal component regression (PCR), which have been successfully applied in many mostly local studies. In order to cope with the increasing size and heterogeneity of growing spectral libraries, the use of more flexible modeling tools have been proposed. Artificial neural networks (ANN), adaptive regression splines (MARS) or support vector regression (SVR) have been reported to deal better with nonlinearities. Many studies have shown that nonlinear approaches result in better predictive capacities especially when used with large spectral libraries. Recent work has shown promising results also for a variety of local calibration models.

In this study, we focus on a local modeling approach which builds on locally linear calibrations known as locally weighted regression (LWR) (Naes et al. 1990).

2 Materials and methods

A total of 725 soil samples have been collected from agriculturally used areas in Tajikistan, covering six different locations with varying climate and mineral composition. 317 samples originate from three relatively fertile loess areas in western Tajikistan (cf. Figure 1), and 408 samples from three cool and less productive mountain valleys in the eastern part of the country with shallow soils. Generally, the samples cover very low contents of organic carbon (0.05-0.15 g/kg), but come from very diverse geological backgrounds, which reportedly is a challenge for calibration model development.

Figure 1. Study site locations in Tajikistan.

Due to insufficient capacity of local soil chemical laboratories, all samples were sent to facilities abroad (Moscow, MSU and Nairobi, ICRAF) for chemical analysis of soil properties.

All samples were grounded to 2mm particle size and spectrally measured twice using a ASD FieldSpec VNIR spectrometer. Replicate spectra were checked, averaged and resampled to 10nm resolution. The full range spectra (350-2500nm) were used for further processing, as proposed (Viscarra Rossel 2009). The sample set was checked for chemical and spectral outliers using robust detection methods (Varmuza and Filzmoser 2008). While finally no spectral outliers were removed from the dataset, 12 samples with unusually high SOC values reportedly belonging to a different soil population. In order to prevent biased validation results, calibration (~70%) and validation (~30%) samples were separated using a conditioned latin hypercube sampling (CLHS) scheme (Minasny & McBratney 2010). In addition to preserving the integrity of the sampling profiles, the CLHS algorithm was found to produce less biased splits than the Kennard-Stone algorithm. After pretreatment of the spectra (mean scatter correction* and 2^{nd} derivative Savitzky-Golay filtering**), calibration models were first developed locally site-wise and

consecutively merged based on PCA analysis to larger models, following a global modeling approach using partial least square regression (PLSR) and support vector machine regression (SVMR). Apart from a global modeling strategy, also a local modeling approach was tested using locally weighted regression (LWR) (Naes et al. 1990). PLSR and SVMR models were developed using a conventional cross-calibration procedure. LWR models, which can handle non-linearity in the data by selecting a subset of the calibration data (local training samples) to create a localized model for a new sample. The samples which are closest to a new sample are identified in the PCA space. LWR models are built using the number of components used for the local selection model, and the number of local samples selected as local points. Various options exist for selecting locally nearest samples (Gogé et al. 2012). In the case of LWR, two models are reported in table 2, which correspond to different local sample selection algorithms applied. LWR(x) only uses the spectral x matrix for identifying nearest samples, while LWR(xy) also uses the y dimension. The algorithm applied in the latter case tries to select samples which are near in the PCA space but which also have similar y-values. This is achieved by repeating the prediction step multiple times. In a first step, samples are selected only in the PCA space. Then, in a next step, predicted y-value of the new sample and the measured y-values of the calibration samples are compared to identify the closest samples. These two model parameters were optimized stepwise using cross validation, and in the final step the best models (RMSEP) were used to predict the samples kept aside for validation purposes.

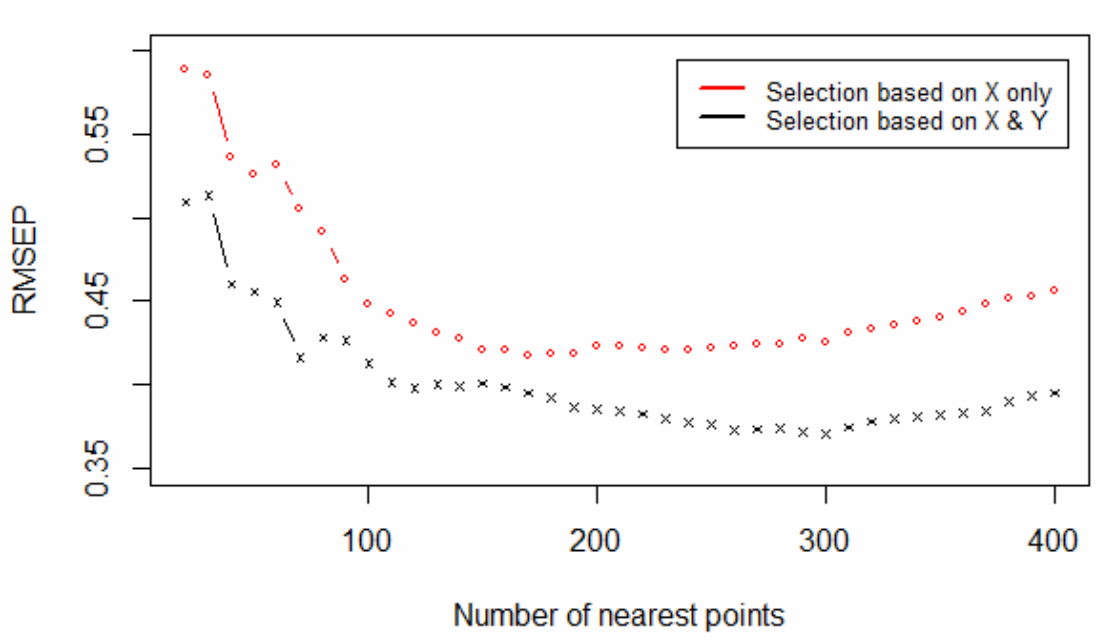

Figure 2. Parameter optimization (number of nearest points) for the two LWR models

The results for all models were finally compared and evaluated in terms of accuracy (RMSEP) and robustness (RPD), which are given in table 1.

3 Results

Due to the diverse nature of the samples collected, the development of a regional spectral library suffered from the high heterogeneity of the soil sample set. While site-wise calibration models performed in an expected range, regional spectral libraries tend to be less accurate and less stable. The results for the regional calibration models ("western set" and "eastern set") as well as for the overall model ("full set") are listed in the table below. While on the sub regional level PLSR and especially SVMR perform satisfactorily and are even outperforming LWR, the local modeling approach excels on the full set (regional) level.

Table 1. Model performance properties

	PLSR	SVMR	LWR(x)	LWR(xy)
RMSEP				
- western set	0.38	0.34	0.43	0.35
- eastern set	0.43	0.31	0.39	0.36
- full set	0.45	0.38	0.42	0.37
R^2				
- western set	0.65	0.70	0.65	0.69
- eastern set	0.61	0.80	0.68	0.74
- full set	0.61	0.71	0.68	0.73
RPD				
- western set	1.75	1.96	1.80	1.89
- eastern set	1.68	2.33	1.85	2.02
- full set	1.5	1.79	1.63	1.84

The listed results correspond largely to our expectations and are also in line with results reported from other authors and studies in the region (Wolfgramm 2007, Seiler et al. 2007), but also globally (Terhoeven-Urselmans et al. 2010, Shepherd and Walsh 2002). PLSR models are known to lack the ability to model data with strongly non-linear structures, and the advantage and flexibility of SVMR models over PLSR is visible on all levels. On the full set level, LWR is performing as good as SVMR and in the case of LWR(xy), it is even outperforming all the global approaches.

4 Conclusions

Based on the results presented here, we tend to conclude that in our case, the best strategy to predict organic carbon from our regional spectral library is to use a local modeling approach on the full set spectral library.

However, recent research by other authors suggests that further improvements might be achieved in accuracy and stability by applying more advanced memory based learn-

ing algorithms and locally nearest calibration sample selection strategies (Ramirez-Lopes et al. 2013, Gogé et al., 2012).

References

GOGÉ, F., JOFFRE, R., JOLIVET, C., ROSS, I., RANJARD, L. 2012. Optimization criteria in sample selection step of local regression for quantitative analysis of large soil NIRS database. Chemometrics and Intelligent Laboratory Systems 110, 168–176.

MINASNY, B., MCBRATNEY, A. 2006. A conditioned Latin hypercube method for sampling in the presence of ancillary information. Computers & Geosciences 32, 1378–1388.

NAES, T. ISAKSSON, T., KOWALSKI, B.R. 1990. Locally Weighted Regression and Scatter Correction for Near-Infrared Reflectance Data, Anal. Chem. 62, 664-673.

RAMIREZ-LOPEZ, L., BEHRENS, T., SCHMIDT, K., STEVENS, A., DEMATTÊ, J., SCHOLTEN, T. 2013. The spectrum-based learner: A new local approach for modeling soil vis–NIR spectra of complex datasets.

SEILER, B., KNEUBÜHLER, M., WOLFGRAMM, B., ITTEN, KI. 2007. Quantitative assessment of soil parameters in western Tajikistan using a soil spectral library approach. 10th Intl. Symposium on Physical Measurements and Spectral Signatures in Remote Sensing (Schaepman ME, Liang S, Groot NE, Kneubühler M (eds)), Intl. Archives of the Photogrammetry, Remote Sensing and Spatial Information Sciences 36 (7/C50): 451–55. ISPRS, Davos. http://tinyurl.com/cv8z5k7

SHEPHERD, K.D., WALSH, M.G. 2002. Development of Reflectance Spectral Libraries for Characterization of Soil Properties. Soil Science Society of America Journal 66, 988–998.

STENBERG B, NORDKVIST E, AND SALOMONSSON L. 1995. Use of near infrared reflectance spectra of soils for objective selection of samples. Soil Science 159: 109–14.

TERHOEVEN-URSELMANS, T., VAGEN, T.G., SPAARGAREN, O., SHEPHERD, K.D. 2010. Prediction of soil fertility properties from a globally distributed soil mid-infrared spectral library. Soil Science Society of America Journal 74, 1792–1799.

VARMUZA, K., FILZMOSER, P. 2008. Introduction to multivariate statistical analysis in chemometrics. CRC Press, Taylor & Francis Group, Boca Raton.

VISCARRA ROSSEL, R., SOIL SPECTROSCOPY GROUP. 2009. The Soil Spectroscopy Group and the development of a global soil spectral library. EGU General Assembly Conference Abstracts 11, p. 14021, April 2009.

WOLFGRAMM, B., SEILER, B., KNEUBUEHLER, M., LINIGER, H.P. 2007. Spatial assessment of erosion and its impact on soil fertility in the Tajik foothills, EARSeL eProceedings 6 (1): 12–25. http://tinyurl.com/d62uj3s

Part field management: comparison of EC-value, soil texture, nutrient content and biomass in two selected fields

S. Hinck*, N. Emeis, K. Mueller

University of Applied Sciences Osnabrueck, P.O.B. 1940, 49009 Osnabrueck.
**E-Mail: s.hinck@hs-osnabrueck.de*

Abstract

We report on a practical method to generate a small scale field map for use in precision farming. Although this method is not new in theory it is not in actual use today. We start from electrical conductivity values (EC-values) obtained from on-the-go measurements using a geoelectric test set. Those EC-values are then used to define partial areas through cluster-analysis. Subsequently the soil types in the partial areas are determined using an auger sampler and finger testing. Usually different classes of EC-values correspond to different soil types. In the defined partial areas the biomass and the pH-value have been measured together with the content of phosphorous, potassium and magnesium from samples taken at depths of 0 - 30 cm and 30 cm - 60 cm, respectively. The obtained results are well explained by the different soil types.

Keywords: digital soil mapping, geoelectric conductivity (EC), type of soil, part field management, nutrient content.

1 Introduction

A correlation between the EC-value of a soil and the soil type is well known. The storage capacity for water and nutrients is strongly related to the clay and organic matter content of soil (Scheffer & Schachtschabel 2010). Electrolytic conductivity due to a high water and nutrient content causes a high EC-value (Keller and Frischtknecht 1977). According to these observations partial areas with different EC-values may not only differ in their soil types but also in their nutrient content. Finally the biomass formation should be influenced by the water and nutrient capacity. Based on the obtained measurement results partial areas may be defined using cluster analysis (Altenhoff et al. 2012). The cluster classes represent areas showing certain EC-value ranges with different soil types (Hinck et al. 2006). Following the clustering, a relatively small number of auger samples in the identified partial areas have been taken. At the different locations the soil type is determined using a finger test and the soil horizon is registered. Within the context of this work, we have not done a systematic sampling on a fixed grid or a random choice of sampling locations.

2 Materials and methods

2.1 Test field

The examinations have been performed on the agricultural crop land “Bloecken” with a size of 5.5 ha and “Eschkorn” with a size of 11.7 ha. Both areas are located in the community “Ebersdorf” in the northwestern part of Germany, in the Elbe-Weser region. The formation history is glacially (glacial loams and glacial sands) and Holocene (moor) affected. The test fields were farmed with maize.

2.2 Used geoelectrical measurement systems

Table 1 specifies the used geoelectric measurement systems and the related depths of measurement.

Table1. Used measurement systems and their depths of measurement

System	measurement mode	depth from surface
EM38	horizontal mode	0 – 60 cm
Veris 3100	measurement set-up shallow	0 – 30 cm
Veris 3100	measurement set-up depth	0 – 90 cm
BOs-1EP	direct measurement in the top soil	0 – 15 cm

2.3 Soil analysis and biomass determination

Soil samples from depths of 0 - 30 cm and 30 - 60 cm have been collected from the partial areas. Their respective phosphorous (P; CAL-method), potassium (K; CAL-method) and magnesium contents (Mg; $CaCl_2$ method) as well as their pH-values ($CaCl_2$ method) have been determined. The number of maize plants and their biomass has been determined at each sample location. To this end all maize-plants on an area of 3 m^2 have been harvested, counted and weighed.

2.4 Processing of obtained data

The GIS-program OPENJump has been used for the data processing and the cluster analysis (K-mean value method) (Brüning et al. 2007). The specific locations for the sampling using an auger sampler have been chosen following the cluster analysis. The soil type has been determined by finger test.

3 Results

As an example for our findings we present the measurement results obtained using the “Veris 3100” (measurement set-up shallow) system. The spatial distribution of the determined EC-values in the two test fields are shown in fig. 1. Using these EC-value a cluster analyses has been done. As displayed in fig. 2 the field “Bloecken” is subdivided into two cluster-classes while the test field “Eschkorn” is grouped into four cluster-classes. To determine the soil-types correlated to the cluster-classes we used finger tests. Within the field “Bloecken” cluster-class 1 correlates with sand while cluster-class 2 indicates loamy sand. One exception from these findings shows up at the sampling location 1 (s. fig. 3) where the soil type is sand. That special place has been used as a deposit site for an extended period of time. Regarding the test field “Eschkorn” cluster-class 1 mostly correlates with sand.

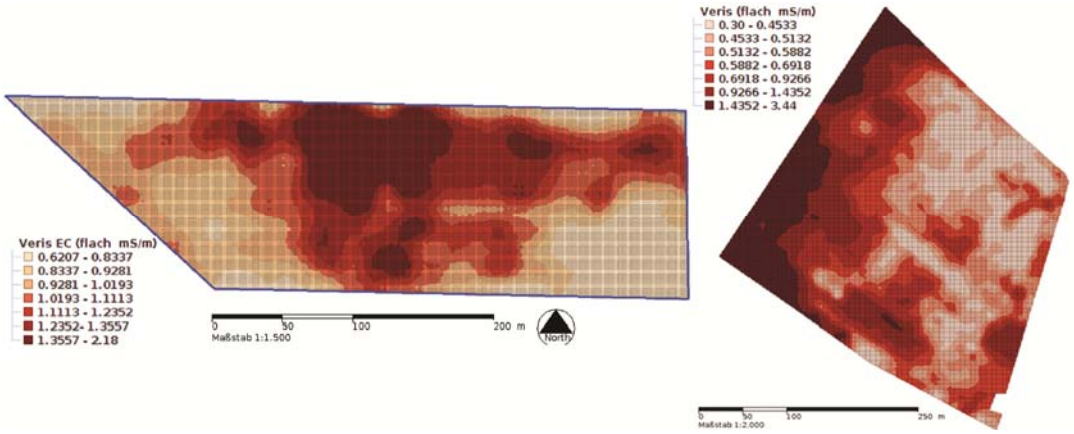

Figure 1. EC-value Veris / shallow (0 – 30 cm measurement depth), above: field „Bloecken“, bottom: field „Eschkorn“

Cluster-class 2 indicates humus rich sand or a transition region between sand and peaty sand. In areas with cluster-classes 3 and 4 predominantly peaty sand has been found (s. fig. 4).

Based on the cluster analysis and the auger sampling a small scale soil map has been generated. Additional information from the EM38 and the BOs-1EP systems as well as from additional soil maps has been used. The cluster classes show the following correlations with soil types:

Field „Bloecken“:
cluster 1 (Ø 0,92 mS/m): sand
cluster 2 (Ø 1,37 mS/m): loamy sand

Field „Eschkorn“:
cluster 1 (Ø 0,55 mS/m): sand
cluster 2 (Ø 0,86 mS/m): sandy soil with high content of organic matter or peat
clusters 3 (Ø 1,34 mS/m) and 4 (Ø 2,2 mS/m): peaty sand. (s. fig 5)

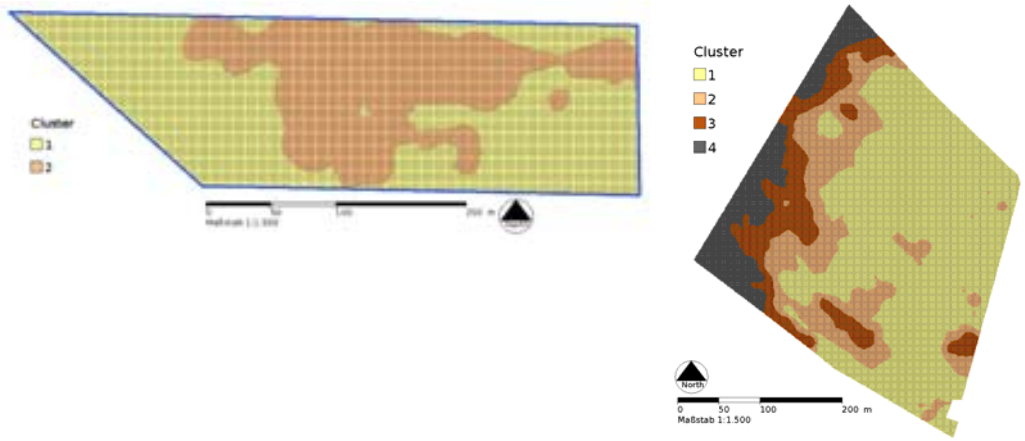

Figure 2. Cluster analysis, left site: field „Bloecken“; right site: „Eschkorn“

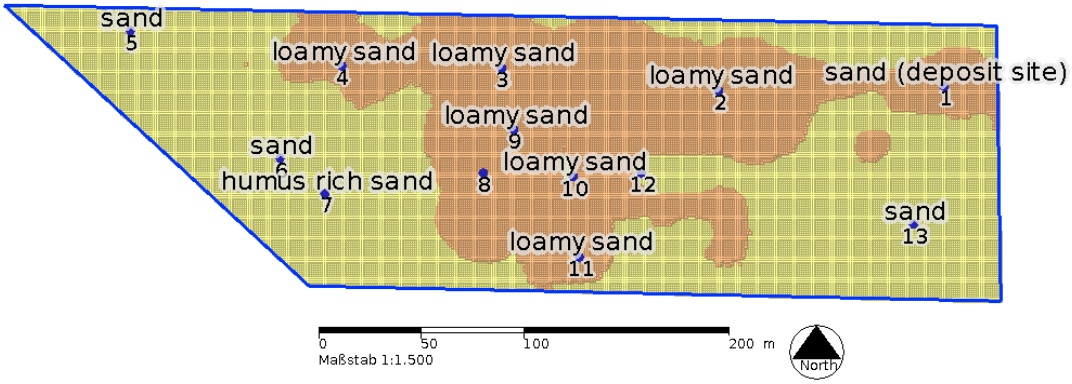

Figure 3. Cluster classes and mapped soil type (0 – 30 cm), field „Bloecken“

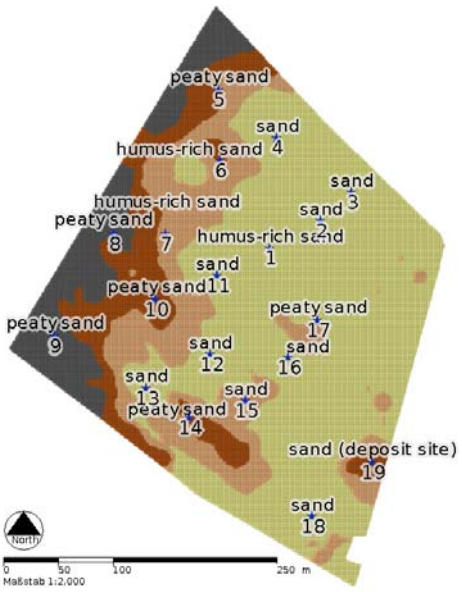

Figure 4. Cluster classes and mapped soil type (0 – 30 cm), field „Eschkorn“

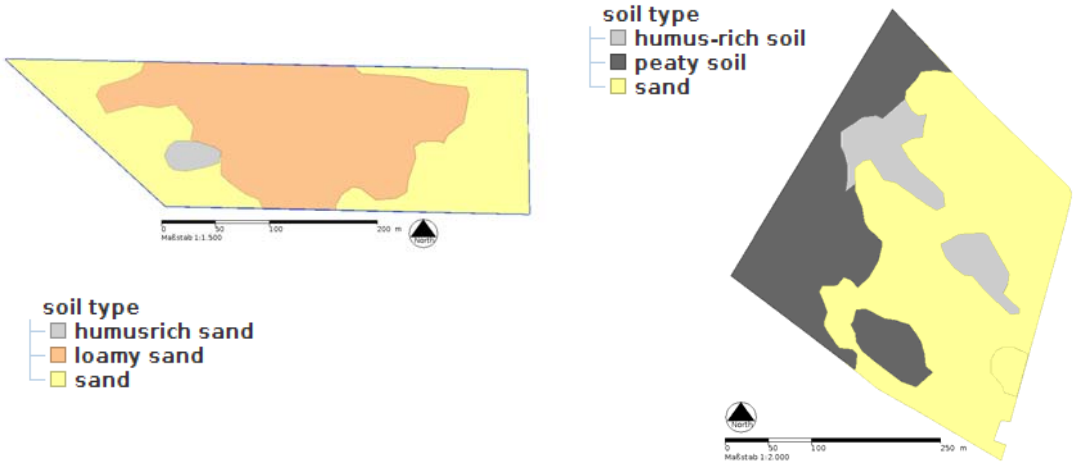

Figure 5. Small scale field map with the soil type of the topsoil, left site: field „Bloecken“; right site: field „Eschkorn“

Due to the sowing density, the number of plants per area was approximately nine plants/m^2. This density could be observed in all partial areas on both test fields. In contrast to this even distribution of plants, the biomass in the sandy areas was significantly lower than in the other partial areas. On the test field “Bloecken” the average value for the biomass was 7 kg/m^2 and on the field “Eschkorn” 5 kg/m^2. Regarding the yields from the partial areas, the biomass from the field “Bloecken” was 9 kg/m^2 for loamy sand. This was considerably more than 7.5 kg/m^2 to 8.5 kg/m^2 as obtained from the field “Eschkorn” for peaty sand.

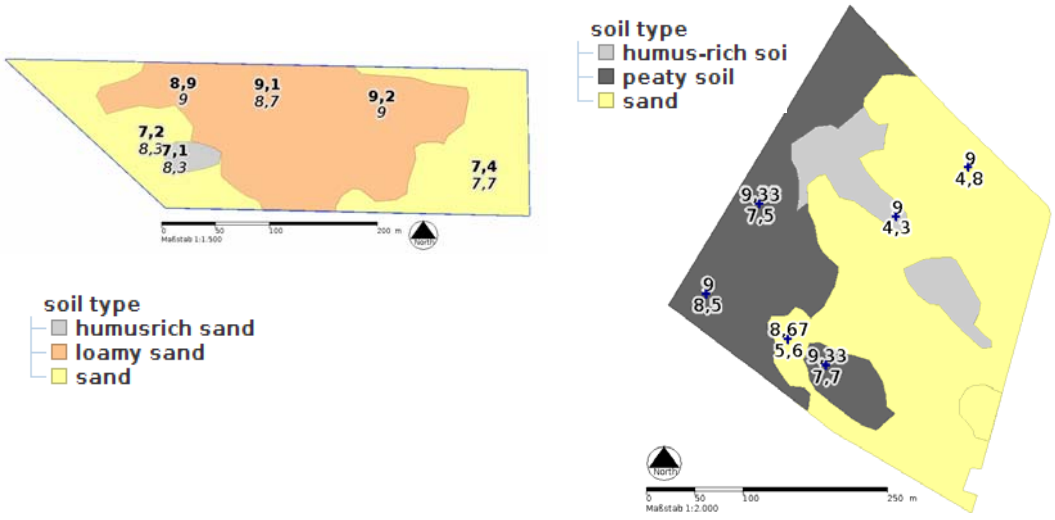

Figure 6. Small scale field map with the soil type of the topsoil and the counted (value above) and weight plants per m^2 (value bottom), left site: field „Bloecken“; right site: field „Eschkorn“.

Partially due to the used cultivation techniques the nutrient contents of the two test fields are different. The areas with loamy sand in the field “Bloecken” exhibits less potassium in the top soil (0 cm - 30 cm) than the areas with sand. This can be explained by withdrawal because of the higher values of biomass in loamy sand. Looking at the potassium content in the partial areas for depths of 30 cm to 60 cm the proportions are opposite. Potassium in sand may be washed out easily, leading to low potassium contents in the soil. The phosphorous values in comparison do not vary that much. The determined magnesium contents at depths of 30 cm to 60 cm follow the same tendencies as the potassium contents. Here a wash out effect from sand can be seen as well.

The pH-value in the top soil is too low for farming. Concerning the soil type, the pH-value in the loamy sand areas should be increased by a higher amount than the respective value in the sandy areas (see fig. 7).

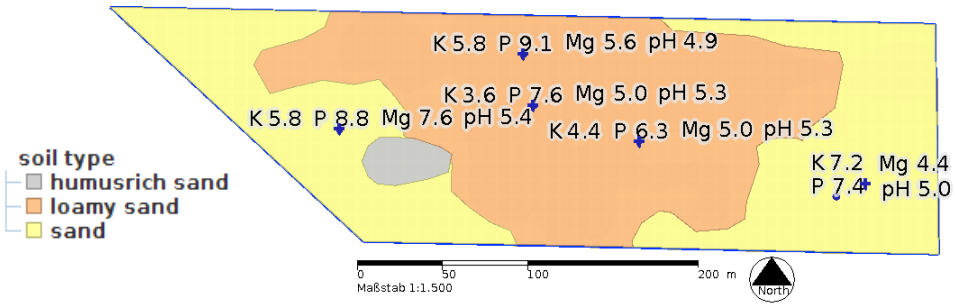

Figure 7. Small scale field map with the soil type of the topsoil and the nutrient content: K, P, Mg and pH-Value; field “Bloecken”

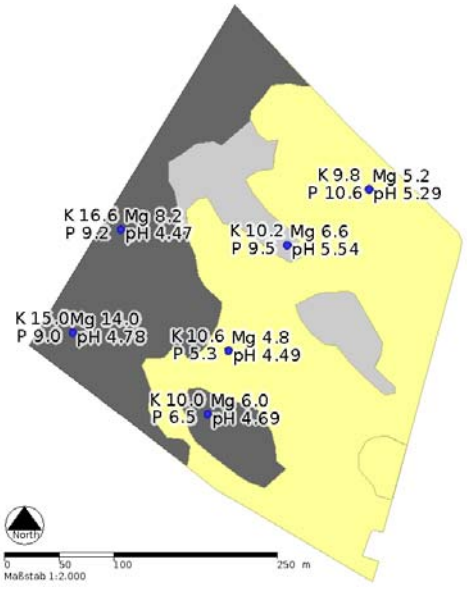

Figure 8. Small scale field map with the soil type of the topsoil and the nutrient content: K P, Mg and pH-Value; field “Eschkorn

In the field “Eschkorn” the nutrient situation is different because of peaty sand as the soil type. The mobilization and fixing of nutrients in organic soils follows different rules than in mineral soils. This has to be considered for fertilization. The field “Eschkorn” is uniformly manured using potassium, phosphorous and magnesium there are high plant available nutrient concentrations in the partial areas with peaty sand. The sandy areas are at least adequately supplied with nutrients. In the sandy partial areas the pH-values are higher than in the areas with peaty soil. A differentiated liming has not been applied. A partial area specific liming resulting in a optimal pH-values (pH: 4,2) in the peaty sand would reduced the unproductive mineralization of organic mass. (s. fig. 8)

4 Discussion and Conclusions

It is well known that the EC-values found by geoelectrical means differ within a given area. These different values may be classified using cluster analysis. Usually those different cluster-classes are related to differences in the soil types. Within this work these facts have been largely verified using a combination of on-the-go geolelectric test sets and classical sampling using an auger and subsequent finger tests.

Different soil types result in different biomasses obtained from a given area. This may be explained by different water and nutrient retention capabilities of the soils. The nutrient content depends on the nutrient withdrawal by the plants. Regarding the potassium and magnesium contents an additional wash out effect has to be considered. This is exemplified specifically clear for potassium in the field “Bloecken”. In the field “Eschkorn” the nutrient situation is different because of the predominant high organic matter content of the soil.

By using the described combination of on-the-go geolelectric measurements and following directed classical auger sampling a reliable subdivision of a field into partial areas with different soil types is feasible. The directed auger sampling reveals different nutrient contents in the partial areas. In that way the fertilization may be optimized.

Acknowledgement

This project is funded by EFRE (EU & federal state of Niedersachsen (WA3 – 801 25 081).

References

BRÜNING, M., KIELHORN, A., BIERMANN, J., GERVENS, T., RAHN, O. 2007. Statistikwerkzeuge in OpenJUMP - Implementationen der PIROL Edition (statistic tools in OpenJUMP - implementationen at the PIROL Edition), Online-Wiki der FOSSGIS-Konferenz, Humboldt-Universität zu Berlin. Internetadresse: http://www.projekt-pirol.de/uploads/media/Statistik_in_OpenJUMP_01.pdf

ALTDORFF, D., DIETRICH, P. 2012. Combination of electromagnetic induction and gamma spectrometry using K-means clustering: A study for evaluation of site partitioning. J. Plant Nutr. Soil Sci., 175, p. 345–35.

HINCK, S., MUELLER, K., EMEIS, N. CHRISTEN, O. 2006. Development of a multi-sensor system for the low-sample recording of soil properties, S. 892 - 896 in Proceedings of the 17. Conference International Soil Tillage Research Organisation (ISTRO), 28.08.2006 - 03.09.2006 in Kiel.

KELLER, G.V., FRISCHSKNECHT, F.C. 1977. Electrical Methods in Geophysical Prospecting. Pergamon Press, New York.

SCHEFFER&SCHACHTSCHABEL, BLUME, H.-P., BRÜMMER, G. W., HORN, R., KANDELER, E., KOEGEL-KNABNER, I., KRETZSCHMAR, R., STAHR, K., WILKE, B.-M. 2010. Lehrbuch der Bodenkunde (textbook of soil sciences), 16. edition. Spektrum Akademischer Verlag Heidelberg.

Comparison of mobile multi-sensor platforms at the test-site Rosslau in Germany

E. Lück[1*], C. Dierke[2], U. Werban[2], T. Wunderlich[3], S.A. Al Hagrey[3], H. Petersen[3], E. Loonstra[4], J. Rühlmann[5]

[1]*University of Potsdam, Germany, Karl-Liebknecht-Str. 24, D-14476 Golm/Potsdam, Germany*
[2]*Helmholtz Centre for Environmental Research - UFZ, Permoserstraße 15, D-04318 Leipzig, Germany*
[3]*University of Kiel, Otto-Hahn-Platz 1, D-24118 Kiel, Germany*
[4]*The Soil Company, Leonard Springerlaan 9, 9727 KB Groningen, The Netherlands*
[5]*Leibniz-Institute of Vegetable and Ornamental Crops, Grossbeeren, Theodor-Echtermeyer-Weg 1, D-14979 Großbeeren, Germany*
[*]*E-mail: elueck@geo.uni-potsdam.de*

Abstract

In the last decades multi-sensor platforms came into the focus to reduce the ambiguity in the interpretation of soil-sensor-data. In this study we compare electrical conductivity and gamma radiation data from several multi-sensor platforms. These sensor-systems are based on commercial available as well as on recently developed components. The main topic of this study is to compare the relatively new sensor Geophilus (recently a combination of electrical and gamma measurements) with data from well established devices.

Keywords: multi-sensor platform, electrical conductivity, gamma radiation.

1 Introduction

Mobile sensors were developed to get rapidly soil information over large areas with a high data resolution. Site specific parameter transfer-functions are used to translate these sensor data into the needed soil properties. Multi-sensor platforms are applied in order to reduce the ambiguity in the interpretation of soil-sensor-data. Especially both, conductivity and gamma-ray measurements are useful for imaging spatial soil heterogeneity in terms of physical soil parameters (Viscarra Rossel et al., 2007).

The gamma-ray measurement is a passive method because it detects the natural gamma radiation without any artificial source. While some gamma probes determine only the total count, gamma-ray spectrometers use energy-sensitive detectors. Conductivity measurements as an active method can be performed either using an electromagnetic method or working with capacitive or galvanic coupled electrodes. The data and the spatial resolution vary in dependence on the specific methods and sensors applied (Gebbers et al., 2009).

In this study we want to present a comparison of multi-sensor data collected at a test site in Rosslau (Germany). Most data were collected within the iSOIL-project (Werban et al., 2009, van Egmond et al., 2009), an EU-project which was coordinated from the Helmholtz Centre for Environmental Research, Leipzig, Germany.

2 Materials and methods

The field site in Rosslau is located next to the Elbe river and can be characterized by fluvial deposits with varying clay content (5 - 50%) (Petersen et al., 2012). The elevation of the test site increases slowly from 56 m in the south to 58 m in the north. Different multi-sensor platforms (Fig. 1) were tested and soil samples within the depth interval 0-0.7 m were taken at a field with a size of 13 ha. The data density varies in depending on the applied sensor combinations.

a) b) c)

Figure 1. Multi-sensor platforms used in Rosslau. a) Combination of EM38 and GMS-Car, b) Geophilus-system, c) the Mole.

Electrical data were collected

1. using electromagnetic induction method (EM38, EM38-DD and EM31, Geonics)
2. working with rolling electrodes (Geophilus (Lueck and Ruehlmann, 2012), University Potsdam and IGZ Grossbeeren). In order to make data comparable, apparent resistivity data were transformed into apparent conductivities (ECa).

Gamma radiation was measured with

1. commercial gamma-ray spectrometers GMS-Car (GF Instruments, Czech Republic), which consist of a thallium-activated 4 l NaI-scintillation crystal in combination with a real time windows spectrum analysis
2. the Mole (The Soil Company, The Netherlands) containing a 1 liter CsI-crystal and post processing full spectrum analysis
3. a new gamma detector, which is used in combination with the Geophilus-system, which consists of polysterene (volume about 10 l) and measures only the total count.

Unfortunately, the applied gamma sensors have different outputs (Bq/kg, dose rate in nGy/h or total count in cps). A transformation between dose rate and total count is not

possible. Thus the results from different gamma sensors will be compared only qualitatively.

Presented data were collected during several field campaigns. First different experimental setups were tested to optimize the field parameters for further surveys. These measurements were concentrated along two transects covering different soil units (Wunderlich and al Hagrey, 2008). Additional mobile surveys were carried out for the whole field (Fig. 2) and on subareas representing the different soil units of the site. The location of the above transect is marked in Fig. 2c.

3 Results

The conductivity as well as the gamma maps confirm once again the stability of the geophysical data. The correlation coefficients 'r' for all conductivity maps vary between 0.86 and 0.98 and also the gamma data show a strong correlation with r = 0.97 between different sensors at several dates. All maps image similar pattern of heterogeneity (Fig. 2). The field can be subdivided into two main regions with a strong differentiation between the glacio-fluvial series in the NW (low conductive area, ECa about 10 mS/m) and the alluvial soil in the SE (ECa mean value of 30 mS/m in the subsoil). This differentiation is not only visible in geophysical data but also obvious in other soil parameters like soil moisture and texture (sand content of about 80% in the North und 20% in the South).

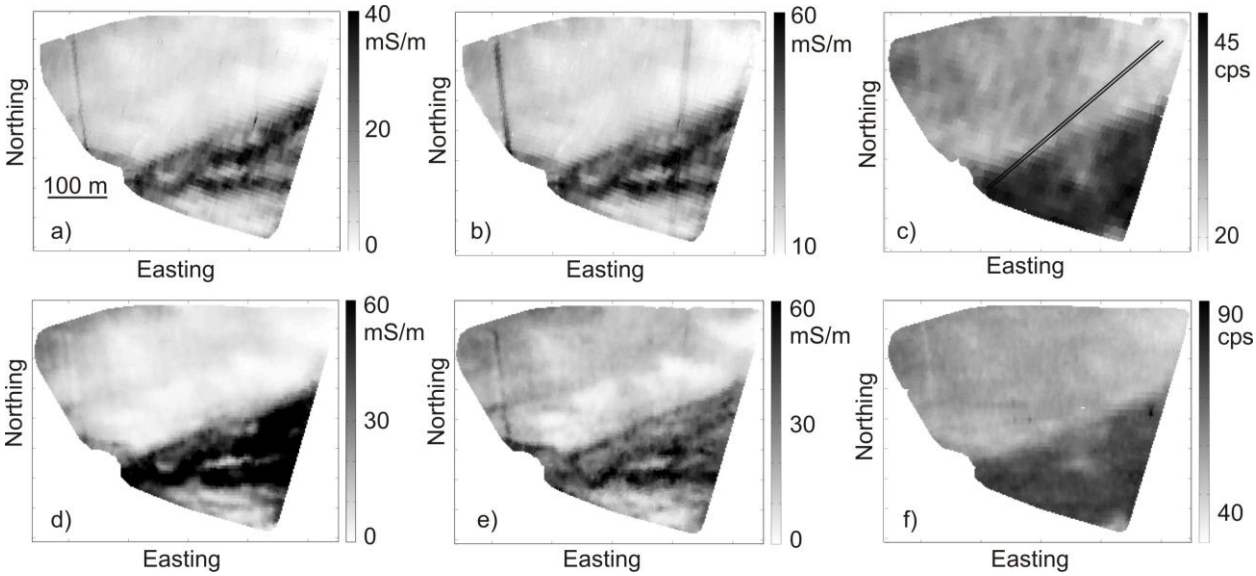

Figure 2. Interpolated conductivity and gamma data from different multi-sensor platformsa) EM38 - horizontal dipole, b) EM38 - vertical dipole, c) GMS-Car - dose rate, d) Geophilus - channel 1, e) Geophilus - channel 5, f) Geophilus - total count. The location of the test transect is given in Fig. 2c.

In a next step the individual gamma data of the used multi-sensor platforms are compared along the transects. While the total count and dose rate data show good correlation for all sensors (0.68 - 0.98), the correlation coefficients vary for the observed spectral windows. Thorium data were also highly correlated (0.61 - 0.87), but Uranium and Potassium showed only an intermediate to poor correlation (U (0.56 - 0.08) and K (0.48 - 0.08)). The correlation coefficients also reveal that the spectrometer of the Soil Company achieves the best repeatability of total count superior to GMS-Car systems. The mapping reliability for Th, K and U was determined to be similar for all three systems. As expected, the spectrometers of the same type show similar correlation coefficients for their measurements.

4 Discussion

Environmental conditions as well as measurement speed have to be considered when data from different methods and sensors should be compared. Weather and soil conditions have an influence on the absolute values of the signal and therefore also on the data quality. For example, measurements from different dates indicate differences in the distribution of soil moisture. Not only the absolute conductivity values but also the spatial patterns and the ratios between the information from several depths may change. In Rosslau both, the EM38 and the Geophilus indicate an increase of ECa with depth. Especially the Geophilus sensor can resolve this well, because it delivers data from five depth levels (channel 1 - channel 5) between 0 and 1.5 m.

The used sensor combinations get information from different depths. Whereas gamma data are mostly influenced by the topsoil, electrical measurements often look deeper. The strongest correlation between gamma data and ECa can be observed for the Geophilus-system. This may be caused by the depth sensitivity of the used methods.

Differences between the existing gamma sensors result from the types and the volumes of the applied crystals as well as from the data processing. Because of its high efficiency, the total count polysterene detectors allow to measure with 0.1 s sampling interval resulting in a high lateral resolution. While the 'total count' measurement only summarizes all radiation within the observed energy window (0 to 3 MeV), the Window Analysis Method allows to distinguish between the radioelement concentrations of K, U and Th and to consider the ratios between these windows. Full Spectrum Analysis (FSA) can be applied to extract more detailed information.

5 Conclusions

The similarity between all conductivity and also between the gamma radiation maps is evident. The data reflect mainly the soil heterogeneity, but also two N-S striking linear elements caused by man-made features. The sensitivity to these objects depends on the applied sensors.

Acknowledgements

We would like to thank the companies 'radic research' and 'BLM Storkow' for their assistance with the sensor development.

References

EGMOND VAN, F.M., NÜSCH, A.-K., WERBAN, U., SAUER, U., DIETRICH, P. 2009. iSOIL: Exploring the soil as the basis for sustainable crop production and precision farming. In: Precision agriculture '09. Joint International Agricultural Conference- JIAC, edited by E. van Henten, D. Goense and C. Lokhorst, pp. 493-499.

GEBBERS, R., LÜCK, E., DABAS, M., DOMSCH, H. 2009. Comparison of instruments for geoelectrical soil mapping at the field scale. Near Surface Geophysics, pp. 179-190.

LUECK, E. RUEHLMANN, J. 2012. Resistivity mapping with GEOPHILUS ELECTRICUS — Information about lateral and vertical soil heterogeneity. Geoderma. (in press)

PETERSEN, H., WUNDERLICH, T., AL HAGREY, S.A., RABBEL, W. 2012. Characterization of some Middle European soil textures by gamma-spectrometry. J. Plant Nutr. Soil Sci., pp. 1-10.

VISCARRA ROSSEL, R.A., TAYLOR, H.J., MCBRATNEY, A.B. 2007. Multivariate calibration of hyperspectral γ -ray energy spectra for proximal soil sensing. European Journal of Soil Science 58, pp. 343–353.

WERBAN, U., BEHRENS, T., CASSIANI G., DIETRICH P. 2009. iSOIL – An EU-level Project to Integrate Geophysics, Digital Soil Mapping and Soil Science. In: Proximal Soil sensing, edited by R.V. Rossel, A. McBratney and B. Minasny, pp. 103-111.

WUNDERLICH, T., AL HAGREY, S.A. 2008. First comparative measurements between geophysical platform sensors, Rosslau, Germany. iSOIL Project Technical Report.

The integration of on-the-go measurements of soil apparent electrical conductivity in an objective and probabilistic model for measuring soil fertility potential in an agricultural field

F.J. Moral[1*], F.J. Rebollo[1], J.M. Terrón[2], J.R. Marques[3]

[1]*Universidad de Extremadura, Departamento de Expresión Gráfica, Badajoz, 06006, Spain*
[2]*Centro de Investigación "La Orden - Valdesequera", Gobierno de Extremadura, Spain*
[3]*Universidade de Évora, Departamento de Engenharia Rural, Portugal*
[*]*E-mail: fjmoral@unex.es*

Abstract

With the aim of quantifying the overall soil fertililty potential in an agricultural field, integrating the main soil physical and chemical properties (clay, silt and sand content, organic matter, pH, total nitrogen, available phosphorus and potassium, cation exchange capacity, and apparent electrical conductivity, ECa), measured at 70 locations, we propose using the ECa obtained with a 3100 Veris sensor, operating in both shallow (0-30 cm), and deep (0-90 cm) mode, as an essential information to be included in an statistical model, the Rasch model. The main outputs include a ranking of all locations according to their fertility potential and anomalies in any location or property.

Keywords: Rasch model, soil apparent electrical conductivity, precision agriculture.

1 Introduction

Quantifying soil fertility in a meaningful way is very problematic. In order to estimate it, three main problems can be distinguished: i) What shall we measure? ii) How do we interpret the data? iii) How can we derive a statement about soil fertility based on the data? The requirements of plants should be met from the elements contained in the soil; thus, initially, it has a fertility potential, but some other soil properties are important in determining a soil's inherent fertility. Generally, the long-term productivity of a soil is greatly influenced by its cation exchange capacity, CEC. The makeup of a soil (soil texture) and its acidity (pH) determine the extent to which nutrients are available to plants. Moreover, soil texture and CEC are related; for instance, soils with high CEC usually have high clay content. However, an ideal soil should contain equivalent portions of sand, silt, and clay, to facilitate the agricultural works. Soil apparent electrical conductivity (ECa) is another soil property closely related to some important physico-chemical properties influencing crop yield across a wide range of soils (e.g., Sudduth et al., 2005). High correlation coefficients have been found between ECa and other variables related to soil fertility as CEC and pH (e.g., Moral et al., 2010). If soil texture properties, CEC, pH, primary nutrients availability and apparent electrical conductivity

(ECa) are considered, it seems that a rational indication about the soil fertility potential can be obtained. However, how do we combine these variables? It seems like a puzzle with pieces out of different pictures; the pieces do not match, no picture emerges.

With the aim of considering and summarizing data from different variables, the Rasch model (Rasch, 1980), which is a statistical measurement model (item response model), constitutes a promising technique. In a previous work, Moral et al. (2012) used the Rasch methodology integrating soil texture properties and ECa to analyse the soil fertility potential. In this case study we propose using more soil properties and analyse the response of the Rasch model to estimate with a rational basis the soil fertility potential, and interpret the outputs of the model as it can generate a striking information to properly manage the field.

2 Material and methods

2.1 The Rasch measurement model

The Rasch model, as a measuring method can be an important and innovative tool to determine soil fertility potential (in the sense the crop production potential is influenced by soil fertility). This latent variable model is based on the mathematical modelling of the behaviour resulting from the iteration of a subject with its item (Tristán, 2002). The purpose of this procedure, in this case study, is to consolidate several heterogeneous measures of soil properties into an overall variable that simplifies interpretation of soil fertility potential. Thus, the Rasch model constructs a line of measurement with the items placed hierarchically on this line according to their importance to subjects. One way to form a single synthesis of the items, which are expressed in different measurement units, is by means of a common referent, latent variable, that holds them all together (soil fertility potential). To achieve an adimensional characterization, first the data corresponding to the considered individual soil properties are categorized. In particular, 5 categories are established for all properties; a measure assigned to level 0 indicates the lowest contribution to soil fertility potential and, on the contrary, a measure assigned to level 5 indicates the highest contribution to soil fertility potential. Through this numerical manipulation, independent scale quantities can be expressed as common ratings ranging from low to high. The data are arranged in matrix form, where the rows are the locations where soil were taken and the columns the soil properties. The Rasch model uses the traditional total score (the sum of the item ratings) as a starting point for estimating response probabilities. Rasch measurement construction applies a stochastic Guttman model to convert rating scale observations into linear measures, to which linear statistics can be usefully applied, and tests for goodness-of-fit to validate its item calibrations and subject measures (Rasch, 1980).

2.2 Soil sampling and data treatment

The field research was carried out at a farm called Cerro del Amo (38º 58' 14" N, 6º 33'394 W, 225 m a.s.l, Datum WGS84), located in the proximity of Badajoz (southwestern Spain), which area is 33 ha approximately. Soil samples were collected using a stratified random sampling scheme from 70 georeferenced places (Moral et al., 2010), and analysed for some soil properties (see Table 1). Deep -ECd- and shallow -ECs- soil apparent electrical conductivity (0-90 and 0-30 cm depth respectively) data for all sampling sites were obtained from different transects of the measurements of soil apparent electrical conductivity conducted using a 3100 Veris (Moral et al., 2010). The formulation of the Rasch model was performed with the WINSTEPS v. 3.69 computer program (Linacre, 2009), which determine the best linear variables for predicting soil potential fertility, supporting by the considered data.

3 Results and discussion

The categorical values were processed by the WINSTEPS program, obtaining a great amount of results in several formats. From the fit statistics, Infit and Outfit mean-square (Linacre, 2009), which expectation is 1, it was obtained that the data fit the model better than expected; both values for soil samples and properties are 0.99. The internal consistency of samples and items, i.e., the degree to which measures are free from error and therefore yield consistent results, are estimated with the separation reliability index (Linacre, 2009); values over 0.70 are considered acceptable. For the data of the present study, their values for samples and items are 0.81 and 0.94 respectively. When individual items were checked, the Infit and Outfit mean-square were between 0.6 and 1.5 (Linacre, 2009). These results (Table 1) demonstrate all considered soil properties support and have an important influence on soil fertility potential; the sand is the only item which values are not in the proposed intervals, but close to their lower limits.

In Fig. 1 the relative distribution of the soil samples and properties is provided. The soil property more to the right in the continuum (Fig. 1), with the highest measure (0.96; see Table 1), is the AK. In consequence, it is the soil property least frequently used to position the samples. On the contrary, to the left, both ECs and ECd are situated, and their measures are practically equal (-0.85 and -0.77 respectively; see Table 1). They are the soil properties most frequently used to position the samples. A ranking of soil samples according to their fertility potential is also available in Fig. 1.

If soil properties are grouped and the mean measure is determined, the most important properties are the ones making up soil apparent electrical conductivity (ECd and ECs), -0.81, followed by texture properties (sand, silt and clay content), -0.27, CEC, -0.17, OM, 0.53, and, finally, the primary nutrients (TN, AP, and AK), 0.69. This provides support for the importance of ECd and ECs as indicators of soil fertility. They both integrates the

effects of various soil variables that govern soil fertility and, so, it seems logical that they are the main source of information about the overall nutritional condition in this soil.

Table 1. Influence of each soil property on the fertility potential in the experimental. Total score, sum of points of the common scale for each soil property considering all samples (70); Measure, position of each soil property along the straight line that represents the latent variable, soil fertility potential

Item	AP	OM	Clay	AK	Silt	CEC	ECd	ECs	TN	Sand
Total Score	174	186	223	164	217	225	258	262	195	251
Measure	0.76	0.53	-0.14	0.96	-0.03	-0.17	-0.77	-0.85	0.36	-0.64
Infit MNSQ	1.36	1.14	1.20	1.13	0.96	1.03	0.90	0.87	0.71	0.56
Outfit MNSQ	1.40	1.24	1.23	1.03	1.04	1.03	0.84	0.81	0.71	0.56

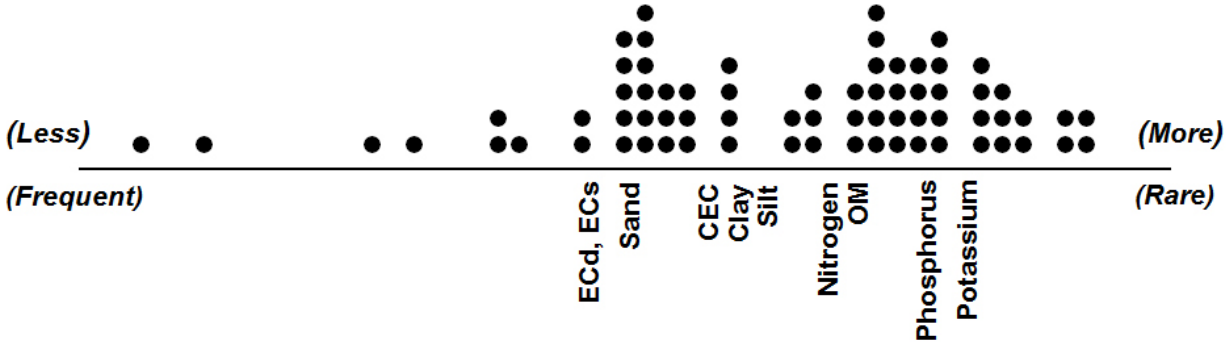

Figure 1: Soil samples and properties in the same scale. The straight line represents the latent variable: soil fertility potential. Distribution of soil samples (points) is above the line: to the right those more potentially fertile; to the left less those less potentially fertile. Soil properties are below the line: to the right less common (rare) properties, with lower importance on soil fertility; to the left more common (frequent) properties, with higher importance on soil fertility.

Table 2. Guttman scalogram for all soil properties (10) and samples (70) considered. Only some sampling points, those with higher and lower fertility potential, are shown

Soil sample	ECs	ECd	Sand	CEC	Clay	Silt	TN	OM	AP	AK
60	5	5	5	5	3	3	5	4	2	5
66	5	5	5	4	4	3	5	4	3	4
...	...	...	...	...	...	...	...	...	...	
31	1	1	1	1	2	2	1	2	2	1
11	1	1	1	1	2	2	1	2	1	1

Soil samples can be sorted according to their measure, displaying those which obtained higher value (the most suitable locations for crops due to their higher fertility potential)

on the top, and the influence of any soil property on each sample can be also showed (Table 2).

4 Conclusions

The use of the Rasch measurement model in soil issues, in this case study to estimate soil fertility potential, constitutes a new application of this method of great practical importance, enabling to rationally determine locations in a field where high soil fertility potential exists and establishing those soil samples or properties which have any anomaly; this information can be necessary to conduct site-specific treatments, leading to a more cost-effective and sustainable field management. The importance of soil apparent electrical conductivity to properly characterize soil fertility in an agricultural field was also highlighted.

Acknowledgements

This research was co-financed by the Gobierno de Extremadura and the European Regional Development Fund (ERDF) through the projects GR10038 (Research Group TIC008) and PRI07B080.

References

LINACRE, J. M. 2009. WINSTEPS (Version 3.69) [Computer Program]. John M. Linacre (Ed.), Chicago, USA.

MORAL, F. J., REBOLLO, F. J., TERRÓN, J.M. 2012. Analysis of soil fertility and its anomalies using an objective model. J. Plant Nutr. Soil Sci., 175 912–919.

MORAL, F. J., TERRÓN, J. M., MARQUES DA SILVA, J. R. 2010. Delineation of management zones using mobile measurements of soil apparent electrical conductivity and multivariate geostatistical techniques. Soil & Tillage Research, 106 335-343.

SUDDUTH, K. A., KITCHEN, N. R., WIEBOLD, W.J., BATCHELOR, W.D., BOLLERO, G. A., BULLOCK, D. G., CLAY, D. E., PALM, H. L, PIERCE, F. J., SCHULER, R. T., THELEN, K. D. 2005. Relating apparent electrical conductivity top soil properties across the North-Central USA. Comp. Electron. Agric., 46 263-283.

RASCH, G. 1980. Probabilistic models for some intelligence and attainment tests. University of Chicago Press., 1960, Denmark. Revised and expanded ed.

TRISTÁN, A. 2002. Análisis de Rasch para todos. Ed. Ceneval. México.

Electrical conductivity analysis of field of highly variable soils

J. Niedźwiecki*, G. Debaene, R. Pudełko

Department of Soil Science Erosion and Land Conservation
** E-mail: jacekn@iung.pulawy.pl*

Abstract

This paper presents electrical conductivity analysis results of soils with high spatial variability. Electrical conductivity (ECa) measurements were taken with the EM38 sensor in Baborówko farm (Western Poland). The objective of the study was to recognise both real spatial variability of soil physical properties and nugget variance, which determines interpolation or interpretation process of such data. Spatial variability was determined in semivariance analyses. Results displayed a great variability of ECa between fields which can be better established using empirical semivariogram. A lag parameter of size 10 meters seems to be optimal for the model semivariogram.

Keywords: electrical conductivity, geostatistical analysis, kriging, spatial variability.

1 Introduction

Effective management of soil resources requires basic information about the spatial distribution of various attributes. Spatial maps of soil properties are invaluable in agriculture for assessing soil quality, planning land use, and determining the suitability of cropping patterns. However, until recently, with the introduction of global positioning systems (GPS) documentation of crop yield and soil variability at field scale was difficult to establish (Sudduth et al, 2005). This, enabled utilisation of a combination of sampling strategies and geostatistics for providing spatial information (Triantafilis & Lesch, 2005). Geophysical methods, such as electromagnetic (EM) induction allow a robust and less expensive approach to gather soil information.

Electromagnetic induction is already a commonly used tool for non-invasive mapping of apparent soil electrical conductivity (ECa). The development of mobile ECa equipment has made it possible to characterise spatial variability of a variety of soil properties both rapidly and cost effectively. ECa data obtained with non-contact Geonics EM38 were documented by Sudduth et al. (2005) who attributed the relationship of ECa data to soil properties. Measurements of electromagnetic soil conductivity by kinematic method allow on-the-go registration (Adamchuck, 2004). Thus, sampling is conducted with a resolution of several meters. Such a large data set may be sufficient for mapping the actual variability of soil physical properties. In the case of high soil mosaic geostatistical analyses are needed.

The purpose of our study was to recognise real soil spatial variability of typical field heterogeneity. Our hypothesis assumed that EC_a sensor working in a continuous registration mode should register real spatial variability, which is not influenced by a nugget effect. Autocorrelation of electrical conductivity for the tested fields was assessed In the second part, a directional variance and the influence of the physical properties of soil was included.

2 Materials and Methods

Data were collected in Baborówko, western Poland (52.58^{O} N; 16.64^{O} E). Soil electrical conductivity was measured with the EM-38 sensor (Geonics Limited, Canada). The distance between passing ways was about 10-12 m. Geostatistical analyses were performed with the Geostatistical Analyst extension of ArcGIS 9.3 software. Semivariance of the data set and directional semivariance were analysed. Experimental semivariograms were modelled by changing lag size parameter of spherical function. The other parameters were calculated automatically. Prediction errors (root mean square error – RMSE) were evaluated by cross validation method of ordinary kriging algorithm.

3 Results and discussion

Based on preliminary modelling of semivariogram's properties, we conclude that a spherical function in comparison to other functions is characterised by a lack of trends in pursuit of function course to achieving low values (nugget effect) and clear sill value. For this reason, it is more sensitive to the analysis of variance random participation into total variance and allows the assessment of the range of data's autocorrelation (parameter "sill").

3.1 Changeability of omni-directional variations

Spatial autocorrelation analyses of the sampled data set were performed separately for each field by using semivariogram for lag size eq. 5, 10 and 20 m with the assumption of ten lag numbers (Figure 1).

Table 1 shows the main parameters of the semivariogram function. The course of a function for lag size 5 m, demonstrated theoretically the best properties, for map interpolating by kriging. In all cases, it received the smallest RMSE of cross-validation and the smallest local variance (nugget effect). Increasing parameter of lag distance, always increases both the RMSE and the proportion of local variance in total variance [Co/(C + Co)].

The range of function, in most cases depends on the total spatial range of analyses and represents approximately 80-90% of its length (lag distance * lag numbers). Only in the case of field No. 2 is observed the dependence of spatial correlation to the much shorter ranges.

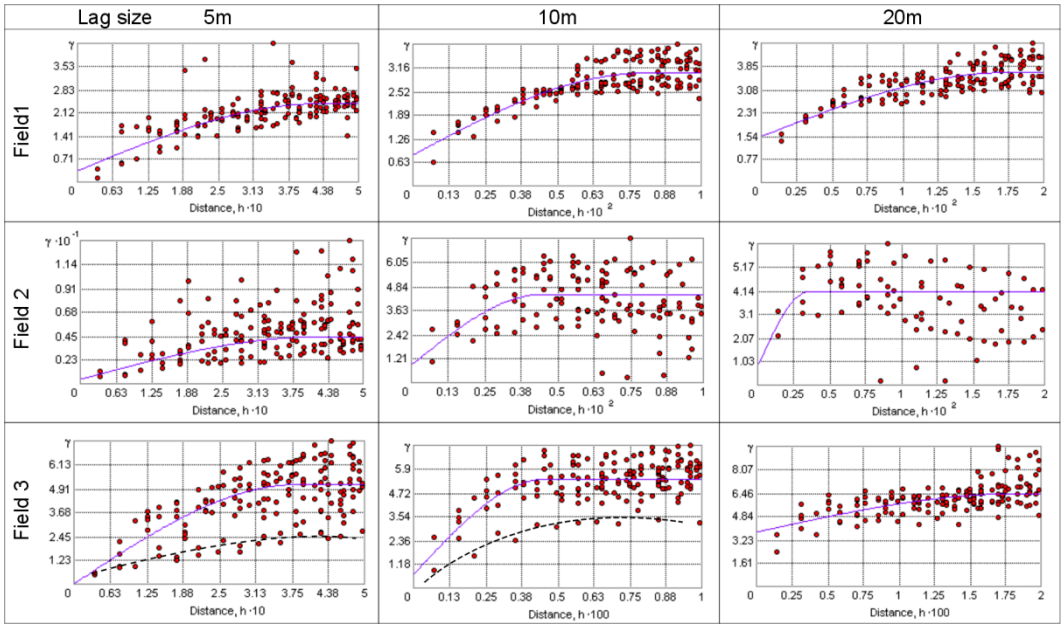

Figure 1. Semivariograms for 5, 10 and 20 m lag size.

Table 1. Properties of semivariograms

Field	Lag size 5 m			Lag size 10 m			Lag size 20 m		
	RMSE	Co/(C+Co)	Range (m)	RMSE	Co/(C+Co)	Range (m)	RMSE	Co/(C+Co)	Range (m)
1	0.96	0.14	43	1.04	0.27	80	1.15	0.42	173
2	0.94	0.09	42	0.96	0.19	45	0.97	0.20	36
3	1.20	0.00	39	1.26	0.12	46	1.70	0.59	184

This dependence most likely results from the smallest, in comparison to other fields, zonal variations. The above results suggest the crucial role of the proper determination of lag size value in modelling semivariogram function, for the interpolation by kriging. Lag size 5 m allows modelling of ECa detailed variability with high resolution (ca. 1 m). Increasing lag size to 10 m allowed the increase detection range of spatial autocorrelation with a minimal increase of nugget effect. But further increase lag size may lead to a wrong model for the kriging interpolation.

3.2 Changeability of directional variations

On the graphs for the lag size 5 and 10 m (field 3) can be observed a subset of points characterised by a different course than the spatial variability of the graph (dashed line on the Figure 1). This may indicate the presence of directional variance. The analyses were performed for three courses (angle of 45, 90 and 135 degrees). The 135 degrees angle corresponds to the direction of technological paths, the angle of 45 degrees to the perpendicular and the angle of 90 degrees can be considered neutral for the detection

of spatial variability associated with the presence of technological pathways. Spatial autocorrelation analysis of data was performed separately for each field, using a directional semivariogram (45, 90, 135 degrees) for the lag size 10 and the lag numbers (Figure 2).

Directions 45 and 90 degrees show a very similar course functions for three of the analysed fields. These courses are also similar to the semivariograms of Figure 2. Spatial autocorrelation in the transversal direction to the azimuth of technological paths showed different properties for the fields 2 and 3. The difference lies mainly in the range of autocorrelation, which in the case of the angle of 135 degrees is about 3 times bigger. This can be explained by the stretching and compacting of the soil along the direction of agricultural machinery. For field 1 there was no differences of variance as a function of the angle. Field 1 has the highest share of very light soils, which can explain by the stretching and compacting of the soil.

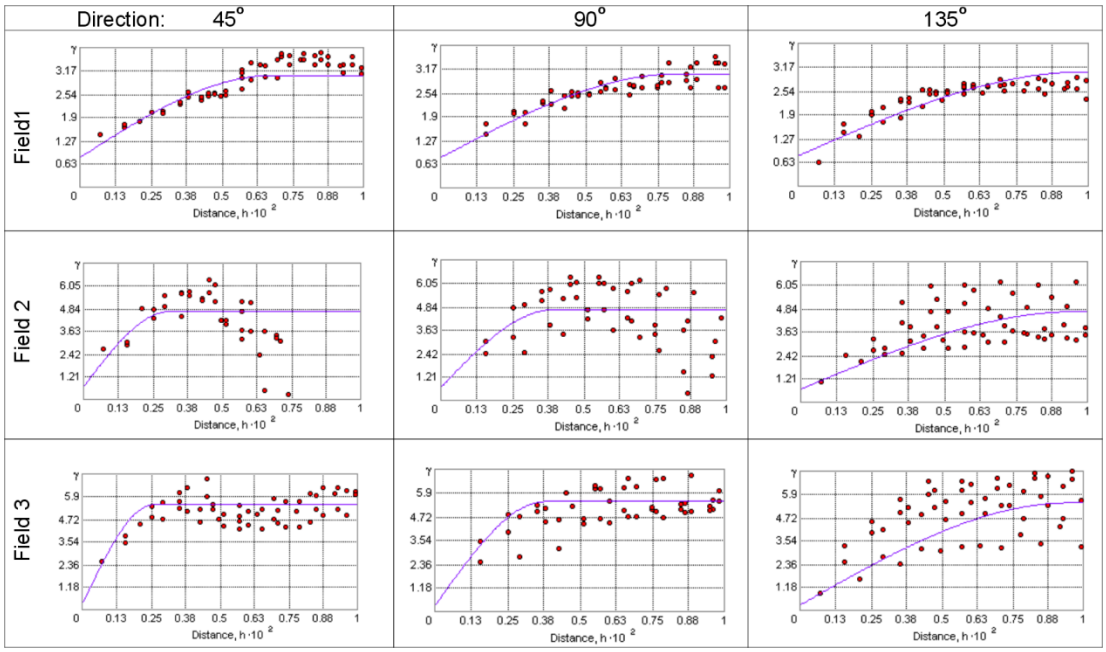

Figure 2. Anisotropy test. Directional semivariograms for 45, 90 and 135 degrees.

Anisotropy test were performed for subsets of heavy and light soils (Figure 3) as for the entire field. This test showed that the variation pattern of heavier soils, in the case of 45m, is similar to the results obtained for box 2 and box 3. For very light soils, to the extent of ca. 60 m, there was no difference between the total variance and the variances codes. Above that range, a sudden increase in the variance (for an angle of 45 degrees) can be observed, which is also visible in the graph of the total variance. This effect is probably a result of agricultural technology, which in light soils is much less observed.

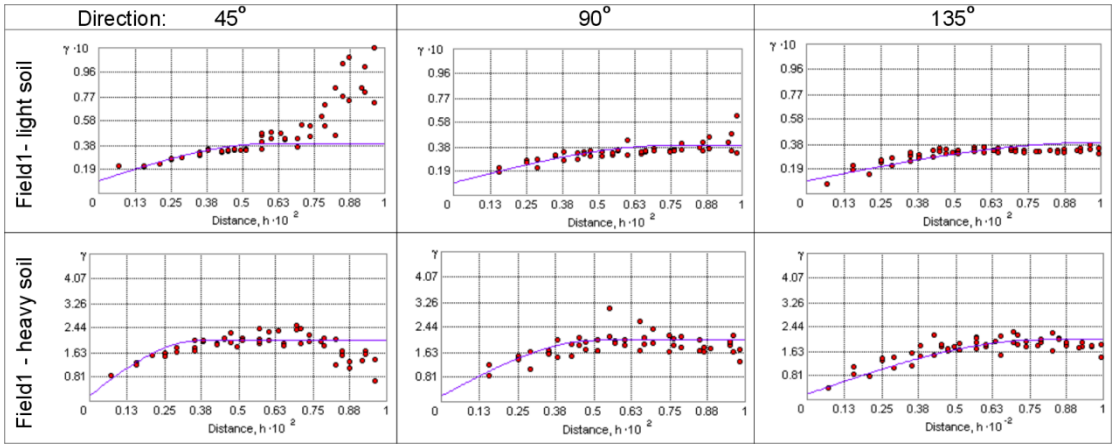

Figure 3. Anisotropy test. Directional semivariograms for 45, 90 and 135 degrees of north field's 1 part (heavy soil) and south field's 1 part (light soil).

4 Conclusions

The electrical conductivity of the soil is to a great extent unique for each field. In case studies of spatial variability it should be considered individually. Because of the possibility of significant differences in the local variance, geostatistical analyses should be conducted based on the empirical semivariogram model. Selection of parameters for semivariogram has a strong impact on the ability to identify significant spatial autocorrelation of data. This is particularly true of lag parameter size and directional analysis of variance. Lag parameter size = 10 m seems to be optimal for the model semivariogram describing the variation field of electrical conductivity of the soil. The influence of azimuth application of agricultural practices on a directional variance of the electrical conductivity of the soil was observed.

Acknowledgements

Work/part of the work has been supported by European Community 7th Framework Program project Proficiency (FP7-REGPOT-2009-1-245751) and by the Ministry of Science and Information Technology within the research project NN310079836 ECCOMP.

References

ADAMCHUCK, V.I., HUMMEL, J.W., MORGAN, M.T., UPADHYAYA, S.K. 2004. On-the-go soil sensors for precision agriculture. Computers and Electronics in Agriculture, 44 71-91.

SUDDUTH, K.A., KITCHEN, N.R., WIEBOLD, W.J., BATCHELOR, W.D., BOLLERO, G.A., BULLOCK, D.G., CLAY, D.E., PALM, H.L., PIERCE, F.J., SCHULER, R.T., THELEN, K.D. 2005. Relating apparent electrical conductivity to soil properties across the North-Central USA. Computers and Electronics in Agriculture, **46**, 263–283.

TRIANFAFILIS, J., LESCH, S.M. 2005. Mapping clay content variation using electromagnetic induction techniques. Computers and Electronics in Agriculture, **46** 203-237.

Electrochemical detection of mercury (II) in bentonite and quartz using anodic stripping voltammetry in presence of different removing agents

I. Robles, J. A. García, E. Bustos*

Centro de Investigación y Desarrollo Tecnológico en Electroquímica, S. C., Parque Tecnológico, Querétaro, Sanfandila, Pedro Escobedo 76703, Querétaro, Mexico.
**E-mail: ebustos@cideteq.mx*

Abstract

There are some techniques for total mercury determination as atomic absorption by hydride generation and cold vapor. For the determination of mercury species is used in general a method of detection by high-performance liquid chromatography with inductively coupled plasma mass spectrometry. However some electrochemical techniques that allow determining mercury species by its different oxidation states is the anodic stripping voltammetry using acid digestion to remove metal from sample or removing agents. In this sense, this research is focused to the electrochemical detection of mercury (II) in bentonite and quartz using anodic stripping voltammetry in presence of different removing agents.

Keywords: mercury, bentonite, quartz, voltammetry, removing agent.

1 Introduction

High mercury concentration in the environment can be dangerous and increases as elemental mercury evaporates and enters the atmosphere. In addition, high concentrations of indoor mercury may pose an inhalation risk. Approximately a third of the mercury circulating in the environment is produced naturally, while the remaining two-thirds are from industrial activity or other human activities. Due to the increase in industrial activity, the quantity of mercury circulating in the environment (atmosphere, soils, lakes, streams and oceans) has increased two to fourfold since the beginning of the industrial era. As a result, mercury levels in our environment are dangerously high (Alloway, 1990).

Techniques for total mercury determination include hydride generation atomic absorption (Chapple, 1990) and cold vapor atomic absorption (US-EPA Method 7471).For a general determination of mercury species, high-performance liquid chromatography with inductively coupled plasma mass spectrometrycan be used (Fodör, 2007). However, some electrochemical techniques can determine all the different mercury species and oxidation states.One such technique is anodic stripping voltammetry (ASV), which uses three electrodes to quantify the mercury found in an aqueous solution.

Stripping methods use a variety of electrochemical procedures, which share a characteristic initial stage. First, the analyte is deposited on a microelectrode, usually starting from a stirring solution. After an exact period of time, electrolysis is interrupted, stirring is stopped and the quantity of analyte deposited is measured using voltammetry procedures. During the second stage of the analysis, the analyte is re-dissolved or liberated from microelectrode. In anodic stripping voltammetry, the microelectrode behaves as a cathode during deposition and as an anode during re-dissolution, where it is oxidized by the analyte again and returns to its original form. Using ASV, the concentration of mercury in liquid samples can be determined. For the determination of mercury in soil, ASV is used after an acid digestion which removes mercury from soil samples (Lamble and Hill, 1998). Some alternative methods for the removal of mercury in soil samples also exist, such as the use of removing agents (Robles et al, 2012).In this research we compared the efficiency of eight previously mentioned removing agents, in the ability to remove mercury from contaminated bentonite and quartz.

2 Material and methods

Samples of quartz and calcium bentonite were polluted with mercuric chloride ($HgCl_2$) and mercuric oxide (HgO) at 10, 25 and 1 000 mgL^{-1}. Eight removing agents were probed to select the best: 0.1 M KI, 0.1 M KCl, 0.1 M KOH, 0.1 M $HClO_4$, 0.1 M EDTA, 10 % hydroxypropyl-β-cyclodextrine (HPCD) in deionized water; 275 mg L^{-1} EDTA + 1.15 % cysteine + 0.5 % NaCl, and 0.01 M chitosan. All of the agents, with the exception of chitosan, had previously been tested for the ability to remove metals in soil samples. Control experiments were carried out with water.

The quantity of mercury removed was quantified by ASV doing an extraction of the liquid from bentonite / quartz samples using an electrochemical cell, which was used with a system of three electrodes: glassy carbon, platinum and Ag/AgCl as working, auxiliary and reference electrode respectively. Experimental conditions for ASV were: potential to pre-concentration of –0.6 V vs. Ag/AgCl, deposition time of 6 min, quiet time of 30 s and scan rate of 70 mVs^{-1}.

3 Results

To account for experimental conditions, re-dissolution potentials were determined for Hg2+ in 0.1M HCl to detect concentrations on the scale of ppm. An increase in signal due to increasing mercury was monitored and recorded along with the increment in current associated with the addition concentration. Calibration curves were created for all the different removing agents for the addition of both HgCl2 and HgO. Table 1 shows the equations of the calibration curves for all the different removing agents.

4 Discussion

Linear regression was used to create fitting equations from the calibration data. These equations were used to determine the quantity of mercury remaining in solution for all the different removing agents. Due to structural differences in bentonite and quartz, mercury removal behaved differently for both. Quartz is ordered as a strong matrix of oxygen-silicon bonds, which prevent metal ions from penetrating its structure. On the other hand, metal ions can easily slip into bentonite, which is formed of stacked layers, due to the gaps between the layers. Because of the strong organized bonds in quartz, mercury is more easily removed from quartz than bentonite. Moreover, the particle size of bentonite is lower than quartz, and therefore has a bigger surface area and as a synthetic colloid, has negative charges which attract positive ions.

Table 1. Equations of calibration curves obtained corresponding to each removing agents.

Removing agent	Calibration curves			
	HgO		$HgCl_2$	
	Equation	Fitting (R^2)	Equation	Fitting (R^2)
HCl	y=0.0077x+0.0980	0.993	y =0.009x+0.0576	0.995
KCl	y=0.0093x+0.0421	0.999	y=0.0092x+0.0538	0.993
KI	y=0.0141x+0.1194	0.982	y=0.0106x+0.1018	0.980
KOH	y=0.0035x+0.0280	0.994	y=0.0005x+0.0484	0.970
EDTA	y=0.0039x+0.0369	0.988	y=0.0033x+0.0421	0.975
HPCD	y=0.0069x+0.0730	0.982	y=0.0056x0.0487	0.995
Cys+EDTA+NaCl	y=0.0083x+0.0162	0.999	y=0.0163x-0.1353	0.987
Chitosan	y=0.0054x+0.0401	0.992	y=0.0046x+0.0406	0.986

Once bentonite and quartz samples were contaminated with HgO or $HgCl_2$, removing agents were added. After 24 h the sample was collected and analyzed by ASV. Bentonite adsorbed chitosan easily, swelling up dramatically which made it difficult to remove the supernatant. Therefore, the removal of mercury from bentonite using chitosan was inefficient. Removing agents can be divided into two classes: extracting agents and complexing agents. Extractant agents remove metals by electrostatic forces, forming ionic bonds. Thus, magnitude depends on ionic charge.

On the other hand, complexing agents act differently with metallic ions. Metals tend to lose electrons during chemical reactions, creating metallic ions. The positive charge of these cations attracts negative ions to form complexes held together by covalent bonds. Donating species (ligands) needs to have a lone pair of electrons which can be donated to form a bond. Water, ammonia and halides are common inorganic ligands (Buffle, 1990). Stronger compounds tend to remove more mercury contamination present in the

bentonite and quartz samples. In this sense, HCl, KCl, KI and KOH are denominated as extractant agents, while complexing agents are EDTA, HPCD, Cys and chitosan, by its own properties.

5 Conclusions

ASV was used to quantify the percentage of mercury removed in liquid samples that were derived from bentonite and quartz samples previously polluted with two mercury compounds (HgO and $HgCl_2$). Eight removing agents were analyzed, using both extracting (ionic bond complexes) and complexing agents (covalent bond complexes). Better results were obtained with complexing agents. For bentonite, the most effective removing agent was EDTA which removed 17 % of both Hg compounds. In quartz, chitosan was the best removing agent, removing 62 % of HgO and 53 % of $HgCl_2$. Chitosanis both biodegradable and easy to obtain (derived from shrimp exoskeleton). While chitosan had never been tested previously, in these experiments chitosan was proven to be a good new alternative complexing agent.

Acknowledgements

The authors would like to thank Consejo Nacional de Ciencia y Tecnología de los Estados Unidos Mexicanos (CONACyT), Academia Mexicana de Ciencias (AMC), Fundación México – Estados Unidos para la Ciencia (FUMEC) and International Cooperation Program across Bilateral Cooperation Mexico – Hungary for the funding of this research.

References

ALLOWAY, B. J. 1990. Heavy metals in soils, John Wiley and Sons, Inc.New York.

BUFFLE, J. 1990. Complexation reactions in aquatic systems, an analytical approach, Editorial Ellis Horwood, Great Britain.

CHAPPLE, G. 1990. The determination of arsenic, selenium and mercury levels in U.S. EPA quality control samples using the GBC HG3000 continuous-flow hydride generator, GBC AA Aplications, Nº 17, Australia.

FODÖR, P. 2007. Selenium speciation studies in Se- enriched chives by HPLC-ICP-MS, Food Chemistry, 101, 1398 – 1406.

HAHEB, P. 2012. Reduction of mercury from meckerel filled using combined solution of cysteine, EDTA, and sodium chloride, Journal of Agricultural and Food Chemistry, 60, 6069 - 6076.

LAMBLE, K. J., HILL, S. J. 1998.Microwave digestion procedures for environmental matrices, Analyst, 123, 103R – 133R.

ROBLES, I., GARCÍA, M. G., SOLÍS, S., HERNÁNDEZ, G., BANDALA, Y., JUARISTI, E., BUSTOS, E. 2012. Electroremediation of mercury polluted soil facilitated by complexing agents, International Journal of Electrochemistry Science, 7, 2276 – 2287.

On-line measurement of soil extractable P and pH with visible and near infrared spectroscopy

S. M. Shaddad[1,2,3*], B. Kuang[2], S. Madrau[1], A. M. Mouazen[2]

[1] *Department of Agriculture, Sassari University, Sassari, Italy*

[2] *Environmental Science and Technology Department, Cranfield University, Cranfield, United Kingdom*

[3] *Soil Science Department, Faculty of Agriculture, Zagazig University, Zagazig, Egypt*

[*] *E-mail: shaddadsm@gmail.com*

Abstract

Visible and near infrared spectroscopy (vis-NIRS) is considered as one of the proximal soil sensing technologies, which is widely used to predict soil properties. The aim of this study was to evaluate the on-line measurement accuracy for soil extractable phosphorus (P) and pH using a vis-NIR on-line sensor. The partial least squares regression (PLSR) analysis resulted in calibration models with a good to excellent prediction performance for pH and P with ratio of prediction deviation (RPD) values of 2.03 and 2.89 and root mean square error (RMSE) values of 0.35 and 3.96 mg/kg, respectively. The validation of the calibration models using on-line collected spectra of the prediction set provided moderate to good performance with RPD values of 2.04 and 1.72, and RMSEP values of 0.44 and 8.87 mg/kg for pH and P respectively.

Keywords: Vis-NIR spectroscopy, on-line measurement, PLSR.

1 Introduction

In precision agriculture, the use of on-line proximal soil sensors is highly recommended, as these can provide high resolution data on spatial variation in soil properties (Stenberg et al., 2010). Visible and near infrared spectroscopy (vis-NIRS) is used as one of the proximal soil sensing technologies for laboratory, in situ and on-line measurement conditions. This is fast, cost effective, easy and does not require expert operators to perform the analyses. In this study the on-line measurement of soil extractable phosphorous (P) and pH is reported in one field in the UK, as these properties affect greatly soil fertility and productivity.

2 Materials and methods

2.1 On-line measurement and soil sampling

On-line survey by a vis-NIR multiple-sensors platform developed by Mouazen (2006) was conducted in 18 ha field located in Wilstead, Bedfordshire, UK. During the on-line measurement, 183 soil samples were collected for calibration and validation of the vis-

NIR sensor. Samples were divided into two parts. The first part was dried, grinded and subjected to chemical analysis to determine pH and P. pH was measured using a glass electrode in a 1:5 (volume fraction) suspension of soil in water and P was extracted in sodium hydrogen carbonate solution according to ISO 11263:1994.

2.2 Laboratory optical measurement and spectra pre-treatment

The second part of soil samples was used for optical scanning under laboratory measurement conditions using the same mobile, fibre type, vis-NIR spectrophotometer (AgroSpec from tec5 Technology for Spectroscopy, Germany), as that used for on-line scanning. A 100 % white reference was used before scanning. Each sample was replicated three times in three cups and a total of 10 scans were collected from each cup, and these were averaged in one spectrum. Soil spectra were first reduced to 371 - 2150 nm to eliminate noise at both edges of spectra. Spectra were further reduced by averaging three successive points in the vis range, and 6 points in the NIR range. The Savitzky-Golay smoothing, maximum normalisation and first derivation were successively implemented using Unscrambler 7.8 software (Camo Inc.; Oslo, Norway).

2.3 Model development and mapping

The chemical and spectral data were used to develop calibration models of P and pH using partial least squares regression (PLSR), with full-cross validation. Samples used for calibration and validation of pH and P were, 135 and 71 and 48 and 23, respectively (Table 1). All maps for both properties were developed by the inverse distance weighting method using an ArcGIS 10 (ESRI, USA) mapping software.

3 Results and discussion

3.1 Accuracy of calibration models and on-line validation

The results of the PLSR cross-validation (Table 1) showed good to excellent calibration models (Viscarra Rossel et al., 2006) for pH and P with RPD values of 2.03 and 2.89, respectively. Calibration RMSEP values were 0.35 and 3.96 mg/kg for pH and P, respectively, which is in line with results obtained by others (Shepherd and Walsh, 2002, Cohen et al., 2005, Mouazen et al. 2006). The validation of the calibration models using on-line spectra of the prediction set provided RPD values of 2.04 and 1.72 mg/kg, and RMSEP values of 0.44 and 8.87 mg/kg for pH and P, respectively, which is better than the result of Mouazen et al., (2009) and Mouazen et al. (2007).

The regression coefficients plots for both soil parameters show either positive or negative bands in the vis and NIR ranges (Figures 1 & 2). Most significant bands are in the visible 400-600 nm, associated with colour and in the NIR range > 1450 nm, associated with water and carbon absorption bands.

Table 1. Partial least squares regression (PLSR) results in cross-validation and on-line prediction.

property	Calibration				On-line Validation			
	Sample no	R^2	RMSEP	RPD	Sample no	R^2	RMSEP	RPD
pH	135	0.73	0.353	2.03	48	0.75	0.438	2.04
Extr_P	71	0.77	3.96	2.89	23	0.64	8.87	1.72

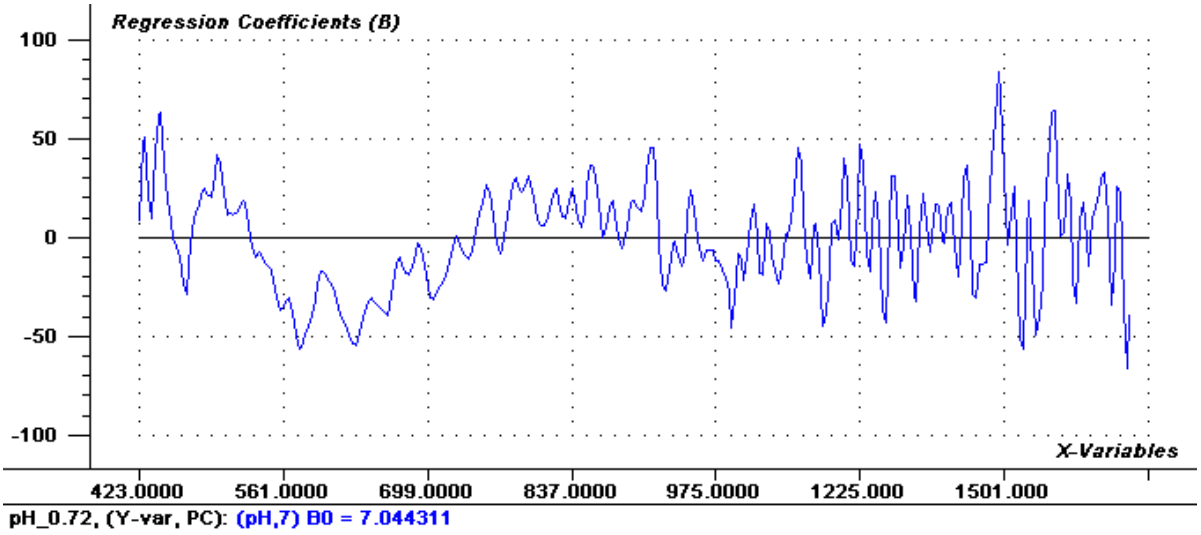

Figure 1. Plot of regression coefficients for pH.

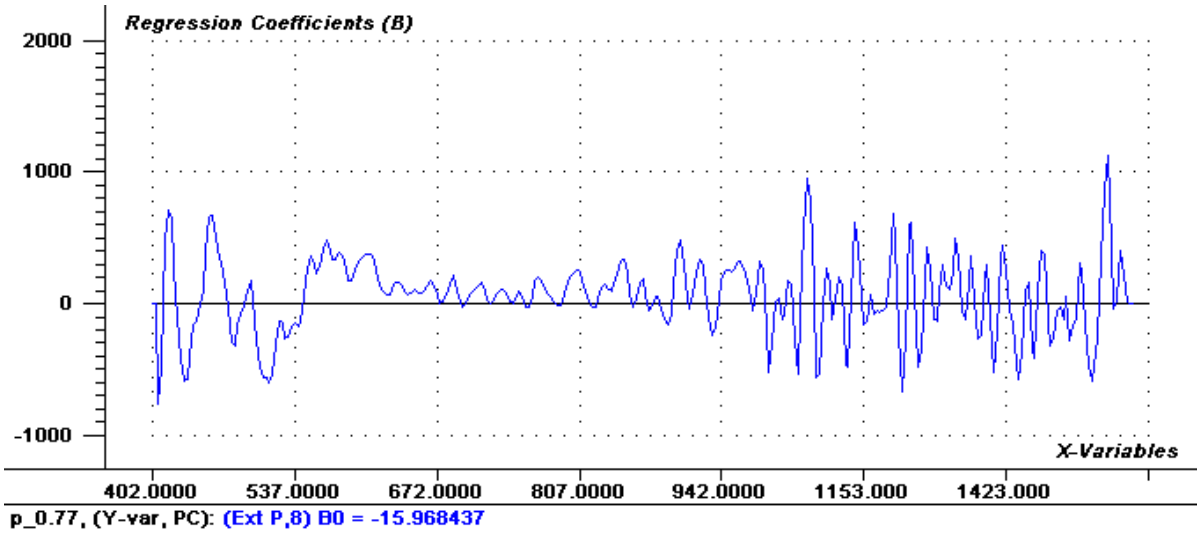

Figure 2. Plot of regression coefficients for P.

3.2 Mapping

Maps for laboratory measured and on-line predicted values for pH and extractable P confirm spatial similarity, and the accuracy on the on-line sensor (Figures 3 & 4).

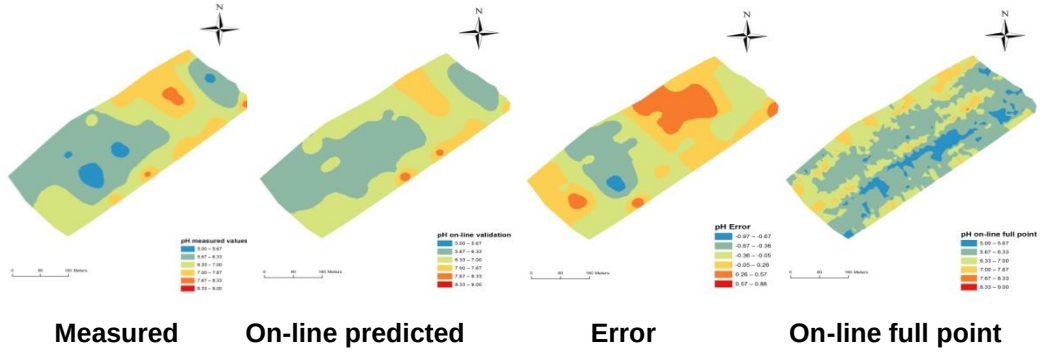

Figure 3. pH measured, on-line predicted, error and on-line full point maps

However, the spatial similarity between full-point map and prediction map is poor, suggesting the need for on-line sensors that can provide different spatial distribution of soil properties as compared to manual sampling considered in precision agriculture.

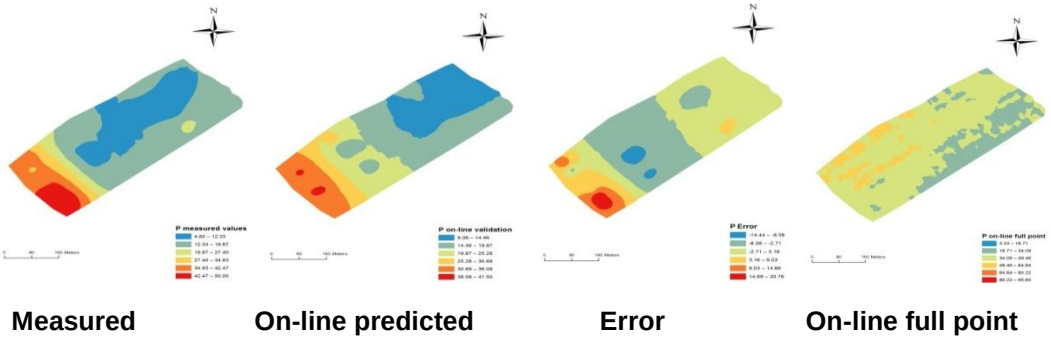

Figure 4. P measured, on-line predicted, error and on-line full point maps

4 Conclusions

Although both soil properties considered in the current work, do not have direct spectral responses in the NIR range, the prediction accuracy obtained is considered appropriate for site specific land management.

Acknowledgment

Authors acknowledge the European Commission for financial support provided to the first author under LLP Programme Erasmus Placement 2012/2013 Prot.16525.

References

COHEN, M. J., PRENGER, J. P., DEBUSK, W. F. 2005. Visible-near infrared reflectance spectroscopy for rapid, nondestructive assessment of wetland soil quality. J. Environ. Qual. 34, 1422–1434.

MOUAZEN, A. M., DE BAERDEMAEKER, J., RAMON, H. 2006. Effect of wavelength range on the measurement accuracy of some selected soil constituents using visual-near infrared spectroscopy. J. Near Infrared Spectrosc. 14, 189–199.

MOUAZEN, A.M. 2006. Soil Survey Device. International publication published under the patent cooperation treaty (PCT). World Intellectual Property Organization, International Bureau. International Publication Number: WO2006/015463; PCT/BE2005/000129; IPC: G01N21/00; G01N21/00.

MOUAZEN, A.M.; MALEKI, M.R.; COCKX, L.; VAN MEIRVENNE, M.; VAN HOLM, L.H.J.; MERCKX, R.; DE BAERDEMAEKER, J.; RAMON, H. 2009. Optimum three-point linkage set up for improving the quality of soil spectra and the accuracy of soil phosphorous measured using an on-line visible and near infrared sensor. Soil & Tillage Research, 103(1): 144-152.

MOUAZEN, A.M.; MALEKI, M.R.; DE BAERDEMAEKER, J.; RAMON, H. 2007. On-line measurement of some selected soil properties using a VIS-NIR sensor. Soil & Tillage Research, 93(1), 13-27

SHEPHERD, K. D., WALSH, M. G. 2002. Development of reflectance spectral libraries for characterization of soil properties. Soil Sci. Soc. Am. J. 66, 988–998.

STENBERG, B., VISCARRA ROSSEL, R. A., MOUAZEN, M. A., WETTERLIND, J. 2010. Visible and Near Infrared Spectroscopy in Soil Science. Adv. Agron. 107, 163–215.

VISCARRA ROSSEL, R. V., MCGLYN R. N., MCBRATNEY, A. B. 2006. Determining the composition of mineral-organic mixes using UV–vis–NIR diffuse reflectance spectroscopy. Geoderma 146, 403-411.

Analysis of spatial pattern and temporal stability of soil apparent electrical conductivity and relationship with yield in a soil of high clay content

J.M. Terrón[1], F.J. Moral[2*], J.R. Marques da Silva[3], F.J. Rebollo[2]

[1]Centro de Investigación "La Orden - Valdesequera", Gobierno de Extremadura, Spain
[2]Universidad de Extremadura, Departamento de Expresión Gráfica, 06006 Badajoz, Spain
[3]Departamento de Engenharia Rural, Instituto de Ciências Agrárias e Ambientais Mediterrânicas (ICAAM), Escola de Ciências e Tecnologia, Universidade de Évora, 7002-554 Évora, Portugal
[*]E-mail: fjmoral@unex.es

Abstract

If ECa zones are used to manage agricultural inputs across the field for multiple years, both the spatial variability and the temporal stability of Eca are important. Maps of ECa in different years (2009, 2011, and 2012) are highly correlated (for all cases r > 0.69) which suggest that single ECa mapping is sufficient to delimit stable zones. Moreover, the relationship between ECa and crop yield (three-year average standardized yield map) was considerable, with important correlations of both spatial patterns. Thus, ECa mapping is an inexpensive tool to accurately characterize soil differences, being closely related to yield in soils with high clay content.

Keywords: soil apparent electrical conductivity, precision agriculture, clayey soil, crop yield.

1 Introduction

Efficient techniques for accurately measuring within-field variation in soil properties are very important for site-specific crop management. The traditional soil sampling is costly and labour-intensive, so taking into account the necessity of many soil samples to achieve a reliable representation of any soil property, this traditional method is not viable from a precision agriculture perspective. The geospatial measurement of soil apparent electrical conductivity (ECa) is an efficient new ground-based sensing technology to provide high density information, which is essential to implement a real site-specific management.

In a previous work, Moral et al. (2010) found that ECa responds well to some soil variables related to soil fertility, as pH, cation exchange capacity and total nitrogen which, in turn, all of them are highly correlated with sand and clay. Thus, it seems that ECa is an excellent variable to delineate different homogeneous subfields. But, if delineated ECa zones are to be used to manage agricultural inputs across the field for multiple years, not only the spatial variability of ECa is of significance importance but

also understanding its temporal stability is equally essential. Multiple ECa mappings should generate similar spatial patterns at a relative scale for ECa maps to have utility in site-specific management. If ECa is highly corretated to stable soil properties as texture, it is also expected that ECa does not change spatially.

In dryland fields the main limiting factor for crop yield is the plant available water, which is highy related to soil texture. Particularly in clayey soils, in which ECa and clay content are highly related, it seems that the relationship between ECa and the crop yield should be important. One of the man objectives in this work is to analyse this relationship.

2 Material and methods

The work was carried out in a 33-ha field located in Badajoz, southwestern Spain. The mean clay content in the experimental field is about 32 %, but there are areas where it is more than 50 % (Moral et al., 2010). ECa measurements were conducted with a 3100 Veris sensor operating in both shallow (0-30 cm), ECs, and deep (0-90 cm), ECd, mode, in February 19 and April 24, 2009, and January 27, 2011. Yield map data were collected in 2007, 2010 and 2011, using a combine harvester equipped with a yield sensor, when there was a non tilled sunflower crop. Thus, a few hundred values of both ECs and ECd, and yield per hectare were obtained. Due to the high density data, the ordinary kriging algorithm can be used to generate maps showing the spatial distribution of ECs (ECd data were not used) and yield.

With the aim of comparing the spatial patterns, the smoothed interpolated 5x5 m grid surfaces were used; they provide better-defined delineations with less isolated patches.

To analyse the temporal variability of both ECs and yield patterns across the field, and due to the fact that the range of values which defines a particular delineation for both variables changes over time, a standard normalization of data was computed. The three maps corresponding to normalized ECs were used as input layers in a principal component analysis (PCA) to compress data by eliminating redundancy. The same was done with the three normalized yield maps. Later, a geographically weighted regression (GWR) was performed with the first principal components resulting in each analysis to model spatially varying relationships. All works were conducted in ArcGIS v.10.0 (ESRI, Redlands, CA).

3 Results and discussion

Descriptive statistics for both variables are shown in Tables 1 and 2. In all cases, mean and median values are very similar, the skewness is low, and the coefficients of kurtosis are close to 3, which is typical of a normal distribution. There was a large difference between yields from year to year, probably due to the overall weather conditions in each year. Coefficients of variation for all dates and years denote significant spatial variability

for both ECs and yield, suggesting the convenience of defining different management zones.

Table 1. Descriptive statistics of shallow (0-30 cm) soil apparent electrical conductivity data, ECs (mS m^{-1}), for different sampling campaigns; SD = Standard Deviation, CV = Coefficient of variation

Measurement date	Mean	Median	SD	Max	Min	Skewness	Kurtosis	CV (%)
February 19, 2009	16.14	18.50	5.84	26.30	0.50	-0.79	2.45	36.18
April 24, 2009	10.63	10.90	3.59	20.90	1.20	-0.22	2.99	33.77
January 27, 2011	17.56	19.50	6.22	33.50	0.50	-0.76	2.64	35.42

Table 2. Descriptive statistics of yield (t ha-1), for different years; SD = Standard Deviation, CV = Coefficient of variation.

Year	Mean	Median	SD	Max	Min	Skewness	Kurtosis	CV (%)
2007	0.53	0.49	0.24	1.70	0.12	0.93	4.14	45.28
2010	0.87	0.89	0.33	1.80	0.10	-0.13	2.55	37.93
2011	1.67	1.69	0.47	2.98	0.47	-0.02	2.12	28.14

Kriged maps of normalized ECs (NECs) and yield (NY) were generated with the point ordinary kriging method, integrating the spatial correlation structures described with spherical variograms. A striking coincidence is that the mean values of ranges for the three ECs and yield variograms are equal, 283 m, which is an initial evidence about similar spatial patterns can be expected. Thus, after interpolating, spatial distributions of NECs and NY obtained for different dates were very similar. This can suggest that the spatial pattern for both variables are stable. To quantify the degree of similarities between patterns, grid-by-grid comparisons of maps between two dates were carried out. Correlations between NECs and NY maps are shown in Tables 3 and 4. High correlation coefficients are apparent for NECs, whereas more moderate, but also considerable correlation coefficients, are obtained for NY.

Table 3. Correlation matrix between normalized shallow (0-30 cm) soil apparent electrical conductivity maps, NECs, for different dates.

	February 19, 2009	April 24, 2009	January 27, 2011
February 19, 2009	1		
April 24, 2009	0.79	1	
January 27, 2011	0.95	0.80	1

Table 4. Correlation matrix between normalized yield (t ha^{-1}), for different years.

	2007	2010	2011
2007	1		
2010	0.45	1	
2011	0.60	0.69	1

After the PCA was performed, the first principal component describe more than 90 % and 74 % of the variance of the three NECs and NY maps, respectively. Eigenvectors show that contribution of all maps to the first component were practically similar. Thus, the maps of the first principal components can be an useful tool to estimate the spatial trends of ECs and yield (Fig. 1, maps 1 and 2). Visually, both maps have similar trends and there is an important coincidence between areas of high NECs and NY values and areas where the sand content is also higher (Moral et al., 2010). This fact can be interpreted as the sandy areas, which are the less productive in rainfed fields, bear a greater stability in ECs and yield patterns than clayey zones. Soil ECs is more dynamic in the presence of clay particles because of the chemical processes involved and the interactions with soil water, and available nutrients is also higher in clayey soils (e.g., King et al., 2001).

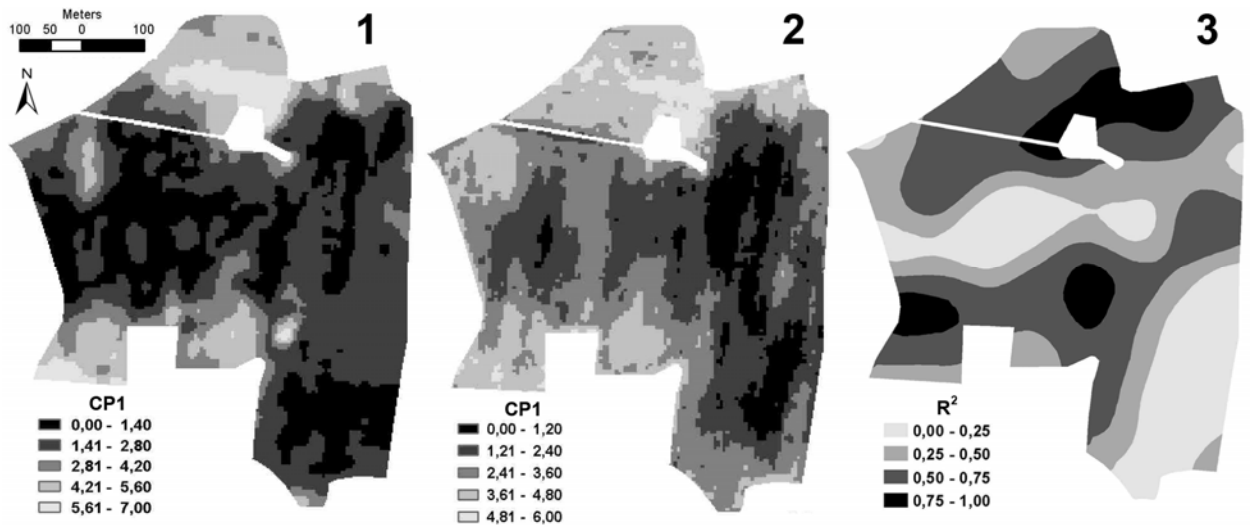

Figure 1. Spatial distributions of the first principal components considering as input layers the kriged maps of normalized shallow (0-30 cm) soil apparent electrical conductivity in February 19 and April 24, 2009, and January 27, 2011 (1), and yield in 2007, 2010, and 2011 (2), and the coefficient of determination after conducting a geographically weighted regression between both variables (3).

Grid-by-grid comparison of both NECs and NY first principal component maps leads to a correlation coefficient of 0.73, denoting that their similarity are not only visual or qualitative but also quantitative. Thus, a GWR was conducted to evaluate how this

relationship varies locally across the experimental field. Fig. 1, map 3, shows the spatial distribution of the determination coefficient, R^2. This is higher than 0.5 in around half of the field, indicating that NY can be predicted well considering NECs as the explanatory variable. It is important to denote the general coincidence of the zone where R^2 is higher and the more sandy and less productive areas, corroborating the aforementioned fact that they are the areas with higher temporal stability. In future works, the type of ECs-yield relationships will be analysed in more detail because they have not to be linear; the more important finding in this case is the fact that the ECs-yield relationship is significant and spatially variable in this clayey soil.

4 Conclusions

The soil of the experimental field is very typical in the south of Spain, so it seems that in similar cases ECa is an important variable integrating the most important soil properties affecting crop productivity. Spatial patterns of ECs were highly stable over time due to the fact that they reflect the stability in the soil factors, such as sand, clay, and cation exchange capacity; thus, single ECs mapping is sufficient to delimit stable zones. Moreover, ECs and yield spatio-temporal patterns are very similar, so it can help delineate homogeneous management zones.

Acknowledgements

This research was co-financed by the Gobierno de Extremadura and the European Regional Development Fund (ERDF) through the projects GR10038 (Research Group TIC008) and PRI07B080.

References

KING, J. A., DAMPNEY, P. M. R., LARK, M., MAYR, T. R., BRADLEY, R. I. 2001. Sensing soil spatial variability by electro-magnetic induction (EMI): Its potential in precision agriculture. In: Third European Conference on Precision Agriculture, Agro Montpellier, Montpellier, France, pp. 419-424.

MORAL, F. J., TERRÓN, J. M., MARQUES DA SILVA, J. R. 2010. Delineation of management zones using mobile measurements of soil apparent electrical conductivity and multivariate geostatistical techniques. Soil & Tillage Research, 106 335-343.

Geophysical investigation of peatlands: assessment of the carbon storage function

J. Walter[1*], E. Lück[2], J. Zeitz[1]

[1]*Humboldt-Universität zu Berlin, 14195 Berlin, Albrecht-Thaer-Weg 2, Germany*
[2]*University of Potsdam, Germany, Karl-Liebknecht-Str. 24, D-14476 Golm/Potsdam, Germany*
[*]*E-mail: judith.walter.1@agrar.hu-berlin.de*

Abstract

Peatlands have an important function for the storage of global carbon, due to intensive agricultural drainage this function is reduced significantly. In order to sustainably protect these ecosystems, information about current state of peatlands, especially about thickness and properties describing the condition of peat, are crucial. Geophysical techniques have the potential to deliver such information. Therefore, we firstly analysed the relation between electrical- and pedogenetic properties of peat of samples that derived from different study sites in the laboratory. Secondly, we conducted surveys of electrical resistivity in the field. Our results show that solute concentration in soil solution, followed by cation ion exchange capacity are the main factors explaining the variability in bulk soil conductivity.

Keywords: electrical conductivity, peat thickness, peat-decomposition.

1 Introduction

Peatlands have an important function for the storage of global carbon. This function has been reduced significantly through intensive agricultural drainage in central Europe for the last 200 years. Drainage of peatlands leads to mineralisation and humification processes and finally to the decomposition of peat material. These processes go along with a loss of organic carbon, especially as carbon dioxide. In order to reduce these losses, assessments of the peatlands in their current function as a carbon sink, and adequate management are required. Therefore, information about both, peat conditions (degree of peat decomposition) and thickness are crucial. Practical methods, which can estimate such data in-field other than time-consuming conventional coring techniques, are still missing.

Non-invasive geophysical techniques, such as electrical resistivity (ER) or ground penetrating radar (GPR), have the potential to support conventional coring methods on peatlands, especially by bringing selective information on a larger scale. GPR, measuring dielectric permittivity of a soil volume, has been used on peatlands successfully in order to determine the thickness of peat (Comas et al., 2011; Sass et al., 2010; Lowry et al., 2009). However, the application of these techniques has mostly been limited to peatlands in a natural state that show low degrees of decomposition. In contrast techniques,

which measure electrical conductivity of the soil, have not yet been applied frequently to peatlands (Slater & Reeve, 2002; El-Galladi et al., 2007) and rarely on degraded fen soils that show very high degrees of decomposition.

ER measures the electrical conductivity (reciprocal of electrical resistivity) of bulk soil (EC_b). According to site conditions EC_b of peat is correlated to parameters such as cation exchange capacity (CEC), organic carbon (OC), dissolved ions in soil solution (EC_e – conductivity is proportional to dissolved ions in soil solution) and bulk density. These parameters are functions of the peat condition. For example organic carbon decreases with increasing decomposition (Kalbitz & Geyer, 2002), whereas CEC increases with increasing decomposition (Seybold et al., 2005, Asadi et al., 2011). In most studies, which were conducted on peatlands, high EC_b were correlated to peat material in general, without explaining the physical reasons for this relationship in detail (Slater & Reeve, 2002; Triantafilis et al., 2002). Additionally, less is known about the quantities of electrical properties of peat at different degrees of decomposition.

Our aim is to gather information about the thickness and the condition of peat in fen soils of north-east Germany by means of non-intrusive geoelectrical techniques measuring EC_b. Therefore, the objectives of this study are to identify the main peat properties influencing EC_b and, subsequently, to find appropriate calibration functions between peat and electrical parameters, which can be applied either multi- sited or site-specifically.

2 Materials and methods

To assess the field-applicability of geophysical technique on peatlands and of ER in particular, we examined the electrical properties of peat on different scales. First, we measured EC_b of undisturbed samples on a small scale in the laboratory with a 4-point-light (LGM-Lippman, Germany). Samples derived from various study locations in north east Germany. We took peat samples of different decomposition stages, classified after the scale of von Post (1920) (ranging from H1 to H10). All parameters, which may potentially influence the EC_b of peat (EC_e, CEC, OC, bulk density, pH-value and volumetric water content) were analysed simultaneously. Second, to assess, if the basic principles discovered on the small scale in the laboratory could be transferred on the field scale and if peat thickness and peat condition can be identified, we conducted electrical resistivity profile measurements with a stationary multielectrode array (GeoTom from GeoLog, Germany) on different sites in north-east Germany. In order to reference field measured EC_b, additional soil samples were taken, which are currently being analysed. In order to reveal relations between EC_b and peat properties, statistical evaluations of laboratory data were performed using weighted multiple regression analysis. The differences in peat properties and EC_b between samples of different degrees of decomposition were checked out using non-parametric significance tests (Wilkoxon rank sum test).

3 Results and discussion

The main factor influencing EC_b is EC_e, showing an almost linear relationship. Figure 1 shows the results of the laboratory analysis in a scatterplotmatrix of EC_b and selected peat properties. Symbols of scatters indicate the degree of decomposition grouped into three classes ranging from low (H1) to medium (H2) and high (H3) degrees. These findings were confirmed by multiple regression analysis, which revealed a strong response of EC_b on EC_e followed by CEC and water content if all samples from different locations were incorporated. After standardisation of regression coefficients, EC_e explained about 60%, CEC 30% and volumetric water content 10% of variability in EC_b. All possible interactions between variables were considered in the regression analysis, but during model simplification process they were deleted out of the model as it did not perform significantly better when including them. However, no direct correlation between EC_b and degree of decomposition could be identified (Figure 1), which was also confirmed by a Wilcoxon test of EC_b between high and low degrees. This could be explained by the strong correlation of EC_b and EC_e, which is due to the fact that EC_e levels varied from site to site. This is pointed out in Figure 2, showing the relation between EC_b und EC_e and the clustering of data according to their origin.

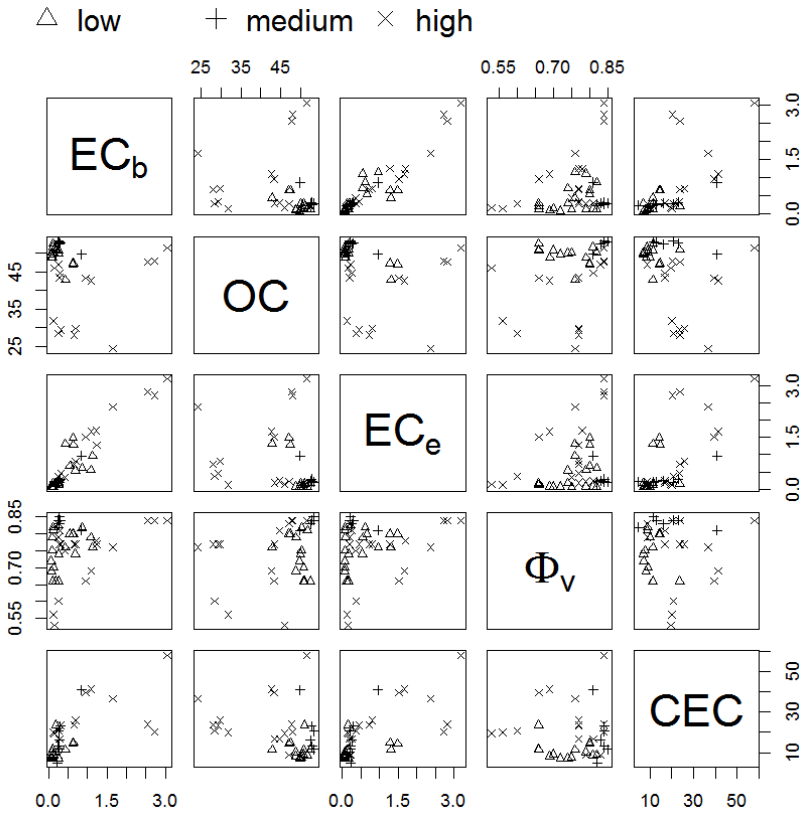

Figure 1. Scatterplotmatrix of electrical conductivity of bulk soil (EC_b, [mS/cm]), electrical conductivity of soil solution (EC_e, [mS/cm]), organic carbon content (OC, [%]), volumetric water content (Θ_v, [%]) and cation ion exchange capacity (CEC, [cmol(+)/kg]) classified in three groups of degree of decomposition, ranging from low, to medium and high degrees.

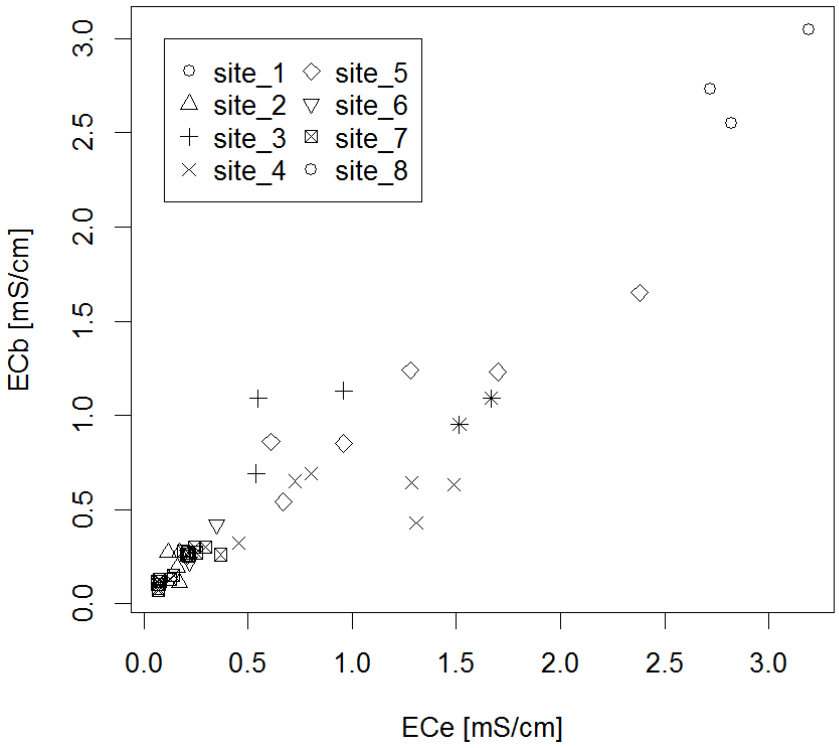

Figure 2. Relation of electrical conductivity of bulk soil (EC_b, [mS/cm]) and electrical conductivity of soil solution (EC_e, [mS/cm]) as a function of location.

As a result the influence of subtrate-connected properties, such as CEC or organic content are masked by the site-specific loads of solutes. There is a slight positive relation between EC_e and degree of decomposition (EC_e between high and low degrees of decomposition is with p-value= 0.04 significant on a 5% level), which can be explained by an increasing release of solutes out of the organic matter during processes of decomposition and humification. However, CEC was primarily a function of the peat decomposition (CEC between high and low degree of decomposition: p-value= 0.0002), which has already been confirmed in other studies (Asadi & Huat 2009; Seybold et al., 2005).

In summary, the laboratory analysis shows that a multi-site analysis of EC_b is mainly controlled by site-specific absolute values of concentration of solutes in the soil solution and no direct correlation with degree of decomposition could be observed. We therefore conclude that the estimation of peat properties describing its condition through electrical measurements is appropriate when using a site specific calibration function.

First results of the field survey of EC_b showed a clear delineation of the peat body with high contrast in EC_b between the peat- and the surrounding mineral material. Figure 3 shows the vertical distribution of resistivity data (reciprocal of conductivity) of one of the ER surveys conducted on a degraded peatland. Bright hatchures indicate high EC_b (low resistivities), which are corresponding to peat layers. Dark hatchures reveal layers of

mineral material and thus low EC_b. Asterisks point out the interface between organic and mineral material, as it was determined by conventional coring techniques. Within peat-structures, such as lower EC_b values until depths of 1 meter between position 30m and 50m, were described as layers of lower degrees of decomposition in the field. These layers presumably possess different chemical properties than the other peat layers, but only the laboratory analysis of samples taken at those sites will clarify the source of variability in EC_b of these layers.

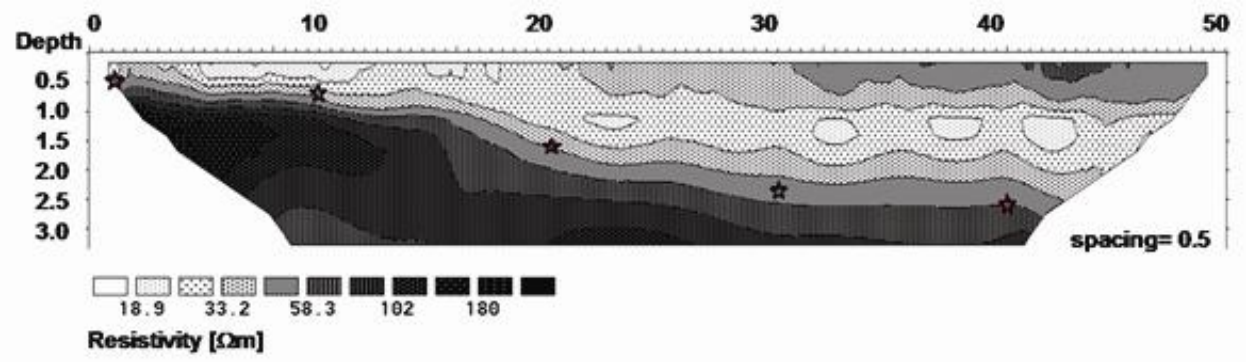

Figure 3. Vertical distribution of resistivity data (reciprocal of conductivity) in [Ωm] along a 50 m section. Electrode spacing was 0.5 meter (Wenner array). Asterisks indicate interface between peat- and mineral material determined by coring.

4 Conclusion

Our results show that if samples from different locations were involved in the calibration function, EC_e, CEC and volumetric water content are dominant factors influencing EC_b, in that order. EC_e is the main factor influencing EC_b. This reflects the specific site conditions of peatlands, because concentrations of dissolved ions depend mostly on the load of solutes of the groundwater in the respective catchment and, hence, vary among sites. Preliminary results suggest that other peat properties, such as CEC and OC can be measured through a site-specific calibration function. In the moment, we focus on developing such a function. Additionally, field surveys of EC_b can delineate the peat body and, hence, can deliver information about the peat thickness, which is also needed if the carbon storage of a specific peatland should be assessed.

References

ASADI, A., HUAT, B.B.K. 2009. Electrical Resistivity of Tropical Peat. Electronic Journal of Geotechnical Engineering, 14, p.1-9.

ASADI, A, HUAT, B.B.K., MOAYEDI, H., SHARIATMADARI, N., PARSAIE, A. 2011. Eletro-Osmotic Permeability Coefficient of Peat with Different Degree of Humification. International Journal of Electrochemical Science, 6, p.4481-4492.

COMAS, X., SLATER, L., REEVE, A.S. 2011. Pool patterning in a northern peatland: geophysical evidence for the role of postglacial landforms. Journal of Hydrology, 399 (3-4), p.173-184.

EL-GALLADI, A., EL-QADY, G., METWALY, M., AWAD, S. 2007. Mapping peat layer using surface geoelectrical methods at mansoura environs, Nile delta, Egypt. Mansoura Journal of Geology and Geophysics, 34 (1), p.59-78.

KALBITZ, K., GEYER, S. 2002. Different effects of peat degradation on dissolved organic carbon and nitrogen, Organic Geochemistry, 33 (3), p.319-326.

LOWRY, C. S., FRATTA, D., ANDERSON, M. P. 2009. Ground penetrating radar and spring formation in a groundwater dominated peat wetland. Journal of Hydrology, 373 (1-2), p.68-79.

POST, VON, L. 1922. SGU peat inventory and some preliminary results. Svenska Mosskultur-foreningens Tidskrift, Jonkoping, Sweden, 36, p.1-37.

SASS, O., FRIEDMANN, A., HASELWANTER, G., WETZEL, K.F. 2010. Investigating thickness and internal structure of alpine mires using conventional and geophysical techniques. Catena, 80, p.195-203.

SEYBOLD, C., GROSSMAN, R., REINSCH, T. 2005. Predicting cation exchange capacity for soil survey using linear models. Soil Science Society of America Journal, 69, p.856-863.

SLATER, L.D., REEVE, A. 2002. Investigating peatland stratigraphy and hydrogeology using integrated electrical geophysics. Geophysics, 67 (2), p.365-378.

TRIANTAFILIS, J., AHMED, M.F., ODEH, I.O.A. 2002. Application of a mobile electromagnetic sensing system (MESS) to assess cause and management of soil salinization in an irrigated cotton-growing field. Soil Use and Management, 18, p.330-339.

Series

Bornimer Agrartechnische Berichte

Heft 1	Technik und Verfahren der Landschaftspflege	1992
Heft 2	Beiträge zur Lagerung und Verarbeitung pflanzenbaulicher Produkte	1993
Heft 3	Technik und Verfahren in der Tierhaltung	1993
Heft 4	Technik und Verfahren der Landschaftspflege und für die Verwendung der anfallenden Materialien	1994
Heft 5	Verfahrenstechnik der Aufbereitung, Lagerung und Qualitätserhaltung pflanzlicher Produkte	1994
Heft 6	Biokonversion nachwachsender Rohstoffe und Verfahren für Reststoffbehandlung	1994
Heft 7	Preußische Versuchs- und Forschungsanstalt für Landarbeit und Schlepperprüffeld in Bornim 1927 bis 1945	1995
Heft 8	Qualitätssicherung und Direktvermarktung	1996
Heft 9	Konservierende Bodenbearbeitung auf Sandböden	1996
Heft 10	Anwendung wärme- und strömungstechnischer Grundlagen in der Landwirtschaft	1996
Heft 11	Computer-Bildanalyse in der Landwirtschaft Workshop 1996	1996
Heft 12	Aufbereitung und Verwertung organischer Reststoffe im ländlichen Raum	1996
Heft 13	Wege zur Verbesserung der Kartoffelqualität durch Verminderung der mechanischen Beanspruchung	1997
Heft 14	Computer-Bildanalyse in der Landwirtschaft Workshop 1997	1997
Heft 15	Technische und ökonomische Aspekte der Nutztierhaltung in großen Beständen	1997
Heft 16	11. Arbeitswissenschaftliches Seminar	1997
Heft 17	Nachwachsende Rohstoffe im Land Brandenburg Stand Aktivitäten und Perspektiven einer zukunftsfähigen und umweltgerechten Entwicklung	1998
Heft 18	Qualität von Agrarprodukten	1998
Heft 19	Computer-Bildanalyse in der Landwirtschaft Workshop 1998	1998
Heft 20	Beiträge zur teilflächenspezifischen Bewirtschaftung	1998
Heft 21	Landnutzung im Spiegel der Technikbewertung – Methoden Indikatoren, Fallbeispiele	1998

Heft 22	Kriterien der Nachhaltigkeit in der Verfahrensentwicklung für die Nutztierhaltung	1999
Heft 23	Situation und Trends in der Landtechnik / Erneuerbare Energien in der Landwirtschaft	1999
Heft 24	Institut für Landtechnik der Deutschen Akademie der Landwirtschaftswissenschaften zu Berlin 1951 bis 1965	1999
Heft 25	Computer-Bildanalyse in der Landwirtschaft Workshop 1999 / 2000	2000
Heft 26	Computer-Bildanalyse in der Landwirtschaft Workshop 2001	2001
Heft 27	Approaching Agricultural technology and Economic Development of Central and Eastern Europe	2001
Heft 28	6th International Symposium on Fruit, Nut, and Vegetable Production Engineering	2001
Heft 29	Measurement Systems for Animal Data and their Importance for Herd Management on Dairy Cow Farms	2002
Heft 30	Produktion, Verarbeitung und Anwendung von Naturfasern	2002
Heft 31	Computer-Bildanalyse in der Landwirtschaft Workshop 2002	2002
Heft 32	Biogas und Energielandwirtschaft - Potenzial, Nutzung, Grünes Gas™, Ökologie und Ökonomie	2003
Heft 33	Sozioökonomische Aspekte zu Perspektiven des Offenlandmanagements	2003
Heft 34	Computer-Bildanalyse in der Landwirtschaft Workshop 2003	2003
Heft 35	Energieholzproduktion in der Landwirtschaft Potenzial, Anbau, Technologie, Ökologie und Ökonomie	2004
Heft 36	High-Tech Innovationen für Verfahrensketten der Agrarproduktion. Statusseminar 2003	2004
Heft 37	Computer-Bildanalyse in der Landwirtschaft Workshop 2004	2004
Heft 38	Die Landmaschinenprüfung in der DDR 1951-1991 und ihre Vorgeschichte	2004
Heft 39	Energieverlust und Schimmelpilzentwicklung bei der Lagerung von Feldholz-Hackgut	2005
Heft 40	Computer-Bildanalyse in der Landwirtschaft Workshop 2005	2005
Heft 41	Demonstration der Langzeitwirkung bedarfsorientierter Fungizidbehandlung mit dem CROP-Meter	2005

Heft 42	Biochemicals and Energy from Sustainable Utilization of herbaceous Biomass (BESUB)	2005
Heft 43	Ozontes Waschwasser zur Qualitätssicherung leichtverderblicher Produkte - Entwicklung einer *Fuzzy-Logic*-Steuerung des Waschprozesses	2005
Heft 44	Messsystem zur Bewertung des Unkrautvorkommens	2005
Heft 45	Anwendung der Thermographie zur Optimierung der Belüftungssteuerung bei der Lagerhaltung landwirtschaftlicher Produkte	2005
Heft 46	Membranbioreaktor zur Aufbereitung von Schlachthofabwässern Prozesssteuerung von Biogasanlagen mit Kofermentation	2005
Heft 47	Verschleißeinfluss auf das Förderverhalten von Drehkolbenpumpen	2005
Heft 48	Qualitätserhaltung und Qualitätssicherung von Bioobst und Biogemüse in der Nachernte	2005
Heft 49	Miniaturisiertes Datenerfassungs-System zum Implantieren in Früchte und zur Messung ihrer mechanischen Belastung durch Ernte- und Nachernteverfahren	2005
Heft 50	Prozesskontrolle der Qualität von frischem Obst und Gemüse mit Hilfe eines Multigas-Sensors	2005
Heft 51	Entwicklung eines Echtzeitsensors für die Stärkebestimmung bei Kartoffeln als funktionaler Bestandteil eines optoelektronischen Verleseautomaten	2005
Heft 52	Optimierte Steuerung von Getreide-Schachttrocknern	2005
Heft 53	Möglichkeiten und Grenzen der energetischen Nutzung von Rizinusöl	2005
Heft 54	Non-Destructive Methods for Detecting Health-Promoting Compounds COST Action 924 Working Group Meeting	2005
Heft 55	4th IFAC / CIGR Workshop Control Applications in Post - Harvest and Processing Technology (CAPPT 2006) 26th - 29th March 2006, Potsdam, GERMANY	2006
Heft 56	Computer-Bildanalyse in der Landwirtschaft Workshop 2006	2006
Heft 57	Kontrolle der Frische in der Nacherntekette von Ökogemüse	2006
Heft 58	Entwicklung eines innovativen Dekontaminationsverfahrens als Technologieantwort auf zukünftiges Qualitätsmanagement im Nacherntebereich	2006
Heft 59	Experimental Studies and Mathematical Modelling of Solar Drying System for Production of High Quality Dried Tomato	2007

Heft 60	13. Workshop Computer-Bildanalyse in der Landwirtschaft & 4. Workshop Precision Farming	2007
Heft 61	Energiepflanzen im Aufwind Wissenschaftliche Ergebnisse und praktische Erfahrungen zur Produktion von Biogaspflanzen und Feldholz	2007
Heft 62	14. Workshop Computer-Bildanalyse in der Landwirtschaft	2008
Heft 63	Experten-Workshop Lagerung von Holzhackschnitzeln	2008
Heft 64	Postharvest unlimited 2008	2008
Heft 65	Vom Agrarrohstoff zu neuen Produkten – Verfahrens-technische Forschung im Nacherntebereich	2009
Heft 66	16. Arbeitswissenschaftliches Kolloquium des VDI-MEG Arbeitskreises Arbeitswissenschaften im Landbau	2009
Heft 67	Monitoring der methanbildenden Mikroflora in Praxis-Biogasanlagen im ländlichen Raum: Analyse des Ist-Zustandes und Entwicklung eines quantitativen Nachweis-systems	2009
Heft 68	Wieviel Biogas steckt in Pflanzen? Abschluss- Symposium des "Biogas-Crops-Network" (BCN) 7. Mai 2009 Potsdam	2009
Heft 69	Image Analysis for Agricultural Products and Processes 27 to 28. Aug. 2009 Potsdam	2009
Heft 70	5th International Technical Symposium on Food Processing, Monitoring Technology in Bioprocesses and Food Quality Management 31. Aug. to 02. Sept. 2009 Potsdam	2009
Heft 71	Einsatz von Biogas in PEM-Brennstoffzellen	2009
Heft 72	Teilflächenspezifische Grunddüngung	2009
Heft 73	16. Workshop Computer-Bildanalyse in der Landwirtschaft 04. Mai 2010 Braunschweig	2010
Heft 74	Erschließung von Nachhaltigkeitspotenzialen durch Nutzung innovativer Sensortechnologien *-Prozesskette Getreide-*	2010
Heft 75	Erschließung von Nachhaltigkeitspotenzialen durch Nutzung innovativer Sensortechnologien *-Prozesskette pflanzliche Frischeprodukte-*	2010
Heft 76	International Workshop The future of the quarter individual milking 14. – 15. September 2010 Potsdam	2010

Heft 77	A flow cytometric approach to monitor the effects of gentle preservation techniques in the postharvest chain	2011
Heft 78	17. und 18. Workshop Computer-Bildanalyse in der Landwirtschaft 05. Mai 2011 Stuttgart und 09. Mai 2012 Osnabrück	2012
Heft 79	2. Öffentliches Symposium des „BCN“ BiogasPOTENZIALE Erkennen, Erforschen, Erwirtschaften	2012
Heft 80	Mechanisms of Bacillus spore germination and inactivation during high pressure processing	2013
Heft 81	19. Workshop Computer-Bildanalyse in der Landwirtschaft 2. Workshop Unbemannte autonom fliegende Systeme in der Landwirtschaft 06. – 07. Mai 2013 Berlin	2013

Contact:

Leibniz-Institut für Agrartechnik Potsdam-Bornim e.V.
Max-Eyth-Allee 100
14469 Potsdam

☎: (0331) 5699-820
Fax.: (0331) 5699-849
E-Mail: atb@atb-potsdam.de

Price for each volume: 13,- €